UNIVERSITY OF CALIFORNIA
RIVERSIDE

Petrology and Stable Isotope Geochemistry of Three Wells in the Buttes Area of the Salton Sea Geothermal Field, Imperial Valley, California, U.S.A.

A Thesis submitted in partial satisfaction
of the requirements for the degree of

Master of Science

in

Geological Sciences

by

Carol Kendall

December 1976

Thesis Committee:

Professor Wilfred A. Elders

Professor Lewis H. Cohen

Dr. Tyler B. Coplen

Dr. Eric R. Olson

DISCLAIMER

ACKNOWLEDGMENTS

I am greatly indebted to Wilfred A. Elders for his support during this research project. Our discussions have been often heated, but both the thesis and I have profited immeasurably from them. I deeply appreciate the freedom he has granted me to make my own decisions and go my own way. I am grateful to Lewis H. Cohen, Tyler B. Coplen, Eric R. Olson, and Patrick R. L. Browne for their critical review of this and earlier versions of the text, and especially to Tyler for introducing me to stable isotope geochemistry. Thanks are also due to Lucy E. Edwards and Paul D. Johnson for serving as sounding boards for my more wild ideas, Pete Collier for making thin sections and preparing samples for X-ray analysis, Candy Mooser for drafting most of the illustrations, Susan Hilton for deciphering my hen-scratches and typing both drafts of this thesis, Libby Benson for cheerfully making last-minute corrections, and to the entire IGPP staff and students for helping out in so many ways. This research was supported by N.S.F. Grant AER 72-03551 and by an N.S.F. Energy Related Traineeship. The X-ray laboratory is supported by U.S.D.I./G.S. Grant No. 14-08-0001-G-244.

PETROLOGY AND STABLE ISOTOPE GEOCHEMISTRY OF THREE WELLS IN THE BUTTES AREA OF THE SALTON SEA GEOTHERMAL FIELD, IMPERIAL VALLEY, CALIFORNIA, U.S.A.

by

Carol Kendall

Master of Science, Graduate Program in Geological Sciences

University of California, Riverside, December 1976

ABSTRACT

This report is based on a detailed investigation of cuttings recovered from three wells in the Salton Sea geothermal field located at the southeast end of the Salton Sea, California. The wells, Magmamax #2, Magmamax #3, and Woolsey #1 penetrate 1340 m, 1200 m, and 730 m, respectively, of altered sandstones, siltstones, and shales of the Colorado River delta. The wells are located at the crest of a thermal anomaly, reach a maximum of 320°C at 1070 m, and produce a brine containing approximately 250,000 mg/l of dissolved solids.

At shallow depths, hydrothermal alteration results in silicification and localized potassium metasomatism of feldspars and montmorillonite to form K-mica. Increasing alteration causes dissolution of silicates and precipitation of abundant calcite. In the highest stage alteration encountered, calcite and detrital silicates are largely replaced by an assemblage of adularia, epidote, anhydrite, tremolite,

pyrite, and hematite. Detrital mica is altered to chlorite, and in the most altered rocks hydrothermal chlorite recrystallized to form biotite; feldspars are albitized and phyllosilicates replaced by albite. Small amounts of garnet, talc, and a high temperature montmorillonite are present in the deepest rocks.

Each mineral assemblage has a limited vertical range. The presence and abundance of secondary minerals is strongly controlled by the matrix content. The impaired permeability of argillaceous rocks impedes water circulation and slows reaction rates so that relict mineral assemblages are preserved outside their usual ranges.

Extensive oxygen and carbon isotope exchange has occurred between geothermal brines and country rocks. Detrital and diagenetic carbonates have exchanged with the brines at temperatures as low as 100-150°C. Both detrital and authigenic quartz in dense, highly altered and mineralized sandstones have completely or almost completely exchanged at temperatures as low as 290°C. Hydrothermal epidote oxygen del values are approximately 4 °/oo lighter than coexisting quartz. Hydrothermal hematite is in apparent oxygen isotopic equilibrium with quartz at measured borehol temperatures (∿300°C).

Superimposed on the gross trend of lower del values at increasing temperature is another important effect due to permeability variations in the reservoir rocks. Aquifers are characterized by low del values, and aquitards by high values. The oxygen del values of vein calcite are 0-1 °/oo lighter than calcite cement in sandstones, which in turn is 1-7 °/oo lighter than calcite in shale. Hydrothermal alteration is more extensive in zones characterized by low del values, and differs

significantly from the alteration assemblages in less permeable horizons.

Aquifer permeability is predominantly secondary and lithologic variation has a strong effect on the creation of microfractures. Water circulation is largely restricted to horizontal aquifers which have been correlated between wells using del values. Fluids within veinlets are locally derived and vertical fractures have been relatively unimportant as circulation channels.

TABLE OF CONTENTS

LIST OF TABLES

LIST OF FIGURES

INTRODUCTION

Active geothermal areas provide an invaluable opportunity to study on-going hydrothermal alteration. In these areas it is possible to directly measure the temperature and depth at which minerals are forming and also to analyze the circulating fluids. Similarly, the study of hydrothermal alteration is an essential prerequisite to understanding the hydrology of a geothermal reservoir so that it can be investigated and developed intelligently.

The intent of this study is to investigate the effect of original permeability variations on the alteration and oxygen and carbon isotopic composition of the rocks. Three adjacent wells, Magmamax #2, Magmamax #3, and Woolsey #1, were studied in order to trace these effects laterally as well as vertically. These particular wells were chosen because they had not yet been studied, sample recovery was excellent, and temperature and geophysical data were available.

This study has been arranged into two semi-independent chapters--petrology and stable isotope geochemistry--each with a final discussion and summary of the data contained in it. The metric system is used throughout except for recording depths at which samples were recovered in order to conform with the drillers' records.

LOCATION AND PREVIOUS WORK

The Salton Sea geothermal field is located in an alluvial plain at the southeast end of the Salton Sea in the Imperial Valley of California (Fig. 1). The field exhibits anomolously high heat flow (Rex, 1966), and is associated with a strong positive gravity anomaly (Elders and others, 1972). The compound positive magnetic anomaly of the area is only partly due to the exposed rhyolite volcanoes (Griscom and Muffler, 1971).

Since 1961 the Salton Sea field has been the site of extensive exploration for geothermal power. Some 20 wells (Fig. 2) ranging in depth from 1700' to 8100' have tapped an exceedingly saline brine with over 250,000 mg/l dissolved solids. Temperatures in the brine reservoir range up to 360°C at 7100'.

The Magmamax #2, Magmamax #3, and Woolsey #1 wells are located in Section 33, T11S, R13E in the southwest end of the Salton Sea geothermal field (Fig. 2). The wells were drilled and logged by Magma Power Company in 1972. Magmamax #2 and #3, and Woolsey #1 were drilled to 4400', 4000', and 2400', respectively. Cuttings were collected at approximately 30' intervals. The lease, including nearby Magmamax #1 and #4, is controlled by the Imperial Magma Company which is presently setting up an experimental two-stage heat exchange unit.

Magmamax #2, #3, and Woolsey #1 are located on the crest of the thermal anomaly (Randall, 1974); temperature profiles of the three wells are shown in Fig. 3. Magmamax #2 shows a slight, broad temperature

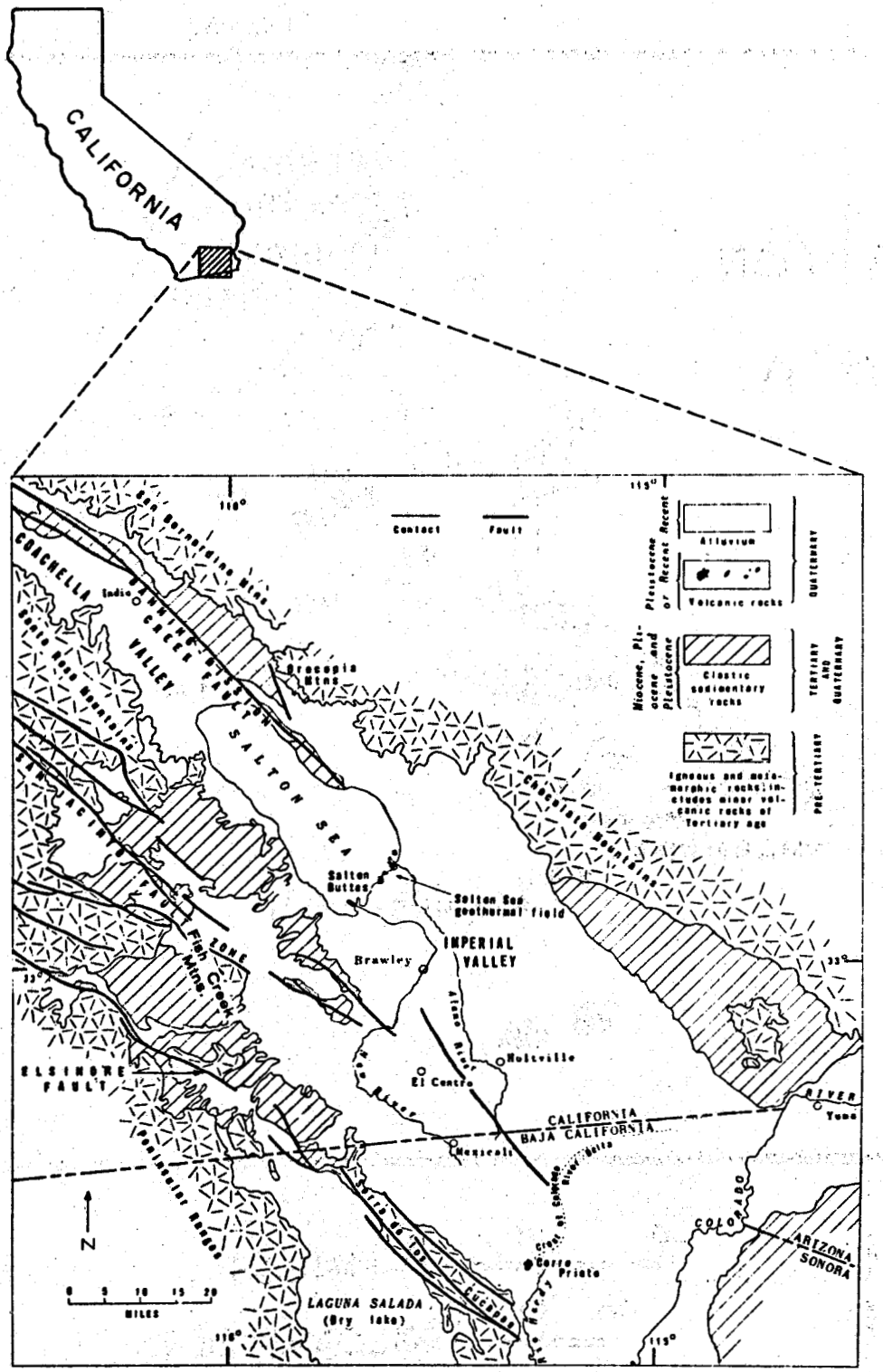

Figure 1. Generalized geologic map of the Imperial Valley and adjacent areas. (after Robinson and others, 1976)

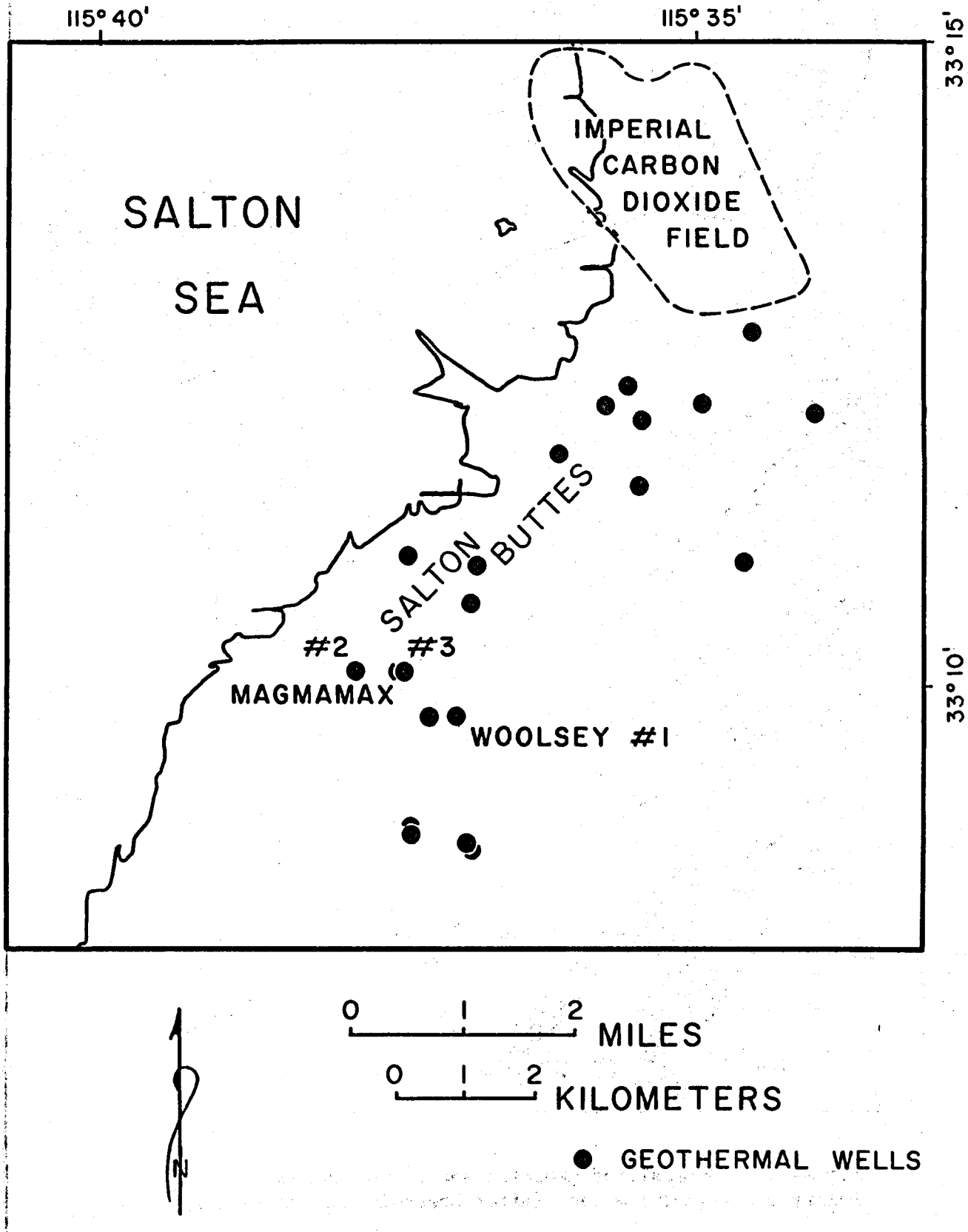

Figure 2. Map of the Salton Sea geothermal field.

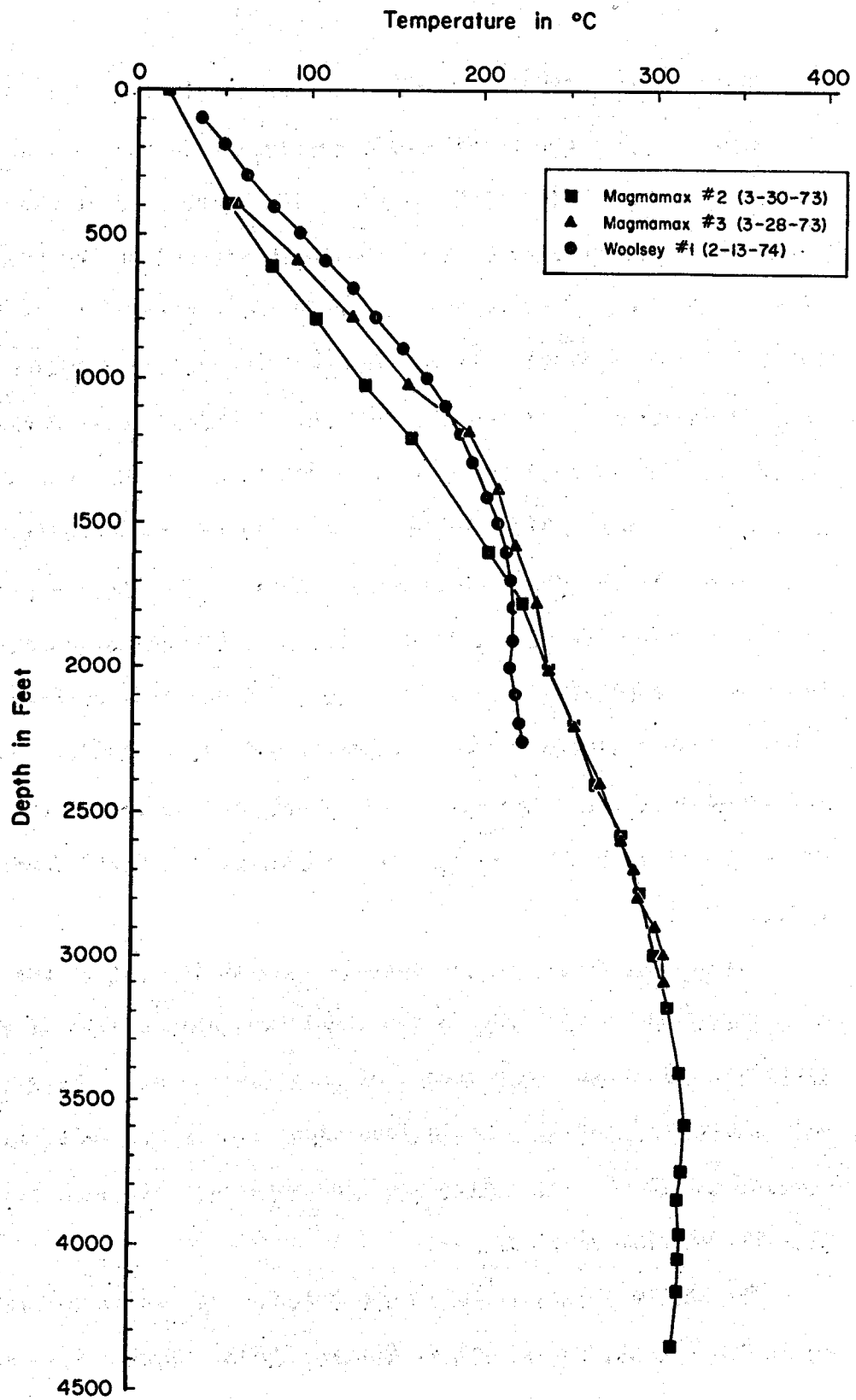

Figure 3. Temperature profiles; data from Randall (1974).

reversal at about 3600'. Temperatures were only logged to 3100' in Magmamax #3, but the profile appears similar to that of Magmamax #2.

Muffler and White (1969) studied the mineralogy of cuttings and core from IID #1 and Sportsman #1 at the northeast end of the anomaly and compared these to samples from a deeper well, Wilson #1, drilled in the center of the Imperial Valley. The wells penetrate a sequence of fine-grained sandstones, siltstones, and shales which range in age from Recent at the surface to late Pliocene at 8000' (Clayton and others, 1968). In response to the elevated temperatures at depth, these sediments are being transformed to low grade metamorphic rocks of the albite-epidote hornfels facies (Muffler and White, 1968). The most common metamorphic assemblage at temperatures greater than 300°C is quartz + epidote + chlorite + K-feldspar + albite ± K-mica (Muffler and White, 1969). Decarbonation reactions during metamorphism are probably the source of the abundant CO_2 produced from the Imperial Carbon Dioxide Gas Field (Muffler and White, 1968).

Subsurface stratigraphic correlations in the Salton Sea area are very difficult to make due to the highly variable nature of the sand-shale sequences and the presence of many fault zones. Randall (1974) made parastratigraphic correlations among Salton Sea wells based on the percent volume of sand bodies per 500' interval; his work suggests the presence of many minor faults.

The saline brines contain over 250,000 mg/l dissolved solids, primarily Cl, Na, Ca, K, and Fe (White, 1968). Brines from IID #1 deposited metal-rich siliceous scale containing an average of 20% Cu and 6% Ag at a rate of 2-3 tons per month (Skinner and others, 1967).

This brine is a potential ore-forming fluid (Doe and others, 1966). Lead and strontium isotopic evidence is compatible with an origin of the heavy metals by leaching and recrystallization of sediments in the brine reservoir (Doe and others, 1966). Coplen (1973) analyzed over 200 well, spring, and geothermal water samples from the Imperial Valley and concluded that most of the subsurface water is derived from the Colorado River.

Clayton and others (1968) studied carbonates and silicates in bulk samples from River Ranch #1 and found extensive oxygen isotope exchange between hydrothermal solutions and the country rocks. Carbonates and some silicates have reached isotopic equilibrium as low as 150°C. There was generally good agreement between the measured borehole temperatures and those derived from the calcite-water geothermometer using an estimated oxygen isotopic composition for water of 2.0 ± .5 $^{o}/_{oo}$ relative to SMOW. They reported a volume ratio of water-rock reaction at depths between 3000'-6000' of approximately 1.

There are five small rhyolite domes along the crest of the thermal, gravity, and magnetic anomalies. These volcanics contain abundant xenoliths composed largely of basalt, with lesser amounts of granitic, sedimentary, and metasedimentary rocks. The origin of this bimodal rhyolite-basalt assemblage is attributed to possible two-stage fusion of mantle peridotite (Robinson and others, 1976). Randall (1974) found that the geometry of isotherms in the Salton Sea Field was not controlled by local stratigraphic or structural relationships, but by the distance from a hypothesized magma instrusion that generated the anomaly. However, seismic refraction studies in the vicinity of the Salton Buttes found

no evidence for a significant intrusive body in the 6 km of sediments above basement (Biehler, pers. com. 1975). An impermeable caprock of shale has acted as an insulating barrier to retain most of the volcanic-related heat within the water reservoir (Helgeson, 1968; Muffler and White, 1969; Randall, 1974).

REGIONAL SETTING

The Salton Trough, the landward extension of the Gulf of California, is a closed sedimentary basin about 200 km long and 5-130 km wide partially filled with late Tertiary and Quaternary deltaic and lacustrine sediments. It is a complex rift valley bordered by steep, step-faulted mountains of Mesozoic and other crystalline rocks and is apparently controlled by en-echelon faulting of the San Andreas and related fault systems. To the south, it is separated from the Gulf of California by the apex of the Colorado River delta. The Salton Sea, 70 m below sea level, presently occupies the lowest point of the Salton basin.

The Salton trough was probably a morphotectonic low as early as the Miocene (Downs and others, 1961) when a marine embayment extended as far north as the Fish Creek Mountains (Durham and Allison, 1962). The Colorado River began to empty into the northeastern Gulf of California in latest Miocene or early Pliocene (Longwell, 1954), and has since been the predominant source of detritus for the basin (Merriam and Bandy, 1965) although lesser volumes of material are also derived from the basin margins. The Colorado Plateau-derived deltaic clastics are distinctly less arkosic than basin margin sediments (Van de Kamp,

1973). These marginal alluvial fans have complex facies relationships with the deltaic deposits and lacustrine clays and silts that dominate the sediments of the central portion of the Salton basin (Van de Kamp, 1973; Bird, 1975).

Growth of the Colorado River delta perpendicular to the Gulf of California-Salton trough during the mid-Pleistocene resulted in the isolation of the Salton basin from the Gulf of California (Van de Kamp, 1973). The present delta forms a low divide which marks the boundary between the Imperial Valley of California and the Mexicali Valley of Mexico.

The major faults in the region are shown in Fig. 1. Movement along the Banning-Mission Creek and San Jacinto faults is known to be right lateral and was probably initiated in the Tertiary (Crowell, 1962). Faults in the basin itself are more difficult to identify due to their usual lack of surface expression. Fault locations have been deduced mainly from seismic reflection (Sigurdson and others, 1971), electrical resistivity (Meidav and Ferguson, 1972), and microearthquake studies (Combs and Hadley, 1973). The Salton trough is believed to have formed by a combination of tensional and right-lateral strike-slip movements associated with the opening of the Gulf of California (Elders and others, 1972).

The Salton trough is characterized as an area of high heat flow (Rex, 1966; Helgeson, 1968). The localized high thermal gradients at the Salton Buttes, Cerro Prieto, Heber, and East Mesa are associated with high heat flows. Only at Salton Buttes and Cerro Prieto is there

surface expression of these thermal anomalies in the form of warm springs and Quaternary volcanic domes. One of the Salton Buttes domes has been dated, using the K-Ar method, at between 16,000 and 50,000 years old (Muffler and White, 1968). Thermal springs northeast of the Salton Sea are aligned along two northwest trending lineaments parallel to local fault orientation.

According to Elders' (1972) model for the Salton trough, tensional zones or rhombochasms are developing between en-echelon faults. These areas of crustal depression and thinning are the sites of partial melting in the mantle, which result in the formation of young volcanic rocks which penetrate the thick sedimentary accumulations, as at the Salton Buttes and Cerro Prieto, Mexico. The heat generated by magmatic activity may be trapped within a circulating water reservoir by an impermeable shale sequence, as suggested by Randall (1974) for the Salton Sea. At the Dunes hydrologic system, hot water is trapped in the subsurface by cap rocks produced by self-sealing (Combs, 1971; Elders and Bird, 1974).

METHODS OF STUDY

This thesis is based primarily on studies of cuttings retrieved from the three wells. Major emphasis is given to isotopic, petrologic and x-ray diffraction investigations.

The oxygen and carbon isotopic analyses were made on a double-focusing, double-collecting isotope ratio mass spectrometer (Coplen,

1973) in the stable isotope laboratory at the University of California at Riverside (UCR). Most of the analyses were of carbonate cement in sandstones and shales. A few detrital and authigenic silicates and oxides were also analyzed.

Petrological investigations were made using a variety of techniques. Cuttings were examined under binocular microscope, and about 100 grain mounts made of grains from more interesting intervals. While some of the grain mounts consisted of random grains from an interval, most of them consisted of handpicked grains. Major attention was given to textural and mineralogical changes in sandstones and veins. The scanning electron microscope at UCR and MAC-5 electron microprobe at California Institute of Technology were used for more detailed textural and chemical studies. X-ray analyses were made on an automated Picker diffractometer at UCR. Clay and silt-sized fractions of bulk samples chosen at 100'-200' intervals in all three wells in addition to selected shale chips were analyzed.

INHERENT PROBLEMS WITH CUTTINGS

Cuttings from a given depth are often contaminated by sloughing of unconsolidated sediment from above, especially in the upper 1000'. In all three wells after drilling down to 1000' casing was cemented in at the approximate base of the clay layer. The cement plug was then drilled; thus below 1000' this casing prevents sloughing from shallower sediments so that rocks here are less contaminated. However, minor

amounts of red shale in cuttings below 1800' in Magmamax #2 and #3 and below 1500' in Woolsey #1 are probably due to sloughing. Although in a strict sense only the first appearance of a mineral or rock type is a totally reliable indicator of its depth, in general slumping appears to be only a minor problem and is readily recognized. Rocks of low abundance which resemble rocks from shallower depths should always be considered suspect. Evidence that sloughing is only of minor importance is shown by consistent isotopic trends and by internal consistency in the petrologic data (Clayton and others, 1968; Muffler and White, 1969).

In addition to contamination by slumping, the cuttings often contain debris and drilling additives, commonly including lignite, casing cement, rust chips from the drill barrels, plant fibers, rubber, paint chips, gypsum, and montmorillonite or other clays in the drilling mud. Montmorillonite is a problem only in shallow, unconsolidated sediments. Mud and lignite are removed by washing, and the others are easily recognized and can be usually handpicked and removed. Besides lignite, the most confusing contaminant is the casing cement. Cuttings collected from about 1000' in all three wells have large quantities of casing cement composed of volcanic glass plus sanidine and quartz which resembles a volcanic tuff.

All samples were washed repeatedly to remove all drilling mud and lignite. Unfortunately, this also removed virtually all of the clay from the unconsolidated shales in the clay layer above 1000'. Almost all that remains after washing shallow cuttings are anhydrite nodules and veinlets, pyritized grains, minor sand and silt, and rare shales. Hence,

the shallow cuttings samples are highly biased, and the lithology of the original sedimentary sequence can best be interpreted from drilling logs.

There is a variable lag-time between the time the drilling bit cuts through a particular interval and when the cuttings from this interval are carried to the surface and collected. Cuttings are labeled with the depth of the bit when collected, and therefore the true depth is unknown. Actual depths can usually be estimated by comparing cuttings logs with well logs.

PETROLOGY

STRATIGRAPHY AND SEDIMENTATION

Lithology

Cuttings recovered from Magmamax #2, #3, and Woolsey #1 consist of interbedded terrigeneous sediments with an overall average of 70% shales, 5% siltstones, and 25% fine to very fine-grained sandstones. An upper sedimentary unit extending from the surface down to about 1000' is composed largely of tan and gray-brown clays and shales with rare interbedded siltstones and sandstones. A lower unit below about 1000' consists of interbedded sandstone, siltstone, and gray, red, and green shales which have been extensively metamorphosed to the quartz-albite-epidote-biotite subfacies of the greenschist facies (Turner, 1968). Locally the boundary between the two sedimentary units is an unconformity (Dibblee, 1954).

Detrital Mineralogy and Fabric

Evidence presented by Muffler and Doe (1968) indicates that the sediments deposited in the Salton Trough have been of similar chemical and mineralogical composition throughout the late Cenozoic, and were

derived largely from the upper Colorado River drainage basin (Merriam and Bandy, 1965). These Colorado River sediments have a uniform mineralogical composition: quartz + calcite + plagioclase + K-feldspar + dolomite + montmorillonite + illite + kaolinite + accessories. Lesser amounts of Salton Trough sediments are derived from Holocene alluvial fan deposits at the base of mountains adjacent to the Salton Trough which differ mineralogically from the Colorado River sediments, primarily in the small amount of calcite, the absence of dolomite, and the presence of large quantities of chlorite and amphibole.

Sandstones in the three wells contain abundant feldspar and lithic fragments, and vary from subarkose to sublithic arenites (classification of Pettijohn and others, 1972). The feldspars are largely microcline, but orthoclase, albite and calcic plagioclase are locally abundant. About two-thirds of the lithic clasts are nonsedimentary, usually igneous, and one-third are sedimentary. Olivine basalt chips and pyroxenes are occasionally common, but altered rhyolite chips are rare; these may represent subsurface volcanics. Accessory detrital minerals include biotite, muscovite, sphene, tourmaline, amphibole, pyroxene, magnetite, zircon, and apatite. Heavy mineral layers are occasionally present.

In each 30' sampling interval there are at least two distinct varieties of sandstone--one with little or no matrix, and one with phyllosilicate matrix material. In shallow, relatively unaltered sandstone, it is clear that this difference is detrital, and that the two sandstone varieties can be labeled arenites and wackes, respectively (Pettijohn and others, 1972). However, in deeper, highly altered meta-

sandstones the phyllosilicate abundance is no longer entirely detrital and may have been diminished or augmented during hydrothermal alteration; therefore sandstone classifications are no longer applicable. For the purposes of this study, sandstones and meta-sandstones are loosely grouped into two categories based on the amount of phyllosilicate matrix: argillaceous sandstones, usually containing >15% matrix, and non-argillaceous sandstones, with <15% matrix. Siltstones also are grouped into argillaceous and non-argillaceous siltstones based on matrix content.

The color and induration of the sediments are variable mainly due to differences in the type and intensity of post-depositional alteration. Sandstones and siltstones are mainly tan-white, but red, green-gray, and brown types are locally abundant. Shales from the upper 1000' are tan and gray-brown. Slightly deeper shales are of various shades of red due to finely disseminated iron oxides. The upper 1000' is poorly consolidated, with the exception of several beds of iron sulfide-cemented sandstone and anhydrite-mineralized shale. Below 1000' the sediments are all lithified, generally with increasing cementation with increasing depth.

The sand-size fraction of sandstones is fine to very fine, well sorted, and subangular to subrounded. Quartz grains are usually more rounded and spherical than feldspar or lithic clasts of the same size.

Stratigraphy and Parastratigraphy

The sedimentary fill of the central part of the Salton Trough is up to 6 km thick (Biehler, 1964), and consists of a complex sequence

of alluvial, fluvial, lacustrine, and marine deposits (Dibblee, 1954). The stratigraphy of the Buttes area is relatively simple. The dense clay-shale section in the upper 1000' is probably a facies of the Brawley-Borrego Formation (Dibblee, 1954). Below this, arkosic sandstone with intermittent argillaceous beds are probably a Colorado River delta facies of the Palm Springs Formation (Helgeson, 1968).

It is extremely difficult to correlate subsurface sandstone-shale sequences in the Salton basin due to the wide spacing of wells, many local faults, and rapid facies changes in the deltaic sediments. Randall's (1974) correlation of subsurface data from Magmamax #1, #2, #3, and Woolsey #1 is shown in Fig. 4. His technique was to measure the thickness of sand bodies as interpreted from electrical logs, plot their percent volume per 500', and correlate these "units" between wells.

Figure 5 shows a correlation of the cuttings lithology in Magmamax #3 with the electrical induction log as interpreted by Randall (1974, Appendix III). In general, the lag-time for the retrieval of cuttings samples from a particular horizon results in a difference of about 100' between the depth of the horizon on the drilling logs and the depth attributed to the cuttings collected from this horizon. Hence cuttings samples labeled 4000' are from about 3900' on the well logs.

An attempt was made to correlate the lithologies of the three wells, using both geophysical and cuttings logs. Figure 6 shows the sandstone-siltstone-shale ratios and shale colors. Lines between the wells indicate proposed correlations. The lithologies of Magmamax #2 and #3 appear to be virtually identical down to 2600'-2700'. Cuttings

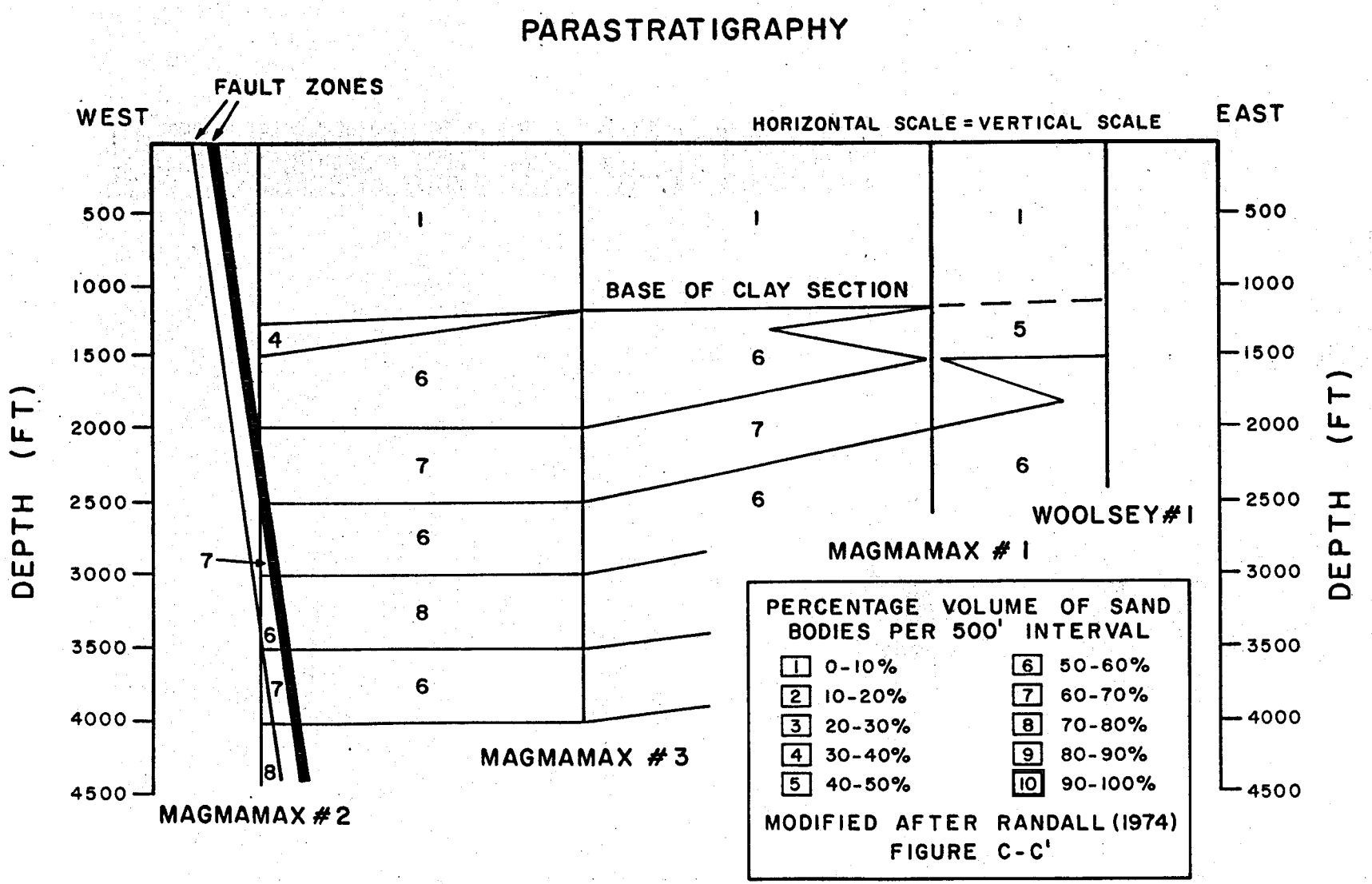

Figure 4. Parastratigraphy of the Buttes area.

Figure 5. Correlation of Cuttings and Geophysical Logs

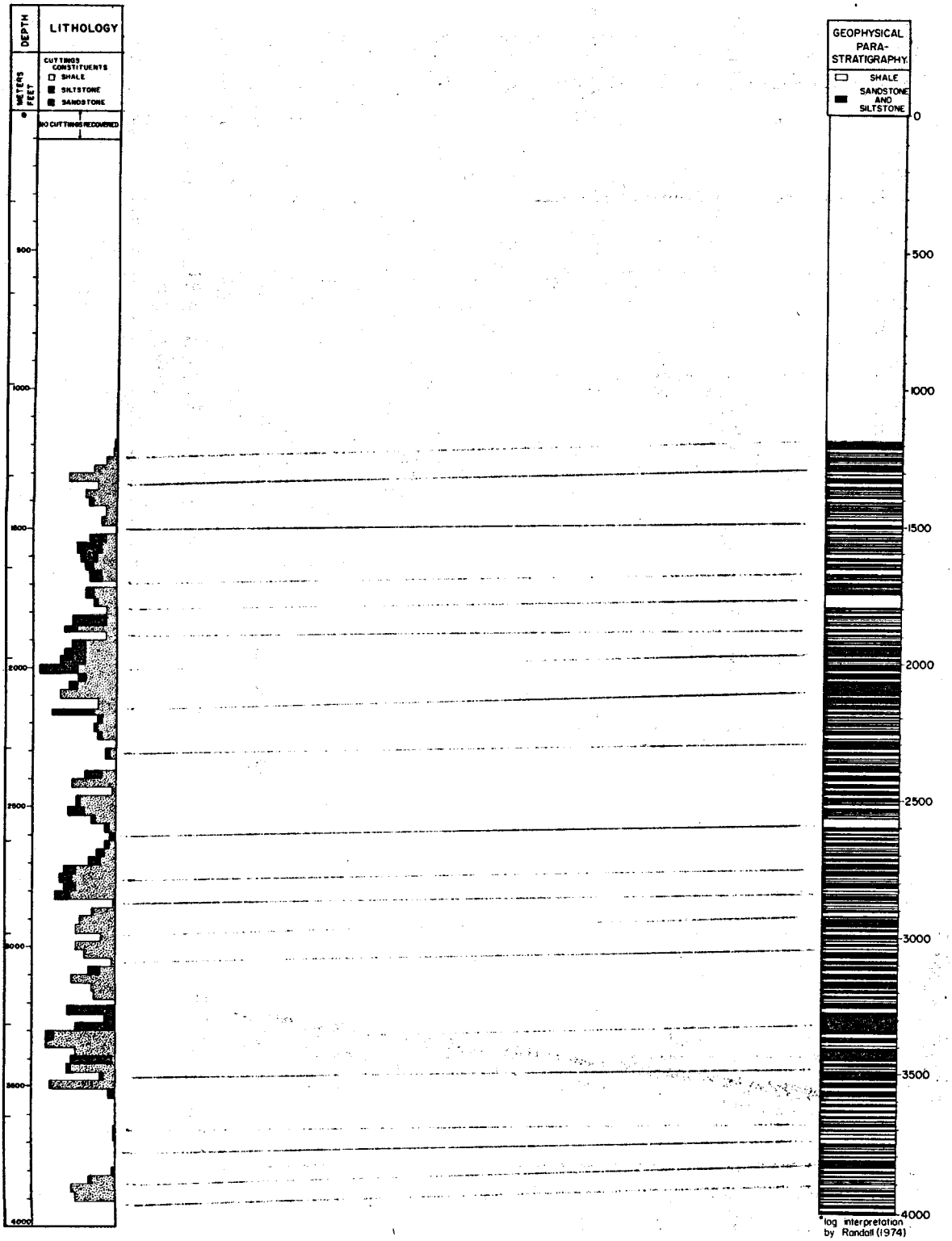

Figure 6. Lithologic Correlations

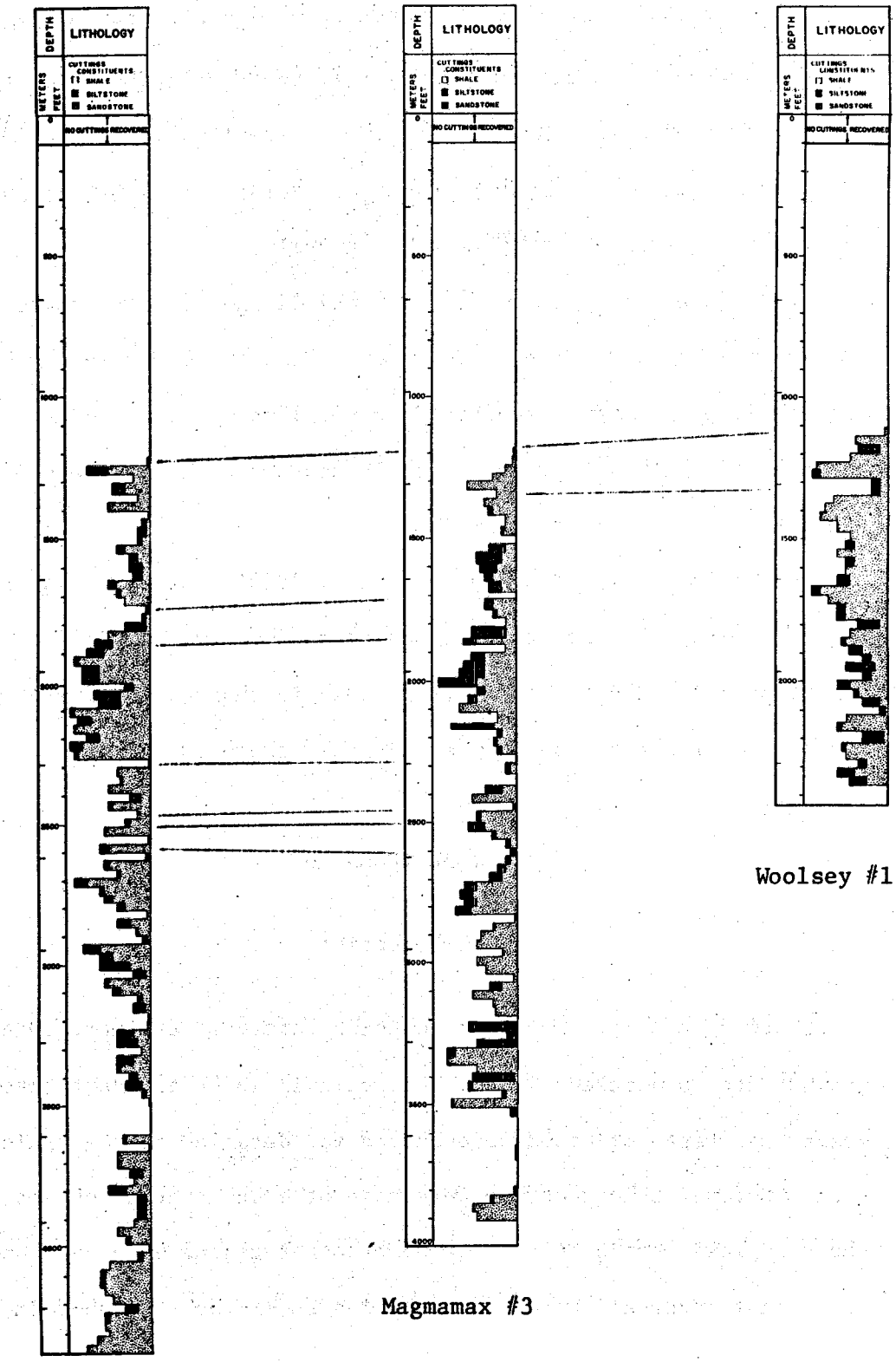

from the interval 2690-2720' in Magmamax #2 include abundant mineralized breccia fragments, suggesting a major fracture cuts the well at this depth. This breccia zone coincides with a fault inferred by Randall (1974) by dipmeter survey (see Fig. 4). Below this there is no apparent lithologic correlation between the two wells.

Red shales are abundant in Magmamax #2 and #3 down to about 1750', and in Woolsey #1 down to 1450'. Their base and the base of the upper shale unit are the only apparent correlations between Woolsey #1 and Magmamax #3; thinning of units to the southeast is in agreement with Randall's (1974) parastratigraphy.

Green shales first appear at 3300', 2800', and 2100' in Magmamax #2, #3 and Woolsey #1 respectively, but this boundary, as will be discussed later, does not denote a primary lithologic change, but instead marks the incipient alteration of gray to green shales.

ANALYTICAL TECHNIQUES

Sample Selection

During description of each cutting interval, the more interesting grains were handpicked; later, intervals in which abundant interesting grains had been collected were chosen for detailed petrographic examination. Several thin sections were made of each interval chosen, using the handpicked grains plus a group of other grains added at random. Additional intervals were then selected to improve the uniform coverage of the well.

Since Magmamax #3 was investigated first, 39 intervals were examined using thin sections. Using the experience gained, only 21 intervals were thin-sectioned in Magmamax #2, and 5 in Woolsey #1. The locations of the intervals where thin sections were studied are shown on Figs. 8-26.

Two different groups of samples were selected, prepared, and analyzed on the diffractometer: the first and major group are bulk samples collected at 100'-200' intervals in all three wells. These were collected to provide a general picture of mineralogic changes in the wells. The second group consists of handpicked, homogeneous, shale grains selected at 100'-200' intervals in Magmamax #2 and #3. The <2μ fraction of each sample was also analyzed because finer grained particles have much greater surface areas and would be more sensitive to variations in temperature and chemical environment than coarser grained material.

Sample Preparation

The preparation procedure used is a modified version of that formerly employed by the Deep Sea Drilling Project X-ray Mineralogy Laboratory at UCR. The same technique is used for both handpicked and bulk samples, except that bulk samples were passed repeatedly through a splitter to obtain random samples. All samples were divided; one portion was ground to clay-size, and analyzed as the bulk fraction. The other portion was disaggregated, dispersed with .05% $(NaPO_3)_6$ solution, and size-fractionated by centrifuge. The suspended <2μ fraction was flocculated, dried, and analyzed as the clay fraction. The samples were run

on an automated Picker x-ray diffractometer using CuK_{α} radiation, a graphite crystal monochrometer, and a scanning speed of 2°2θ per minute. Both fractions were then glycolated and analyzed again.

Diffractogram Interpretation

The interpretation of the diffractograms is done mainly by hand. The minerals present are identified by comparing the glycolated and unglycolated diffractograms with strip-charts showing the major peaks of each mineral. Once the peaks are identified, the intensity above the background scatter of a single, diagnostic peak for each mineral is measured. Using empirically derived intensity factors, the raw intensity measurements for the minerals are computed as mineral percentages, and normalized to 100% (see Cook and others, 1974). Clay fraction data are usually reported qualitatively using a 0 to 5 scale of increasing abundance indicating absent, trace, present, major, and abundant, respectively.

HYDROTHERMAL ALTERATION

Presentation of the Data

Study of the minerals and textures of different rock types, together with their isotopic compositions, revealed that rocks with different original apparent permeabilities had very different responses to water-rock interaction. For this reason, data on argillaceous and non-argillaceous sandstone, argillaceous and non-argillaceous siltstone, and

gray and non-gray shales are presented separately. This facilitates study of progressive changes in rocks of the same original lithology.

Figures 8-26 (pages 28-47) are a set of diagrams, all drawn to the same scale, which show the alteration and mineralization of the sediments. Data on the diagrams are primarily from handsample (cuttings) and thin section examinations. The organization of the data and definitions of terms are explained below.

Cuttings were collected approximately every 30'. The relative amounts of shale, siltstone, and sandstone (or their metamorphic equivalents) in each interval are shown in histogram form in the "lithology" column. Intervals where petrographic or x-ray examinations were made are blacked in. Data on the diagram outside these intervals are from handsample examinations, or are due to interpolation.

Since sandstone and siltstone types are not readily distinguished in handsample, relative abundance data are only available at thin sectioned intervals. Relative quantities of argillaceous and non-argillaceous rocks are indicated by the following symbols:

* >70% of the total sandstone (or siltstone)

\+ the two sandstone (or siltstone) types are of subequal abundance

\- <30% of the total sandstone (or siltstone).

Relative abundances of gray and non-gray shales are easily estimated from handsamples and hence are illustrated as spindle diagrams.

For the purpose of illustration, each lithologic type is considered to have three components--sand or silt, matrix, and cement in sandstones and siltstones; and sand plus silt, matrix, and mineralization in

shales. The relative abundances of each component are shown on the figures.

The categories of sand and silt include all detrital grains, excluding phyllosilicates, greater than .05 mm and .005 mm, respectively.

Matrix includes all phyllosilicates, regardless of grain size or origin, and all other clay-sized (<.005 mm) grains. Sand or silt-sized detrital phyllosilicates are minor constituents, rarely exceeding 1%; hence grouping them with matrix phyllosilicates does not appreciably alter the sand-matrix ratio. All phyllosilicates are grouped together because of the great difficulty in distinguishing among unaltered, altered, or authigenic phyllosilicates. The alteration and recrystallization of phyllosilicates are shown in the "Alteration" column.

The terms cement or mineralization as used here include all neocrystalline non-detrital minerals, excluding phyllosilicates or recrystallized detritals. "Alteration minerals" applies to grains formed by the breakdown or recrystallization of detritals such as feldspars or phyllosilicates; there is no "Alteration" column for siltstones due to lack of data. Neocrystalline, void-filling phyllosilicates rarely exceed 1%, and hence are not shown on the figures. Alteration and mineralization are distinguished because the former probably requires much less change in the total rock chemistry than the latter.

The relative abundances of the twelve most common neocrystalline minerals are shown in the "Mineralization" column. Due to the difficulty in distinguishing between recrystallized and authigenic carbonate, both types are grouped together. Carbonaceous material is also included with

the neocrystalline minerals although it probably consists of slightly remobilized detrital organic matter. Note that the sum of the percentages of minerals at each depth in the "Mineralization" column is equal to the total cement or mineralization shown in the "Components" column.

The basic textures of neocrystalline minerals as shown on the figures are explained below:

Disseminated grains--crystals >.005 mm which are distinct and isolated from each other by matrix or by another type of cement; in shales this category only includes crystals <.25 mm.

Fine grained patches--aggregates or clots of <.05 mm crystals

Micrite--cement composed of grains <.005 mm

Interlocking grains--cement composed of intergrown crystals >.005 mm

Poikilitic cement--texture formed when cement filling several pores is in optical continuity and encloses detrital grains.

Overgrowths--minerals which grow on and partially enclose the sand grains.

Mega-porphyroblasts--very large mineral grains (>.25 mm) in shale, often euhedral; some as large as 2 mm. Equally large grains in sandstones and siltstones generally are poikilitic.

Replacement banding--texture formed when mineralization occurs within selected sedimentary beds.

Data are shown in this column only where petrographic examinations were made. Each mineral present with an abundance greater than 1% has a symbol in the column which best describes its texture. The symbols used are as follows:

A = anhydrite
C = calcite
D = dolomite
E = epidote
F = feldspar (alkali)
G = gypsum
H = hematite
M = carbonaceous material
O = other iron oxides
P = pyrite
Q = quartz
T = tremolite

The relative abundances of the six main phyllosilicate types in shale are derived largely from x-ray analyses of handpicked shales; data on the column outside the x-rayed intervals are due to interpolation, extrapolation from x-ray analyses of bulk samples, and minor petrographic observations. "Mica" includes both muscovite and biotite since these are difficult to distinguish in x-ray patterns. The presence of mega-biotite was noted during petrographic examination, they are >.05 mm, euhedral, oriented crystals.

The "Fracture Mineralization" column displays the relative abundances of the eight most common vein minerals. The abundance of fracture minerals in any 30' interval rarely exceeds 1-5%, and usually is well under 1%. No percentage scales are included because of the difficulty of accurate estimation.

Blackened intervals in Figures 24-26 indicate the locations of the 22 most common mineral assemblages seen in veinlets. The mineral components of each assemblage are listed in the most common paragenetic order. For example, for the assemblage "epidote-tremolite-hematite" epidote was the first mineral formed. In assemblages where two minerals are usually contemporaneous or where the order of mineralization is variable, the minerals are listed: "epidote + calcite."

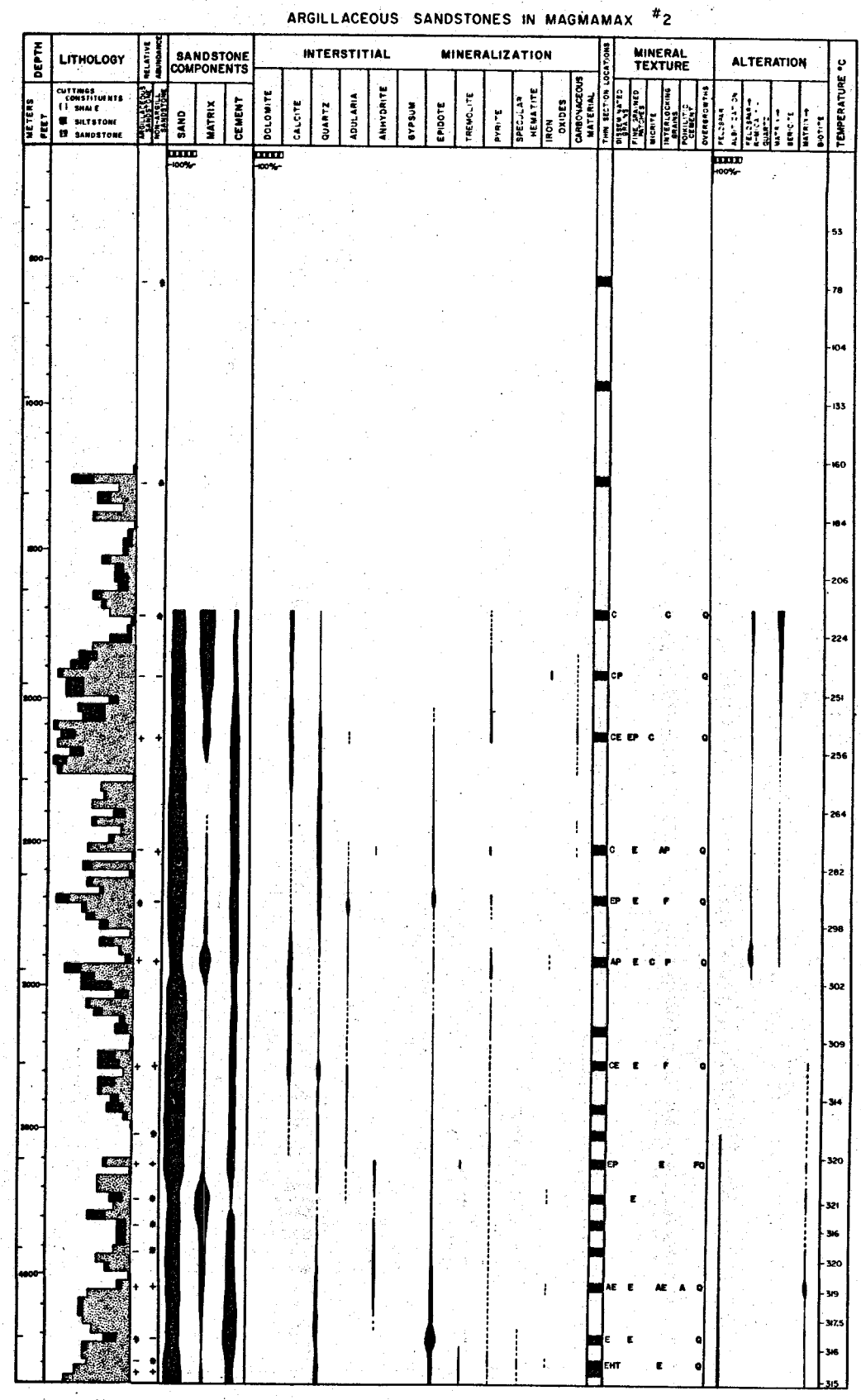
ARGILLACEOUS SANDSTONES IN MAGMAMAX #2
DEPTH
METERS
FEET
LITHOLOGY
CUTTINGS CONSTITUENTS
SHALE
SILTSTONE
SANDSTONE
RELATIVE ABUNDANCE
ARGILLACEOUS SANDSTONE
NON-ARGILLACEOUS SANDSTONE
SANDSTONE COMPONENTS
SAND
MATRIX
CEMENT
INTERSTITIAL MINERALIZATION
DOLOMITE
CALCITE
QUARTZ
ADULARIA
ANHYDRITE
GYPSUM
EPIDOTE
TREMOLITE
PYRITE
SPECULAR HEMATITE
IRON OXIDES
CARBONACEOUS MATERIAL
THIN SECTION LOCATIONS
MINERAL TEXTURE
DISSEMINATED GRAINS
FINE-GRAINED MATRIX
MICRITE
INTERLOCKING GRAINS
FOSSILIFEROUS CEMENT
OVERGROWTHS
ALTERATION
FELDSPAR
ALBITIZATION
FELDSPARS REPLACED BY QUARTZ
MATRIX
SERICITE
MATRIX
BIOTITE
TEMPERATURE °C
100%
C
CP
CE EP C
C E AP
EP E F
AP E C P
CE E F
EP E FQ
E
AE E AE A
E E
EMT E
53
78
104
133
160
184
206
224
251
256
264
282
298
302
309
314
320
321
316
320
319
317.5
316
315

Figure 7

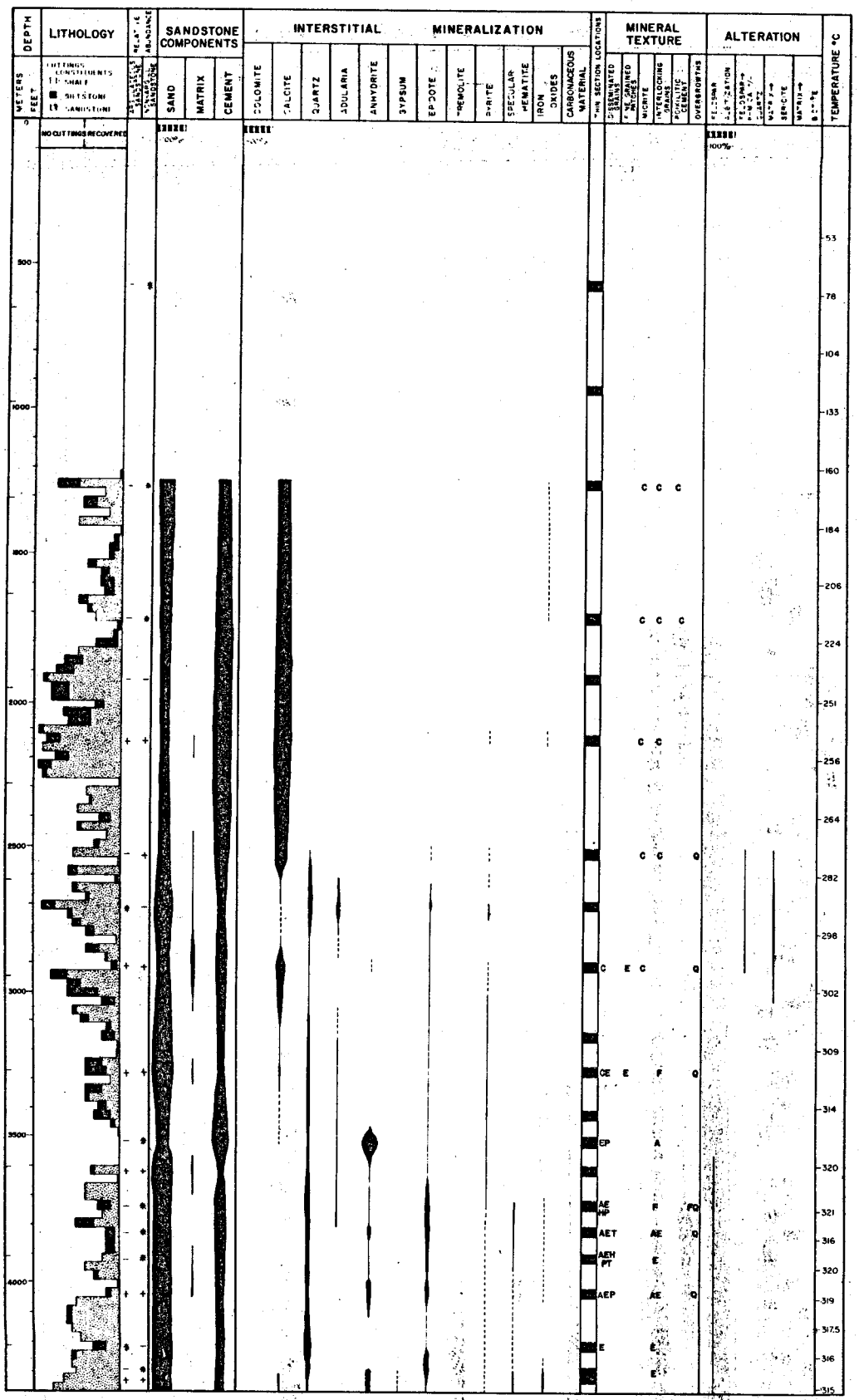
NON-ARGILLACEOUS SANDSTONES IN MAGMAMAX #2
DEPTH
METERS
FEET
LITHOLOGY
SANDSTONE COMPONENTS
SAND
MATRIX
CEMENT
INTERSTITIAL MINERALIZATION
DOLOMITE
CALCITE
QUARTZ
ADULARIA
ANHYDRITE
GYPSUM
EPIDOTE
TREMOLITE
PYRITE
SPECULAR HEMATITE
IRON OXIDES
CARBONACEOUS MATERIAL
THIN SECTION LOCATIONS
MINERAL TEXTURE
MICRITE
INTERLOCKING GRAINS
OVERGROWTHS
ALTERATION
SERICITE
MATRIX
TEMPERATURE °C
NO CUTTINGS RECOVERED
500
1000
1500
2000
2500
3000
3500
4000
53
78
104
133
160
184
206
224
251
256
264
282
298
302
309
314
320
321
316
320
319
317.5
316
315

Figure 8

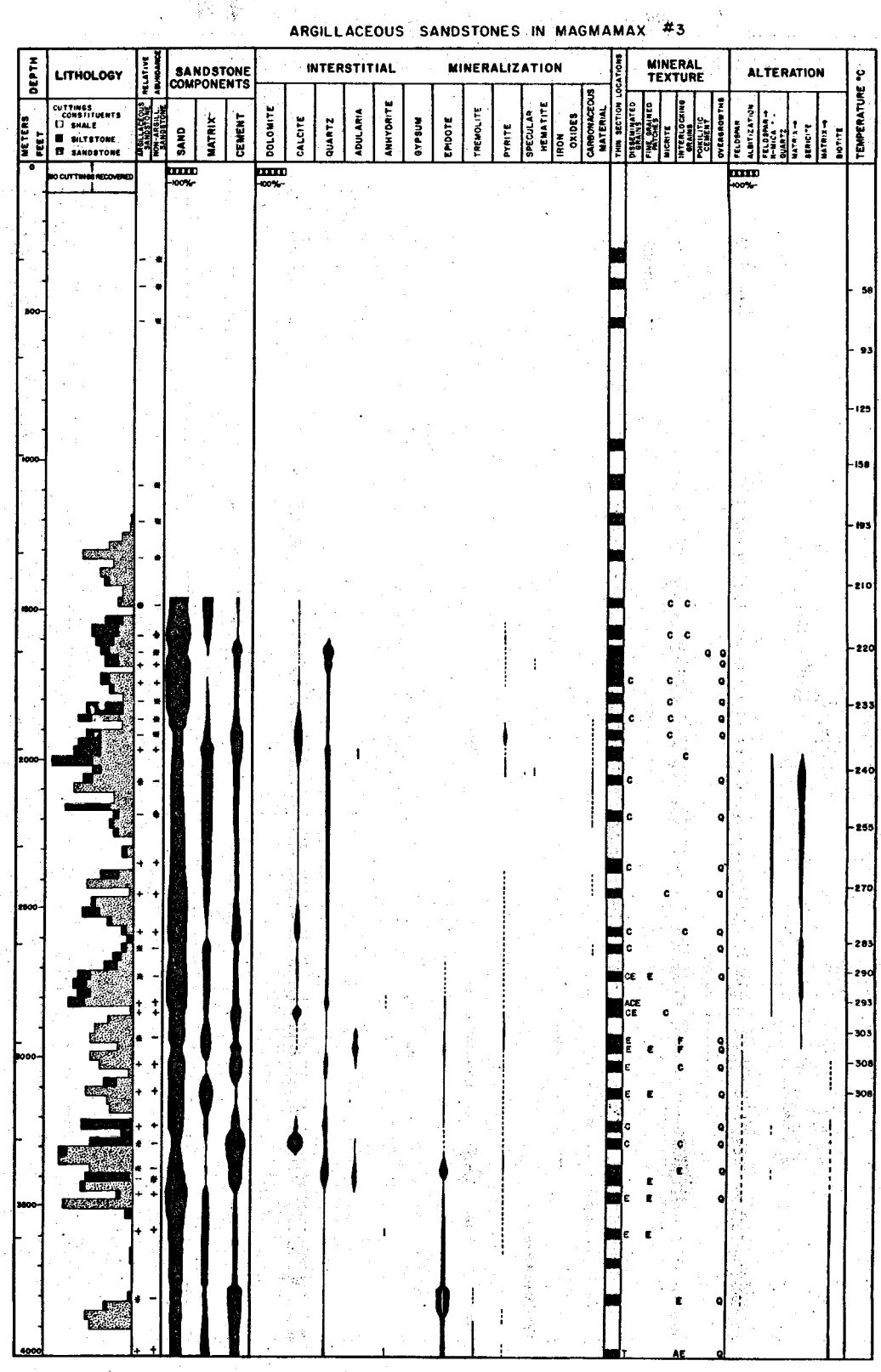
ARGILLACEOUS SANDSTONES IN MAGMAMAX #3
DEPTH
METERS
FEET
LITHOLOGY
CUTTINGS CONSTITUENTS
SHALE
SILTSTONE
SANDSTONE
RELATIVE ARGILLACEOUS ABUNDANCE
SANDSTONE COMPONENTS
SAND
MATRIX
CEMENT
INTERSTITIAL MINERALIZATION
DOLOMITE
CALCITE
QUARTZ
ADULARIA
ANHYDRITE
GYPSUM
EPIDOTE
TREMOLITE
PYRITE
SPECULAR HEMATITE
IRON OXIDES
CARBONACEOUS MATERIAL
THIN SECTION LOCATIONS
MINERAL TEXTURE
DISSEMINATED GRAINS
FINE GRAINED MATRIX
MICRITE
INTERLOCKING GRAINS
POIKILITIC CEMENT
OVERGROWTHS
ALTERATION
FELDSPAR
ALBITIZATION
FELDSPAR → SERICITE
QUARTZ
MATRIX → SERICITE
MATRIX → BIOTITE
TEMPERATURE °C
100%
80 CUTTINGS RECOVERED
1000
2000
3000
4000
58
93
125
158
193
210
220
233
240
255
270
285
290
293
303
308
308

Figure 9

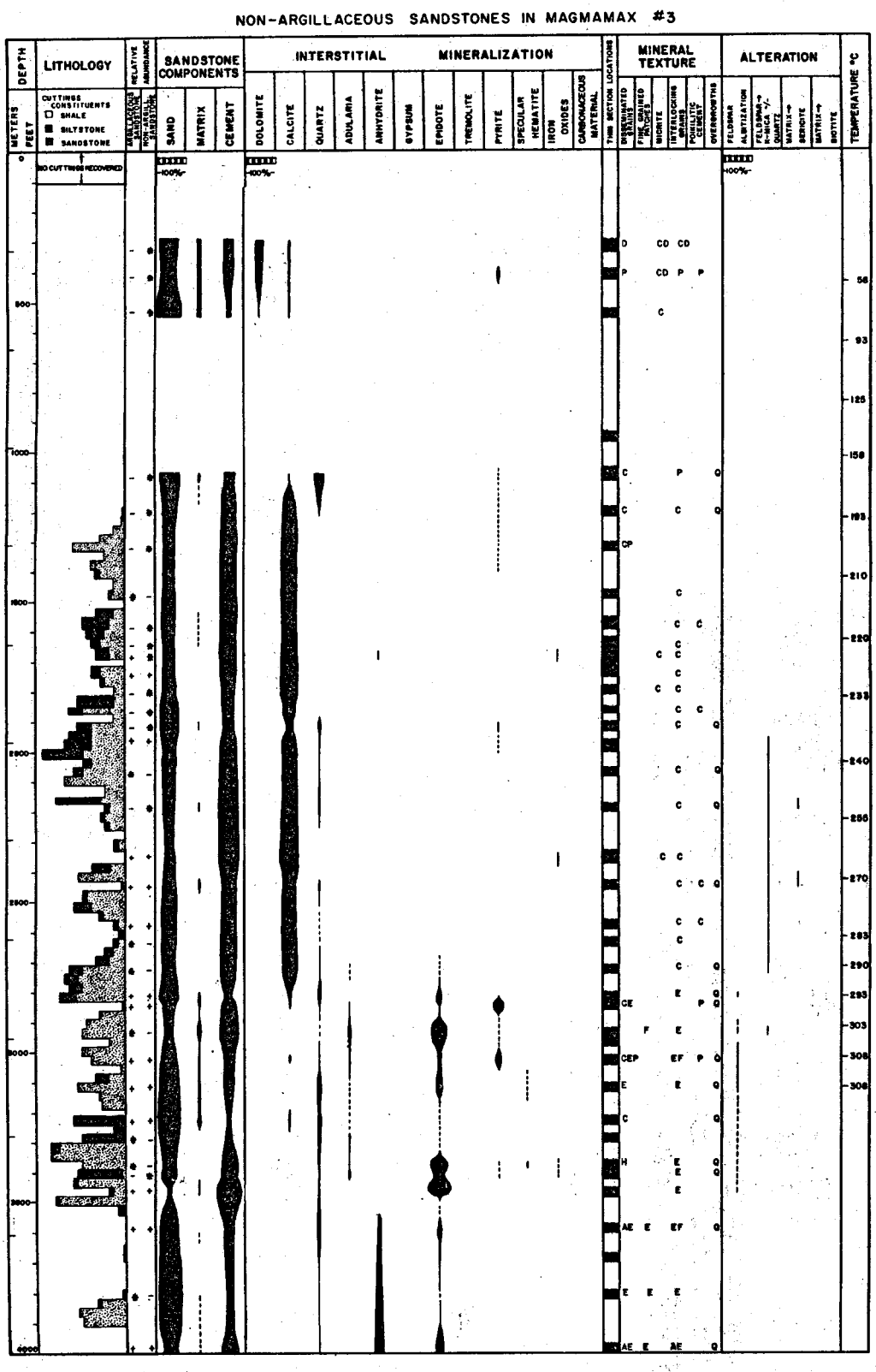
NON-ARGILLACEOUS SANDSTONES IN MAGMAMAX #3
DEPTH
METERS
FEET
LITHOLOGY
CUTTINGS CONSTITUENTS
SHALE
SILTSTONE
SANDSTONE
80 CUTTINGS RECOVERED
RELATIVE ABUNDANCE
CLASTIC/NON-CLASTIC SEDIMENTS
NON-SEDIMENTARY INTRUSIVE
SANDSTONE COMPONENTS
SAND
MATRIX
CEMENT
INTERSTITIAL
MINERALIZATION
DOLOMITE
CALCITE
QUARTZ
ADULARIA
ANHYDRITE
GYPSUM
EPIDOTE
TREMOLITE
PYRITE
SPECULAR HEMATITE
IRON OXIDES
CARBONACEOUS MATERIAL
THIN SECTION LOCATIONS
MINERAL TEXTURE
DISSEMINATED MINERALS
FINE GRAINED PATCHES
BIOTITE
INTERLOCKING GRAINS
POIKILITIC CEMENT
OVERGROWTHS
ALTERATION
FELDSPAR
ALBITIZATION
FELDSPAR→ K-MICA +/- QUARTZ
MATRIX→
BIOTITE
MATRIX→
BIOTITE
TEMPERATURE °C
100%
56
93
125
158
193
210
220
233
240
255
270
283
290
293
303
308
308

Figure 10

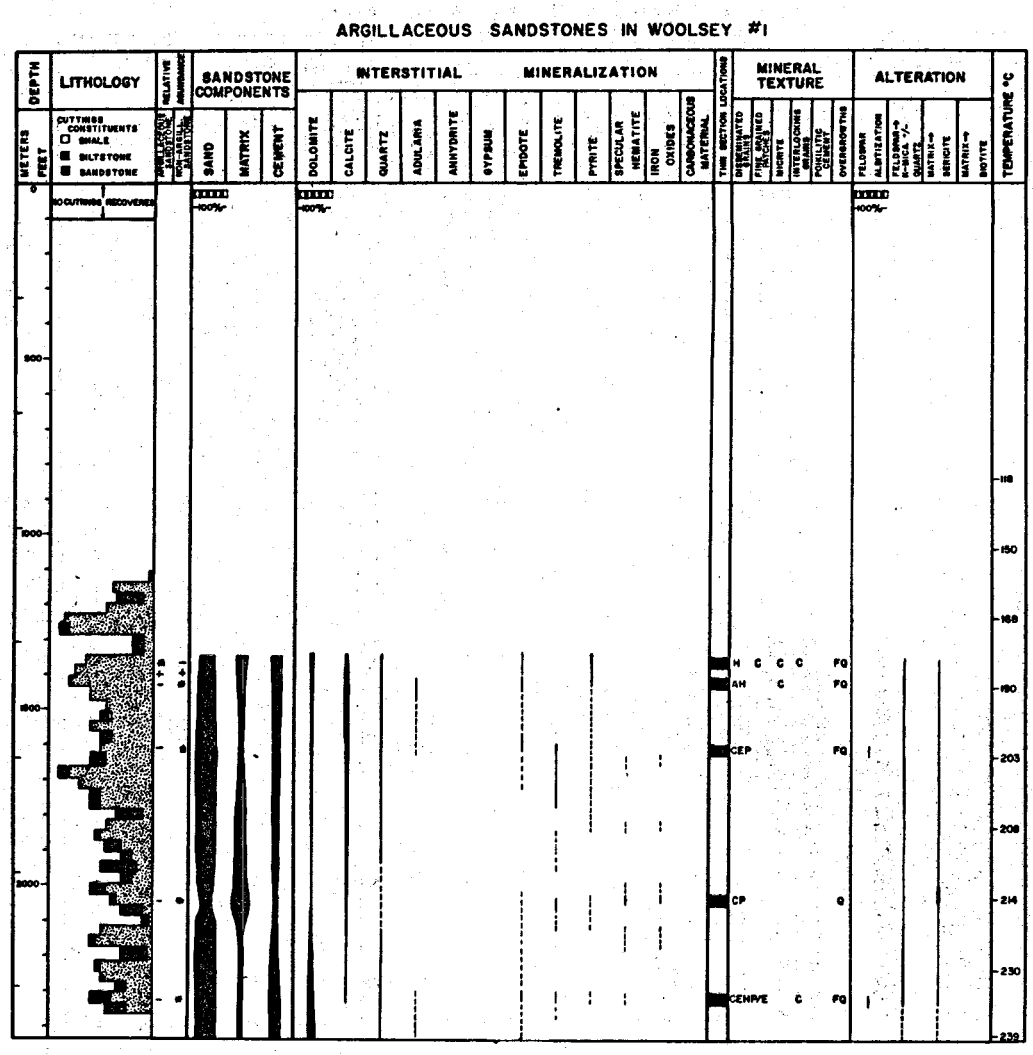
ARGILLACEOUS SANDSTONES IN WOOLSEY #1
DEPTH
METERS
FEET
LITHOLOGY
CUTTINGS CONSTITUENTS
SHALE
SILTSTONE
SANDSTONE
SIDEWALL CORE
RELATIVE ABUNDANCE
SANDSTONE COMPONENTS
SAND
MATRIX
CEMENT
INTERSTITIAL MINERALIZATION
DOLOMITE
CALCITE
QUARTZ
ADULARIA
ANHYDRITE
GYPSUM
EPIDOTE
TREMOLITE
PYRITE
SPECULAR HEMATITE
IRON OXIDES
CARBONACEOUS MATERIAL
THIN SECTION LOCATIONS
MINERAL TEXTURE
DISSEMINATED
FINE-GRAINED PATCHES
SHORTE
INTERLOCKING GRAINS
POIKILITIC CEMENT
OVERGROWTHS
ALTERATION
FELDSPAR
ALTERATION
FELDSPAR→ ALBITE ½
QUARTZ
MATRIX→
SERICITE
MATRIX→
BIOTITE
TEMPERATURE °C
CUTTINGS
RECOVERED
100%
H C C C FQ
AH C FQ
CEP FQ
CP Q
CEMPYE C FQ
118
150
189
190
203
208
214
230
239

Figure 11

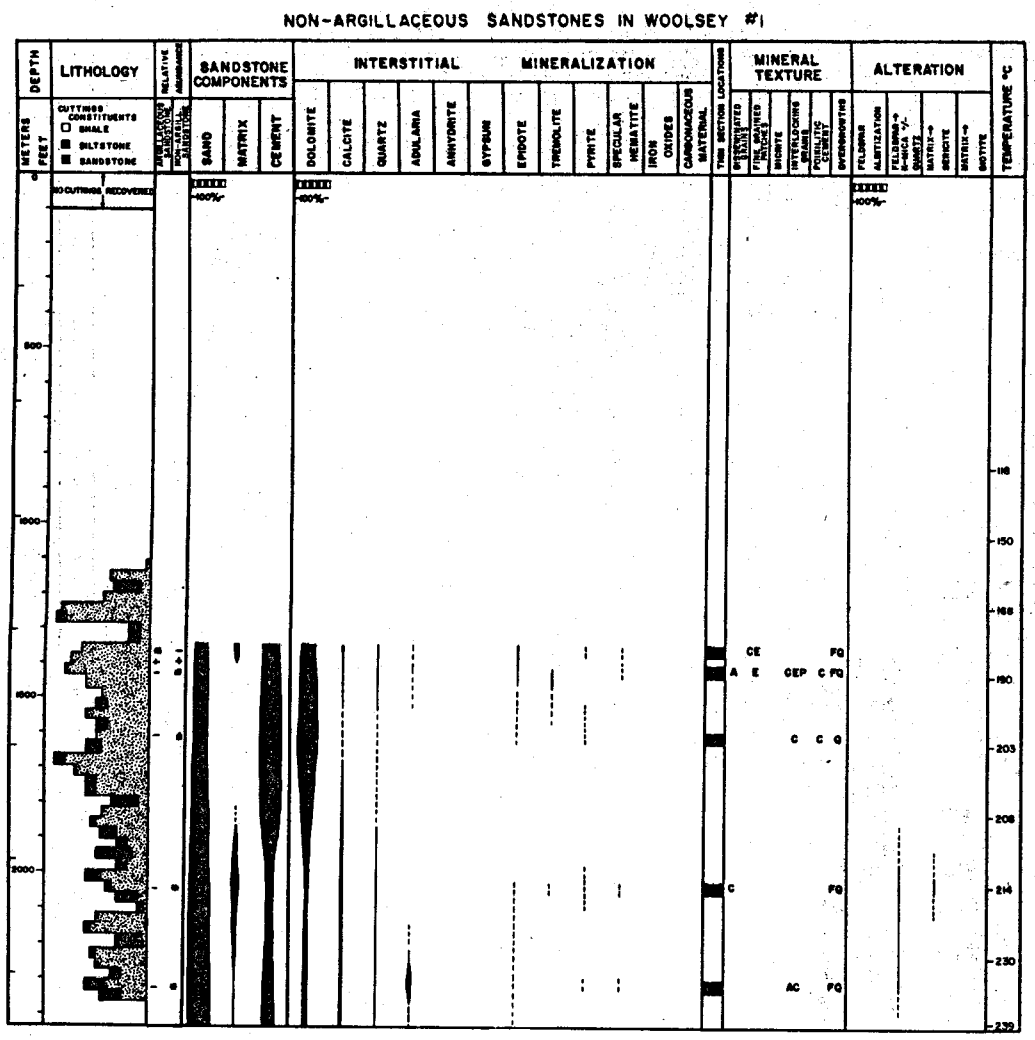
NON-ARGILLACEOUS SANDSTONES IN WOOLSEY #1
DEPTH
METERS
FEET
LITHOLOGY
CUTTINGS CONSTITUENTS
SHALE
SILTSTONE
SANDSTONE
NO CUTTINGS RECOVERED
RELATIVE ABUNDANCE
SANDSTONE COMPONENTS
SAND
MATRIX
CEMENT
INTERSTITIAL MINERALIZATION
DOLOMITE
CALCITE
QUARTZ
ADULARIA
ANHYDRITE
GYPSUM
EPIDOTE
TREMOLITE
PYRITE
SPECULAR HEMATITE
IRON OXIDES
CARBONACEOUS MATERIAL
THIN SECTION LOCATIONS
MINERAL TEXTURE
ALTERATION
FELDSPAR ALTERATION
FELDSPAR → MATRIX + QUARTZ
MATRIX → SERICITE
BIOTITE
TEMPERATURE °C

Figure 12

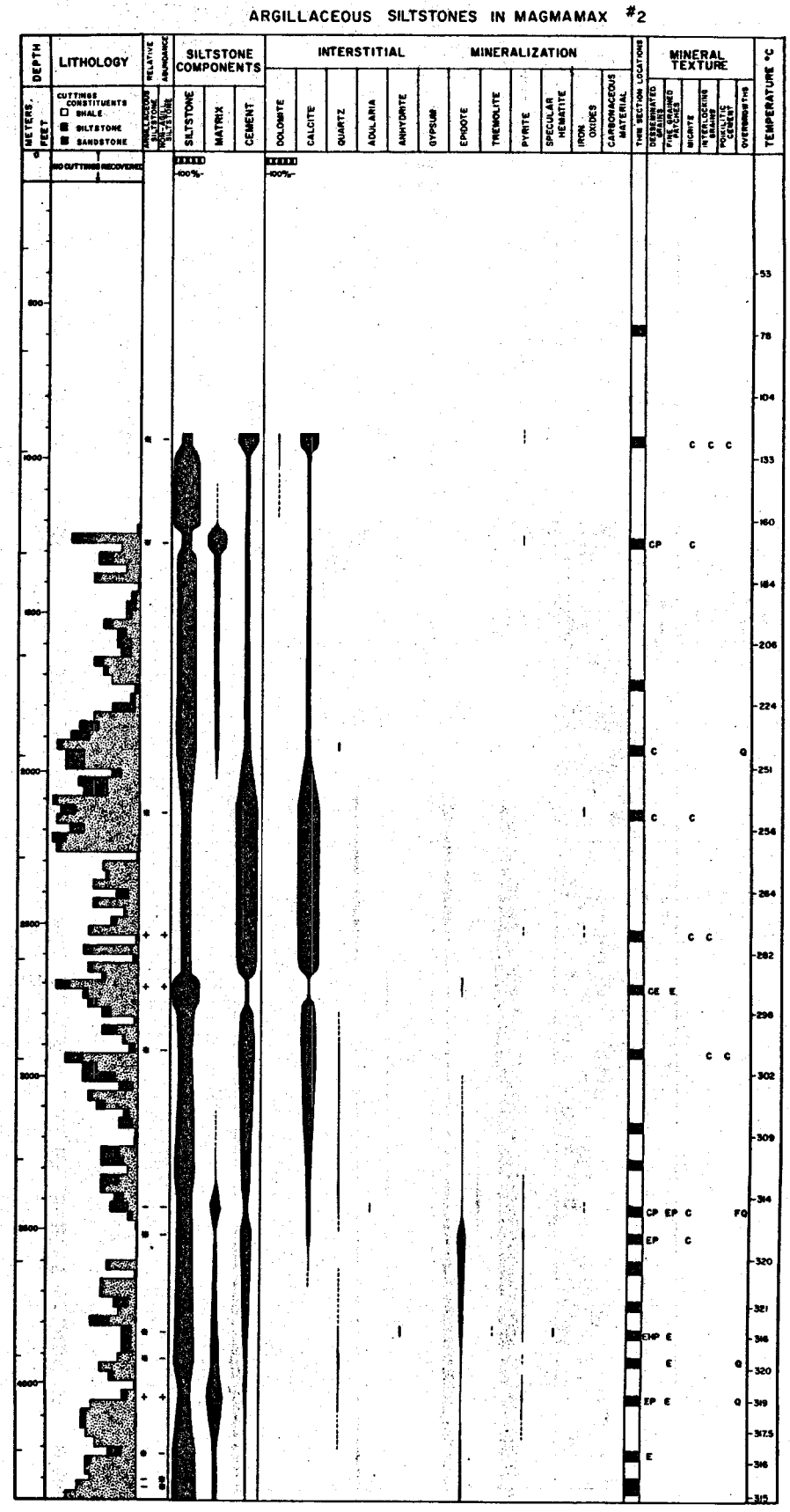
ARGILLACEOUS SILTSTONES IN MAGMAMAX #2
DEPTH
METERS
FEET
LITHOLOGY
CUTTINGS CONSTITUENTS
SHALE
SILTSTONE
SANDSTONE
NO CUTTINGS RECOVERED
RELATIVE ABUNDANCE
SILTSTONE COMPONENTS
SILTSTONE
MATRIX
CEMENT
-100%-
INTERSTITIAL MINERALIZATION
DOLOMITE
CALCITE
QUARTZ
ADULARIA
ANHYDRITE
GYPSUM
EPIDOTE
TREMOLITE
PYRITE
SPECULAR HEMATITE
IRON OXIDES
CARBONACEOUS MATERIAL
THIN SECTION LOCATIONS
MINERAL TEXTURE
DISSEMINATED CRYSTALS
FINE-GRAINED PATCHES
BIOTITE
INTERLOCKING MOSAIC
POIKILITIC CEMENT
OVERGROWTHS
TEMPERATURE °C
53
78
104
133
160
184
206
224
251
254
284
292
298
302
309
314
320
321
316
320
319
317.5
316
315

Figure 13

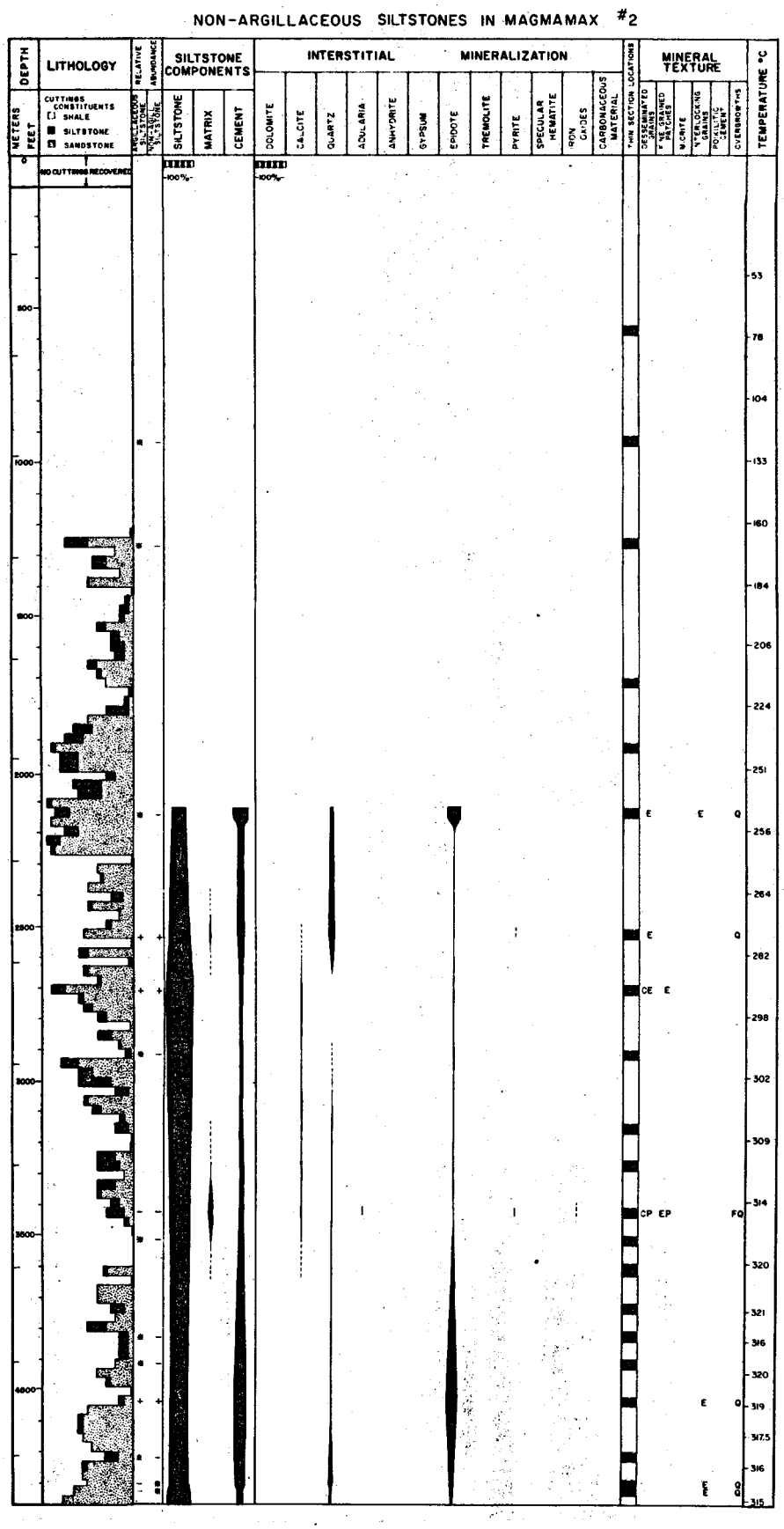
NON-ARGILLACEOUS SILTSTONES IN MAGMAMAX #2
DEPTH
METERS
FEET
LITHOLOGY
CUTTINGS CONSTITUENTS
SHALE
SILTSTONE
SANDSTONE
NO CUTTINGS RECOVERED
RELATIVE ABUNDANCE
ARGILLACEOUS SILTSTONE
NON-ARGILLACEOUS SILTSTONE
SILTSTONE COMPONENTS
SILTSTONE
MATRIX
CEMENT
100%
INTERSTITIAL MINERALIZATION
DOLOMITE
CALCITE
QUARTZ
ADULARIA
ANHYDRITE
GYPSUM
EPIDOTE
TREMOLITE
PYRITE
SPECULAR HEMATITE
IRON OXIDES
CARBONACEOUS MATERIAL
THIN SECTION LOCATIONS
MINERAL TEXTURE
DISSEMINATED ANHYDRITE
FINE GRAINED PATCHES
MICRITE
INTERLOCKING GRAINS
POIKILOTOPIC GYPSUM
OVERGROWTHS
TEMPERATURE °C
E
Q
CE
CP
EP
FQ
mm
53
78
104
133
160
184
206
224
251
256
264
282
298
302
309
314
320
321
316
320
319
317.5
316
315

Figure 14

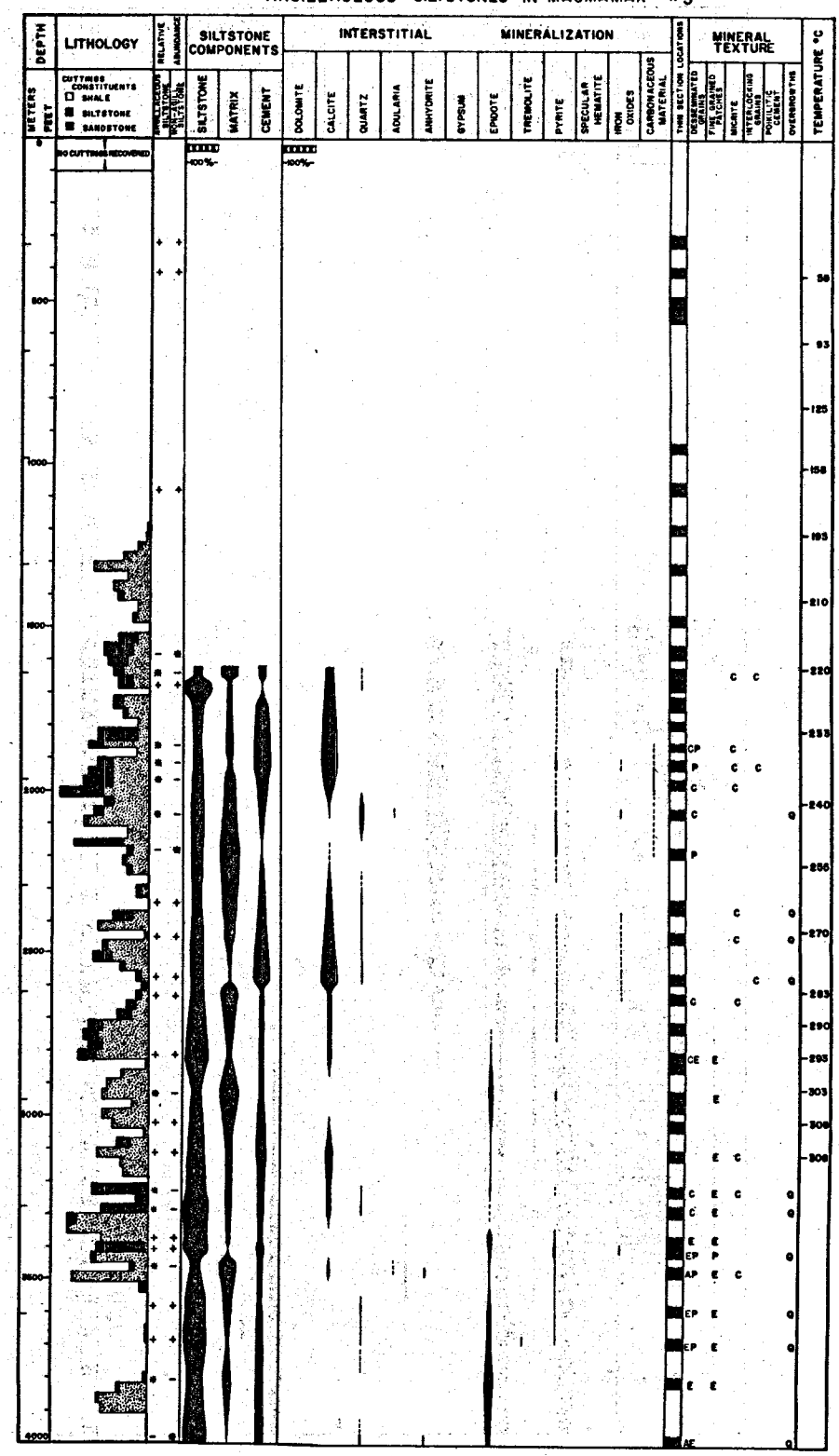
ARGILLACEOUS SILTSTONES IN MAGMAMAX #3
DEPTH
METERS
FEET
LITHOLOGY
CUTTINGS CONSTITUENTS
SHALE
SILTSTONE
SANDSTONE
NO CUTTINGS RECOVERED
RELATIVE ABUNDANCE
SILTSTONE COMPONENTS
SILTSTONE
MATRIX
CEMENT
100%
INTERSTITIAL MINERALIZATION
DOLOMITE
CALCITE
QUARTZ
ADULARIA
ANHYDRITE
GYPSUM
EPIDOTE
TREMOLITE
PYRITE
SPECULAR HEMATITE
IRON OXIDES
CARBONACEOUS MATERIAL
MINERAL TEXTURE
THIN SECTION LOCATIONS
DISSEMINATED DOLOMITE
FINE-GRAINED PATCHES
SHEARED
INTERLOCKING QUARTZ
POROUS CEMENT
OVERGROWTHS
TEMPERATURE °C
2000
2500
3000
3500
4000
50
93
125
158
185
210
220
233
240
256
270
283
290
293
303
308
309

Figure 15

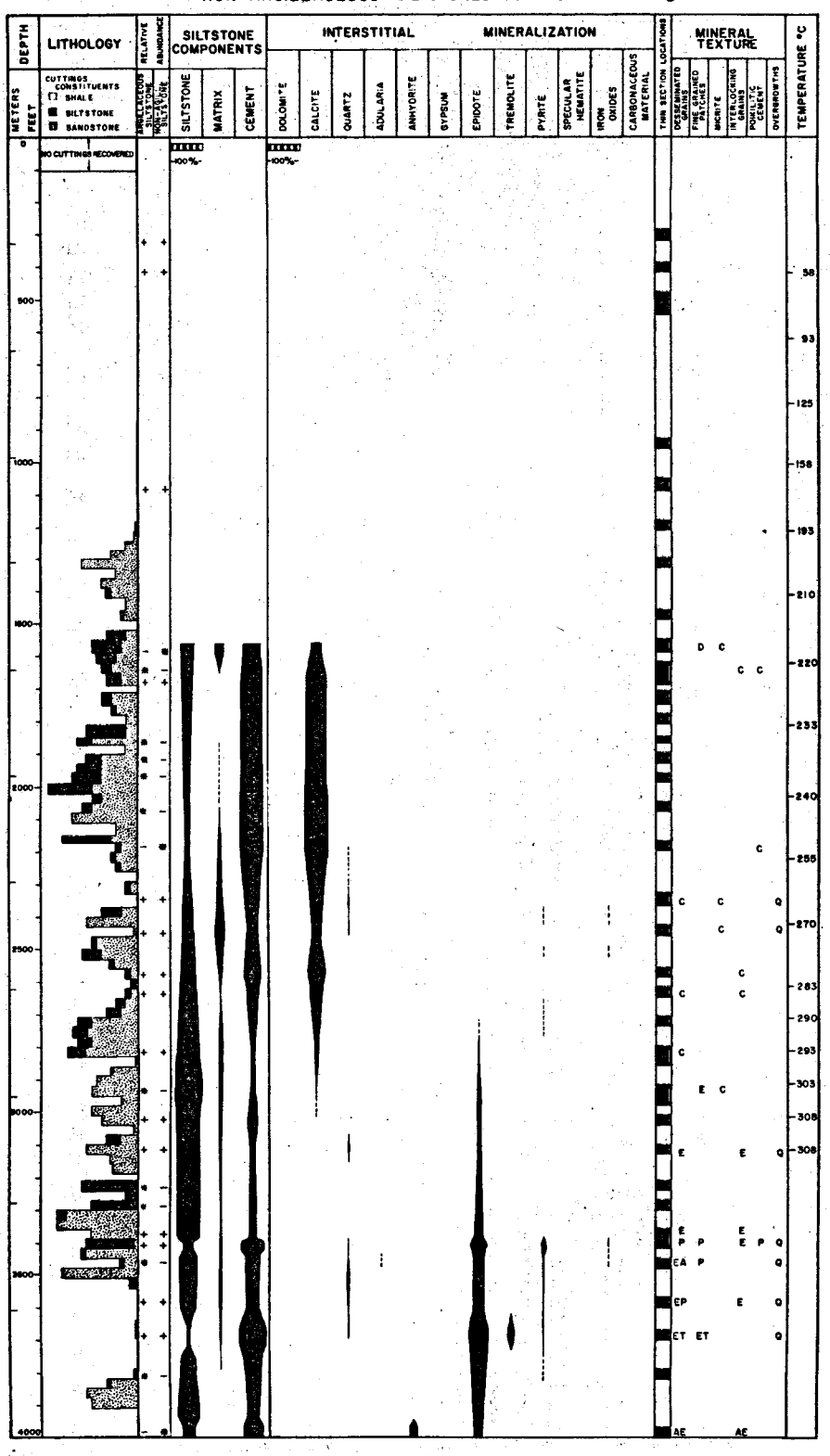
NON-ARGILLACEOUS SILTSTONES IN MAGMAMAX #3
DEPTH
METERS
FEET
LITHOLOGY
CUTTINGS CONSTITUENTS
SHALE
SILTSTONE
SANDSTONE
NO CUTTINGS RECOVERED
RELATIVE ABUNDANCE
SILTSTONE COMPONENTS
SILTSTONE
MATRIX
CEMENT
100%
INTERSTITIAL MINERALIZATION
DOLOMITE
CALCITE
QUARTZ
ADULARIA
ANHYDRITE
GYPSUM
EPIDOTE
TREMOLITE
PYRITE
SPECULAR HEMATITE
IRON OXIDES
CARBONACEOUS MATERIAL
THIN SECTION LOCATIONS
MINERAL TEXTURE
DISSEMINATED CRYSTALS
FINE GRAINED PATCHES
MICRITE
INTERLOCKING GRAINS
POIKILITIC CRYSTALS
OVERGROWTHS
TEMPERATURE °C
500
1000
1500
2000
2500
3000
3500
4000
58
93
125
158
193
210
220
233
240
255
270
283
290
293
303
308
308

Figure 16

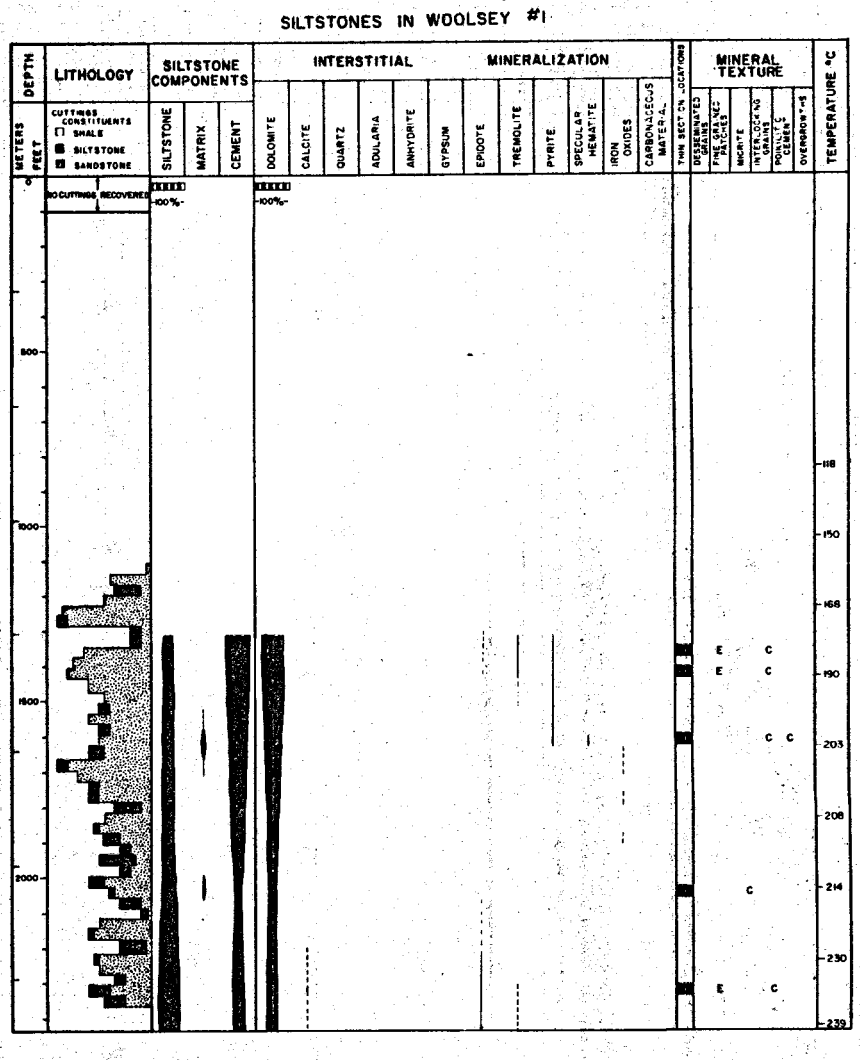
SILTSTONES IN WOOLSEY #1
DEPTH
METERS
FEET
LITHOLOGY
CUTTINGS CONSTITUENTS
SHALE
SILTSTONE
SANDSTONE
NO CUTTINGS RECOVERED
SILTSTONE COMPONENTS
SILTSTONE
MATRIX
CEMENT
-100%-
INTERSTITIAL
MINERALIZATION
DOLOMITE
CALCITE
QUARTZ
ADULARIA
ANHYDRITE
GYPSUM
EPIDOTE
TREMOLITE
PYRITE
SPECULAR HEMATITE
IRON OXIDES
CARBONACEOUS MATERIAL
THIN SECTION LOCATIONS
MINERAL TEXTURE
DISSEMINATED CRYSTALS
FINE GRAINED PATCHES
MICRITE
INTERLOCKING GRAINS
POIKILITIC CRYSTALS
OVERGROWTHS
TEMPERATURE °C
1000
1500
2000
118
150
168
190
203
208
214
230
239

Figure 17

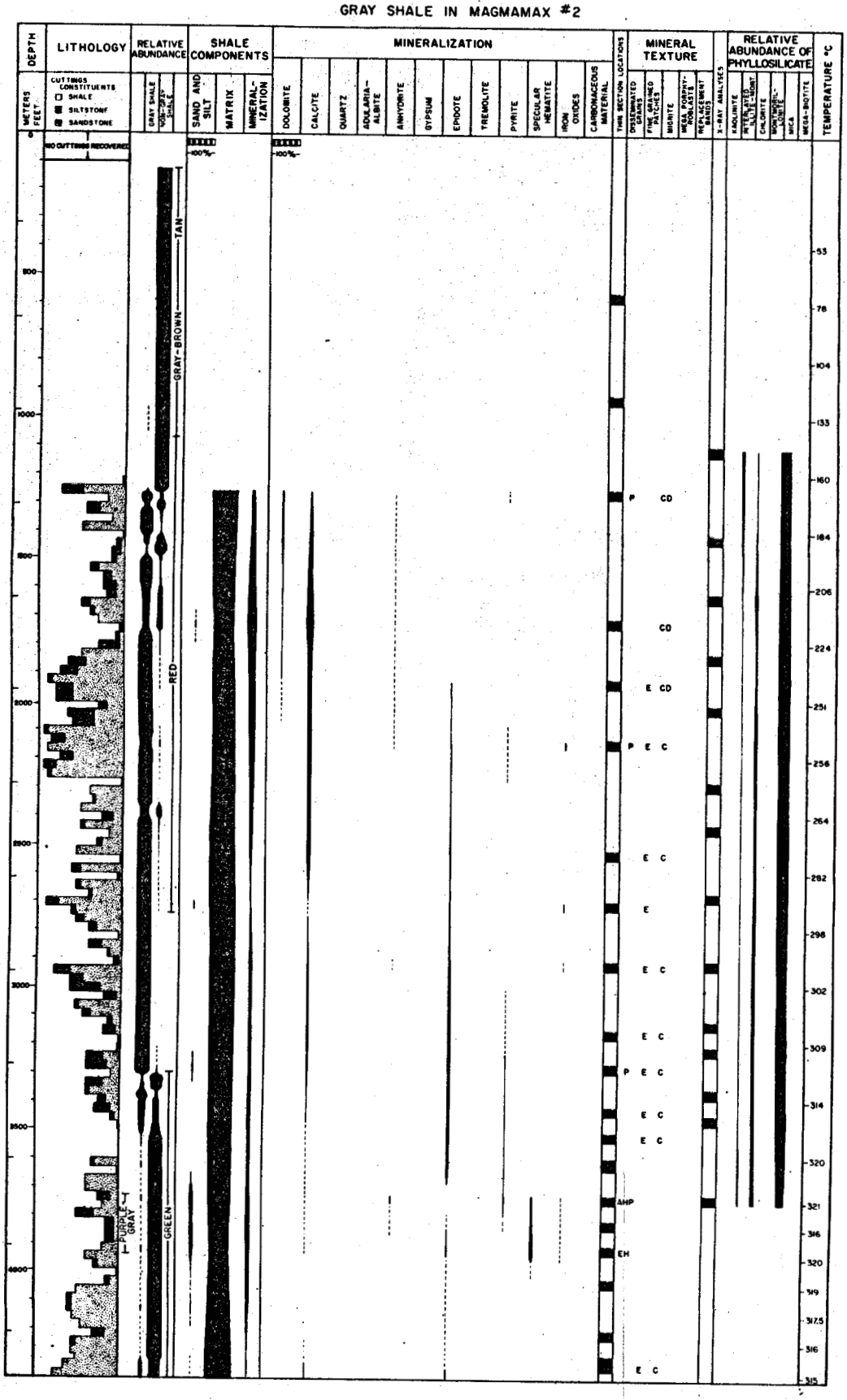
GRAY SHALE IN MAGMAMAX #2
DEPTH
METERS
FEET
LITHOLOGY
CUTTINGS CONSTITUENTS
SHALE
SILTSTONE
SANDSTONE
NO CUTTINGS RECOVERED
RELATIVE ABUNDANCE
GRAY SHALE
RED-TAN SHALE
SHALE COMPONENTS
SAND AND SILT
MATRIX
MINERALIZATION
MINERALIZATION
DOLOMITE
CALCITE
QUARTZ
ADULARIA-ALBITE
ANHYDRITE
GYPSUM
EPIDOTE
TREMOLITE
PYRITE
SPECULAR HEMATITE
IRON OXIDES
CARBONACEOUS MATERIAL
100%
100%
THIN SECTION LOCATIONS
MINERAL TEXTURE
DISSEMINATED CLAYS
FINE GRAINED PATCHES
LIGNITE
MESA PORPHYROBLASTS
REPLACEMENT MESAS
X-RAY ANALYSES
RELATIVE ABUNDANCE OF PHYLLOSILICATE
KAOLINITE
MIXED-LAYER CLAY
CHLORITE
MONTMORILLONITE
MICA
MEGA-BIOTITE
TEMPERATURE °C
TAN
GRAY-BROWN
RED
GREEN
PURPLE-GRAY
P
CD
CD
E CD
P E C
E C
E
E C
E C
P E C
E C
E C
AHP
EH
E C
53
78
104
133
160
184
206
224
251
256
264
282
298
302
309
314
320
321
316
320
319
317.5
316
315

Figure 18

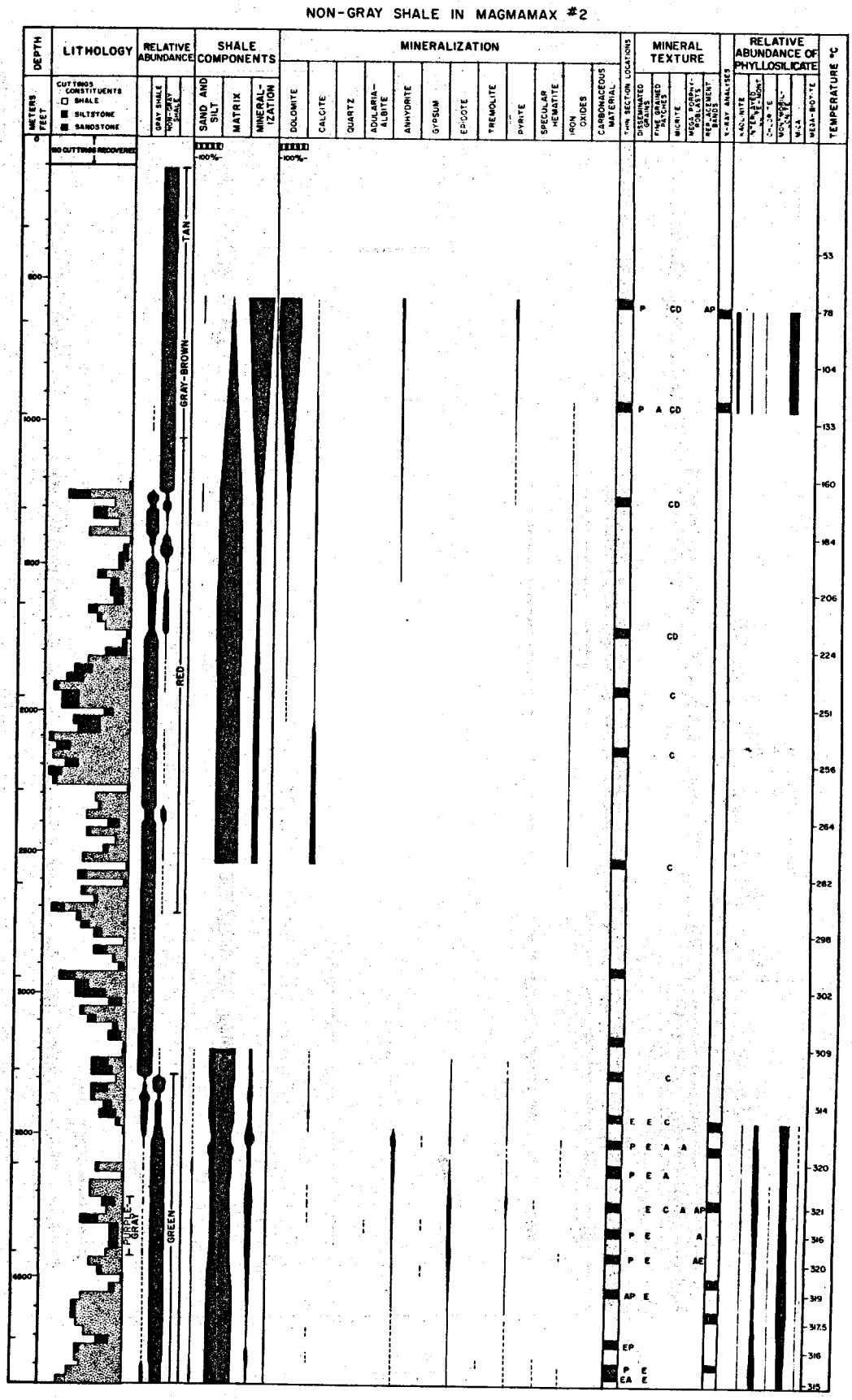
NON-GRAY SHALE IN MAGMAMAX #2
DEPTH
METERS
FEET
LITHOLOGY
CUTTINGS CONSTITUENTS
SHALE
SILTSTONE
SANDSTONE
160 CUTTINGS RECOVERED
RELATIVE ABUNDANCE
GRAY SHALE
NON-GRAY SHALE
SHALE COMPONENTS
SAND AND SILT
MATRIX
MINERALIZATION
-100%-
TAN
GRAY-BROWN
RED
GREEN
PURPLE-GRAY
MINERALIZATION
DOLOMITE
CALCITE
QUARTZ
ADULARIA-ALBITE
ANHYDRITE
GYPSUM
EPIDOTE
TREMOLITE
PYRITE
SPECULAR HEMATITE
IRON OXIDES
CARBONACEOUS MATERIAL
THIN SECTION LOCATIONS
MINERAL TEXTURE
DISSEMINATED GRAINS
PELLETOIDS
MICRITE
MEGA. SPARRY-BOULASTS
REPLACEMENT BANDS
X-RAY ANALYSES
RELATIVE ABUNDANCE OF PHYLLOSILICATE
KAOLINITE
INTERLAYERED CLAYS
CHLORITE
MONTMORILLONITE
MICA
MIXED-LAYER MICA
TEMPERATURE °C
600
800
1000
2000
2500
3000
3500
4000
53
78
104
133
160
184
206
224
251
256
264
282
298
302
309
314
320
321
316
320
319
317.5
316
315

Figure 19

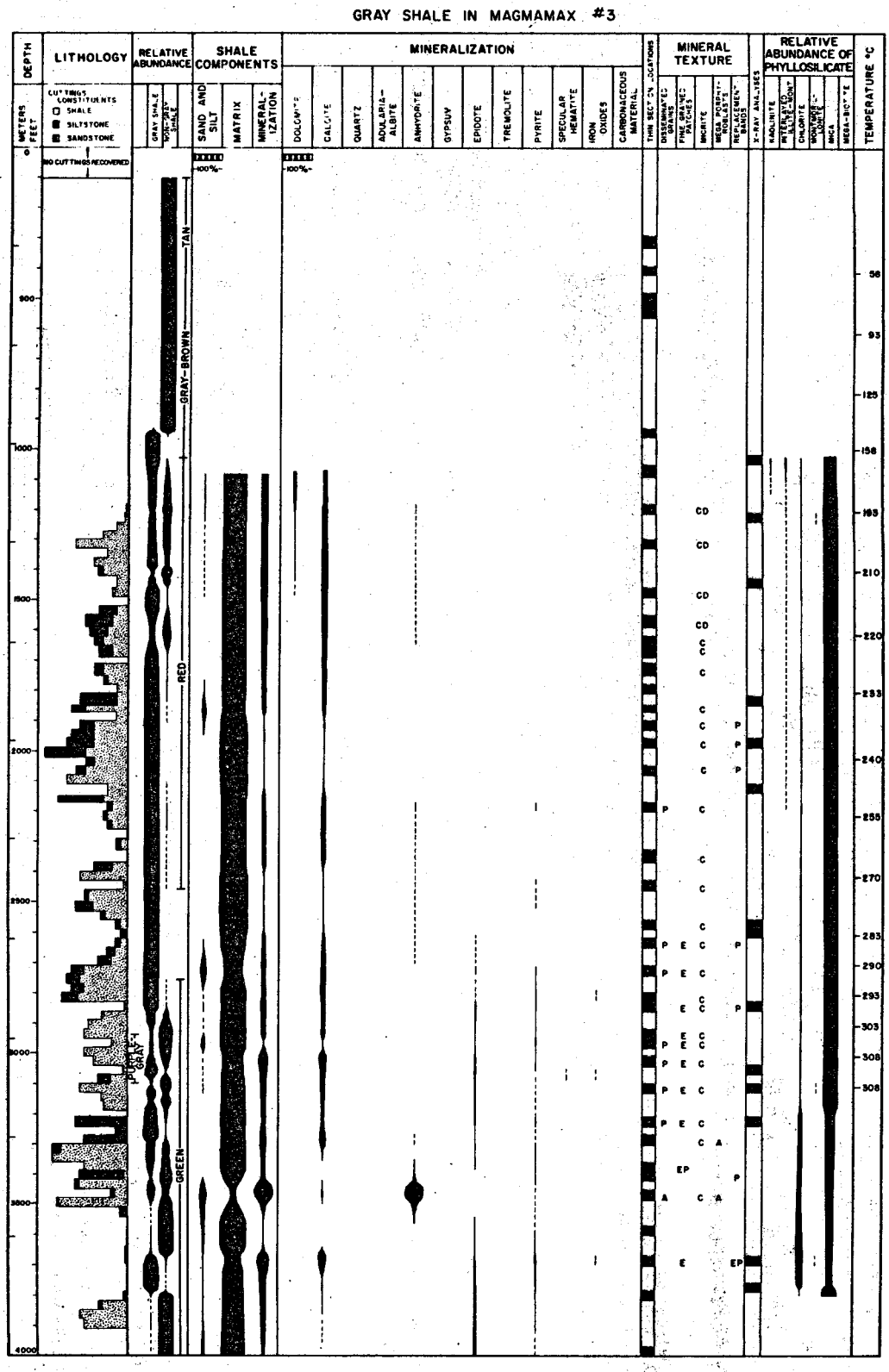
GRAY SHALE IN MAGMAMAX #3
DEPTH
METERS
FEET
LITHOLOGY
CUTTINGS CONSTITUENTS
SHALE
SILTSTONE
SANDSTONE
NO CUTTINGS RECOVERED
RELATIVE ABUNDANCE
GRAY SHALE
RED-GRAY SHALE
SHALE COMPONENTS
SAND AND SILT
MATRIX
MINERAL-IZATION
-100%-
MINERALIZATION
DOLOMITE
CALCITE
QUARTZ
ADULARIA-ALBITE
ANHYDRITE
GYPSUM
EPIDOTE
TREMOLITE
PYRITE
SPECULAR HEMATITE
IRON OXIDES
CARBONACEOUS MATERIAL
THIN SECTION LOCATIONS
MINERAL TEXTURE
DISSEMINATED GRAINS
FINE GRAINED PATCHES
MICRITE
MEGA PORPHYROBLASTS
REPLACEMENT BANDS
X-RAY ANALYSES
RELATIVE ABUNDANCE OF PHYLLOSILICATE
KAOLINITE
MIXED-LAYER
CHLORITE
BIOTITE
MICA
MEGA-BIOTITE
TEMPERATURE °C
TAN
GRAY-BROWN
RED
PURPLE-GRAY
GREEN
1000
1500
2000
2500
3000
3500
4000
56
93
125
158
185
210
220
233
240
255
270
283
290
293
303
308
308

Figure 20

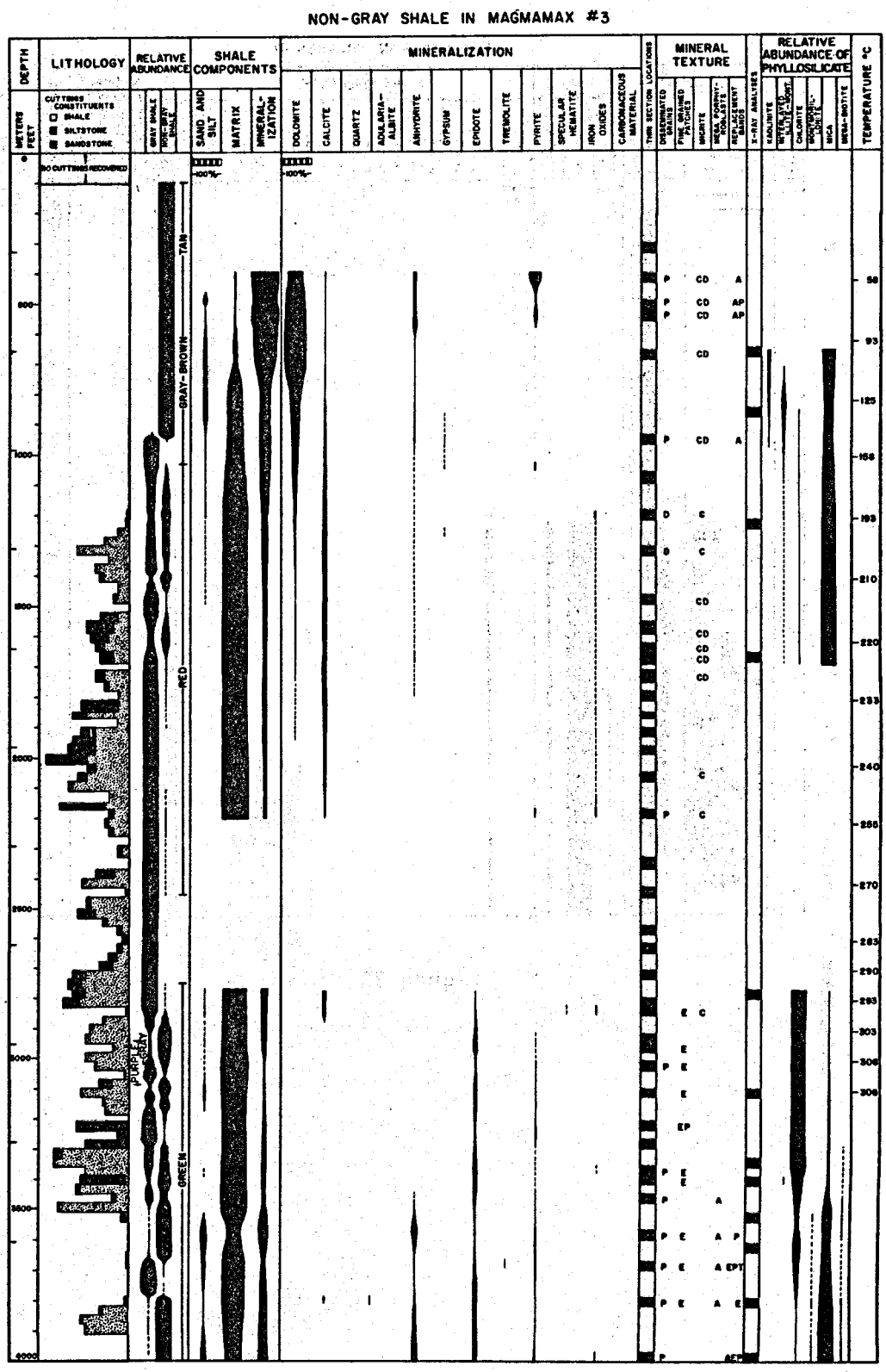
NON-GRAY SHALE IN MAGMAMAX #3
DEPTH
METERS
FEET
LITHOLOGY
CUTTINGS CONSTITUENTS
SHALE
SILTSTONE
SANDSTONE
NO CUTTINGS RECOVERED
RELATIVE ABUNDANCE
GRAY SHALE
NON-GRAY SHALE
SHALE COMPONENTS
SAND AND SILT
MATRIX
MINERAL-IZATION
100%
MINERALIZATION
DOLOMITE
CALCITE
QUARTZ
ADULARIA-ALBITE
ANHYDRITE
GYPSUM
EPIDOTE
TREMOLITE
PYRITE
SPECULAR HEMATITE
IRON OXIDES
CARBONACEOUS MATERIAL
THIN SECTION LOCATIONS
MINERAL TEXTURE
DISSEMINATED GRAINS
FINE GRAINED PATCHES
SPARITE
MICRITE
VEIN, CONVEX-OUTWARD
REPLACEMENT BANDS
X-RAY ANALYSES
RELATIVE ABUNDANCE OF PHYLLOSILICATE
KAOLINITE
INTERMIXED MIXED-LAYER
CHLORITE
MONTMORIL-LONITE
MICA
VERM-IKULITE
TEMPERATURE °C
TAN
GRAY-BROWN
RED
PURPLISH GRAY
GREEN
BASE

Figure 21

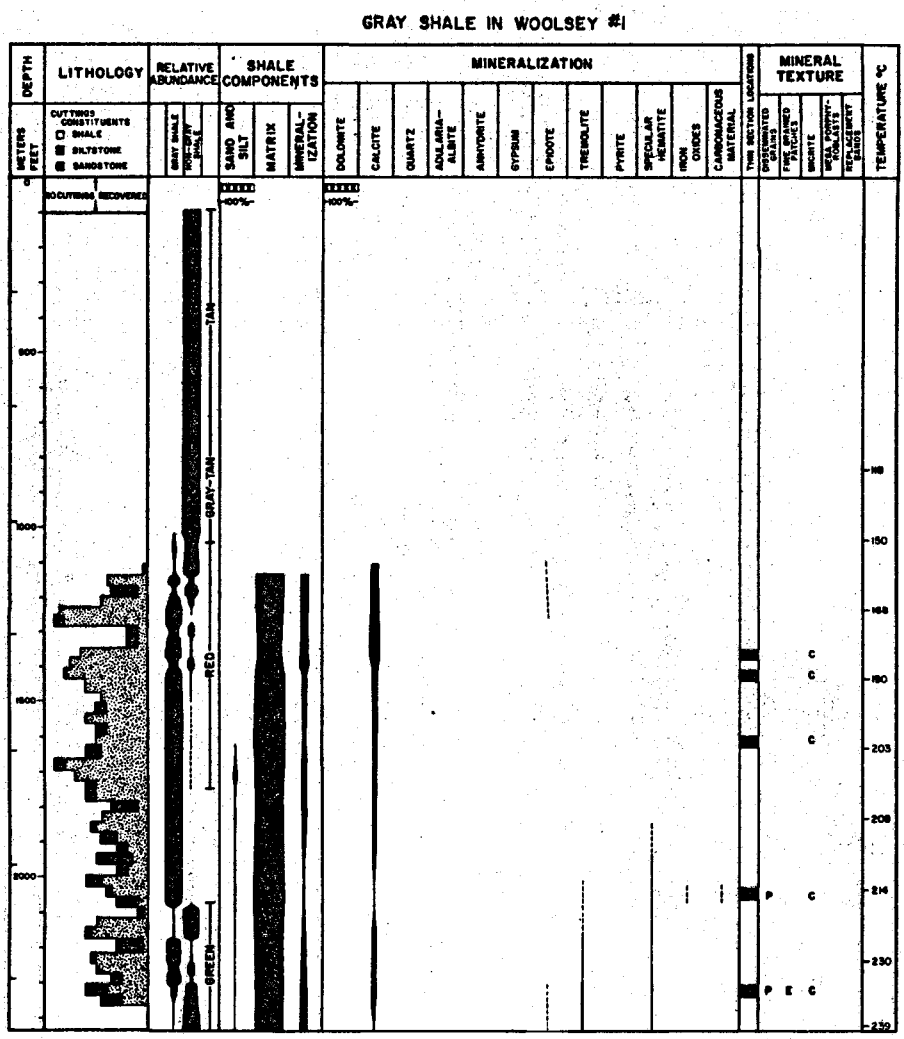
GRAY SHALE IN WOOLSEY #1
DEPTH
METERS
FEET
LITHOLOGY
CUTTINGS CONSTITUENTS
SHALE
SILTSTONE
SANDSTONE
CUTTINGS
RECOVERED
RELATIVE ABUNDANCE
GRAY SHALE
ROSE-BRN SHALE
SHALE COMPONENTS
SAND AND SILT
MATRIX
MINERAL-IZATION
100%
MINERALIZATION
DOLOMITE
CALCITE
QUARTZ
ADULARIA-ALBITE
ANHYDRITE
GYPSUM
EPIDOTE
TREMOLITE
PYRITE
SPECULAR HEMATITE
IRON OXIDES
CARBONACEOUS MATERIAL
THIN SECTION LOCATIONS
MINERAL TEXTURE
DISSEMINATED GRAINS
FINE-GRAINED ROCKS
SPARITE
REPLACEMENT BANDS
TEMPERATURE °C
TAN
GRAY-TAN
RED
GREEN
500
1000
1500
2000
C
P
E
118
150
168
180
203
208
214
230
239

Figure 22

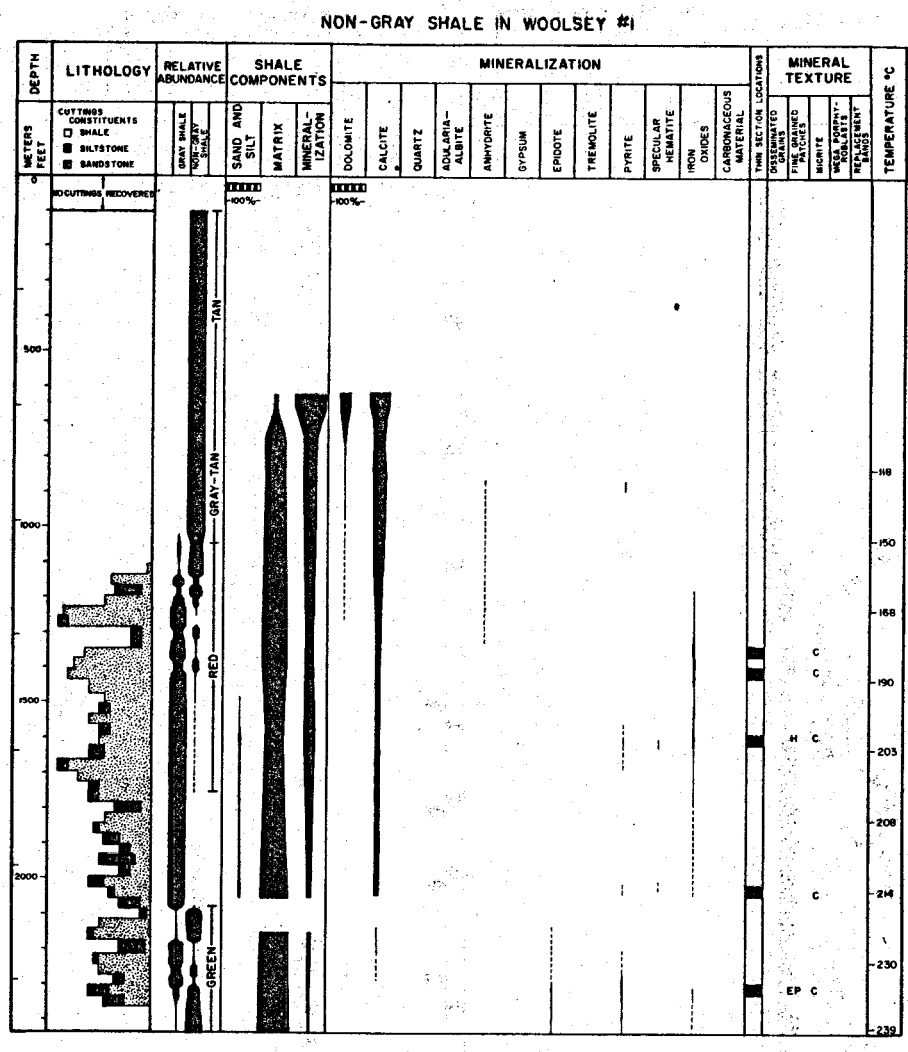
NON-GRAY SHALE IN WOOLSEY #1
DEPTH
METERS
FEET
LITHOLOGY
CUTTINGS CONSTITUENTS
SHALE
SILTSTONE
SANDSTONE
NO CUTTINGS RECOVERED
RELATIVE ABUNDANCE
GRAY SHALE
NON-GRAY SHALE
SHALE COMPONENTS
SAND AND SILT
MATRIX
MINERAL-IZATION
100%
MINERALIZATION
DOLOMITE
CALCITE
QUARTZ
ADULARIA-ALBITE
ANHYDRITE
GYPSUM
EPIDOTE
TREMOLITE
PYRITE
SPECULAR HEMATITE
IRON OXIDES
CARBONACEOUS MATERIAL
THIN SECTION LOCATIONS
MINERAL TEXTURE
DISSEMINATED GRAINS
FINE GRAINED MATRIX
MICRITE
MED. CRYSTALLINE MOSAIC
REPLACEMENT BANDS
TEMPERATURE °C
TAN
GRAY-TAN
RED
GREEN
500
1000
1500
2000
118
150
168
190
203
208
214
230
239
C
H
EP

Figure 23

MINERALIZED FRACTURES IN MAGMAMAX #2

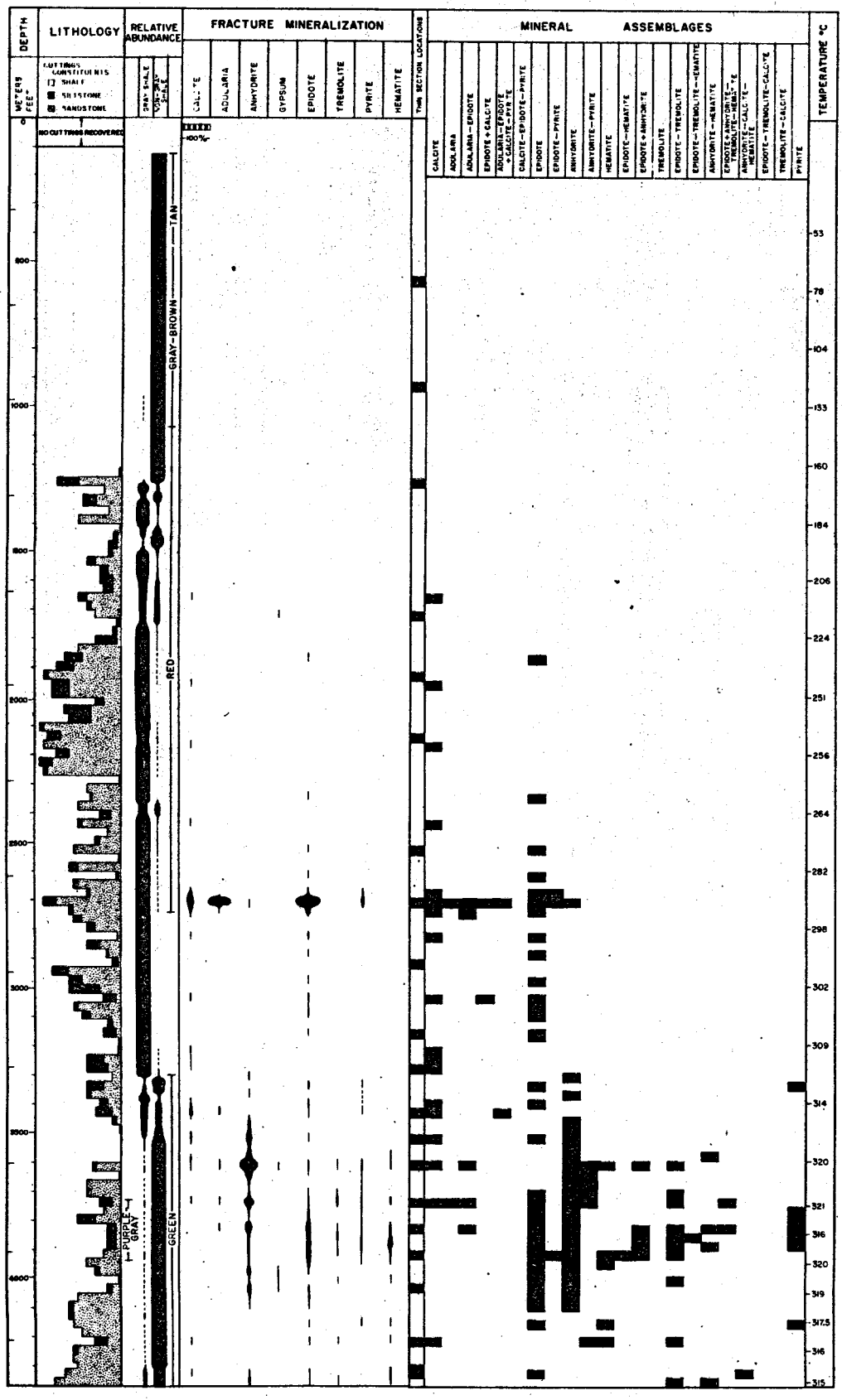

Figure 24

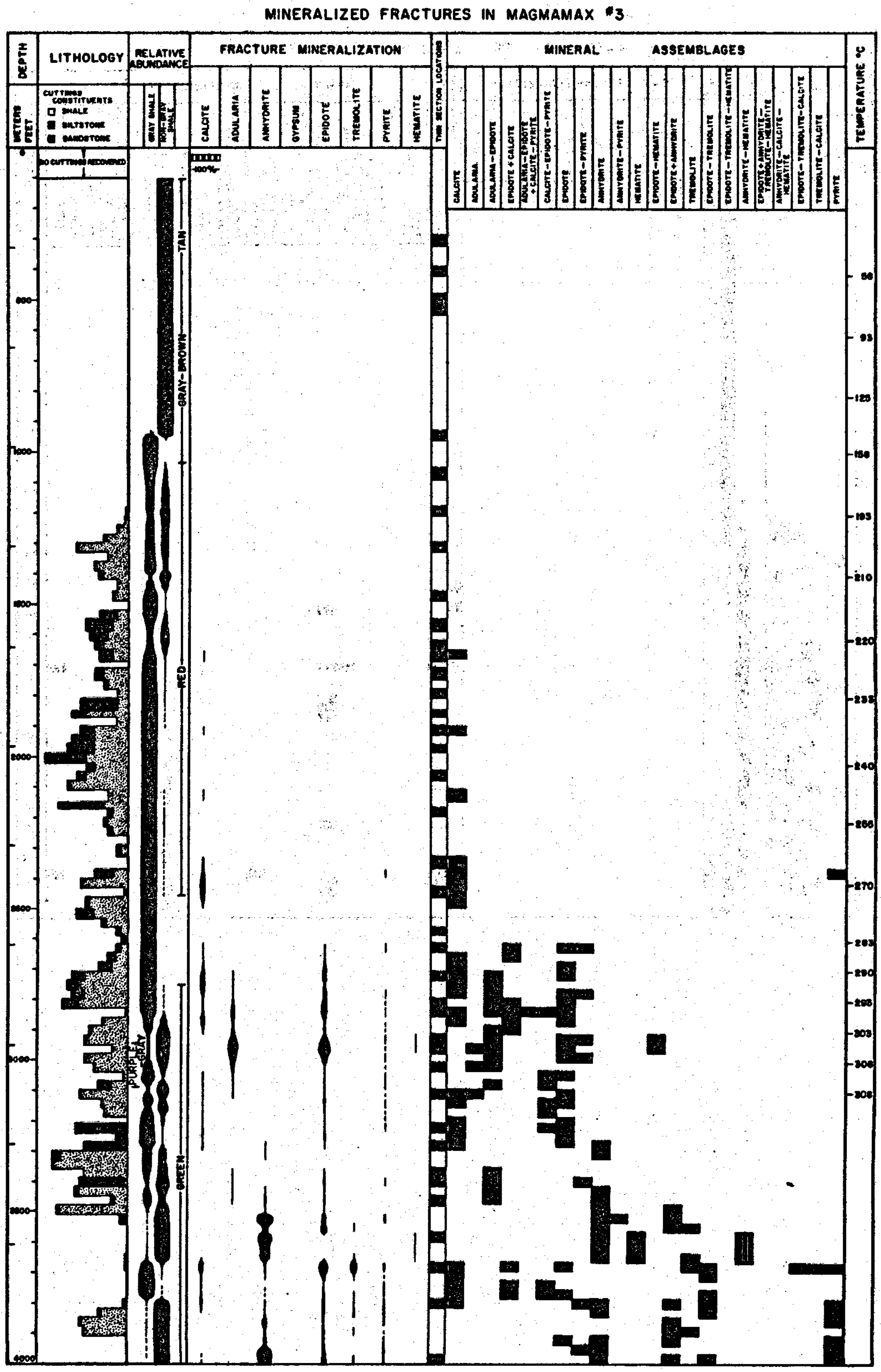
MINERALIZED FRACTURES IN MAGMAMAX #3
DEPTH
METERS
FEET
LITHOLOGY
CUTTINGS CONSTITUENTS
SHALE
SILTSTONE
SANDSTONE
NO CUTTINGS RECOVERED
RELATIVE ABUNDANCE
GRAY SHALE
NON-GRAY SHALE
TAN
GRAY-BROWN
RED
PURPLE GRAY
GREEN
FRACTURE MINERALIZATION
CALCITE
ADULARIA
ANHYDRITE
GYPSUM
EPIDOTE
TREMOLITE
PYRITE
HEMATITE
100%
THIN SECTION LOCATIONS
MINERAL ASSEMBLAGES
CALCITE
ADULARIA
ADULARIA—EPIDOTE
EPIDOTE + CALCITE
ADULARIA—EPIDOTE + CALCITE—PYRITE
CALCITE—EPIDOTE—PYRITE
EPIDOTE
EPIDOTE—PYRITE
ANHYDRITE
ANHYDRITE—PYRITE
HEMATITE
EPIDOTE—HEMATITE
EPIDOTE + ANHYDRITE
TREMOLITE
EPIDOTE—TREMOLITE
EPIDOTE—TREMOLITE—HEMATITE
ANHYDRITE—HEMATITE
EPIDOTE + ANHYDRITE—TREMOLITE—HEMATITE
ANHYDRITE—CALCITE—HEMATITE
EPIDOTE—TREMOLITE—CALCITE
TREMOLITE—CALCITE
PYRITE
TEMPERATURE °C

Figure 25

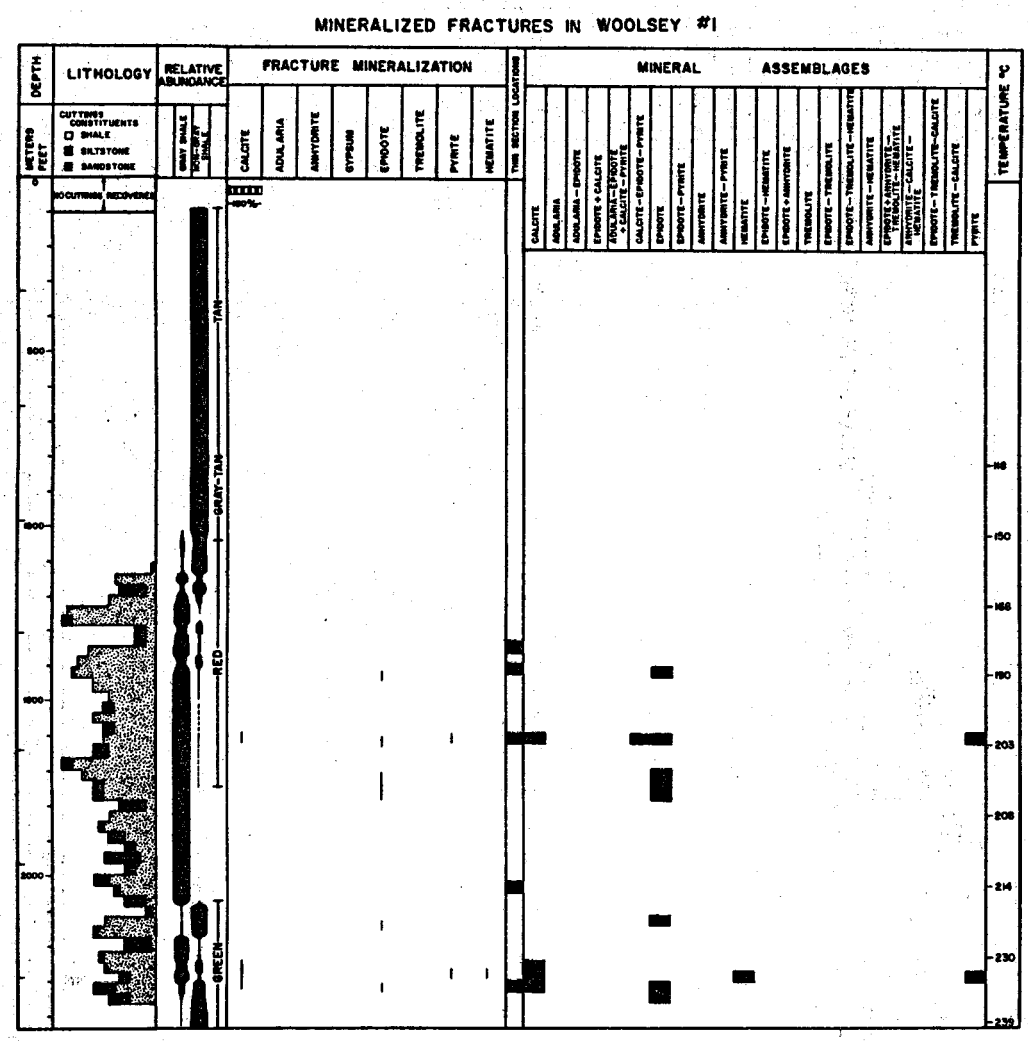
MINERALIZED FRACTURES IN WOOLSEY #1
DEPTH
METERS
FEET
LITHOLOGY
CUTTINGS CONSTITUENTS
SHALE
SILTSTONE
SANDSTONE
80 CUTTINGS RECOVERED
RELATIVE ABUNDANCE
GRAY SHALE
RED-BRN SHALE
FRACTURE MINERALIZATION
CALCITE
ADULARIA
ANHYDRITE
GYPSUM
EPIDOTE
TREMOLITE
PYRITE
HEMATITE
<100%
THIN SECTION LOCATIONS
MINERAL ASSEMBLAGES
CALCITE
ADULARIA
ADULARIA - EPIDOTE
EPIDOTE + CALCITE
ADULARIA - EPIDOTE + CALCITE - PYRITE
CALCITE - EPIDOTE - PYRITE
EPIDOTE
EPIDOTE - PYRITE
ANHYDRITE
ANHYDRITE - PYRITE
HEMATITE
EPIDOTE - HEMATITE
EPIDOTE + ANHYDRITE
TREMOLITE
EPIDOTE - TREMOLITE
EPIDOTE - TREMOLITE - HEMATITE
ANHYDRITE - HEMATITE
EPIDOTE + ANHYDRITE - TREMOLITE - HEMATITE
ANHYDRITE - CALCITE - HEMATITE
EPIDOTE - TREMOLITE - CALCITE
TREMOLITE - CALCITE
PYRITE
TAN
GRAY-TAN
RED
GREEN
TEMPERATURE °C
118
150
166
190
203
208
214
230
239

Figure 26

Sandstones

ARGILLACEOUS VS NON-ARGILLACEOUS SANDSTONES

Two different sandstones with different types and amounts of mineralization--one with abundant matrix and one with little or no matrix--occur in each 30' interval. Data from these two rock types are compiled into separate charts (Figs. 7-12) for the reasons stated earlier.

SANDSTONE COMPONENTS

For each well, the sandstones are composed of 20-80% sand, 0-40% matrix, and 2-80% mineralization (cement); open pore species are rare. In non-argillaceous sandstones, the components are approximately evenly divided between sand and cement, with very minor matrix. In argillaceous sandstones, relative abundances are more variable, but in general 65% is sand and 35% is matrix plus cement. The difference in sand abundance between the two sandstone varieties (50% versus 65%) is mainly due to greater sand dissolution in the non-argillaceous sandstones; the difference is not thought to be a primary sedimentary feature.

The argillaceous sandstones of Magmamax #3 (Fig. 9) show a very pronounced inverse relationship between matrix and cement largely due to replacement of matrix by cement at particular horizons. Matrix in Magmamax #2 (Fig. 7) is predominantly confined to three locations: above 2200', 2850-3000' and 3650-4000'; the percentage of cement is relatively constant throughout the well. The argillaceous sandstones in Woolsey #1 (Fig. 11) are more similar to those of Magmamax #3.

MINERALIZATION

Dolomite. The most abundant cement in shallow sandstones is dolomite. Much of it may be recrystallized detrital grains, but rhombic crystals occasionally replace micrite and phyllosilicates. Below 1000' dolomite never constitutes more than 1% of the sandstone and disappears completely by 1500'. Such small quantities are not observable in thin section or in diffraction patterns but can be interpreted from isotope shifts (p. 146).

Calcite. Near the surface, fine grained diagenetic and detrital calcite cements argillaceous and non-argillaceous sandstones. Some shallow sandstones show quartz overgrowths replacing primary micritic cement and calcareous matrix (e.g., Magmamax #3 at 1050'; Fig. 10), but elsewhere recrystallized and authigenic calcite embays both detrital sand and quartz overgrowths. In non-argillaceous sandstones, with increased depth and/or increased permeability, calcite recrystallizes and generally changes in texture from micrite, to interlocking sparry cement, to large optically-continuous crystals that enclose sand remnants (poikilitic texture). Oxygen isotope studies (page 129) indicate that the degree of recrystallization is very sensitive to changes in permeability. The impaired permeability of the argillaceous sandstones inhibits recrystallization.

Calcite is present in almost all sandstones down to about 3500', but it is very rare below 3000'. Above 2500', non-argillaceous sandstones contain about 50% calcite cement; argillaceous sandstones have much less calcite and its abundance is inversely proportional to that of

quartz overgrowths. Since in this interval calcite replaces quartz, the reaction in the non-argillaceous sandstones is much closer to completion. Calcite in argillaceous sandstones in Magmamax #3 (Fig. 9) is abundant only in four distinct horizons: 1900', 2500', 2850', and 3250'. These horizons are largely composed of shale, with only a few percent of sandstone.

Quartz. Virtually all authigenic quartz occurs as overgrowths. In poorly cemented sandstones, quartz occurs as tiny (.01 mm) euhedral crystals in optical continuity with the detrital sand substrate. As silicification progresses, authigenic quartz forms syntaxial, optically-continuous crystal rims; grain boundaries are usually planar or concave-convex. Epitaxial quartz overgrowths on feldspars or lithic clasts are common in argillaceous sandstones above 3000'. Minor fine-grained quartz or chert is present, both as cement and as an alteration or replacement of detrital minerals.

All argillaceous sandstones below 1000' in all three wells contain authigenic quartz, but its abundance rarely exceeds 20%. Authigenic quartz in the non-argillaceous sandstones has a more limited vertical extent: below 2500', 1900', and 1300' in Magmamax #2, #3 and Woolsey #1, respectively. Above these depths, authigenic quartz is extremely rare, except for ~30% quartz in Magmamax #3 at 1050'. The rare overgrowths present are being actively replaced by calcite. Detrital quartz is also being dissolved, resulting in corresponding low "sand" percentages.

Adularia. Like quartz, adularia occurs mainly as overgrowths. In shallow, poorly cemented sandstones, it forms tiny (.01 mm) rhombic

crystals on detrital K-feldspar. Better cemented sandstones have up to 10% adularia overgrowths, virtually all syntaxial but occasionally epitaxial on detrital quartz or plagioclase. Overgrowths in shallow rocks show no optical continuity with orthoclase or with the orthoclase exsolution lamellae in microcline. Boundaries between detrital and authigenic feldspars are occasionally sutured, suggesting minor replacement of detritals by adularia. Crystals are rarely twinned, but frequently show growth banding.

Adularia is present from 2500-3800' in Magmamax #2 and from 1350-2450' in Woolsey #1; in these wells matrix abundance seems to have no relationship with the range or abundance of adularia. However, matrix content is related to adularia formation in Magmamax #3: in non-argillaceous sandstones adularia is present from 2700-3400', but in argillaceous sandstones it is very abundant (10%) at 2950' and 3400' and elsewhere is absent.

The adularia zone in Magmamax #2 and #3 slightly overlaps the lower temperature zone of feldspar (mainly plagioclase) sericitization and sericite precipitation. The insensitivity of adularia to matrix abundance and therefore to permeability can perhaps be attributed to the former abundance of K-micas in the sandstones, making long distance solution transport of cations less necessary.

Adularia replaces phyllosilicates, quartz and feldspar detritals, and quartz overgrowths. The adularia is partially contemporaneous with calcite, but also often replaces it. Pyrite is frequently rimmed and corroded by adularia.

Anhydrite. The rare sandstones within the upper clay layer occasionally contain anhydrite cement associated with pyrite pseudomorphing marcasite; this anhydrite is probably altered from gypsum. Deep (>3500') anhydrite in Magmamax #2 and #3 is entirely metamorphic and shows no relationship to any sedimentary feature. Anhydrite veinlets are abundant below 3500' (Figs. 24-26).

Anhydrite forms disseminated crystals, interlocking grains, or large poikilitic crystals; euhedral crystals are rare. Fluid inclusions are common. Anhydrite is typically associated with epidote and occasionally replaces it. The two minerals are usually contemporaneous and often seem to compete for room. Finely bedded sandstones commonly have alternate, but overlapping, zones of abundant anhydrite or epidote. Anhydrite rarely embays quartz, but does replace matrix, producing non-argillaceous sandstones with abundant anhydrite.

Calcite and anhydrite are closely related in non-argillaceous sandstones at two locations in Magmamax #2. At 2900' calcite and anhydrite are contemporaneous; both replace the locally abundant matrix in the rare sandstones in a largely shale interval. At 4300', a fine grained mixture of calcite and earthy hematite replaces anhydrite along cleavage traces and grain margins; this may be a retrograde reaction.

In Magmamax #2 and #3 anhydrite is more abundant in the non-argillaceous sandstones, particularly in permeable sandstones in shaley intervals like at 3500' in Magmamax #3. Woolsey #1 sandstones contain anhydrite in two separate locations, with a higher abundance in the non-argillaceous sandstones.

Epidote. Epidote first appears at 1350' in Woolsey #1, 1950' in Magmamax #2, and 2700' in Magmamax #3, and is present from these depths on down. Although it usually constitutes about 5% of the sandstones, locally its abundance may exceed 50%.

At shallow depths, epidote first appears as tiny (.01 mm) needles and needle rosettes. With increased depth, needle patches recrystallize into small disseminated crystals, which in turn grow together to form a "cement" of interlocking, subhedral laths. In argillaceous sandstones, epidote is present usually as small patches of fine grained, turbid crystals.

The depth range of epidote is the same in both types of sandstone, but abundances are greater in non-argillaceous sandstones; epidote abundance shows little vertical variation in Magmamax #2 and Woolsey #1. However, in Magmamax #3 there are several distinct zones with very abundant epidote.

Calcite abundance in non-argillaceous sandstones decreases sharply where epidote first appears. Muffler and White (1969) considered that epidote formed from calcium liberated during the breakdown of calcite, and there is abundant textural evidence to support this. Epidote typically preferentially replaces calcite, but it also replaces detrital and authigenic quartz, adularia, and phyllosilicates. There is also a strong correlation between carbon isotope shifts and the presence of epidote, suggesting fractionation of carbon isotopes during the breakdown of calcite to evolve carbon dioxide (page 146).

Shallow epidote intimately associated with pyrite or hematite is often highly oxidized. Nearby pyrite occasionally is also oxidized, but usually appears little altered. Anhydrite and pyrite are partially contemporaneous with epidote formation, but often replace epidote. Hematite and tremolite are both formed later.

Keith and others (1968) reported on two epidotes from IID #1 and #2 which had compositions of 20 and 32 mole % $Ca_2Fe_3Si_3O_{12}(OH)$, respectively. Figure 27 shows the variation in Fe^{+3} of epidotes in sandstones and veinlets from Magmamax #2 and #3. Although most of the data are from microprobe analyses (Table A-II, Appendix I), some compositions were determined by use of Myer's (1965) X-ray determinative curve for hydrothermal epidote. The epidotes range in composition from 20 to 35 mole %. Although the compositions of epidotes from Magmamax #3 show no relationship to depth, epidotes from Magmamax #2 become progressively more iron-rich from 2700-3850', and are approximately uniform below. This uniformity may be due to the coexistence of hematite with epidote below 3800'; above 3800' the major iron-bearing-mineral is pyrite. Epidote composition is largely a function of oxygen fugacity (Keith and others, 1968). The oxygen isotopic compositions of epidotes are discussed on p. 152.

Tremolite. Sandstones below 3500' commonly contain tremolite; its abundance never exceeds 2%. The most common habit of tremolite is fine-grained fibrous aggregates, and laths are usually only seen in veinlets. Tremolite in both sandstones and veinlets is colorless or extremely pale greenish-white. Analyses by Keith and others (1968) give a composition

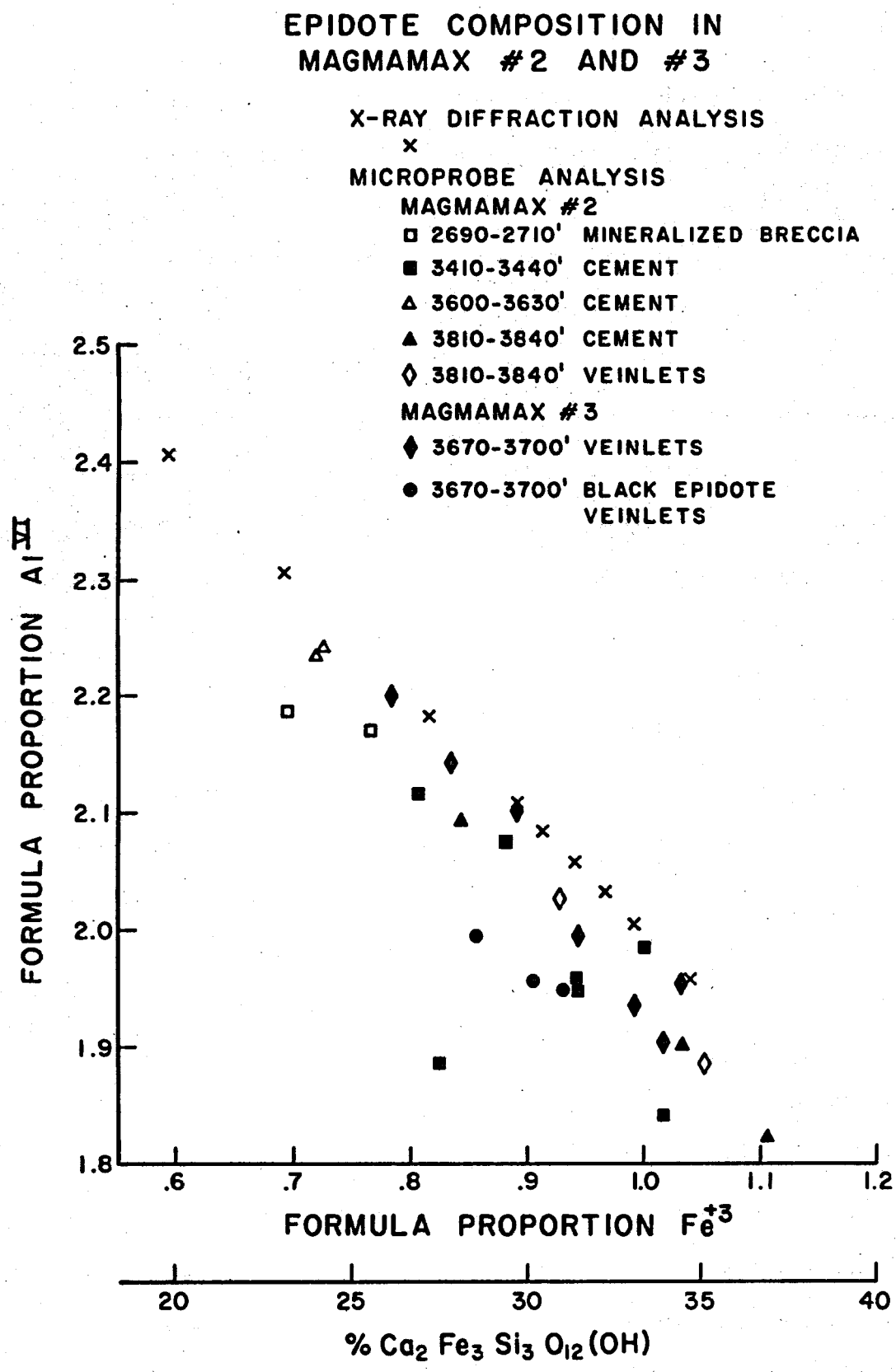

Figure 27. Variability of epidote composition in Magmamax #2 and #3. Microprobe analyses are identified by well and grain-type in the legend. The X-ray compositions are of sandstone cements from both wells which were analyzed for their oxygen isotopic compositions (see Table A-II, Appendix I).

of 17 mole % ferro-actinolite. Microprobe analyses of vein tremolite are shown in Table A-III (Appendix I), with a compositional range of 18-19 mole % ferro-actinolite.

Tremolite sheaves commonly crystallize from fine-grained phyllosilicates. Tremolite often fills in cracks, rims, and replaces quartz and feldspar sand grains. Pyrite is commonly associated with, and occasionally enclosed by, tremolite. Epidote is commonly associated with tremolite, and the two are generally contemporaneous.

Pyrite. Pyrite is ubiquitous in both time and space. It is sporadic above 2500' and very common below, but its abundance rarely exceeds 2%. Pyrite replaces all minerals except hematite, and is replaced by all minerals except quartz and calcite. It generally occurs as disseminated subhedral to euhedral cubes, but when abundant, sandstone interstices may be completely filled with poikilitic pyrite crystals. Minor amounts of chalcopyrite are often associated with pyrite.

Hematite and other Iron Oxides. Iron oxides are divided into two categories on Figures 7-23: specular hematite and other iron oxides (earthy hematite, goethite, limonite, etc.). The specular hematite occurs as discrete crystals, with a needle or blade habit.

Hematite occurs sporadically throughout Woolsey #1. In argillaceous sandstones this hematite is typically hydrated, producing red sandstones; the non-argillaceous sandstones contain unhydrated hematite and are generally white: hematite in Woolsey #1 appears to have been stable during most of the mineralization. It always replaces matrix, but appears to have been contemporaneous with either quartz or calcite in

different intervals. Adularia and hematite are commonly associated, with the adularia enclosing earlier hematite. The relationship between hematite and pyrite is complex; they coexist stably in some intervals, but in others the pyrite is anhedral and appears slightly resorbed, suggesting a change to a more oxidizing environment.

Hematite in Magmamax #2 and #3 is present only below 3500' and appears to be the last mineral formed; it typically replaces epidote grains. Oxygen isotope analyses of hematites are discussed on p. 153.

Other iron oxides are typically present in two areas: in shallow sandstones as fine-grained detrital matrix material which is being replaced by calcite, and in deep sandstones associated with hematite. Shallow sandstones with minor iron oxides are typically red or reddish brown.

Carbonaceous Material. Argillaceous sandstones in all three wells contain minor (usually <1%) carbonaceous material forming elongate, discontinuous bands parallel to the detrital and authigenic micas. The carbonaceous material is black, opaque, and very fined-grained. The material has clearly been remobilized during recrystallization of the rocks, and is closely related to pyrite mineralization. Associated micas often are fretted and replaced by pyrite. It is frequently difficult to distinguish between fine-grained pyrite and the carbonaceous material. In hand samples, these carbonaceous sandstones are characterized by abundant thin, black lamellae.

The carbonaceous material in all three wells is found in very similar argillaceous sandstones, probably within the same stratigraphic

unit (see Figs. 7, 9, 11). The material is present in Magmamax #2, #3 and Woolsey #1 from 1800-2500', 1900-2500', and sporadically from 1400-2350', respectively. The carbonaceous material is probably due to decayed organic matter deposited with this sandstone unit which was later slightly remobilized. The presence of the carbonaceous material probably produced a local reducing environment in the impermeable, argillaceous sandstones, causing the precipitation of pyrite and its replacement of detrital and authigenic micas.

ALTERATION

There are two distinct zones where feldspars and phyllosilicates are being altered and/or recrystallized. In the shallower zone, sandstones are undergoing potassium metasomatism. At higher temperatures feldspars are albitized and chlorite is recrystallized to biotite.

Sericitization. The alteration of plagioclase and minor K-feldspar to sericite plus quartz and the recrystallization of montmorillonite to sericite (illite?) are associated events. Both alterations have approximately the same depth range, with feldspar sericitization at 1700-3000', 1950-2850', and 1200(?)-2450(?)'; and matrix sericitization at 1600-3050', 1950-2950', and 1200(?)-2450(?)' in Magmamax #2, #3, and Woolsey #1, respectively.

Sericite both rims and forms within feldspars, but in general sericitization is minor so that the type of feldspar is still clearly recognizable. Sericite or hydromuscovite recrystallizing from the matrix are arranged subparallel. Sericite rarely fills open pore spaces. The sericite is generally very fine grained (<.01 mm), pale green, and has a

weak pleochroism; it is optically very similar to water-rich K-mica from the Dunes (Bird, 1975) and East Mesa (Hoagland, 1976) hydrologic systems.

The sericitization in Magmamax #2, #3, and Woolsey #1, like that at Dunes and East Mesa, represents an early stage of potassium metasomatism closely associated with silicification. At higher temperatures, a later stage of potassium metasomatism results in adularia formation. The sericite and adularia zones overlap slightly; the sericite here is replaced by both calcite and adularia. There is no evidence that the sericitization zone ever had any greater vertical extent; feldspars above and below the zone show no alteration to mica.

Albitization and Biotite Formation. Albitization of feldspar and the recrystallization of matrix chlorite and muscovite(?) to biotite are associated events. Both alterations appear at approximately the same depths and persist to the bases of the wells. Albitization occurs at 3500' and 2900', and biotite forms at 3250' and 3000' in Magmamax #2 and #3, respectively. Biotite is very rare in non-argillaceous sandstones due to the pre-existing low amount of matrix (generally <1%).

Both plagioclase and K-feldspars are being recrystallized and albitized; twin lamellae in plagioclase and microcline are only poorly preserved, and the feldspars are very turbid. The sandstone albitization is closely associated with the formation of albite in shales. Much of the authigenic feldspar overgrowths in sandstones below 3500' may be albite rather than adularia.

Several hydrothermal alteration studies (e.g., Browne and Ellis, 1970; Naboko, 1970) have noted that feldspar composition is dependent on

permeability; adularia is found to be stable in permeable zones, and albite in less permeable horizons. Comparison of Schlumberger Saraband permeability logs shown in Fig. 28 with Figs. 8-26 indicates that the same relationship between feldspar type and present permeability exists in Magmamax #2 and #3. Hence the albitization is related to the impaired permeability of rocks below 3000' in both wells.

Biotite rarely exceeds 1% in abundance, and the grains are large (≤2 mm), fresh, brown or green-brown, euhedral plates which are oriented parallel to one another and bend around nearby detritals. Biotite is often intimately associated with epidote and anhydrite, and appears to be approximately contemporaneous. Biotite seems to form largely by the replacement of chlorite and muscovite(?), a relationship much more apparent in shales (page 66). Several biotites were microprobed and have an average composition of $K_{.8}Na_{.2}(Mg_{1.41}Fe_{1.09}Al_{.37}Ti_{.13})(Al_{1.30}Si_{2.70})O_{10}(OH)_2$ (C. I. Huang, pers. comm., 1976).

SUMMARY

The paragenesis of mineralization in sandstones is illustrated in Fig. 29. The diagram shows both the sequence of mineral deposition over time and the changes in mineral stability with increased temperature.

The earliest events other than the recrystallization of detrital carbonates were silicification and localized potassium metasomatism which altered feldspars and montmorillonite to form K-mica. In the interval 1000-2500', calcite replaces the earlier formed quartz overgrowths and K-mica. Between 2500' and 3500', adularia, epidote and pyrite replace

Figure 28. Saraband Permeability logs for Magmamax #2 and #3

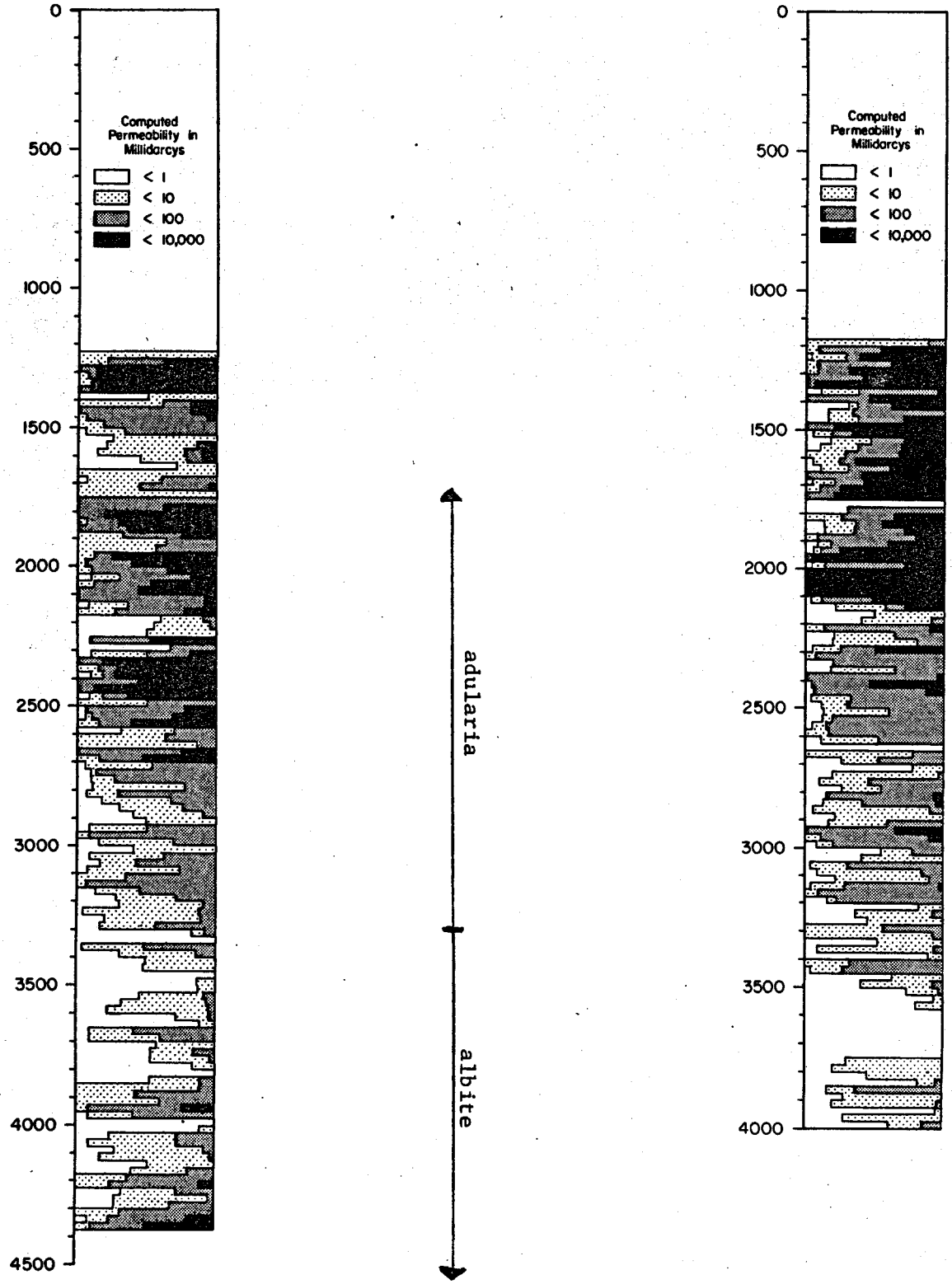

Figure 29

SANDSTONE PARAGENESIS

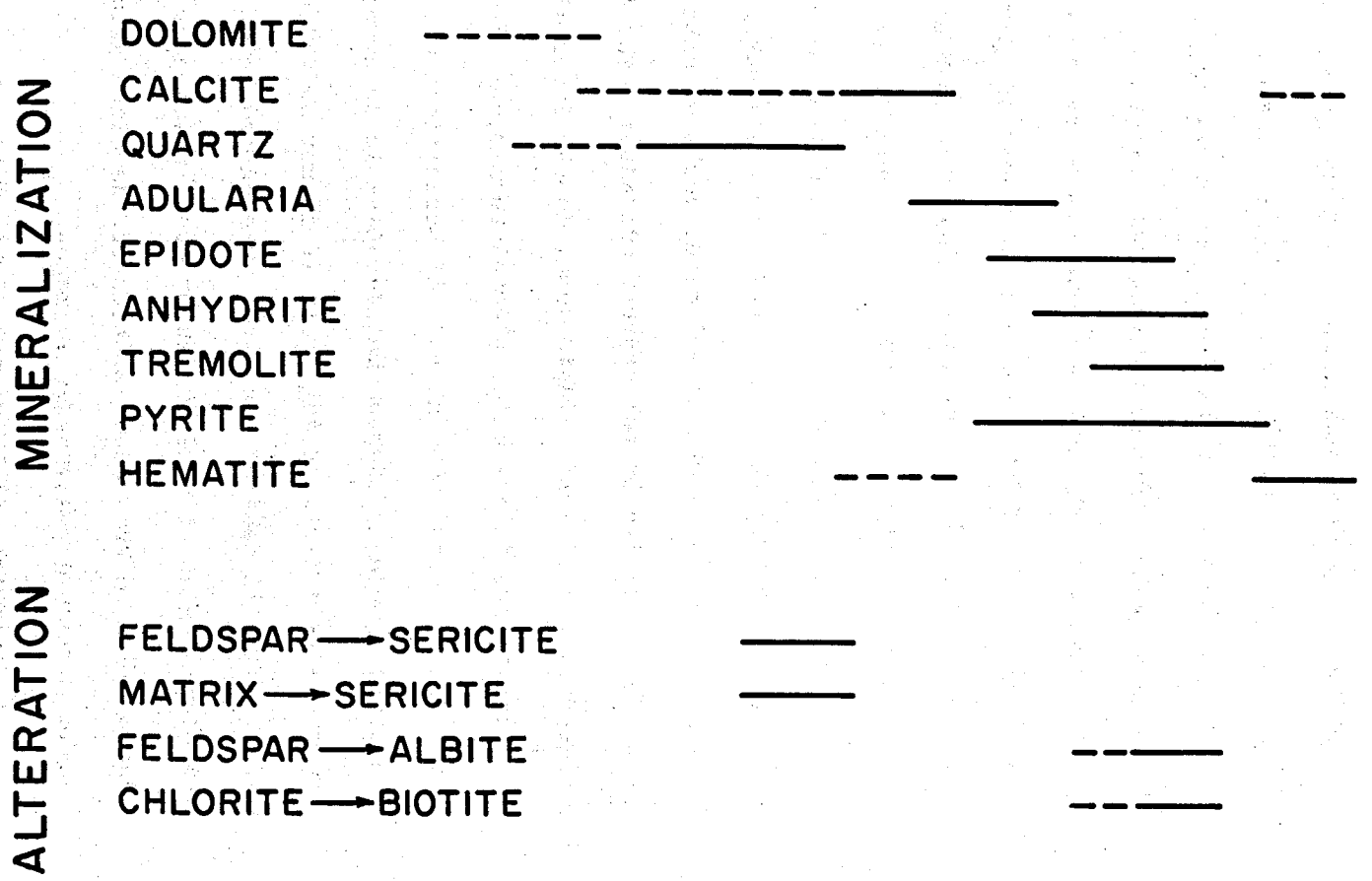

detritals, quartz overgrowths, and calcite. Below 3500', epidote, anhydrite, tremolite, and hematite are deposited, detrital feldspars are albitized, and the matrix recrystallizes to form large biotites.

The earliest mineralization was the development of quartz overgrowths replacing detrital phyllosilicates and carbonate. Quartz overgrowths are found throughout the total vertical extent of the wells, although they are presently being replaced everywhere and are presumably unstable. Since silicification is a common diagenetic change in sandstones, the overgrowths may have been formed in all sandstones early in the history of the sediments, perhaps even before the thermal anomaly developed.

The other mineralogical changes were all superimposed over the original silicification, have limited vertical extents, and are apparently strongly controlled by temperature and water composition. For example, feldspars, particularly plagioclase, in the interval 2000-2900' in Magmamax #2 and #3 are being altered to K-mica. Above and below this interval, feldspars show no sign of sericitization, and plagioclase is abundant. Hence, potassium metasomatism is an event presently superimposed over a distinct interval; it is not a diagenetic change which occurred in all sediments as they were buried below a particular depth. The mineralogies at various depths are, in a sense, a zonation of minerals due to the recent effects of the circulation of hot, saline fluids through a sedimentary sequence.

The presence and abundance of minerals are strongly controlled by the matrix content of the sandstones. Quartz overgrowths are more abundant in the argillaceous sandstones; they are less abundant in the non-

argillaceous sandstones, largely because of later mineralization and replacement by other silicates and calcite. The argillaceous sandstones generally have the same authigenic minerals as the non-argillaceous sandstones, but the minerals are less abundant and first occur at greater depths in argillaceous sandstones. Differences in mineralogy are probably due to relative permeabilities of the sandstones--the non-argillaceous sandstones are more permeable and hence have had more fluid circulation; the impaired permeability of the argillaceous rocks impedes water circulation and hence slows reaction.

Mineralogies are also affected by the permeability of nearby rocks. In intervals largely composed of shale, rare sandstones present are argillaceous and therefore relatively impermeable; sandstones in intervals lacking shales are especially permeable. Calcite in argillaceous sandstones in Magmamax #3 is abundant only in four distinct intervals; these intervals are characterized by abundant calcareous shale. The deepest calcite-rich interval is at 3750'; sandstones just above and below 3750' lack calcite, which is presumably stable at 3750' due to the impaired permeability of the interval caused by the high shale content. There is a faint correlation between zones of abundant epidote and sandstone abundance. Quartz overgrowths are more common in argillaceous sandstones because there has been insufficient mineralization to replace them with calcite, epidote, and other silicates.

Siltstones

ARGILLACEOUS VS NON-ARGILLACEOUS SILTSTONES

Two different siltstones with different types and amounts of mineralization and with different matrix contents occur in each interval. Data from the two rock types are compiled into separate charts for Magmamax #2 and #3 (Figs. 13-16) but are combined into a single chart for Woolsey #1 (Fig. 17).

SILTSTONE COMPONENTS

For each well, the siltstones are composed of 30-90% silt, 0-60% matrix, and 2-80% mineralization (cement). Siltstones in general have a higher abundance of matrix and cement, and a lower abundance of framework grains (silt and sand) than sandstones. The siltstones of Magmamax #3 are all very argillaceous; siltstones in Magmamax #2 and Woolsey #1 are less argillaceous.

MINERALIZATION

The siltstones in the three wells studied are usually rather coarse-grained (.01-.05 mm) and are much more similar to sandstones than shales in their fabric and mineralization. Since the textures and patterns of mineralization are so very similar to those in sandstones, they are considered here only briefly.

The most common siltstone cement, as in sandstone, is calcite. Like the non-argillaceous sandstones of Magmamax #3, the non-argillaceous siltstones have high calcite abundances only in distinct zones which are located at approximately the same depths as zones in the sandstones.

There is no apparent relationship between matrix content and calcite abundance in siltstones. The non-argillaceous siltstones of Magmamax #2 have very little calcite (<5%), probably because earlier silicification filled most of the available pore space. Calcite disappears at about the same depth in both siltstones and sandstones.

Epidote first appears at about the same depths in both siltstones and sandstones of Magmamax #3 and Woolsey #1, and the abundances of epidote are quite similar.

SUMMARY

The textures and mineralization trends in siltstones are very similar to those of sandstone. Siltstones in general have more matrix and cement, and less framework grains than sandstones. Magmamax #3 siltstones are very argillaceous, and hence relatively impermeable.

Shales

GRAY VS NON-GRAY SHALES

For each well, there are two shale diagrams--one for gray and one for non-gray shales (Figs. 18-23). Non-gray shales include two different types: the shallow tan, gray-brown, and red shales; and the deeper green shales. Data on the non-gray shales are grouped together for ease of presentation since these shales have non-overlapping vertical ranges.

There are several reasons for distinguishing among shales of different colors. Most importantly, the variations in shale color are closely related to differences in mineralogy and fabric. Oxygen and carbon isotopic compositions of different colored shales are also different

(page 133), suggesting variable degrees of exchange with the water. Green shales appear to be the metamorphosed counterparts of gray shales.

Shales of different colors have limited vertical ranges. Tan and gray-brown shales are present only in the clay or shale layer above 1000' in all three wells. Red shales are the deeper counterpart of these shales; they extent down to 2500', 2300', and 2000' in Magmamax #2, #3 and Woolsey #1 respectively, but are abundant only down to 1750', 1700', and 1400'. Gray shales are present below 1000' and are abundant down to 3300', 2800', and 2100' in Magmamax #2, #3 and Woolsey #1, respectively. Below these depths, green shales are present also. Relative abundances of gray and green shales are quite variable.

Different shale colors are produced by differences in mineralization. The red color is a result of the higher iron oxide content. Abundant chlorite, and to a lesser extent epidote, produce the green color. The major differences between the red and gray shales from 1000-2500' are the greater dolomite and iron oxide content of the red shales, and the minor epidote in the deeper gray shales. As shown in Figs. 18-23, green shales differ from gray shales mainly by their lack of calcite, higher chlorite and anhydrite contents, slightly higher epidote abundance, and the presence of large biotite porphyroblasts in the green shales (hornfelses).

SHALE COMPONENTS

Figures 18-23 show that shales are composed of 0-20% sand and silt, 5-95% matrix, and 5-95% mineralization (cement). However, the average shale has less than 5% sand and silt, more than 75% matrix, and 20%

mineralization. Non-gray shales generally have more mineralization and less matrix than gray shales.

X-ray diffraction techniques are useful for determining shale constituents since shales are largely too fine-grained for petrographic work. Unfortunately, minerals with abundances less than 5-10% may not be readily detected on diffractograms.

Mineral percentages in the bulk fraction of shales from Magmamax #2 and #3 are presented on Tables I and II. The compositional ranges of shales are as follows: 0-19% calcite, 0-86% other carbonates, 2-40% quartz, 0-41% K-feldspar, 0-59% plagioclase, 0-6% kaolinite, 0-17% interlayered illite-montmorillonite, 0-88% mica, and 0-87% chlorite. The "average" shale has about 6% calcite, 15% quartz, 10% K-feldspar, 12% plagioclase, 1% interlayered clays, 40% mica, and 16% chlorite.

MINERALIZATION

Muffler and Doe (1968) suggest that there is as much as 10% detrital carbonate in Colorado River deltaic deposits. It is extremely difficult to distinguish between detrital and diagenetic carbonate in thin section so therefore both types have been grouped together.

Dolomite. Iron-rich dolomite (ankerite) is the most abundant cement in tan shales. The oxygen and carbon isotopic compositions suggest that some of the dolomite may be diagenetic rather than detrital (page 161). Dolomite is present in shales to at least 2000-2500', but below 1500' the abundance is so low that it is detected only by oxygen isotope analyses.

TABLE I

X-ray Diffraction Analyses of Shales from Magmamax #2

Bulk Fraction Mineral Percentages

DEPTH	COLOR	DOL.	ANK.	CALC.	QTZ.	PLAG.	KSPAR	KAOL.	MIXED LAYER	MICA	CHL.	TOTAL
580'	tan	86	--	--	8	--	--	2	--	5	--	101
910	tan	--	50	5	11	--	--	5	7	21	--	99
1090	tan	--	7	11	8	--	--	--	17	52	5	100
1400	gray	--	--	4	9	--	--	--	15	64	8	100
1610	gray	--	--	3	8	--	--	--	5	70	14	100
1820	gray	--	--	3	7	--	--	--	3	77	10	100
2000	gray	--	--	--	5	--	--	--	--	78	17	100
2220	gray	--	--	7	14	--	--	--	5	59	16	101
2420	gray	--	--	3	10	--	--	--	--	75	13	101
2660	gray	--	--	8	12	--	--	--	2	63	15	100
2900	gray	--	--	8	17	--	--	--	2	57	16	100
3110	gray-green	--	--	5	11	--	--	--	--	70	14	100
3200	gray	--	--	10	21	--	--	--	4	51	14	100
3350	gray	--	--	9	19	--	10	--	--	46	11	100
3440	gray	--	--	7	13	--	23	--	2	38	19	102
3440	green	--	--	5	10	--	24	--	--	40	20	99
3530	green	--	--	2	10	--	21	--	2	36	29	100
3720	green	--	--	3	9	15	22	--	1	25	25	99
3720	green	--	--	2	7	13	16	--	3	22	37	100
3720	purple	--	--	--	18	59	--	--	4	12	7	100
3990	green	--	--	2	5	9	13	--	3	50	19	101
4140	green	--	--	3	8	16	--	--	2	55	16	100
4280	green	--	--	2	4	--	12	--	3	40	39	100

TABLE II

X-ray Diffraction Analyses of Shales from Magmamax #3

Bulk Fraction Mineral Percentages

DEPTH	COLOR	ANK.	CALC.	SID.	QTZ.	PLAG.	KSPAR	KAOL.	MIXED LAYER	MICA	CHL.	TOTAL
630'	tan	72	—	—	14	—	—	2	—	12	—	100
840	tan	30	2	3	10	—	—	6	17	32	2	102
1020	gray	14	4	—	11	—	—	5	7	55	3	98
1210	gray	—	6	—	16	—	—	—	—	77	2	101
1210	red	—	3	—	7	—	—	—	—	88	2	100
1430	gray	—	7	—	20	—	—	—	—	67	6	100
1650	red	—	8	—	10	—	—	—	—	77	5	100
1810	gray	—	11	—	19	3	—	—	—	62	4	99
1960	gray	—	11	—	32	—	—	—	—	53	4	100
2080	gray	—	—	—	16	—	—	—	—	64	20	100
2370	gray	—	4	—	9	—	—	—	—	82	6	101
2560	gray	—	10	—	12	2	—	—	—	68	8	101
2590	gray	—	8	—	18	2	—	—	—	64	7	99
2770	green	—	—	—	13	—	—	—	—	—	87	100
2830	gray	—	6	—	13	4	—	—	—	70	8	101
3040	gray	—	12	—	38	13	—	—	—	33	5	101
3100	green	—	8	—	20	2	—	—	—	61	8	99
3100	green	—	13	—	13	35	—	—	—	6	34	101
3100	purple	—	8	—	18	5	—	—	—	61	8	100
3210	gray	—	4	—	15	41	—	—	—	13	27	99
3330	green	—	—	—	20	12	—	—	—	—	68	100
3390	green	—	—	—	36	20	25	—	—	13	7	101
3510	green	—	—	—	6	18	—	—	—	50	27	101
3610	green	—	—	—	11	26	—	—	—	35	28	100
3670	gray	—	19	—	8	26	—	—	—	24	22	99
3760	gray	—	—	—	32	18	—	—	—	—	50	100
3790	green	—	1	—	2	23	—	—	—	65	10	101
3910	green	—	9	—	13	31	—	—	—	46	2	101
3970	green	—	—	—	3	12	—	—	—	36	50	101
3970	green	—	—	—	5	18	—	—	—	73	4	100

Calcite. Although rare or absent in green shales, calcite is the most abundant cement in red and gray shales. Its abundance rarely exceeds 20%; the texture is usually micritic with calcite randomly intergrown within the phyllosilicate matrix. Calcite is present in all red shales and its abundance in the wells shows little relationship to depth, except that it increases as dolomite decreases in quantity.

The calcite content of gray shales correlates with the relative abundance of gray shale. Gray shales in intervals with abundant gray shale and only minor green shale have higher calcite abundances than in intervals with abundant green shale. Since green shales are altered or metamorphosed gray shales, it seems that calcite abundance is highest in the relatively unaltered (i.e., largely gray shale) intervals. As will be discussed later, calcite is preserved in gray shales due to their lower permeability.

Examples of the close relationship between calcite content and gray shale abundance are as follows: the vertical ranges of gray and green shales in Magmamax #3 and Woolsey #1 overlap for many hundreds of feet, with alternate horizons of abundant gray or green shales. Calcite abundances in Magmamax #3 and Woolsey #1 are greater where the relative abundance of gray shales is high. Stratigraphic overlap of gray and green shales in Magmamax #2 is much less, and in this short interval gray shales gradually decrease and green shales increase in abundance; calcite content gradually decreases as the abundance of gray shales decreases. At about 2700' in Magmamax #2 and #3, the calcite content of the gray shales is rather low. This interval is characterized by abundant

mineralized fractures. Perhaps greater water circulation resulted in the removal of calcite and its replacement by epidote and anhydrite.

Calcite is rare in green shales, and is usually absent in green shales from intervals with abundant green shales and only minor gray ones. It is replaced by epidote, anhydrite, and pyrite.

Carbonate cement in shales was analyzed to determine the oxygen and carbon isotopic compositions of the carbonates (p. 128). Most of the analyses are of gray shales because of their large vertical range. Green shales were rarely analyzed because of their low calcite abundance.

Adularia-albite. Authigenic feldspar was only detected in thin sections of green shales from two intervals: 3790-3820' in Magmamax #3 and 3810-3840' in Magmamax #2. The Magmamax #3 interval contains abundant epidote-anhydrite veinlets within green shales. Fine grained (.05 mm), interlocking albite replaces the shale near the veinlets. A microprobe analysis of this albite is given in Table A-I (Appendix I), along with other authigenic feldspars. Lensoid, .1-.4 mm, porphyroblasts of interlocking albite are often seen in shales in this interval.

In Magmamax #2, the feldspar is also fine grained (.05 mm) and interlocking, and seems to replace some large (2 mm) pre-existing, vaguely tabular crystals, perhaps anhydrite(?). The feldspar pseudomorphs were microprobed and found to be adularia with 95% of the orthoclase endmember and 5% of albite (Table A-I, Appendix I).

The mineralogies of the clay fractions of shales of Magmamax #2 and #3 are given on Tables III and IV. Since feldspars are absent in the clay fraction above 3300', it is likely that all the feldspar below here

TABLE III

X-ray Diffraction Analyses of Shales from Magmamax #2

Clay Fraction Relative Mineral Abundances *

DEPTH	COLOR	ANK.	CALC.	QTZ.	MIXED LAYER	MICA	CHL.	MONT.
580'	tan	3	--	--	2	1	--	--
910	tan	4	--	2	2	1	2	--
1090	tan	--	--	2	2	2	2	--
1400	gray	--	--	2	2	4	2	--
1610	gray	--	1	2	2	4	3	--
1820	gray	--	--	3	--	4	2	--
2000	gray	--	--	2	1	2	4	--
2220	gray	--	--	--	1	4	3	--
2420	gray	--	--	1	1	4	3	--
2660	gray	--	--	1	--	3	4	--
2900	gray	--	--	2	1	3	4	--
3110	gray-green	--	--	2	1	2	4	--
3200	gray	--	--	--	--	2	2	--
3350	gray	--	--	2	1	2	4	--
3440	gray	--	--	2	--	2	2	2
3440	green	--	--	2	--	1	3	--
3530	green	--	--	1	--	1	3	--
3720	green	--	--	--	--	1	4	2
3720	green	--	--	--	1	1	2	4
3720	purple	--	--	1	1	1	4	--
3990	green	--	--	--	1	1	2	4
4140	green	--	--	--	--	1	3	4
4280	green	--	--	--	--	1	3	4

* Relative abundances are reported qualitatively using a 0 to 5 scale of increasing abundance indicating absent, trace, present, major, and abundant, respectively.

TABLE IV

X-ray Diffraction Analyses of Shales from Magmamax #3

Clay Fraction Relative Mineral Abundances

DEPTH	COLOR	ANK.	CALC.	QTZ.	FELD.	KAOL.	MIXED LAYER	MICA	CHL.	MONT.
630'	tan	--	--	2	--	2	--	2	--	--
840	tan	--	--	2	--	2	--	3	--	--
1020	gray	--	--	2	--	2	2	3	--	--
1210	gray	--	--	2	--	2	2	3	--	--
1210	red	--	--	2	--	--	2	3	2	--
1430	gray	--	--	2	--	--	2	3	2	--
1650	red	--	--	2	--	--	2	3	2	--
1810	gray	---	--	2	--	--	2	3	--	--
1960	gray	--	--	2	--	--	1	3	2	--
2080	gray	--	--	2	--	--	1	3	3	--
2370	gray	--	1	2	--	--	--	4	3	--
2560	gray	--	--	2	--	--	--	3	3	--
2590	gray	--	--	2	--	--	--	3	3	--
2770	green	--	--	--	--	--	--	1	4	--
2830	gray	2	--	2	--	--	--	3	3	--
3040	gray	2	--	2	--	--	--	3	3	--
3100	green	--	--	1	--	--	--	2	4	--
3100	green	--	--	--	--	--	--	--	4	--
3100	purple	--	--	2	--	--	1	3	3	1
3210	gray	--	--	1	2	--	--	2	4	--
3330	green	--	--	--	--	--	--	--	4	--
3390	green	--	--	2	2	--	--	2	4	--
3390	green	--	--	--	2	--	2	--	4	--
3510	green	--	--	1	2	--	--	1	3	3
3610	green	1	--	1	2	--	--	3	4	--
3670	gray	1	--	2	--	--	--	--	3	2
3760	gray	--	--	1	2	--	--	1	4	--
3790	green	--	--	--	2	--	--	2	3	4
3910	green	--	--	1	2	--	--	2	3	2
3970	green	--	--	1	2	--	--	1	3	3
3970	green	1	--	1	--	--	--	1	1	--

is authigenic. The clay fraction data suggest that appreciable fine grained feldspar is forming in shales, probably by replacing mica.

Anhydrite. Anhydrite is present in two distinct zones in the wells: from 0-2000', and below 3400'. Shallow anhydrite occurs both as nodules and lath-aggregates, and is frequently associated with pyrite. The nodules are white, spherical to botryoidal, .1-10 mm balls of very fine grained (.005-.05 mm), fibrous anhydrite; x-ray analyses show that they contain small amounts of gypsum and hemimorphite. Nodules form within shallow shales and are especially abundant in the unconsolidated clay layer. Below 1000', tiny nodules are occasionally seen within lithified shales; much of the larger loose anhydrite nodules in the cuttings are probably contaminants.

Anhydrite aggregates, rosettes or random clusters of silt and sand-size anhydrite laths, often form within the shallow shales by the progressive recrystallization of anhydrite nodules which act as nuclei for further shale replacement. Aggregates often have fine grained, fibrous cores, and shale remnants are common in interstices. Anhydrite aggregates are only found in the upper 500' of the section. Shales rarely have beds of isolated, rounded, and oriented detrital anhydrite laths which were probably removed from pre-existing shales by stream channeling, and then redeposited.

The deeper anhydrite which forms in shales below 3400' is associated with abundant anhydrite-filled veinlets. Shale anhydrite is clearly metamorphic; the euhedral porphyroblasts commonly disrupt the meta-shale foliation. Phyllosilicates in shales lacking porphyroblasts are all

extremely well oriented parallel to each other. However, where porphyroblasts are present, the shale fabric is disturbed and is divided into very irregular zones with slightly different phyllosilicate orientations.

Anhydrite in these deep shales typically occurs as single crystals or rosettes ranging in size from .05-5 mm. Anhydrite occasionally selectively replaces certain shale beds, producing banded shales. Epidote and anhydrite are largely contemporaneous. The anhydrite porphyroblasts replace both phyllosilicates and pre-existing fine grained epidote patches. Pyrite commonly rims or forms within the anhydrite by the reduction of the calcium sulfate.

Other than at 3400' in Magmamax #3 where gray shales are largely replaced by pink anhydrite, metamorphic anhydrite is very rare in gray shales; it is more abundant in the green shales where it locally constitutes up to 20% of the shale. Anhydrite abundance in Magmamax #2 decreases steadily downwards from a maximum at about 3500'. The abundance in Magmamax #3 has a minimum at 3600-3800', perhaps related to the high shale abundance in the interval, and consequent very low permeability.

Gypsum. Traces of gypsum and hemimorphite are present in shallow anhydrite nodules in shales; anhydrite textures frequently suggest recrystallization from gypsum. Gypsum has also been tentatively identified in association with deeper, metamorphic anhydrite. Small (.05-.2 mm), subhedral to euhedral gypsum crystals occasionally recrystallize from anhydrite in sandstones, shales, and veinlets.

Epidote. Gray and green shales below 2000-2500' commonly contain epidote which typically occurs in small (.01-.1 mm) patches or aggregates

of clay and silt sized grains. The constituent crystals are usually pale yellow-green, turbid, anhedral grains and are intimately intergrown with very fine grained albite-adularia, iron oxides, and phyllosilicates.

Epidote patches are commonly elongate and arranged subparallel to phyllosilicate orientation. In a few shales, the elongate patches are connected to form thin, swirly, crenulate fine grained bands. In other locations, selected shale beds are largely replaced by abundant epidote. Shales below 3600' commonly have epidote, anhydrite, pyrite, or iron oxide-rich bands.

At 3670' in Magmamax #3, thin dark gray shale lamellae within lighter gray shales are selectively replaced by silt-sized, interlocking epidote with minor disseminated iron oxides. This epidote is black rather than the usual yellow-green, perhaps due to disseminated material. Microprobe analyses of the black epidote are given in Table A-II (Appendix I). The black epidotes are within the range of other epidote compositions.

Epidote abundance in shales rarely exceeds 15% and is inversely proportional to the calcite content; the correlation is best seen in the green shales Magmamax #2 and #3. Green shales have less calcite and more epidote than gray shales of the same depth. Anhydrite porphyroblasts usually occur in green shales with less than normal epidote contents, perhaps because fluids in these shales are less calcium depleted.

Tremolite. Tremolite is an extremely rare constituent of green shales and is present in only two locations (Figs. 19 and 21). In both instances,

fibrous tremolite replaces phyllosilicates within largely-epidotized shales.

Pyrite. Although pyrite is a common shale constituent, it rarely exceeds 2%. It is extremely rare in red shales due to the prevailing oxidizing environment. Pyrite is abundant in the shallow tan shales where it is associated with, and replaces, anhydrite. Although the pyrite shows the cockscomb habit typical of marcasite, x-ray analysis indicates that the sulfide is now entirely pyrite; it is apparently pseudomorphous after marcasite.

Pyrite in Magmamax #2 and #3 is virtually absent in shales in the interval 1000-2700'. Gray shales below 3000' and 2700' in Magmamax #2 and #3 respectively contain pyrite; pyrite is also present in all green shales. The depth at which pyrite first appears in gray shales is approximately the depth at which green shales begin to form. Hence pyrite occurs in all co-existing gray and green shales. The same relationship between the appearance of pyrite and green shale formation exists in Woolsey #1, but at a different depth. Pyrite and green shales here start at about 1950' and 2100' respectively.

Pyrite formation is apparently related to incipient shale metamorphism and consequent formation of green shales. The major reaction in the progressive alteration of green shales is the breakdown of chlorite to form muscovite and biotite, apparently liberating iron. The excess iron produces pyrite as well as the higher epidote content of the green shales.

Pyrite below 2500' occurs as subhedral to euhedral cubes ranging from .005-.2 mm. The cubes are sometimes randomly distributed, but more commonly are arranged in small (.05-5 mm) patches elongate parallel to the bedding. Pyrite patches in well laminated shales often grow together and replace surrounding shale to form broad, pyrite-rich bands parallel to the bedding. Pyrite preferentially forms in the more silty lamellae.

Hematite and Other Iron Oxides. Specular hematite is a rare constituent in shales and is more common in gray than green shales. It is present in rare red shales, but usually in the form of finely disseminated, earthy, iron oxides. Shales with specular hematite are commonly purplish-gray in color due to the earthy iron oxides associated with the hematite. The specular hematite is usually randomly disseminated throughout the shale in the form of silt-sized, blade-like crystals.

In Magmamax #2 and #3, shales with hematite generally contain very little pyrite. Below 3800' in Magmamax #2, the pyrite content of gray shales decreases as hematite becomes more abundant. Small pyrites in these gray shales are oxidized, but the larger cubes are still fresh. Hematite replaces minor pyrite in green shales below 4250'.

PHYLLOSILICATE ABUNDANCE

The data in the column labeled "Relative Abundance of Phyllosilicates" are derived largely from x-ray analysis of handpicked shales. Complete shale compositional data are given in chart form on Tables I-IV.

Kaolinite is present only in shallow shales above 1000'. Muffler and White (1969) suggest that kaolinite, ankerite, and dolomite react in the interval 1200-2300' in IID #1 to form chlorite, calcite, and CO_2.

Mixed-layer clays are not detected below 2000' in Magmamax #3. In Magmamax #2, they are abundant only above 1500', but traces of mixed-layer clays are present in gray and green shales throughout the well.

Mica is the most abundant phyllosilicate. The term "mica" here includes both muscovite and biotite since it is very difficult to distinguish between them in diffraction patterns and in thin sections of shale. Mica constitutes 80% of phyllosilicates in tan, red and gray shales of above 3500' in Magmamax #2, and 90% of the phyllosilicates in the same shales above 3100' in Magmamax #3. Regardless of the phyllosilicate content of shales in these intervals, the ratio of mica to total phyllosilicates remains remarkably constant (Figs. 18-21). The remaining 10-20% of the phyllosilicates are composed of kaolinite, mixed-layer clays, and chlorite above 1500'; below 1500' the kaolinite and mixed layer clays are largely converted to chlorite.

The consistent ratio of mica to total phyllosilicates (mica/phyllosilicates) in tan, red and gray shales throughout the upper 3100' or 3500' of the wells suggests that the argillaceous detritus deposited in the Salton Trough had a remarkably consistent mineralogical composition. Muffler and Doe (1968) reported that the bulk chemical and mineralogical composition of the sediments has been very similar throughout the late Cenozoic.

The invariance of the mica/phyllosilicates ratio also suggests that the mica in the tan, red, and gray shales is stable down to 3100' in Magmamax #3 and 3500' in Magmamax #2. Gray shales below these depths show a progressive decrease in the mica percentage and an increase in

the chlorite percentage of the total phyllosilicates. The decrease in the mica/chlorite ratio is probably indicative of the breakdown of detrital mica to form authigenic chlorite. Two microprobe analyses of chlorite in green shales are given in Table A-III (Appendix I). The chlorites are magnesium and alkali rich and iron poor, with an average composition of $(Mg_{6.4}Al_{2.6}Fe_{1.2}Ti_{.6})\ Al_{1.7}Si_{6.3}O_{20}\ (OH)_2$.

Although the mica/chlorite ratio is constant from 1500-3100', both mica and chlorite have recrystallized considerably in this interval. The width of the 10 Å mica peak is closely related to mica crystallinity; as the mica becomes better crystallized, the mica peak becomes sharper (de Segonzac, 1970). Figures 30 and 31 show the changes in shale mica peak width with increasing depth in Magmamax #2 and #3.

In Magmamax #2 shales, the peak widths of mica in both the clay and bulk fraction (Fig. 30) show the same pattern of decreasing peak width with increasing depth. There is considerable scatter above 1700', but in the interval 1700-3400' the peak width is approximately constant. Below 3400' the peak width decreases again. Clay-size micas are better crystallized than bulk micas, presumably due to their greater surface areas. The mica/chlorite ratio increases below 3500' and chlorite is being recrystallized to form well crystallized hydrothermal mica.

Magmamax #3 shales also show a pattern of decreasing mica peak width with increasing depth (Fig. 31). This pattern is best developed in the bulk fraction; the peak width decreases rapidly to 2100', and then gradually below. There is considerable scatter in the clay fraction

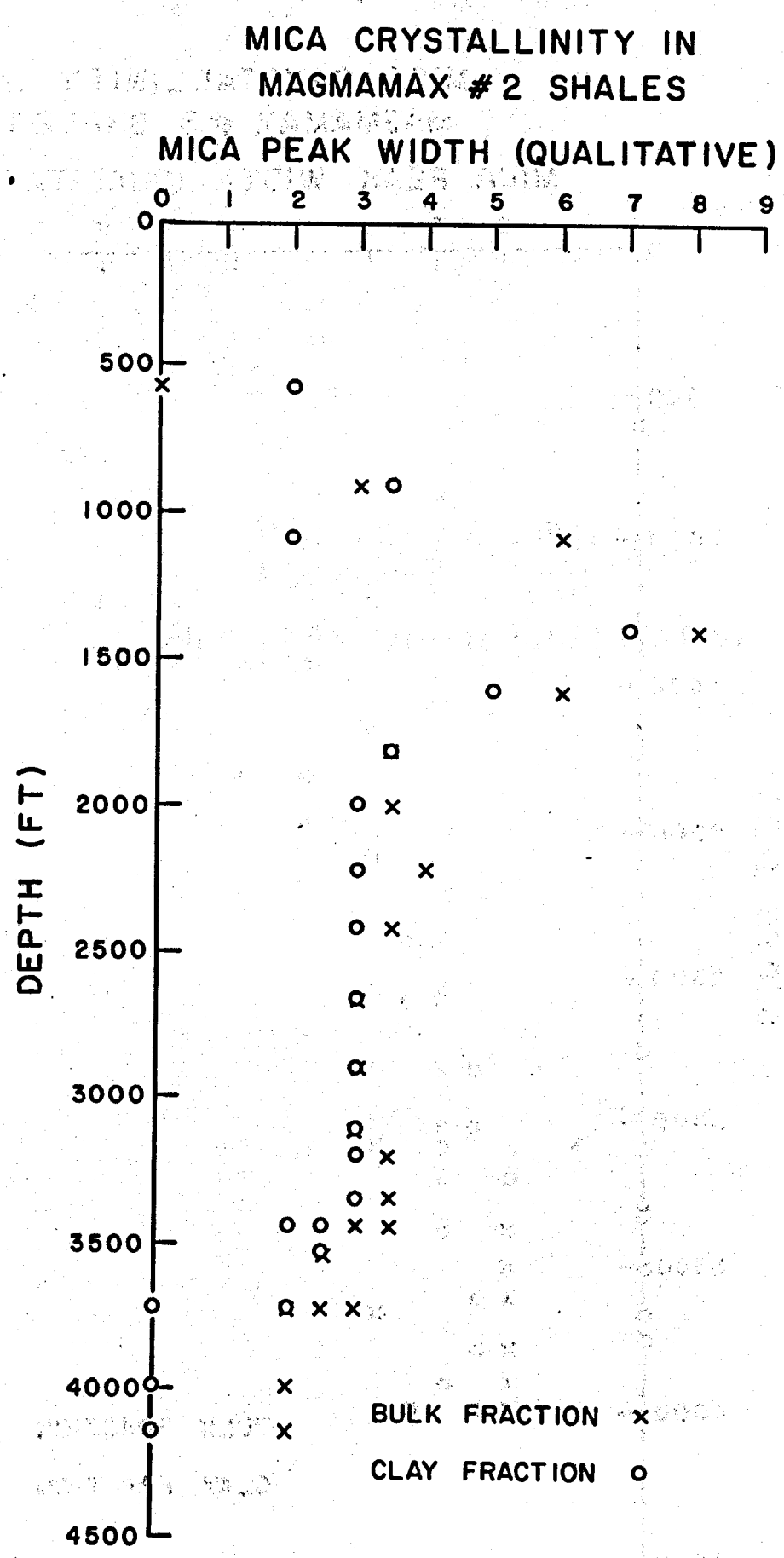
MICA CRYSTALLINITY IN
MAGMAMAX #2 SHALES
MICA PEAK WIDTH (QUALITATIVE)
0 1 2 3 4 5 6 7 8 9
0
500
1000
1500
2000
2500
3000
3500
4000
4500
DEPTH (FT)
BULK FRACTION ×
CLAY FRACTION o

Figure 30

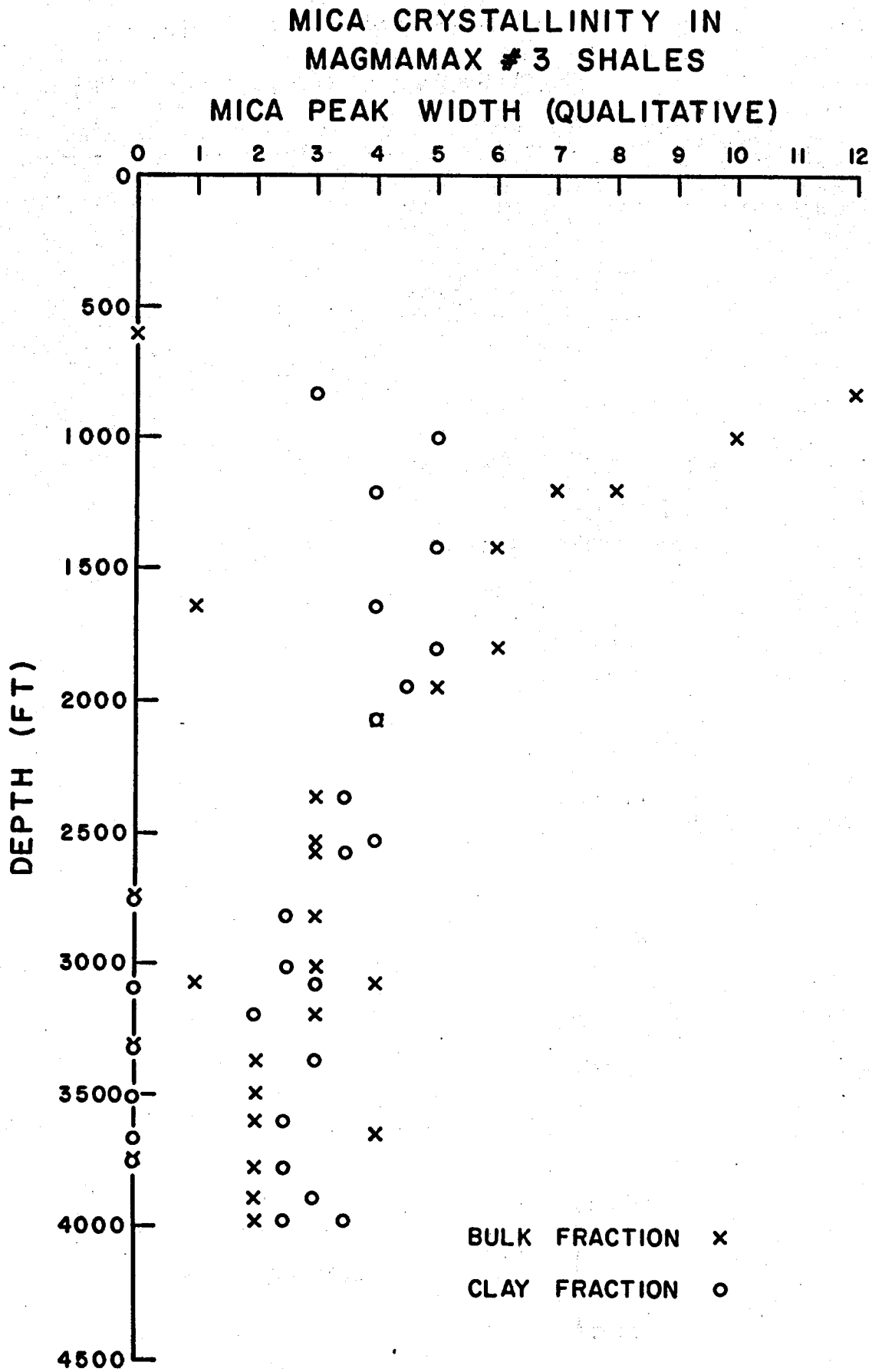
MICA CRYSTALLINITY IN
MAGMAMAX #3 SHALES
MICA PEAK WIDTH (QUALITATIVE)
0
1
2
3
4
5
6
7
8
9
10
11
12
DEPTH (FT)
0
500
1000
1500
2000
2500
3000
3500
4000
4500
BULK FRACTION ×
CLAY FRACTION o

Figure 31

data, but the same trend is present. There is no apparent correlation between the shale color and mica peak width.

The Fe content of chlorite can be calculated from diffraction patterns according to the method given by Brindley (in Brown ed., 1961). Figure 32 shows the variation in the Fe content of chlorite with depth in the clay fraction of shales in Magmamax #2 and #3. There is considerable data scatter, but the Fe content in Magmamax #2 vaguely increases and that of Magmamax #3 vaguely decreases with increasing depth.

Green shales of Magmamax #3 show a very close relationship between mica and chlorite. Green shales at 2800' have a phyllosilicate content of 5% mica and 95% chlorite. The mica/chlorite ratio decreases slightly down to 3350'. Between 3350' and 3800' the ratio decreases rapidly; below 3800' it decreases slightly to the bottom of the well where phyllosilicates consist of 95% mica, 3% chlorite, and 2% miscellaneous. The progressive decrease in chlorite and increase in mica content suggest that mica is replacing the previously-formed chlorite. Thin sections in this interval show the development of coarse-grained biotite which appears to replace finer-grained phyllosilicates.

The green shales of Magmamax #2 show a different relationship between mica and chlorite; their relative abundances show less variation with increased depth than in Magmamax #3. The mica/chlorite ratio increases slightly from 3450-3550', and then slowly decreases from 3550' to the bottom of the well where the phyllosilicate content is 75% mica, 20% chlorite, and 5% miscellaneous. The trend below 3550' is the same as in Magmamax #3, but the ratio changes less with increased depth. In

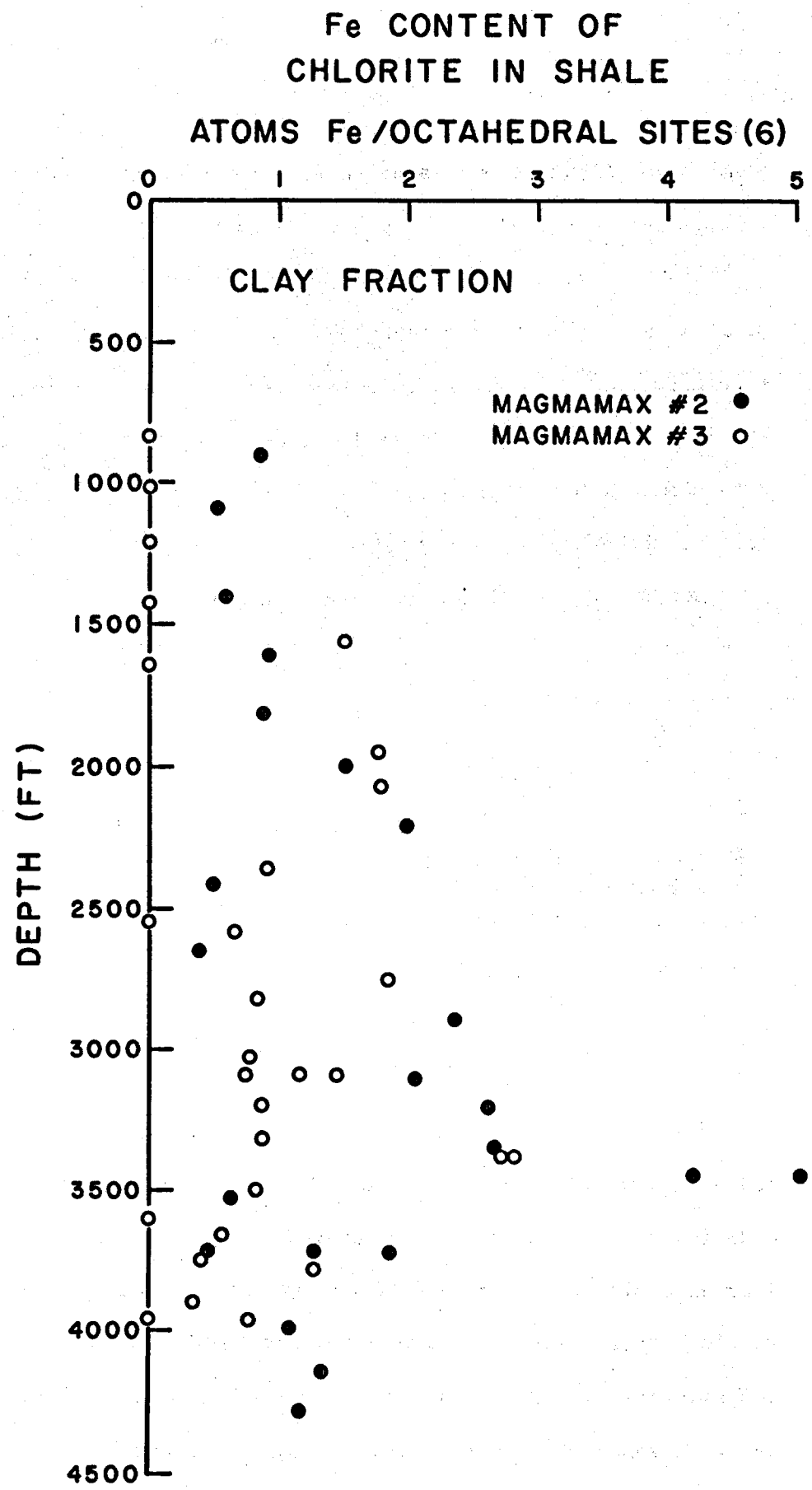
Fe CONTENT OF
CHLORITE IN SHALE
ATOMS Fe / OCTAHEDRAL SITES (6)
0
1
2
3
4
5
CLAY FRACTION
MAGMAMAX #2
MAGMAMAX #3
DEPTH (FT)
500
1000
1500
2000
2500
3000
3500
4000
4500

Figure 32

general, chlorite is being progressively replaced by mica within the green shales.

Authigenic biotite is forming in green shales below 3250' in Magmamax #3 and 3400' in Magmamax #2. The biotites are large (up to 2 mm), euhedral tablets generally oriented parallel to the bedding. The biotite is partially contemporaneous with epidote and anhydrite formation.

Associated with the neo-crystalline micas is a montmorillonite-like clay. The clay is expandable, and diffractograms before and after glycolation are shown in Fig. 33. The montmorillonoid is present in the clay fraction of green shales below 3500' in Magmamax #3 and 3700' in Magmamax #2 (Figs. 19 and 21). The abundance of the montmorillonoid never exceeds 2%.

Although montmorillonites are generally considered to be low temperature clays (Brown, 1961), de Segonzac (1970) notes that montmorillonite has been identified in other metamorphic rocks and attributes their presence to local, very special geochemical conditions or to late hydrothermal phenomena. Experimental studies have shown a close relationship between composition and thermal stability (Sand and others, 1957). Sodium montmorillonites with high Mg/Al ratios are stable up to 750°C (Ames and Sand, 1958). The interval containing the montmorillonite is characterized by albite and by magnesium-rich minerals such as talc, tremolite, chlorite, and biotite; hence, the montmorillonite is probably sodium and magnesium-rich.

Talc was identified only in diffractograms of the clay fraction of shales from 3600-3800' in Magmamax #3. This internal contains abundant and presumably impermeable gray shale.

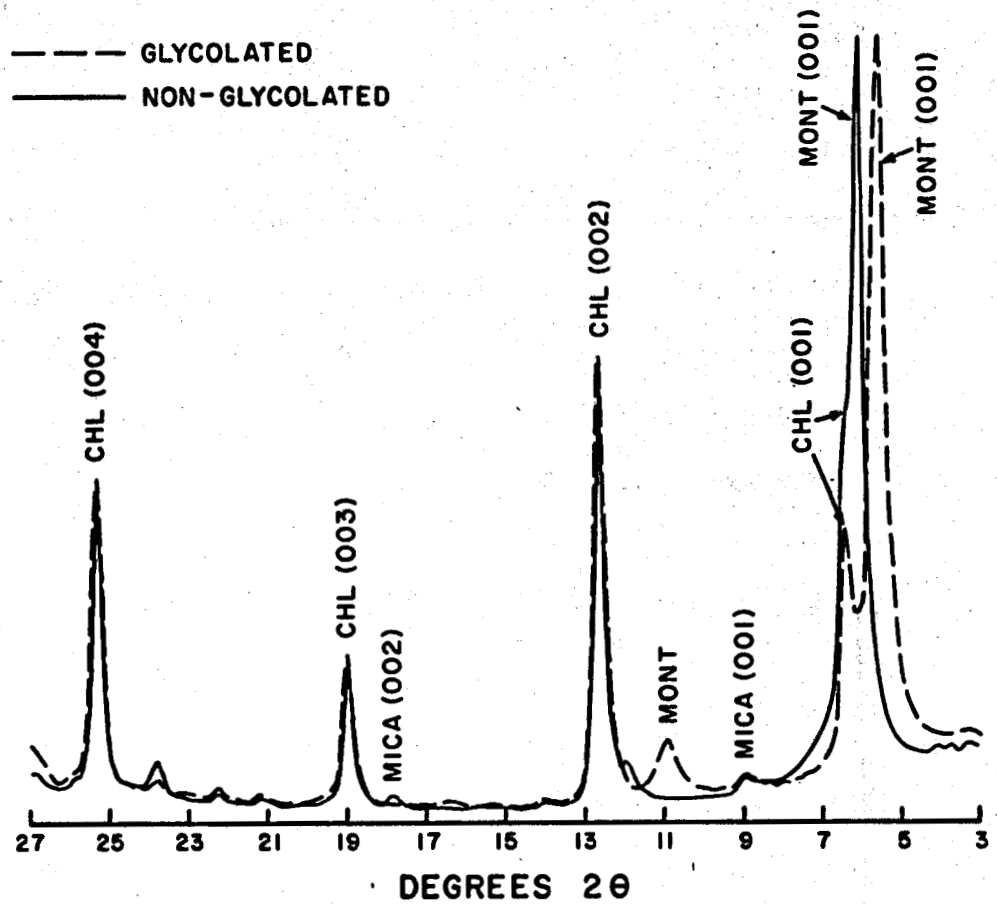

Figure 33. Diffractogram of shale from 3790-3820' in Magmamax #3 showing the shift in the 17 Å (001) peak after glycolation which is diagnostic of montmorillonite.

The following is a summary of changes in phyllosilicates with increased depth: Detrital kaolinite and mixed layer clays are transformed into chlorite above 1500'. The mica/phyllosilicate ratio of tan, red, and gray shales above about 3000' is approximately constant due to the stability of mica below about 300°C. Gray shales below about 3000' show a progressive decrease in the mica/chlorite ratio due to alteration of detrital mica to chlorite. The recrystallized chlorite in green metashales is progressively altered to fine grained muscovite and biotite porphyroblasts with increased depth. The iron liberated in the breakdown of chlorite is converted into pyrite and epidote.

RELATIONSHIP BETWEEN GRAY AND GREEN SHALES

Green shales first appear at 3250', 2800', and 2100' in Magmamax #2, #3 and Woolsey #1, respectively. Below these depths, both gray and green shales co-exist, with variable relative abundances. Gray shales are rare below 3550' in Magmamax #2. Although the shales here have been categorized as either gray or green shales, there are a wide variety of colors gradational between gray and green. Generally, the shale colors are more gradational in those intervals where the abundances of gray and green are subequal than in intervals consisting primarily of only one shale type. The colors become less gradational and more distinct toward the bottom of the wells. The gradations in color seem to predominantly reflect variations in the abundance of chlorite (and epidote?), and hence gradations in the degree of metamorphism.

Green shales begin to appear at about the same depth at which sandstones begin to be mineralized by epidote and adularia. Gray and green

shales share the same alteration and mineralization trends, but the changes occur at shallower depths in the green shales. For example, calcite is very rare and is present only in the shallowest green shales; in gray shales the calcite content decreases with increasing depth, but disappears only near the bottoms of the wells. Metamorphic minerals such as anhydrite and epidote are more abundant in green shales. The inference is that gray shales are the less altered counterparts of green shales.

Magmamax #2 shows a general trend of decreasing gray shales and increasing green shales downhole. This pattern is consistent with a progressive metamorphism of gray to green shales with increasing temperature. Magmamax #3 shows the same basic trend of increased abundance of green shales with depth, but gray shales continue to persist in abundance down as deep as 3800'. In Magmamax #2 and Woolsey #1, gray shales coexist with green shales for only 200-300'; in Magmamax #3, the shales coexist for 1000'.

There is an excellent correlation between the relative abundance of gray shale and the bulk lithology of the interval. Where sandstones are rare or lacking, gray shales are more abundant. For example, in Magmamax #3 sandstones are virtually absent from 3600-3800'; the interval 3650-3800' contains virtually no green shales, only gray ones. Sandstones are also rare from 3050-3100' and 3150-3300'; these intervals also have abundant gray shales.

Since sandstones have a higher original permeability than shales, intervals with abundant sandstone have had more water circulation than

all-shale areas. Shales in the sandy intervals are more highly altered due to water circulation in the adjoining sandstones. Cuttings often show that shales bordering sandstone beds are greener than shales farther away. The conclusion is that gray shales are found in zones of low permeability where minerals persist outside their stability ranges due to the lack of water circulation.

In summary, there is a general trend of progressive alteration of gray shales to green shales with increasing depth and temperature. However, superimposed on this basic pattern is the effect of local low permeability which preserves otherwise unstable assemblages within the gray shales. Magmamax #3 has many zones of abundant gray shale below 2800' where green shales first appear. Magmamax #2 has few comparable zones of gray shale. The inference is that zones of local impermeability have more effect on the mineralogy of shales in Magmamax #3 than in Magmamax #2.

SUMMARY

The paragenesis of mineralization in shales is illustrated in Fig. 34. The diagram shows both the sequence of mineral deposition over time and the changes in mineral stability with increased temperature. In the first 2000', kaolinite and mixed-layer clays are replaced by chlorite, and dolomite is gradually replaced by calcite; gypsum dehydrates to anhydrite which is partially replaced by pyrite pseudomorphic after marcasite. In the interval 2000-3500', the major mineralogical change is that epidote patches replace calcite. The mica/chlorite ratio is constant down to about 3200' where chlorite begins to recrystallize

Figure 34

SHALE PARAGENESIS

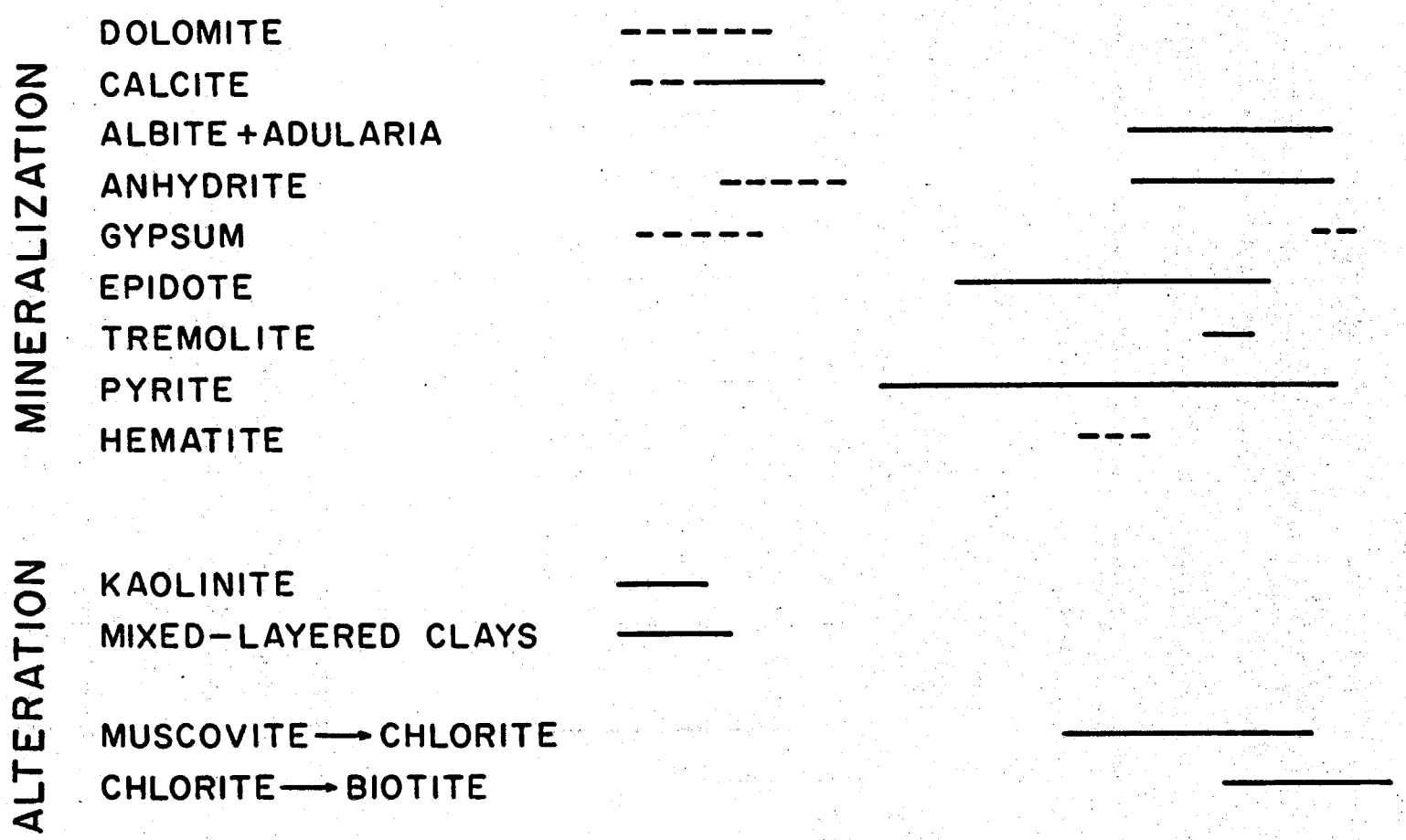

from detrital mica. Below 3500' biotite and muscovite(?) replace chlorite within green shales. Anhydrite and pyrite, as well as epidote, develop within shales. Minor tremolite and hematite are present. The abundance of epidote and pyrite patches, and anhydrite porphyroblasts produces a generally "spotted" fabric; the meta-shales could reasonably be termed "spotted hornfelses".

The different shale colors are produced by the differences in mineralization of the shales. The red color is a product of the higher iron oxide content. The purple tint of the purple-gray shales is produced by finely disseminated specular hematite and earthy hematite. Abundant chlorite, and to a lesser extent epidote, causes the green color.

The green shales differ from the gray shales mainly by the lack of calcite, higher chlorite and anhydrite contents, slightly higher epidote abundance, and the presence of large biotite porphyroblasts in the green shales. Green shales are the metamorphosed counterparts of gray shales. There is a general trend of progressive alteration of gray shales to green shales with increasing temperature. However, superimposed on this basic pattern is the effect of local permeability. Gray shales are present in zones of low permeability where minerals persist outside their normal stability ranges due to insufficient water circulation.

Fracture Mineralization

The eight major vein minerals are calcite, adularia, anhydrite, gypsum, epidote, tremolite, pyrite, and hematite. The relative abun-

dances of these minerals throughout the three wells are illustrated in Figs. 24-26. Minor fracture minerals include: sphene, chalcopyrite, sphalerite, and garnet. Fluid inclusions are common, but were not investigated. The mineral associations seen in multi-mineral veinlets are also shown on the figures. Nearly all the mineralized fractures are within shales, with about 75% of them oriented parallel to the bedding. Veinlets range in width from .005 to 3mm. Only in cuttings from the fault zone at 2700' in Magmamax #2 are there remnants of potentially much wider veinlets.

MINERAL ASSEMBLAGES

The mineral occurrence and mineral association data can be interpreted as three major vein mineral assemblages, each with a distinct downhole range.

Calcite. The first, and shallowest mineral zone is characterized by calcite veinlets and extends from about 1600' down to 2300' in Magmamax #2 and 2600' in Magmamax #3. Within this zone, veinlets are quite rare, and almost all are composed entirely of calcite. Epidote or pyrite veinlets are extremely rare.

The calcite veinlets are almost always in gray shales. Veinlets rarely exceed 2 mm in width and usually have a cockscomb fabric of tiny crystals growing in from the walls; some veinlets are recrystallized into a solid, optically-continuous mass. Vein calcite from all three wells have been analyzed to determine their oxygen and carbon isotopic compositions (page 128).

Adularia-epidote-calcite. The second assemblage is characterized by the assemblage of adularia, epidote, and calcite. Pyrite, hematite and

sphene are locally abundant. The zone containing this mineral association extends from 2300'-3300' in Magmamax #2, 2600'-3500' in Magmamax #3, and from 1400' to the bottom of the well in Woolsey #1.

In the interval 2690'-2720' in Magmamax #2 the cuttings consist largely of highly brecciated rocks cemented by the assemblage of adularia, epidote, and calcite. There are minor similarly brecciated and healed rocks at 2710-2740' in Magmamax #3. Randall (1974) has inferred a fault at this location in Magmamax #2 based on dipmeter surveys.

Within the brecciated interval there are abundant veinlets. Typically, the open spaces are first lined with euhedral adularia rhombs; epidote needles or laths grow inward from the adularia rims, frequently corroding the earlier adularia. Epidote interstices are sometimes later filled with adularia, but often the interstices are left unfilled. Euhedral sphene and pyrite are quite common. Calcite replaces both adularia and epidote.

Fractures in the interval 2830'-2950' in Magmamax #3 were repeatedly reopened and rehealed; one veinlet had been reopened and healed at least six times. Each time it opened, euhedral adularia formed on the wall rocks, and epidote later partially corroded the adularia and filled the remaining open space. The veinlet reopened each time along the veinlet-wall rock boundary; shale remnants are usually trapped in each new fracture. The repetitive veinlet fabric is suggestive of hydrofracturing during boiling; each time the rocks fractured, the same fluid flowed in and followed the same crystallization path.

Where hematite is associated with epidote, the epidote is often oxidized to a reddish-green, turbid color. Microprobe analyses indicate

that the red epidotes are largely replaced by iron oxides; nearby pyrite is also oxidized.

Epidote-anhydrite-tremolite-pyrite-hematite. The third and deepest mineral assemblage is characterized by epidote, anhydrite, tremolite, pyrite, and hematite; calcite and adularia are locally abundant. The zone containing this mineral assemblage begins at 3300' in Magmamax #2 and 3500' in Magmamax #3, and extends to the bottoms of the wells.

Epidote-anhydrite veinlets are common. The minerals are partially contemporaneous, and replace each other. Sixteen vein epidotes were microprobed, and the analyses are given in Table A-II (Appendix I). They range in composition from 23-37 mole percent $Ca_2Fe_3Si_3O_{12}(OH)$.

In the interval 3810-3840' in Magmamax #2, a few rare veinlets contain the assemblage: garnet-epidote-anhydrite-hematite. The garnet has been partially replaced by epidote and anhydrite; hematite was deposited last. The garnet is zoned, and microprobe analyses of two of the zones are given in Table A-IV (Appendix I). The garnet is honey-colored with first order gray birefringence colors. The inner zone has a composition of 74.6% andradrite, 24.3% grossularite, .7% spessartine, and .4% pyrope; the outer zone is 62% andradite, 37% grossularite, .7% spessartine, and .4% pyrope. The basic shift in composition is from high Fe and low Al to high Al and Low Fe. The coexisting epidote in this veinlet was microprobed, and the analyses are given in Table A-II (Appendix I).

Epidote and tremolite are commonly associated. Typically, the fracture is rimmed by epidote, and fibrous tremolite replaces some epidote and fills the remaining open space. Tremolite is virtually

always fibrous, and the fibers are usually aligned parallel to each other and at some angle to the veinlet. Microprobe analyses of tremolite at 3670-3700' in Magmamax #3 are given in Table A-III (Appendix I). The totals are all too low due to epoxy volatization. Compositions range from 18-19 mole percent ferro-actinolite. Calcite occasionally replaces epidote and tremolite.

Anhydrite is commonly associated with pyrite; pyrite is always the later mineral and forms as cubes within anhydrite or as rims enclosing it. Therefore, the normal sequence is to deposit anhydrite under oxidizing conditions, and then to later reduce the sulfur to form pyrite.

In one interval, 4310-4340' in Magmamax #2, the anhydrite-pyrite association was later oxidized. In sandstones, shales, and veinlets in this interval, the earlier anhydrite and pyrite are replaced by a fine grained mixture of calcite and fine grained earthy hematite which replace anhydrite along veinlet margins, between grains, and along cleavage traces. Pyrite cubes are oxidized and there are several hydrated hematite veinlets.

Within this depth zone there are sporadic gypsum veinlets. The gypsum forms honey-colored, drusy aggregates within green shales. There is no evidence of dehydration to anhydrite and the relationship between the drusy aggregates and anhydrite veinlets is unknown. The gypsum was identified by x-raying, and since it occurs as veinlets in green shales it cannot be sloughed from shallower than 3000' where temperatures and salinities are approximately the same. The presence of gypsum veinlets at temperatures greater than 300°C and at salinities

of approximately 250,000 mg/l is anomalous; under these conditions anhydrite is the stable phase (Blount and Dixon, 1973).

FRACTURE MINERALIZATION AND WALL ROCK CHEMISTRY

The mineralogy of veinlets is very closely related to the mineralogy of the surrounding rocks. Intervals where gray shales are relatively abundant have veinlets containing calcite; intervals where green shales are abundant are characterized by anhydrite-bearing veinlets.

This relationship is most apparent in Magmamax #3 where the relative abundance of gray and green shales fluctuates greatly (Fig. 20). Green shales begin to appear at about 2900', and are abundant down to 3100'; in this interval vein calcite is rare. From 3050-3300', gray shales are abundant, and calcite mineralization is present. Green shales gradually replace gray shales in the interval 3300'3650'; no calcite is present and anhydrite is very abundant. Between 3650' and 3800', virtually all the shale is gray; calcite mineralization is abundant, and anhydrite is uncommon. Below 3800', all the shales are green and calcite disappears and anhydrite is abundant.

The relationship between wall rocks and vein mineralization is less apparent in Magmamax #2 because the two shale types coexist only over a short interval. Green shales begin to appear at about 3250'; anhydrite veinlets first occur at about this depth. In the interval 3250-3550', gray and green shales coexist in approximately equal abundance; both calcite and anhydrite veinlets are present. Between 3550' and 4300', gray shales never constitute more than 1% of the total shales; the rest are green. In this interval, anhydrite is very abundant, and the rare

calcite veinlets are found only in intervals with minor gray shales. Below 4300', gray shales are more common, and calcite plus hematite replaces anhydrite in veinlets here.

Woolsey #1 is relatively unmineralized. No anhydrite veinlets were seen. Calcite veinlets are very abundant in the interval 2250-2350' where the shales are mostly gray rather than green.

The question is: why should the relative abundance of calcite and anhydrite veinlets be related to shale color? As discussed earlier, green shales are the metamorphic counterparts of gray shales, and hence intervals where green shales are locally abundant are the most highly metamorphosed zones.

Probably the major differences between gray and green shales are their calcite and anhydrite abundances in both the shale ground masses and in veinlets. Gray shales are characterized by their abundance of calcite and very rare anhydrite; green shales lack calcite and have abundant anhydrite. The pyrite contents of gray and green shales are quite similar; green shales have slightly more epidote. Therefore, veinlet mineralogy is similar to the mineralogy of the wall rocks, with calcite veinlets developing in calcite-bearing rocks, and anhydrite veinlets where anhydrite is stable in the wall rocks.

The mineralogies of all three wells show great variation with depth. As an example, at about 2700' in Magmamax #2 and #3 the mineral assemblage is: quartz + adularia + mica + epidote + calcite + chlorite; at 3900' the assemblage is: quartz + albite + biotite + muscovite + chlorite + epidote + anhydrite + tremolite + pyrite. It is unreasonable

to expect that the waters within these two intervals which deposited many of these minerals would be the same. Helgeson (1969) indicates that the salinity of Salton Sea geothermal fluids increases with depth. Isotopic studies of hydrothermal minerals also suggests that the waters in different horizons are different (page 153).

Petrographic observations suggest that the veinlets were formed concurrently with metamorphism of the rocks. The paragenesis of minerals seen in veinlets and seen in the mineralization of sandstones and shales is almost identical, suggesting that the simplest model for veinlet mineralization might be that the vein minerals were formed from the same fluids which were altering and mineralizing the wall rocks. Therefore, when shales were fractured, fluids within microfractures in nearby rocks flowed into the open spaces and healed them with sequences of minerals similar to those being deposited in the nearby host rocks. In rocks where calcite was present, and presumably metastable, the hydrothermal fluids deposited calcite in fractures. Where anhydrite was stable in the wall rocks, anhydrite veinlets were developed.

This simple model basically implies that all vein waters are locally derived. An alternative model would be that the waters were derived from elsewhere, but mixed with the rock microfracture fluids and reacted with the wall rocks to deposit mineral assemblages similar to those of the enclosing rocks. Both models are geologically reasonable and suggest that the microfracture fluids control the mineralogy of larger veins; there is no evidence to distinguish between them. However, isotopic evidence suggests that most of the water circulation is within

horizontal aquifers, and that vertical fracture flow is relatively unimportant.

SUMMARY

The paragenesis of fracture mineralization is illustrated in Fig. 35. Mineral occurrence and mineral association data can be interpreted as three major vein mineral assemblages, each with a distinct vertical range. The shallowest mineral zone, which extends to about 2400', is characterized by calcite veinlets. The second assemblage consisting of adularia, epidote, and calcite, with locally abundant pyrite, hematite, and sphene extends from about 2400-3400'. The third assemblage is present below 3400' and is composed of epidote, anhydrite, tremolite, pyrite, and hematite with occasionally abundant calcite and adularia; garnet is rare.

The mineralogy of veinlets is very similar to the mineralogy of the wall rocks. Where local impermeability has preserved lower temperature mineral assemblages in shales, the associated fractures are filled with approximately the same mineral assemblages. Vein mineralization appears to have been concurrent with metamorphism of the rocks. The parageneses of fracture and shale mineralization are very similar. Since the major fluid circulation within the rocks appears to be within horizontal aquifers, the fracture fluids are likely to be locally derived from the enclosing shales.

Figure 35

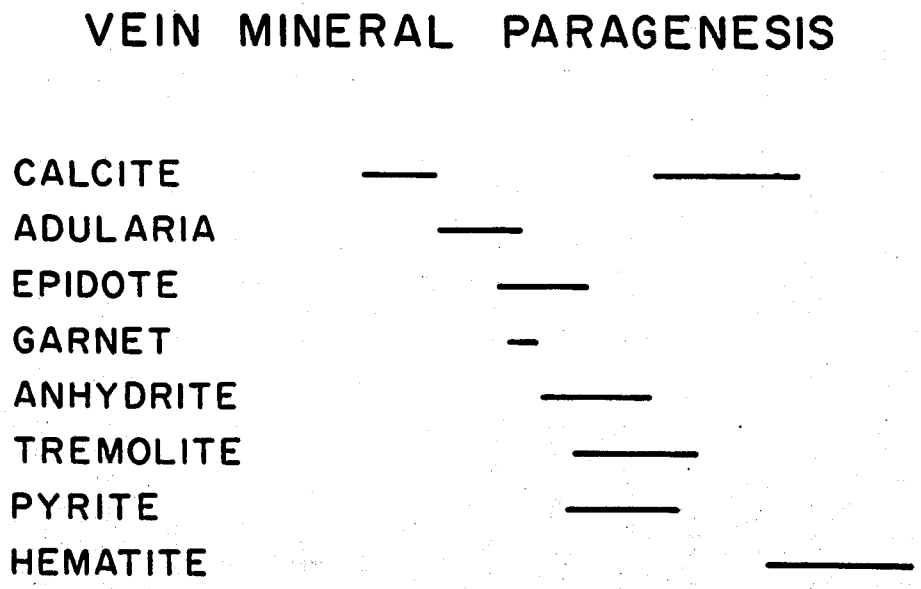
VEIN MINERAL PARAGENESIS
CALCITE
ADULARIA
EPIDOTE
GARNET
ANHYDRITE
TREMOLITE
PYRITE
HEMATITE

DISCUSSION AND CONCLUSIONS

The mineralization and alteration of sandstones, siltstones, shales, and veinlets have been discussed independently, and the conclusions summarized at the end of each section. The rocks show a very distinct vertical mineral zonation; hydrothermal reactions occur within discrete intervals. Differences in original sediment composition, permeability, and water chemistry result in slightly different mineralization and alteration of the various rock types. The presence and abundance of minerals is strongly controlled by the matrix content of the rocks; the impaired permeability of argillaceous rocks impedes water circulation and hence slows reaction rates. Therefore, metamorphic mineralogy is strongly affected by permeability. Although there is a general progressive metamorphism with increased depth, superimposed on this basic pattern is the effect of variations in permeability. Mineral assemblages in zones of low permeability persist outside their normal stability ranges due to insufficient water circulation. Vein mineralization appears to have been concurrent with the metamorphism of the rocks; the parageneses of minerals in the metasediments and the veinlets are very similar. The mineralogy of fractures is very closely related to the mineralogy of the enclosing wall rocks. Fluids within the fractures are probably locally derived from the enclosing shales.

The petrologic differences among Magmamax #2, #3, and Woolsey #1 have been discussed in previous sections. Figures 36 and 37 summarize the differences in bulk mineralogy of the wells and provide a simple means of comparing the wells by ignoring the effect of lithology. The

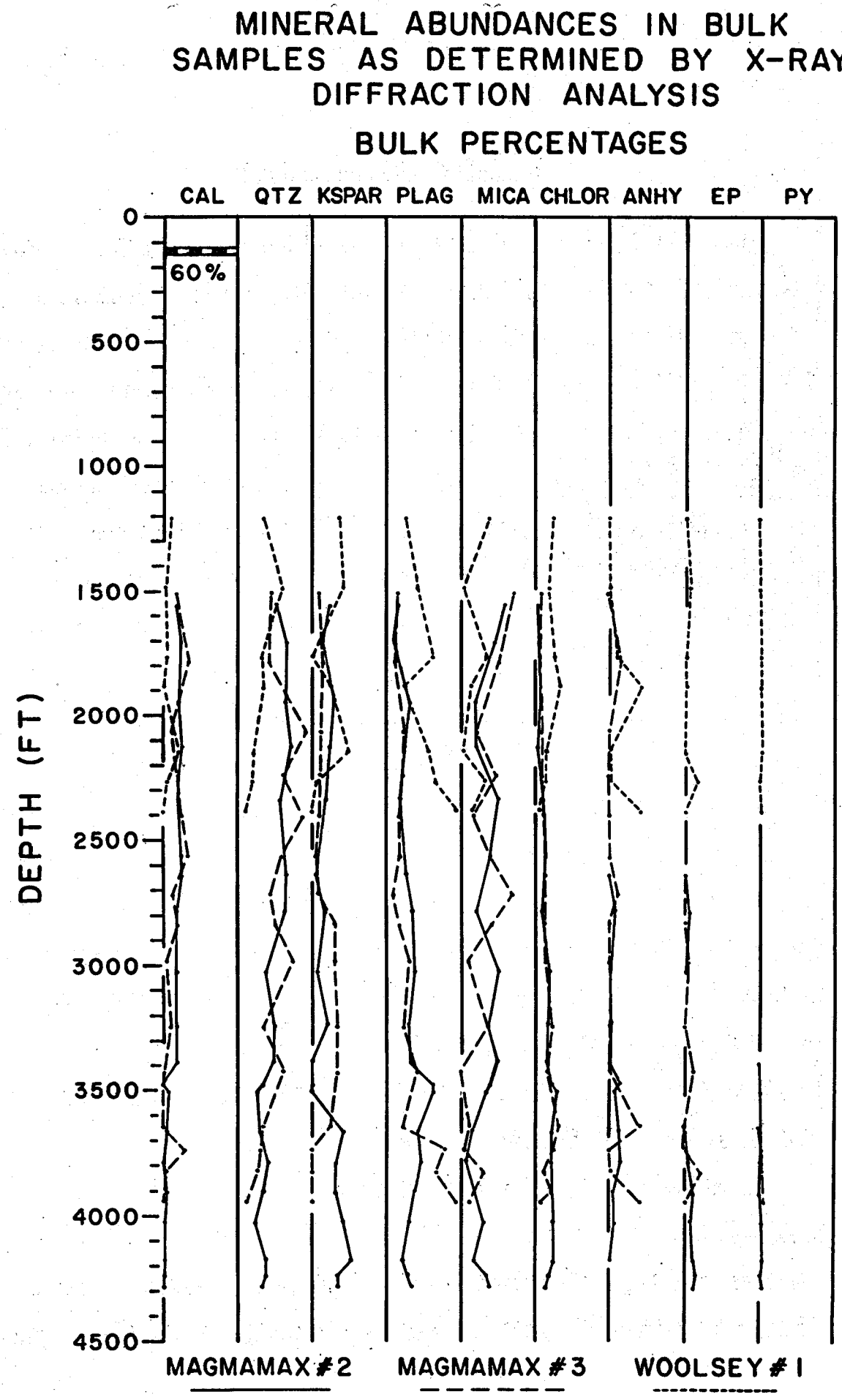
MINERAL ABUNDANCES IN BULK SAMPLES AS DETERMINED BY X-RAY DIFFRACTION ANALYSIS
BULK PERCENTAGES
CAL
QTZ
KSPAR
PLAG
MICA
CHLOR
ANHY
EP
PY
60%
DEPTH (FT)
0
500
1000
1500
2000
2500
3000
3500
4000
4500
MAGMAMAX #2
MAGMAMAX #3
WOOLSEY #1

Figure 36

MINERAL ABUNDANCES IN CLAY FRACTION AS DETERMINED BY X-RAY DIFFRACTION ANALYSIS

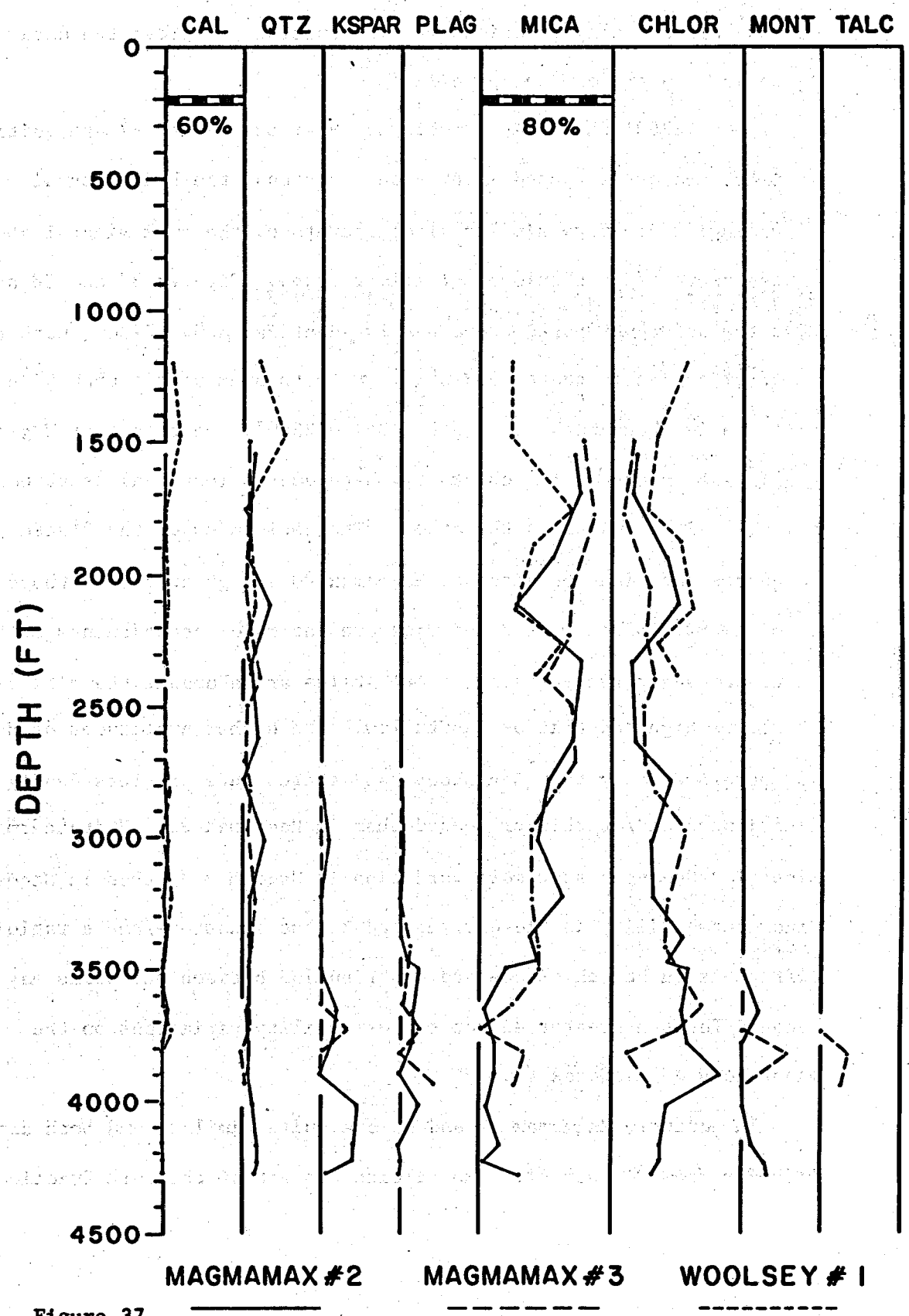

Figure 37

mineral abundances shown were determined by x-ray diffraction analysis of the bulk and clay fractions of bulk cuttings samples; the data are given in tabular form in Appendix II.

Above 2700' the stratigraphies of Magmamax #2 and #3 are quite similar, and as discussed in previous sections, the hydrothermal mineralogies are very similar also; therefore, the bulk mineral abundances above 2700' should be closely related. Figures 37 and 38 show that the abundances are indeed nearly identical above 2700', with two major exceptions: quartz and mica. Both these minerals show wide fluctuations in abundance with depth. Below 2300', the trends of Magmamax #2 and #3 are inverses of each other; where quartz (or mica) is abundant in one well, it is minor in the other. The amplitudes of the fluctuations in quartz and mica abundance of Magmamax #3 are greater than those of Magmamax #2. Since quartz and mica are the major constituents of sandstone and shale respectively, where shales are abundant the mica content should be high and that of quartz low. The higher amplitudes of Magmamax #3 therefore imply that sandstones and shales here are less evenly distributed and/or thicker bedded than in Magmamax #2. Hydrothermal mineral abundances show more variation in Magmamax #3 than in Magmamax #2. Since permeability is closely related to the sandstone/shale ratio, the difference in bed thickness and distribution between the wells may account for the greater effect of permeability variations on the mineralogy of Magmamax #3.

In general, Magmamax #2 and #3 are quite similar, and both differ markedly from Woolsey #1. The calcite content of the bulk fraction

of Woolsey #1 samples is considerably lower and that of the clay fraction higher than in Magmamax #2 or #3; thin section observations indicate that in general Woolsey #1 rocks contain more calcite than the other wells. Quartz is generally much less abundant in Woolsey #1 than in the other two wells although sandstones are more common in Woolsey #1. The decrease in quartz abundance with depth is due both to a decrease in sandstone content and to quartz replacement. The high feldspar and low quartz contents of Woolsey #1 suggest that the abundant authigenic feldspar seen in thin section (Figs. 11 and 12) is replacing large amounts of quartz. Chlorite, epidote, and anhydrite are all much more abundant in Woolsey #1 than at the same depths in Magmamax #2 or #3. The close geographic proximity of the wells makes it unlikely that the difference in mica/chlorite ratio is detrital. The most reasonable explanation is that mica is being recrystallized into chlorite at anomalously shallow depths in Woolsey #1. Epidote and most of the anhydrite are also hydrothermal.

The diffraction study indicates that the whole-rock mineralogical trends of Woolsey #1 are distinctly different from those of Magmamax #2 and #3 at the same depths. In fact, the mineral abundances of Woolsey #1 from 1200-2400' (190-260°C) are generally much more similar to the interval 3000-4200' (310-320°C) in Magmamax #2 and #3 than to 1200-2400'. Green shales are present at 2100' in Woolsey #1, but do not appear until 3200' and 2800' in Magmamax #2 and #3 respectively. Woolsey #1 is presently slightly colder than either of the other two wells, but it is possible that it was once hotter and the mineralization occurred at this time. It is, however, unlikely that the temperature in the interval

1200-2400' in Woolsey #1 was ever as high as the present temperature of the same mineral assemblage in Magmamax #2 and #3. Sandstones are much more abundant in Woolsey #1; permeability may be more important than temperatures in regulating mineralogical changes.

Muffler and White (1969) studied the mineralogies of cuttings from two Salton Sea geothermal wells, IID #1 and Sportsman #1, and one cooler well outside the field, Wilson #1. Their data were derived largely from x-ray diffraction studies of bulk cuttings samples, and may be compared with the mineral abundances determined by x-ray analysis of bulk cuttings from Magmamax #2, #3, and Woolsey #1 as shown in Fig. 36. Unfortunately, their data are given in terms of peak intensities rather than in mineral percentages, so quantitative comparisons are difficult.

Muffler and White (1969) show that ankerite, dolomite, and kaolinite are abundant in shallow rocks but disappear at about 1800' by reacting to form chlorite and calcite. Cuttings above 1200-1500' in Magmamax #2, #3, and Woolsey #1 were not analyzed because the rocks were so poorly indurated that most of the clay was removed during washing. Ankerite, dolomite, and kaolinite are present only above 1100' in Magmamax #2 and #3 shales (Tables I and II).

Below 2000' mineral abundances and distributions in IID #1 and Sportsman #1 are quite similar to those of Magmamax #2 and #3 (Fig. 36). All four wells show an abrupt decrease in calcite in the interval 3000-3500' associated with an increase in epidote abundance, an increase in K-feldspar below 3000', and an increase in chlorite with increasing depth. In IID #1 and Sportsman #1 mica abruptly decreases in abundance

and chlorite increases at about 3500'. Mica and chlorite abundances are much more complicated in Magmamax #2 and #3, with mica apparently replacing chlorite below 3500-4000'. Muffler and White (1969) found only sporadic anhydrite; it apparently is much more abundant in Magmamax #2, #3, and Woolsey #1.

The geothermal wells in the Salton Trough penetrate a sequence of sediments which are being metamorphosed at depth in response to the elevated temperatures and pressures. The metamorphic grade of the deeper rocks has been described as the albite-epidote hornfels facies by Muffler and White (1968) and as low grade greenschist facies by Muffler and White (1969). These two different facies are the appropriate categories for the observed mineral suite in contact and regional metamorphic terrains, respectively. The localized nature of the metamorphism, the presumed relationship with magmatic activity at depth, and the lack of pressure effects suggest that the metamorphic environment is probably more similar to contact than regional metamorphism.

The locations of isograds based on the first appearance of hydrothermal minerals are shown on Fig. 38. The differences in depth between the first appearances of minerals in Magmamax #2 and #3 is largely due to differences in the sandstone/shale ratio, or permeability, between the two wells. Above 2700', Magmamax #2 has the higher sandstone/shale ratio and epidote and adularia are first formed at shallower depths. Below 2700', Magmamax #3 is more permeable, and biotite, albite, and anhydrite are crystallized at shallower depths than in Magmamax #2. Isograds are about 1000' shallower in Woolsey #1, probably due to its

Figure 38

ISOGRADS BASED ON THE FIRST APPEARANCE OF HYDROTHERMAL MINERALS

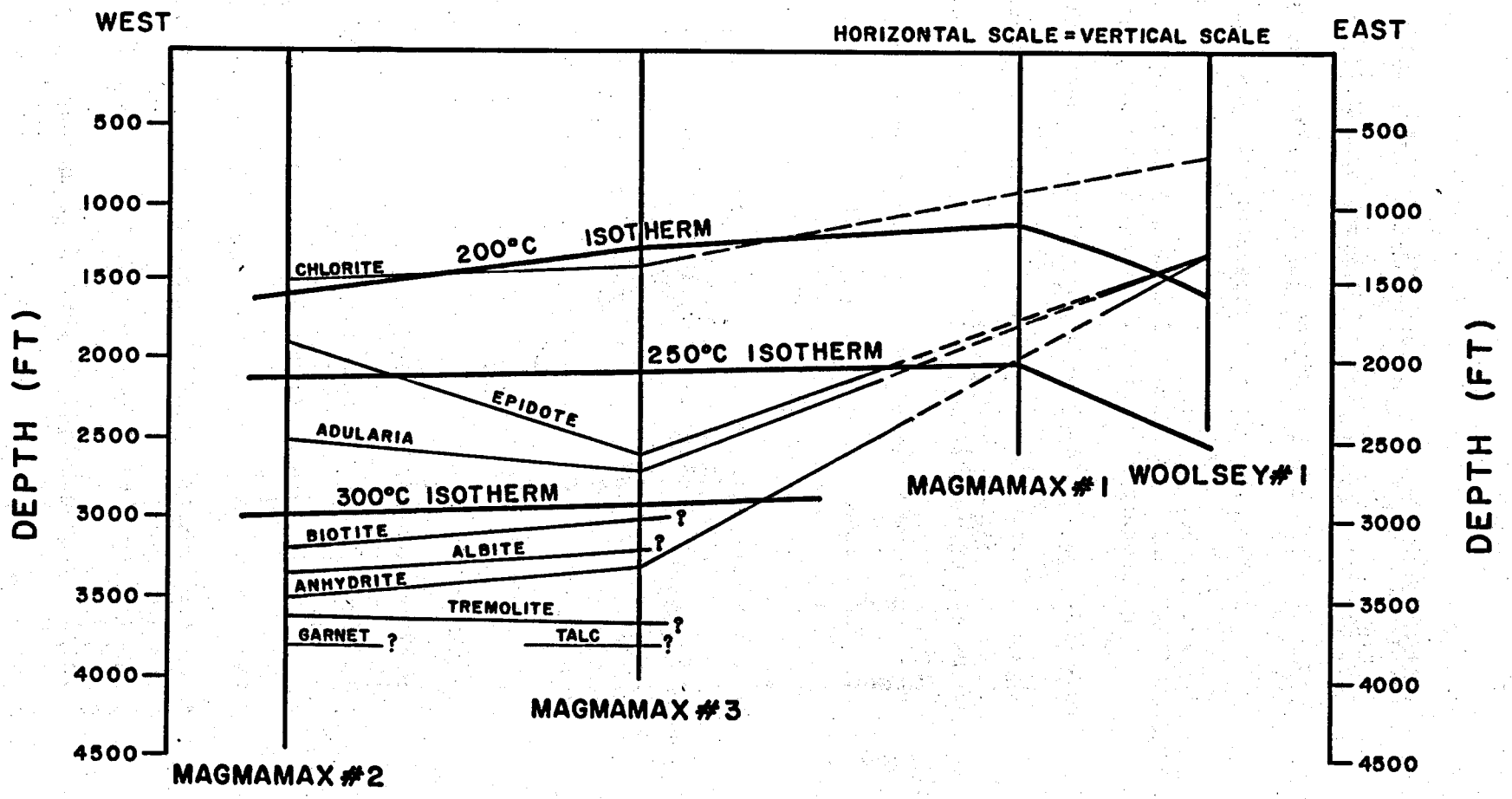

greater permeability. As it is difficult to distinguish between detrital and hydrothermal muscovite, and since there is a continual gradation between hydrothermal illite and muscovite, no muscovite isograd could be drawn.

The mineralogies of the three wells studied show a continuous gradation between a typical sedimentary assemblage of quartz + calcite + plagioclase + K-feldspar + dolomite + montmorillonite + illite + kaolinite plus minor accessories, and a metamorphic assemblage of quartz + albite + epidote + anhydrite + tremolite + chlorite + biotite, with minor hematite, talc, garnet, and pyrite. Figure 39 consists of five ACF diagrams showing the mineral assemblages present at increasing temperatures. Available microprobe analyses (Tables I-IV) were used to locate mineral positions as accurately as possible. There were insufficient data to illustrate variations in the compositions of solid solution minerals with temperature.

Hydrothermal alteration in the interval 25-210°C results in the destruction of the assemblage seen in diagram #1 (Fig. 39) and the formation of that in diagram #2. Chlorite might be formed by a decarbonation reaction such as:

$$\text{dolomite} + \text{ankerite} + \text{kaolinite} + Fe^{+3} \rightleftharpoons \text{chlorite} + \text{calcite} + CO_2$$

with the iron required coming from the iron-rich brine. Potassium metasomatism results in the formation of illite-sericite by the breakdown of montmorillonite, kaolinite, and plagioclase. These reactions precipitate quartz, and release sodium and calcium into solution; some

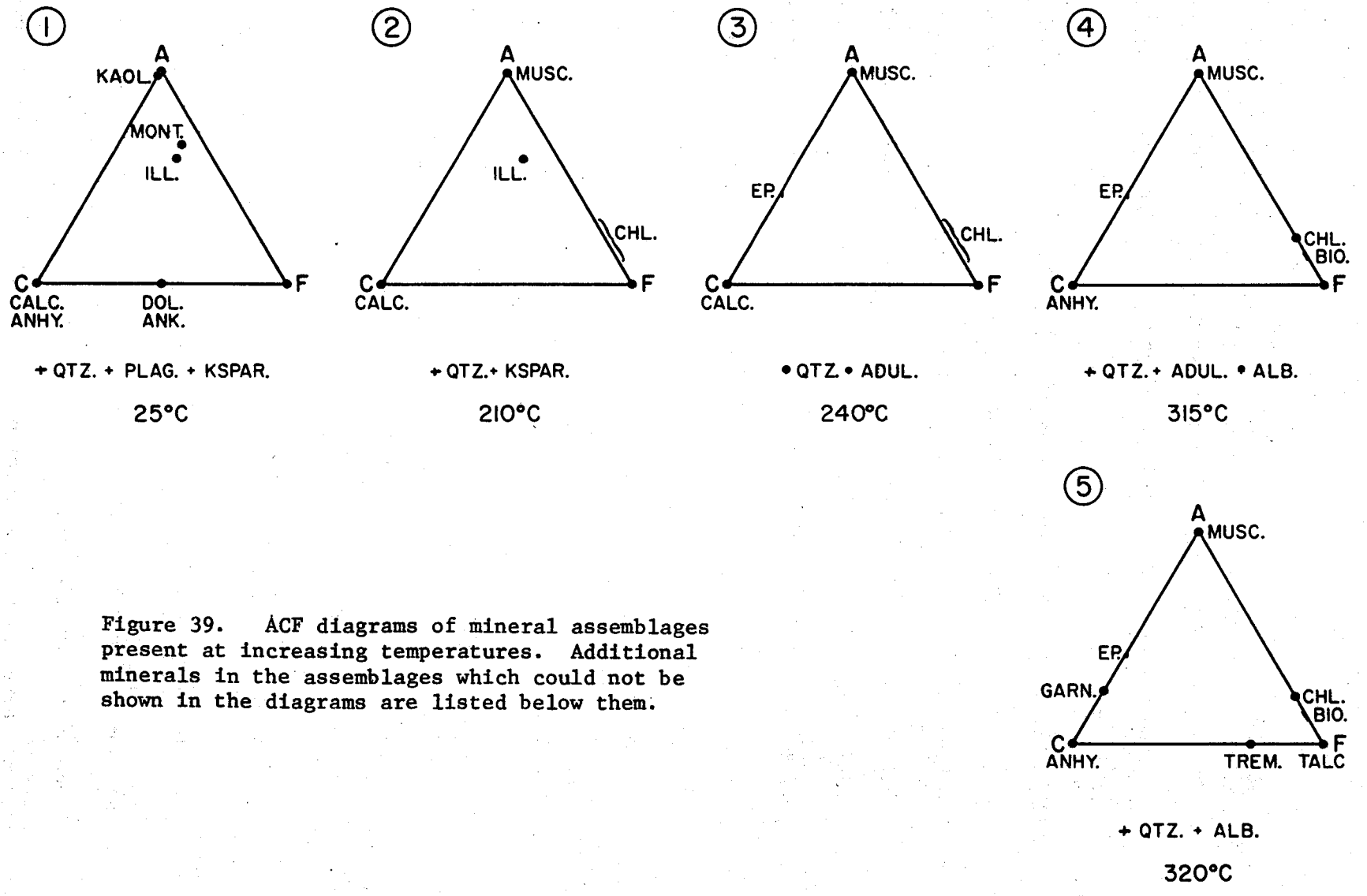

Figure 39. ACF diagrams of mineral assemblages present at increasing temperatures. Additional minerals in the assemblages which could not be shown in the diagrams are listed below them.

of the calcium reacts with bicarbonate and precipates as calcite. The relationship between pyrite and ferric oxides is complex, but in some rocks hydrothermal solutions are capable of reduction reactions such as:

$$\text{anhydrite} + \text{carbon} + \text{ferric oxides (hematite)} \rightleftharpoons \text{pyrite} + Ca^{++} + CO_2$$

Sulfur is also derived from the breakdown of sulfur-bearing organic compounds; organic bands (carbonaceous material) in sandstones are often selectively replaced by pyrite.

The major changes between the mineral assemblages at 210° and 240°C are the disappearance of illite and the formation of epidote and adularia, perhaps by a decarbonation reaction like:

$$\text{illite} + \text{calcite} + \text{quartz} + K^{+} + Fe^{+3} \rightleftharpoons \text{epidote} + \text{adularia} + Mg^{+2}$$

The abundance of epidote in sandstones is clearly inversely related to that of calcite and quartz.

Biotite, albite, and anhydrite are formed in the temperature range 240-315°C, and calcite generally disappears. The abundances of chlorite and mica are inversely related, presumably due to reactions such as:

$$\text{chlorite} + \text{adularia} + S^{-2} \rightleftharpoons \text{biotite} + \text{muscovite} + \text{pyrite} + Mg^{+2}$$

Excess iron is precipitated as pyrite or hematite, depending on local conditions. Adularia and albite coexist in this interval and may form by the breakdown of muscovite:

$$\text{muscovite} + \text{quartz} + Na^{+} \rightleftharpoons \text{adularia} + \text{albite}.$$

Sodium is derived from the brine. The abundances of anhydrite and calcite are inversely related as shown below:

$$CaCO_3 + SO_4^{=} \rightleftharpoons CaSO_4 + CO_3^{=}$$

The reaction is largely controlled by the CO_2 pressure. The brine sulfur content is negligible due to reactions favoring the precipitation of pyrite and anhydrite.

The mineral assemblage at 320°C can be generated by reactions of the following types:

$$\text{chlorite} + \text{calcite} + \text{quartz} + Na^{+} \rightleftharpoons \text{tremolite} + \text{albite} + CO_2$$

$$\text{chlorite} + \text{quartz} + Na^{+} \rightleftharpoons \text{talc} + \text{albite} + Fe^{+2}$$

$$\text{chlorite} + \text{quartz} + Na^{+} + Ca^{+2} \rightleftharpoons \text{talc} + \text{garnet} + \text{albite} + Mg^{+2} + Fe^{+2}$$

These reactions all involve the dissolution of chlorite and quartz, and the addition of sodium. Magnesium released by the breakdown of chlorite is precipitated as talc or tremolite; excess iron may be deposited as pyrite by reducing the sulfur in anhydrite.

Studies of other hydrothermally altered rocks have indicated a relationship between feldspar composition and permeability (Naboko, 1970; Browne and Ellis, 1970). Adularia is deposited in permeable zones, and albite in less permeable horizons. Boiling in permeable beds, by causing a loss of CO_2 and a consequent increase in pH, results in the

deposition of adularia; calcite may also be precipitated. Albite and albitization occur in zones where the CO_2 is still in solution, often below the adularia zone.

In Magmamax #2 and #3, adularia is common in sandstones and veinlets from 2500'-3800', and it typically replaces calcite. Detrital feldspars below 3000' are being albitized. Authigenic albite and adularia coexist in shales below 3500' where they are apparently recrystallizing from K-mica. According to the Saraband computed permeabilities (Fig. 28), the adularia zone is presently more permeable than the deeper adularia-albite zone. Below 2000' carbon isotopic compositions become progressively lighter; this trend could be due to fractionation of carbon isotopes during CO_2 formation and escape (p. 138).

The boiling curve for Magmamax #2 is plotted in Figure 40. The curve was plotted using the .0287 bar/foot hydrostatic gradient measured in Magmamax #2. This is only slightly different from the .0291 bar/ft gradient measured in six other geothermal wells in the Salton Sea field (Helgeson, 1968). The boiling curve for pure water intersects the thermal profile at about 3000' under present conditions.

However, Salton Sea geothermal fluids have salinities as high as 250,000 mg/l (Muffler and White, 1969). Helgeson (1968) indicates that the salinity of the fluids increases steadily with depth to about 3000'; below which it is approximately constant. Salinity elevates the boiling temperature, and the boiling curves for 150,000 and 250,000 mg/l (15% and 25%) NaCl solutions are plotted on Figure 40. The data are from Haas (1971), but are corrected for the observed hydrostatic gradient (Haas uses .0216 bar/ft.).

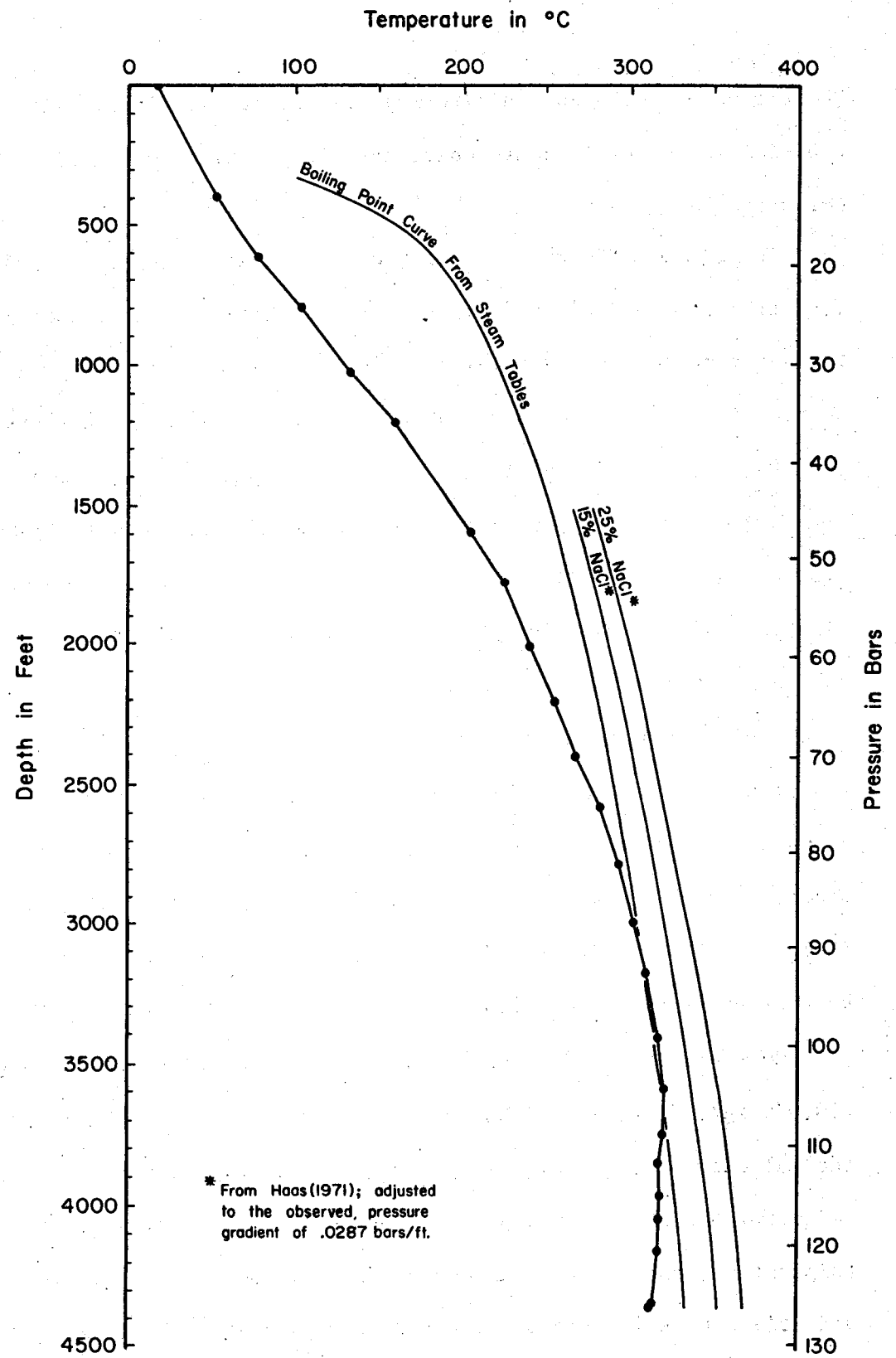

Figure 40. Effect of salinity on the boiling temperature in Magmamax #2. The present temperature profile, and the boiling curves for pure water and for 15% and 25% NaCl solutions are plotted.

The effect of dissolved gases on the boiling curve of Magmamax #2 is negligible. The calculated values for P_{CO_2} and P_{H_2S} at 112 bars (319 C) are .61 and 1012 bars respectively (Truesdell and Singers, 1971). Therefore, the dissolved gas content lowers the vapor pressures by only .62 bars. At Broadlands where the P_{CO_2} is calculated to be 11 bars at 261°C (Truesdell and Singers, 1971), the effect of dissolved gas far outweighs the effects of dissolved salts.

Figure 41 shows that the brine is not boiling under present conditions. However, the adularia may have been deposited during an earlier episode of boiling, or perhaps feldspars were formed by some other mechanism.

Variations in the relative abundance of calcite and anhydrite closely parallel fluctuations in the sandstone/shale ratio. The higher the sandstone/shale ratio, the greater the hydrothermal alteration, and the more anhydrite present. The dissolution of calcite in the more premeable rocks and its replacement by anhydrite is apparently due to a change in the $CO_3^{++}/SO_4^{=}$ ratio for a given Ca^{++} activity. There is a vague correlation of carbon isotopic composition and anhydrite/calcite ratio (p. 146) which is consistent with greater CO_2 escape in intervals where abundant anhydrite has been deposited.

Due to gradational nature of the contact between sedimentary and metasedimentary rocks, it is consequently difficult to decide where to establish a boundary between sandstones, siltstones, and shales, and their metamorphic equivalents--granofels and hornfels. Metamorphic textures and mineralogies develop at different depths in different rock types, so a sandstone with a metamorphic mineralogy is often found at

shallower depths than a typically sedimentary shale. The rocks above 2000' are definitely sedimentary; if one wanted to establish a contact, it should probably be located within the interval 2000-3000' in these three wells. There are several reasonable criteria that one might use for establishing the onset of metamorphism: first appearance of epidote, coexistence of both epidote and adularia, transformation of gray to green shales, breakdown of detrital clays to form chlorite, or disappearance of calcite.

STABLE ISOTOPE GEOCHEMISTRY

Stable isotope studies in active geothermal areas have provided important information about present and past mineralization temperatures, about the existence of equilibrium or non-equilibrium among coexisting minerals and about the origin, nature, and quantity of hydrothermal fluid involved in water-rock interactions (Taylor, 1968). If temperatures are sufficiently high there is oxygen isotope exchange between the water and country rock, resulting in a depletion in O^{18} in the country rocks concurrent with an enrichment in the hydrothermal fluid (Craig, 1966). This report describes the results of an investigation similar to the study of River Ranch #1 by Clayton and others (1968) in that it concentrates primarily on changes in oxygen and carbon isotopic composition of host rocks as a result of interaction with hydrothermal brines.

METHODOLOGY

Notation and Terminology

Isotopic analyses are reported in the δ notation which is the deviation in parts per thousand (permil, or $^{o}/oo$) of the isotope ratio of the sample from that of a standard. Oxygen analyses in this study are

reported relative to Standard Mean Ocean Water (SMOW) (Craig, 1961b). Carbon analyses are reported relative to the Chicago Pee Dee Belemnite (PDB) standard (Epstein and others, 1951; Craig, 1957). Letting $R = (O^{18}/O^{16})$

$$\delta O^{18} = \left[\frac{R(\text{sample})}{R(\text{standard})} - 1\right] \times 1000$$

δC^{13} is similarly defined in terms of the C^{13}/C^{12} ratios of a sample and a standard.

If there is an isotopic fractionation between coexisting phases (A and B) in isotopic equilibrium, the fractionation factor, denoted as α is defined as:

$$\alpha_{A-B} = \frac{R(A)}{R(B)} = \frac{1+(\delta A/1000)}{1+(\delta B/1000)}$$

A useful alternate expression for the fractionation is:

$$\Delta_{A-B} = \delta A - \delta B \approx 1000 \ln \alpha_{A-B}$$

Isotopic Exchange Reactions

Variations in isotopic composition in nature can result from equilibrium or kinetic processes, or from physical processes such as aqueous diffusion or ultrafiltration. Equilibrium processes are of the type:

$$aA + bB^* \rightleftharpoons aA^* + bB$$

where A and B are two substances (such as $CaCO_3$ and H_2O) with exchangeable isotopes. The asterisk indicates a molecule which contains the heavy isotope. Molecules without an asterisk contain the light isotope. The reaction, like any reaction, will proceed toward equilibrium, or toward a configuration of minimal free energy. The equilibrium constant can be written:

$$K = \frac{(A^*)^a (B)^b}{(A)^a (B^*)^b}$$

If all isotopically substituted molecular positions are equivalent, if there is no intermolecular fractionation, and if $\underline{n}$ atoms are exchanged in the reaction:

$$\alpha_{A-B} = \frac{(R)A}{(R)B} = K^{\frac{1}{n}}$$

If the exchange reaction is written such that only one atom is exchanged, $\alpha \approx K$.

Geothermometry

The magnitude of the isotopic fractionation between two coexisting phases is a function of temperature. If the temperature dependence of the fractionation factor is known, the temperature at which the two phases become isotopically equilibrated can be determined from their δO^{18} values.

The possibility of using equilibrium distributions of oxygen isotopes between two or more phases as a geothermometer was first discussed by Urey (1947) who emphasized with fractionation of oxygen isotopes between H_2O and $CaCO_3$. It is not necessary that water be one of the phases used in the geothermometer, nor is oxygen the only element which can be used. What is needed is an accurate calibration of the temperature dependence of the isotope distribution, or fractionation factor, of the phases in question. Such calibrations may be obtained <u>experimentally</u> by equilibrating two phases over the desired temperature range and measuring the isotopic fractionation, <u>empirically</u> by analysis of mineral pairs in rocks equilibrated under known or determinable temperatures, <u>theoretically</u> using spectroscopic and thermodynamic data for each phase, or <u>eclectically</u> by utilizing all available fractionation data.

The calcite-water fractionation equation is the only well-established mineral-water fractionation which has been experimentally studied at both high and low temperatures. The variation of 1000 ln α (calcite-water) is linear with $1/T^2$ between 0 and 500°C. For lack of any experimental evidence to the contrary, other mineral-water fractionations are assumed also to vary linearly on such a plot, and linear extrapolations have been used in this study for constructing isotopic geothermometers for temperatures outside experimental ranges.

Successful application of isotope geothermometry requires that the variation of the isotopic fractionation with temperature be accurately known, and that the phases must have reached equilibrium and maintained

their equilibrium compositions regardless of later temperature changes. In metamorphic and igneous systems, the mineral isotopic compositions are usually "frozen in" at the highest temperature reached (Taylor and Epstein, 1962). Geothermal systems may or may not be the same.

ANALYTICAL TECHNIQUES

Sample Selection

Both carbonates and silicates were selected, analyzed, and plotted on graphs in several batches. The first samples were selected at more or less discrete intervals. Successive samples were selected to elucidate patterns seen in previous plots, or to investigate intervals which were lithologically or mineralogically anomalous.

Virtually no bulk samples were analyzed; almost all samples were handpicked for homogeneity. For example, sandstone chips collected in a particular 30' interval were all of the same color, grain size, and mineralogy; hence all the chips are from the same or very similar types of sandstones. By choosing uniform samples isotopic trends can more easily be correlated with fluctuations in textural and mineralogical parameters. In bulk samples these trends are masked by the superposition of isotopic patterns of other types of grains, and by the relative abundances of different grain types. The major drawback to handpicked versus bulk samples is that many more samples are needed to document the trends of several distinct grain types than to illustrate one bulk trend.

Approximately 175 carbonate samples were collected. These are divided into three distinct groups--cement in shales, cement in sandstones, and calcite veinlets. The characteristics of these samples are listed in Appendix III. The percent carbonate in grains decreases with increased depth and below 3000' calcite is often very rare or absent, making sampling difficult or impossible. Shales generally have more carbonate than sandstones. 10-2000 mg of chips were handpicked for each sample, depending on the type of grain and depth.

Epidote is a common constituent of sandstones, shales, and veinlets below 2500', and 15 samples were analyzed. It was frequently difficult to identify the original lithology of an epidotized grain, but an attempt was made to select grains which appeared to be highly epidote-mineralized sandstones and siltstones. Magmamax #2 and #3 were sampled by handpicking at 100-200' intervals. Approximately 50-200 mg of epidote-rich grains were collected for each sample.

Two distinct types of quartz samples were handpicked and analyzed. The first was a group of 33 sandstones from Magmamax #3, selected at 100-200' intervals. Each sample was homogeneous in grain size, color, and mineralization. All of these sandstones were predominantly cemented by quartz and/or calcite, with minor pyrite, epidote, adularia, or tremolite. The second group of quartz samples were derived from the quartz-rich fractions of the epidote samples. Sample size was 50-200 mg.

Hematite rarely occurred in sufficient amounts for isotopic analyses. Because of the low abundance of hematite, each of the 9 samples analyzed

consisted of hematite in veinlets combined with minor hematite from sandstones in the same interval.

Sample Preparation

Carbonates are very simple to prepare. The chips are ground with a mortar and pestle so that the grains will pass through a 100 mesh (.15 mm) sieve.

The preparation of silicates and oxides involves more elaborate techniques. The purpose of these procedures is to remove all other mineral phases from the desired mineral without utilizing any method which would appreciably alter the isotopic composition of this desired mineral. The techniques used are different for different minerals.

Quartz from sandstones includes both detrital quartz and authigenic overgrowths; samples are disaggregated as gently as possible so as not to pulverize the overgrowths. Boiling for 15-30 minutes in 6N HCl removes carbonate, sulfate, and iron oxide cement (Syers and others, 1968). Depending on the percent of heavy minerals, they may either be handpicked or removed by heavy liquid techniques. Remaining clays, micas, and feldspars are removed by gently boiling in HBF_4 (fluoroboric acid) for 15-30 minutes. The reaction products produced by boiling are easily removed by ultrasonic disaggregation and decanting. The samples are then examined with a binocular microscope or x-rayed to determine purity; minor handpicking is usually necessary. The quartz should be >95% pure.

Epidote and hematite are purified by using heavy liquids. Samples are first ground to pass through the 100 mesh but rest on the 200 mesh; ultrasonic disaggregation is very helpful to break apart minerals. About 50-100 mg of sample is placed in a conical centrifuge tube along with a solution of the appropriate specific gravity. After centrifuging, the tube is partially lowered into a dewar of liquid nitrogen. This freezes the heavy material and allows easy removal of the lighter material before the bottom unfreezes. Repeated separations are usually necessary to beneficiate a sample to >95% pure; minor handpicking is usually necessary. Samples are examined by binocular microscope and/or x-rayed to determine purity.

Techniques of Gas Extraction

Carbon dioxide was evolved from carbonates by reaction with 100% H_3PO_4 (phosphoric acid) at 25°C (McCrea, 1950). Samples from above 2500' in the wells contained both calcite and dolomite-ankerite. These two carbonate species could not be physically isolated for separate extraction, but the gas evolved from the two species could be separated by the differing reaction rates of the carbonates in H_3PO_4 using a modification of the procedure of Epstein and others (1964). The CO_2 evolved during the first hour is almost entirely from the dissolution of calcite, and is collected and analyzed. The CO_2 evolved between 1 and 24 hours is from both calcite and dolomite, and is discarded. The CO_2 evolved between 24 hours and 1 week is collected and analyzed for the δO^{18} and δC^{13} of dolomite. The gas from samples from below 2500'

where dolomite is absent is collected from 1 to 24 hours. In order to reduce fractionation due to isotopic variations in grain size, all samples were crushed as little as possible, and sieved to pass through a 100 mesh sieve (Walters and others, 1972).

The preparation and extraction of silicates and oxides for oxygen isotope analysis is described by Clayton and Mayeda (1963). About 10-20 mg of sample is placed in a dry box for 24 hours. The sample is then loaded into tubes, outgassed, preheated to remove adsorbed water, and reacted with BrF_5 for 9 hours at 550° for quartz, and 650° for epidote and hematite. Oxygen is liberated quantitatively from the mineral and is converted into carbon dioxide by passage over hot carbon catalyzed by platinum. The carbon dioxide is collected, measured, and analyzed for oxygen isotopic composition. If the measured gas yield differs from the theoretical yield by more than 3%, the gas sample is considered suspect.

Mass Spectrometer

The CO_2 from all samples was analyzed for its isotopic composition on a double-focusing, double-collecting isotope ratio mass spectrometer (Coplen, 1973).

Reproducibility of Isotopic Analyses

The average deviation of repeated analyses of a single gas sample on the mass spectrometer is less than .1 °/oo from the mean (Coplen, 1974). Duplicates of each sample were prepared, extracted, and analyzed. If the δO^{18} values of the pair were within .2 °/oo, they were averaged and

plotted. Additional analyses were very rarely required for carbonates, but were commonly necessary for silicates. If the δO^{18} values of the carbonate pair were acceptable, only one sample was analyzed for δC^{13}, because past experience has indicated that δC^{13} values are almost always reproduced to within ± .06 °/oo (Coplen, pers. comm., 1976).

Only one silicate, NBS #28, was prepared, extracted, and analyzed sufficient times to provide data on silicate reproducibility. The mean composition of NBS #28 was 9.03 and the average deviation from the mean was .23 °/oo (Coplen and others, 1975); this standard was interspersed between sample analyses to check the reproducibility of silicate preparation. Small corrections (± .02 °/oo) were made to sample δO^{18} compositions to correct for drift in the composition of NBS #28.

Data Corrections

In the reaction of a carbonate with phosphoric acid, only two-thirds of the oxygen is evolved as CO_2, and an isotopic fractionation occurs. It is thus necessary to apply a correction to the observed isotopic ratio. These corrections, called acid fractionation factors, are defined as:

$$\alpha = \frac{R\ CO_2}{R\ \text{carbonate}} \qquad \text{where} \quad R = O^{18}/O^{16}$$

For calcite and dolomite the factors are 1.01008 and 1.01090 respectively, as modified after Sharma and Clayton (1965). Isotopic compositions were calculated using $\alpha(CO_2 - H_2O) = 1.04112$ (Coplen, pers. comm., 1976). Machine corrections were made after Mook (1968); tail corrections are trivial.

WATER-ROCK INTERACTION

Carbonates

There are at least three different types of carbonate in the reservoir rocks--detrital, diagenetic, and hydrothermal; the relative proportions of these in any sample are variable and generally unknown. Petrographic studies (Figs. 7-17; "Mineral Textures" columns) indicate that with increasing temperature both detrital and diagenetic carbonates recrystallize from micrite to sand-size poikilitic grains. Isotope exchange by solid diffusion is probably minimal, but during recrystallization appreciable exchange can occur between carbonates and brines. Concurrent with recrystallization, additional hydrothermal carbonate was precipitated in isotopic equilibrium with the brine. Therefore, deeper rocks contain a mixture of totally and partially exchanged carbonate. All of the carbonate may be in isotopic equilibrium in horizons where temperatures and permeabilities are sufficient for recrystallization to totally exchange original carbonate.

Results of oxygen and carbon isotope analyses are presented in Appendix III. Figures 41-43 show oxygen isotope data and Figures 46-48 carbon data for calcite and dolomite from Magmamax #2, #3, and Woolsey #1, respectively. The size of the data points approximates the uncertainty in depth (30') and composition (.2 $^{o}/_{oo}$). Analyses of mixed carbonates are also given in Appendix III, but are not plotted.

All carbonate samples were homogeneous and handpicked, and are of three types: carbonate cement in sandstones, carbonate cement in shales,

and vein calcite. Data are sparse below 3000-3500' due to the low abundance of calcite in the host rocks, especially in sandstones.

CALCITE

Oxygen Isotopes. Oxygen in rocks can exchange with the oxygen of the water circulating through the rocks; the effect of this exchange is to enrich the water and deplete the rock in O^{18}. The magnitude of this δO^{18} shift depends on the temperature, degree of equilibrium, δO^{18} of the water and rock prior to isotope exchange, and the ratio of mass of water to rock which depends on permeability.

As shown in Figs. 41-43, the range of δO^{18} for calcite covers 18 °/oo. There is a general decrease in δO^{18} with increasing depth down to about 3000', below which it increases slightly to the bottoms of wells. The variation with depth is most simply interpreted as resulting from variation in the degree of isotope exchange between calcite and water with increasing temperature. Superimposed on this general trend are two lesser patterns: (1) calcite in veinlets is usually lighter (lower ratios of O^{18}/O^{16}) than in adjacent sandstone, and that calcite in shale is heavier; and (2) δO^{18} values show a distinct zig-zag pattern with variable amplitudes.

The pattern of alternating isotope maxima and minima (isotope inversions) is produced by variations in the degree of isotopic exchange between rocks and circulating water. The temperature profiles (Fig. 3) show smooth thermal gradients with no evidence of repeated temperature inversions. It is possible that an earlier thermal regime did have multiple thermal inversions to which the rocks were equilibrated, but

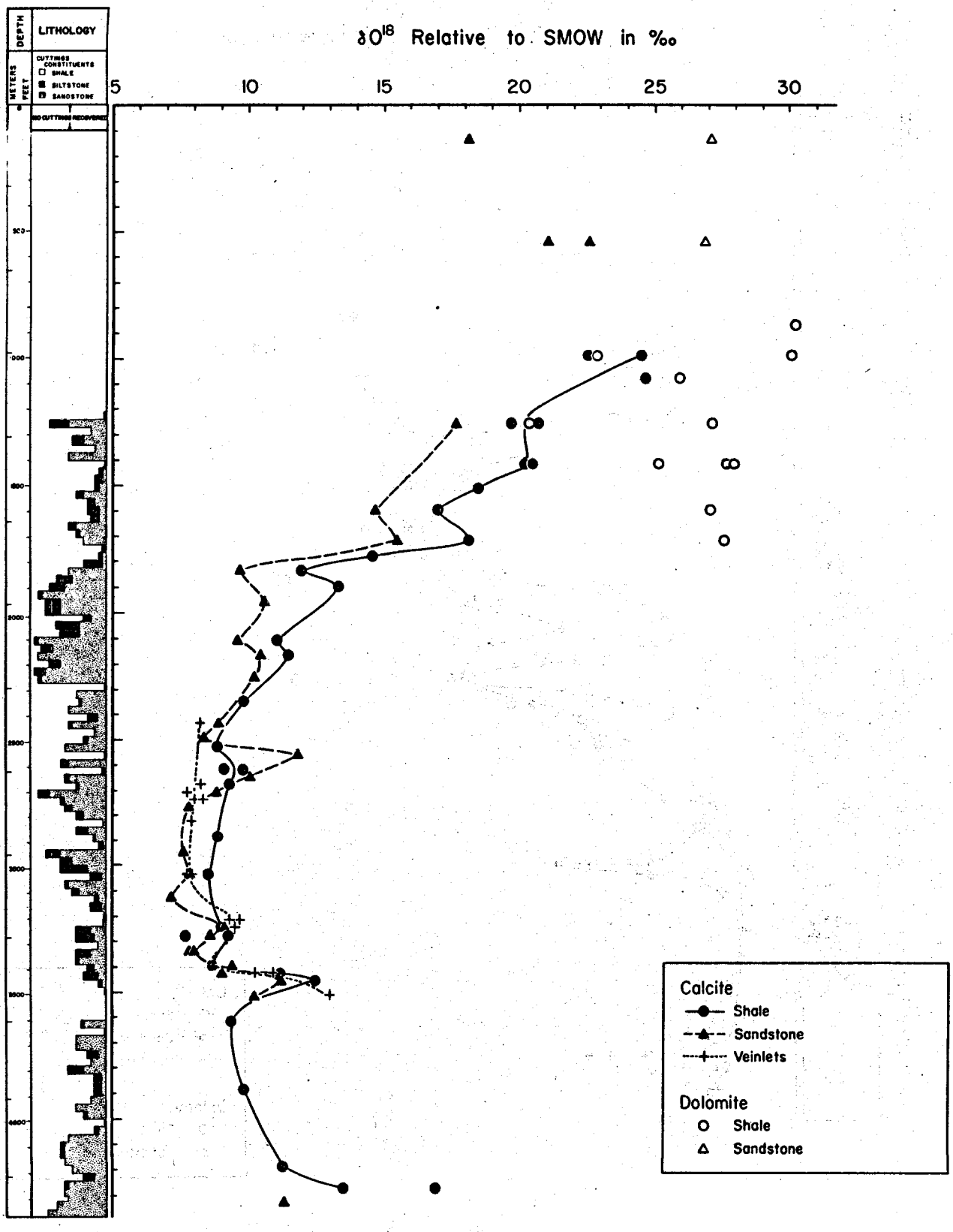
Carbonate in Magmamax #2
δO18 Relative to SMOW in ‰
5
10
15
20
25
30
DEPTH
METERS
FEET
LITHOLOGY
CUTTINGS CONSTITUENTS
SHALE
SILTSTONE
SANDSTONE
NO CUTTINGS RECOVERED
Calcite
Shale
Sandstone
Veinlets
Dolomite
Shale
Sandstone

Figure 41

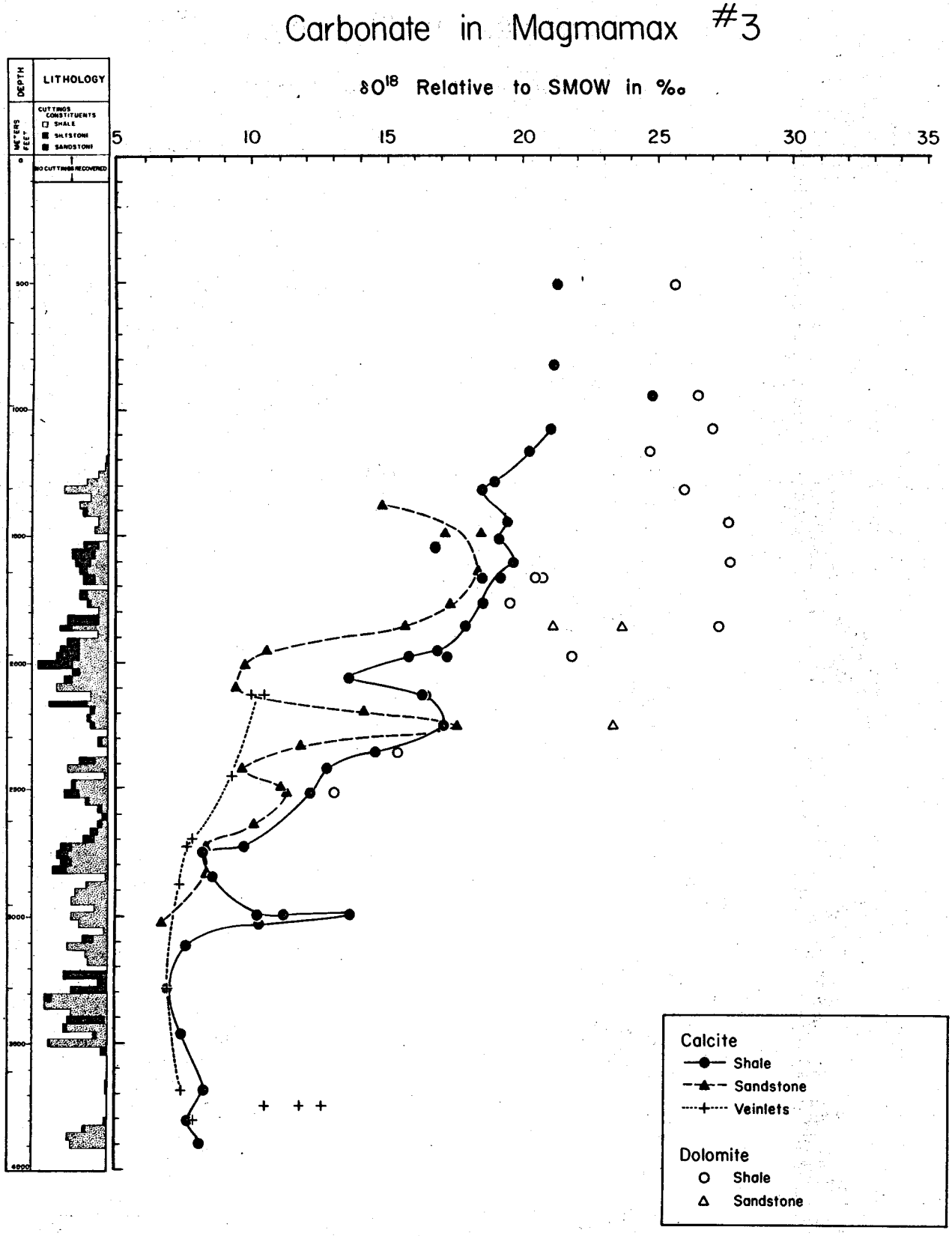
Carbonate in Magmamax #3
δO18 Relative to SMOW in ‰
5
10
15
20
25
30
35
DEPTH
METERS
FEET
LITHOLOGY
CUTTINGS CONSTITUENTS
SHALE
SILTSTONE
SANDSTONE
NO CUTTINGS RECOVERED
500
1000
1500
2000
2500
3000
3500
4000
Calcite
Shale
Sandstone
Veinlets
Dolomite
Shale
Sandstone

Figure 42

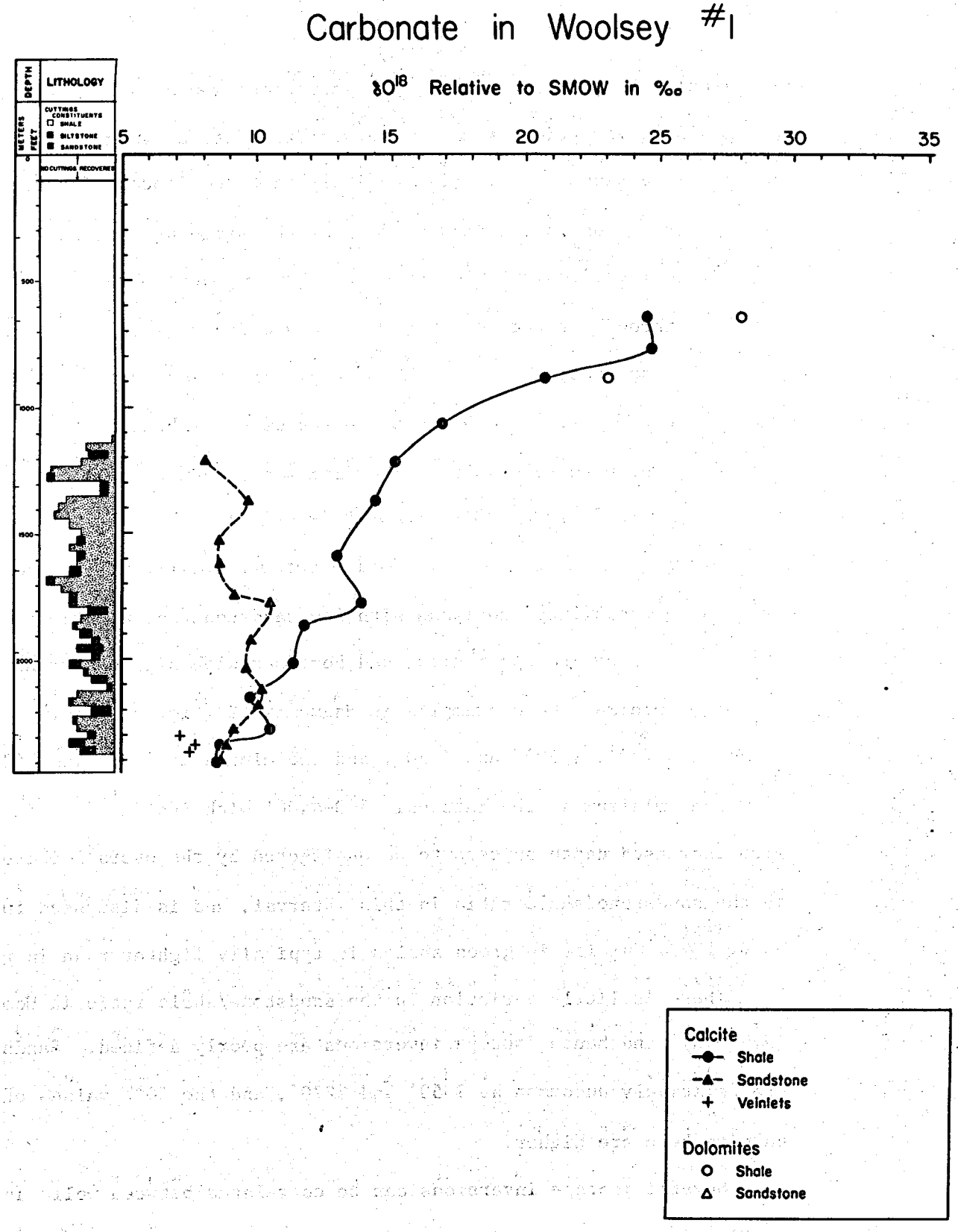
Carbonate in Woolsey #1
δO18 Relative to SMOW in ‰
5
10
15
20
25
30
35
DEPTH
METERS
FEET
LITHOLOGY
CUTTINGS CONSTITUENTS
SHALE
SILTSTONE
SANDSTONE
NO CUTTINGS RECOVERED
500
1000
1500
2000
Calcite
Shale
Sandstone
Veinlets
Dolomites
Shale
Sandstone

Figure 43

it is unlikely that the temperature variations would be as extreme as the 25-100°C variation in only a few hundred feet as suggested by the isotope inversions. It is also unlikely that the isotope inversions are due to variations in the initial δO^{18} of the sediment carbonate; the depositional environment and source of the sediments were approximately constant throughout the section (Merriam and Bandy, 1965). The most plausible explanation is that the multiple inversions are due to variations in permeability and hence to degree of equilibration. The lower the δO^{18}, the more permeable the horizon was. Sandstone calcite is generally 1 to 7 °/oo lighter than shale calcite.

There is an excellent correlation between isotope inversions and original permeability; horizons with low sandstone/shale ratios are characterized by isotope maxima, and horizons with high sandstone/shale ratios by minima. Good examples in Magmamax #2 (Fig. 41) include the maxima at 1720', 2550', and 3450', and the minima at 2100' and 2500'. The broad minimum in the interval 3500-4400' with its increase in δO^{18} with increased depth appears to be unaffected by the overall increase in the sandstone/shale ratio in this interval, and is discussed further on p. 136. Calcite in green shales is typically lighter than in gray shales.

There is little variation in the sandstone/shale ratio in Woolsey #1 (Fig. 43), and hence isotope inversions are poorly defined. Sandstones are relatively uncommon at 1350' and 2270', and the δO^{18} values of calcite here are higher.

Several isotope inversions can be correlated between wells as shown in Fig. 44. No correlations can be made below 2700' where the rocks in

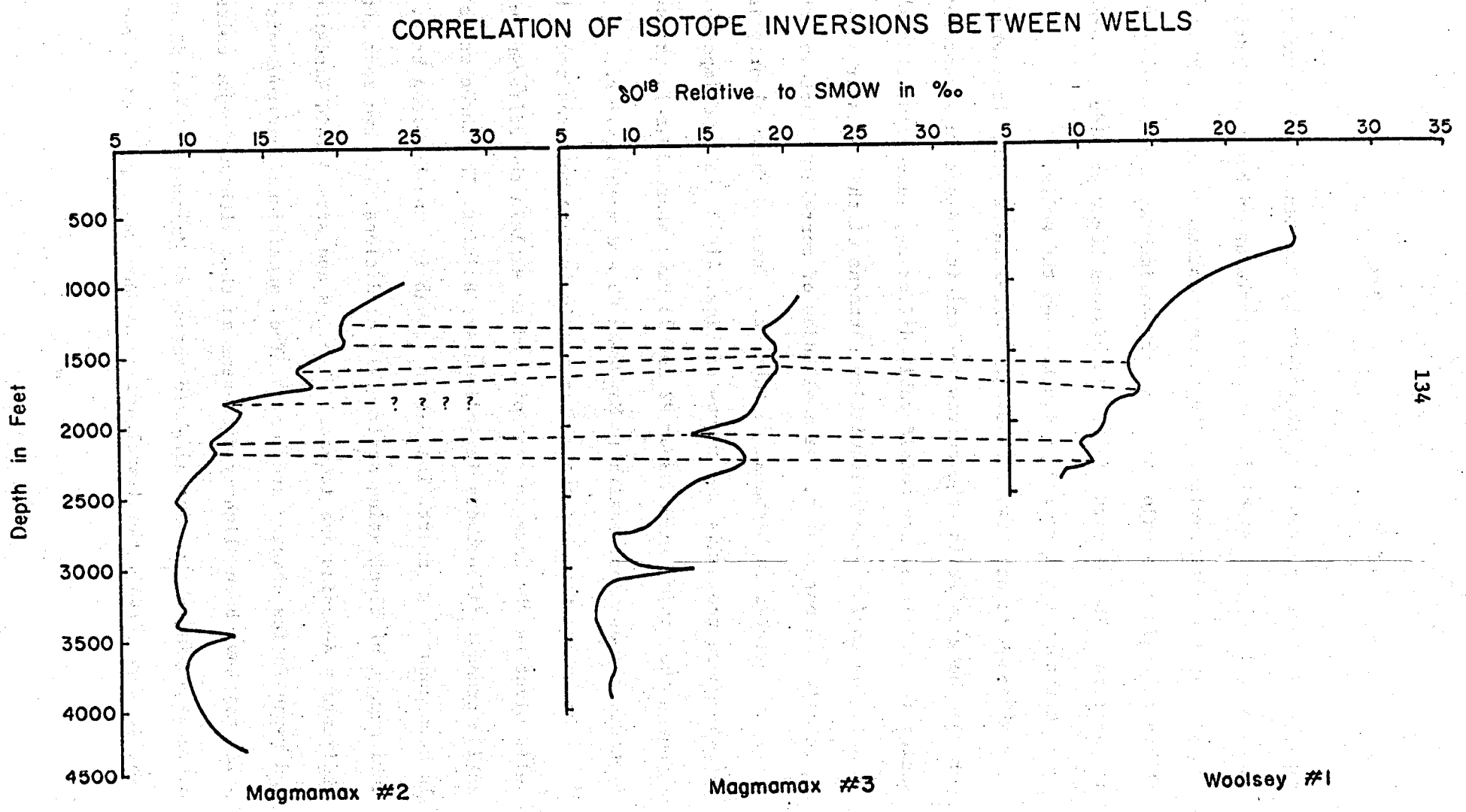

Figure 44. The lines between the isotope profiles show proposed correlations.

Magmamax #2 have apparently been offset by faulting. The correlation between isotope inversions is really a correlation between stratigraphic horizons in the three wells. The strong minimum at about 2000-2100' in all three wells is a major aquifer; the maximum at approximately 2300' is an aquitard. The pattern of δO^{18} inversions hence provides information about horizontal water circulation between the wells.

Although it has been possible to correlate several stratigraphic horizons between wells, the curves for calcite cement in sandstones and shales (Figs. 41-43) are considerably different, suggesting that the lithologies and/or water circulation patterns of the wells are different in detail. In particular, the amplitudes of correlated isotope inversions are greater in Magmamax #3 than #2. This is shown clearly in Fig. 45 where the sandstone curves of Figs. 41-43 are superimposed. Although the minima in Magmamax #2 and #3 have approximately the same isotopic composition, maxima in Magmamax #3 are much heavier.

The explanation for the difference in isotope patterns among the wells might be the same as that offered to explain the different mineralization trends: differences in sedimentary bedding. The three wells are located about 1 km apart. The Salton Trough is, and has long been, an environment of fluctuating sedimentary conditions. The two most common sedimentary deposits are lacustrine shales and stream-laid sandstones, and rapid facies changes are common. The depositional environments of the wells may have been slightly different so that although major units are correlative and the sandstone/shale ratios of Magmamax #2 and #3 are very similar above 2700', the distribution may have been quite different.

If the sandstone and shale beds are thinner and more evenly distributed in Magmamax #2 as discussed earlier (page 105), there would be only a small difference in water flow between the finely interbedded sandstones and shales, and hence only a small difference in the isotopic compositions of adjacent rock types. In Magmamax #3 the beds could be thicker and/or less evenly distributed so that water flow would be restricted to major aquifers, and therefore adjacent rock types would have large differences in isotopic composition. Minor sandstones within large shale beds would be affected by the impermeability of the enclosing shale. Another possibility is that Magmamax #3 might contain more discontinuous sandstone beds which, because of their lack of continuity, have impaired water flow.

Figures 44 and 45 show that above 1800' both the shale and sandstone curves of Woolsey #1 are considerably lighter than those of Magmamax #2 and #3. The higher sandstone/shale ratios of Woolsey #1 in this interval presumably accounts for the greater isotope exchange of the rocks. Data from Magmamax #2 are lighter at shallower depths than in Magmamax #3, reflecting the impaired circulation of the latter well.

Both Magmamax #2 and #3 have broad isotope minima beginning at about 2700' with inversion points at 3100-3300' and below this a gentle increase in δO^{18} with depth. The temperature profiles (Fig. 3) also show that the thermal gradients flatten at about 3000'; therefore, the broad isotope minima are at least partially due to the lower thermal gradients. The increase in δO^{18} below 3300' in Magmamax #3 is probably caused by the increase in shale abundance and hence lower permeability.

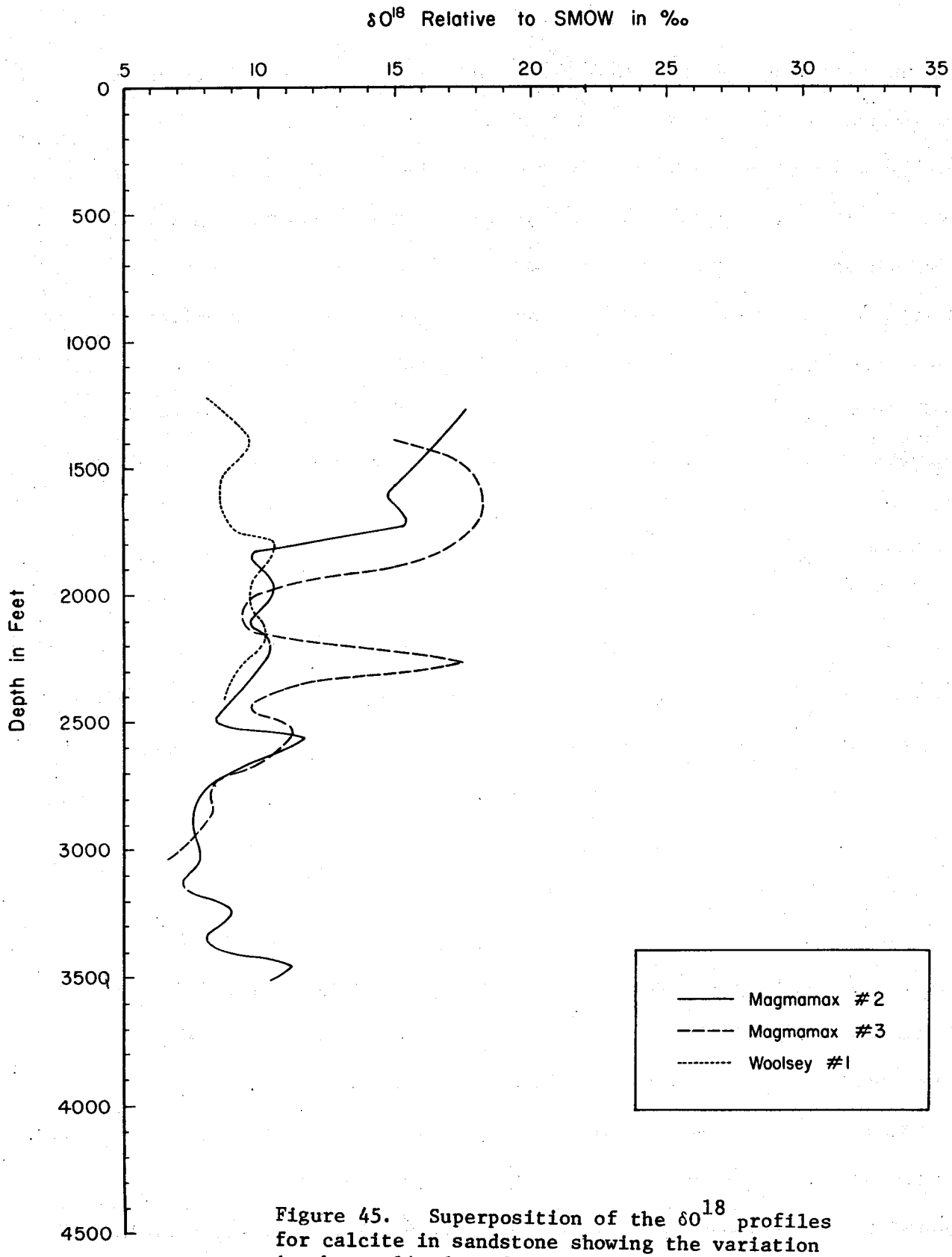

Figure 45. Superposition of the δO^{18} profiles for calcite in sandstone showing the variation in the amplitudes of correlatable isotope inversions for Magmamax #2, #3, and Woolsey #1.

However, in Magmamax #2 the shale content generally decreases below 3100' and the increase in δO^{18} may be related to the decrease in fracture abundance below 3600' (Fig. 25); with fewer fractures, there is less water circulation in the rocks, and hence the δO^{18} is greater.

The δO^{18} trends of calcite in sandstones, shales, and veinlets are very similar, but in general sandstone calcite is 1 to 7 °/oo lighter than shale calcite, and vein calcite is generally lighter than sandstone calcite. The isotopic compositions of calcite in shales, sandstones, and veinlets all converge to within ± 1 °/oo with increasing depth. Convergence occurs at about 2700' (300°C) in Magmamax #2 and #3, and at 2300' (225°C) in Woolsey #1. Since vein calcite, unlike sandstone and shale calcite, is entirely authigenic, it presumably was deposited in isotopic equilibrium with the water. Therefore, as a first approximation, all the calcite present below the convergence depths, regardless of origins, is approximately in equilibrium with the circulating brines.

Carbon Isotopes. The range of δC^{13} for calcite covers 7 °/oo. As shown in Figs. 46-48, there is considerable scatter in the data above 1500'. Below 1500', there is a general decrease in δC^{13} with increasing depth. The variation with depth is most simply interpreted as resulting from isotope exchange between carbonates and the dissolved CO_2 in the circulating water.

Superimposed on this general trend of decreasing δC^{13} with depths are two lesser patterns. The first is that calcite in veinlets is usually lighter (lower ratio of C^{13}/C^{12}) than in sandstones, and that calcite in shale is heavier than in sandstones. The second pattern is that the

Carbonate in Magmamax # 2

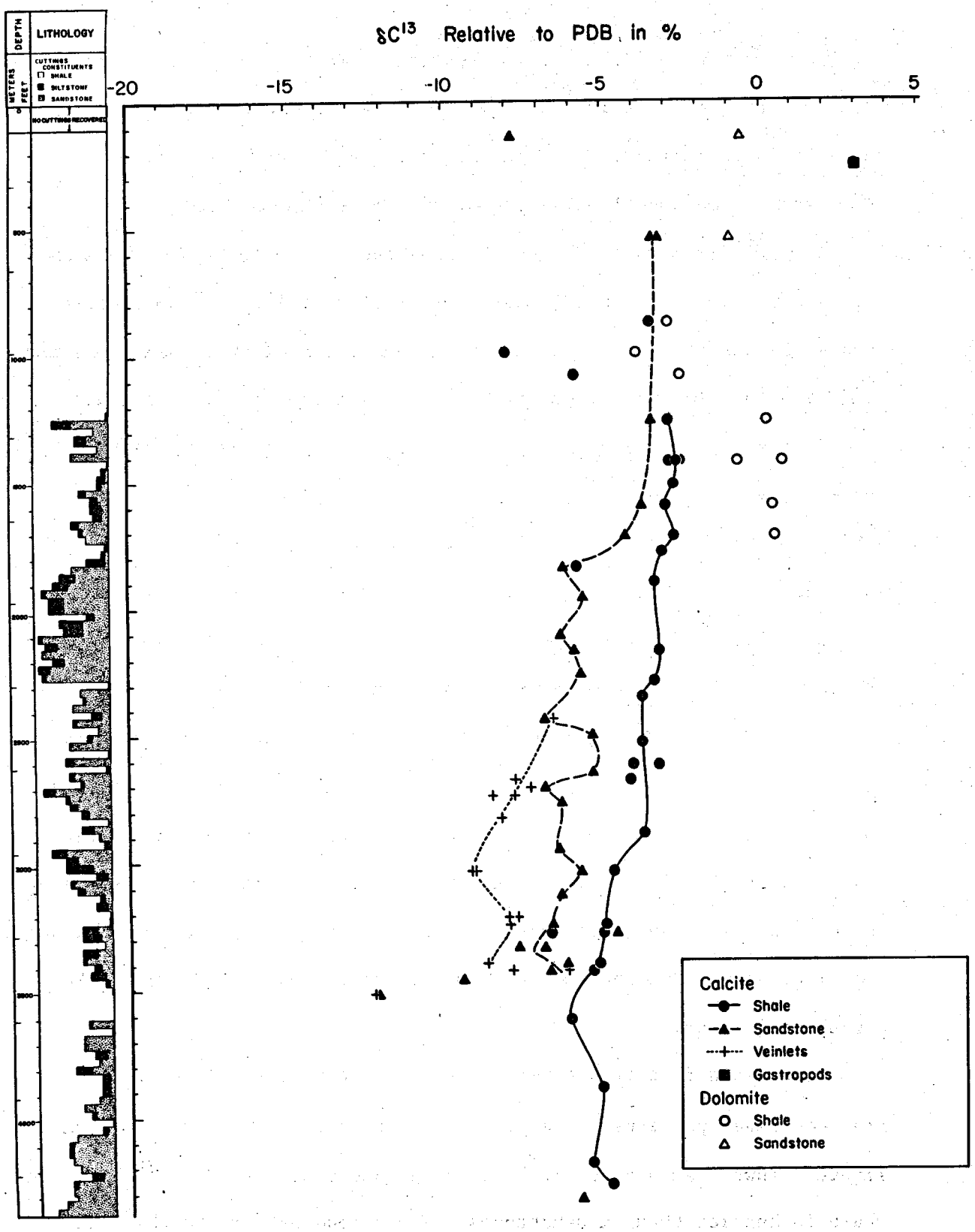

Figure 46

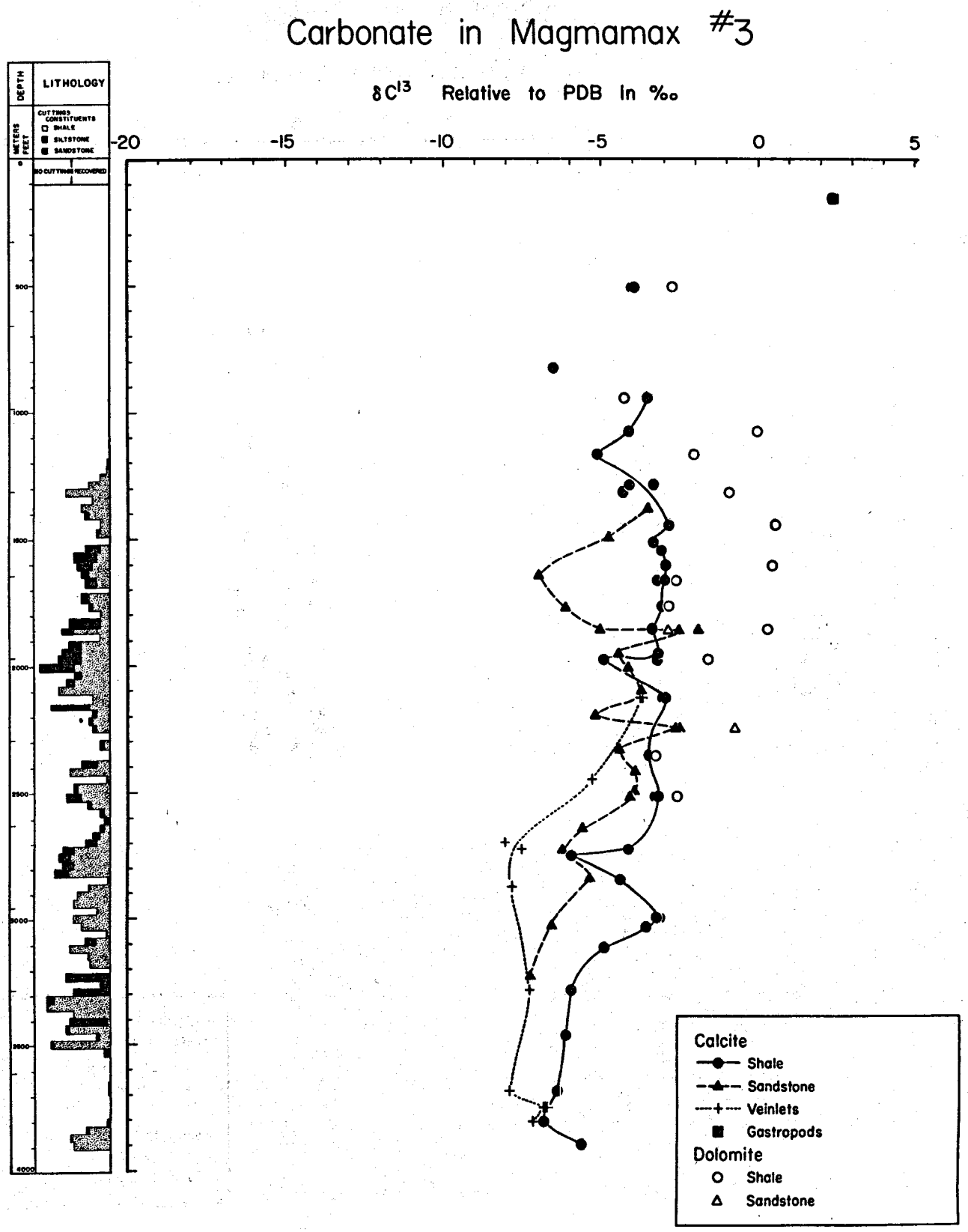
Carbonate in Magmamax #3
δC13 Relative to PDB in ‰
-20
-15
-10
-5
0
5
DEPTH
METERS
FEET
LITHOLOGY
CUTTINGS CONSTITUENTS
SHALE
SILTSTONE
SANDSTONE
NO CUTTINGS RECOVERED
Calcite
Shale
Sandstone
Veinlets
Gastropods
Dolomite
Shale
Sandstone

Figure 47

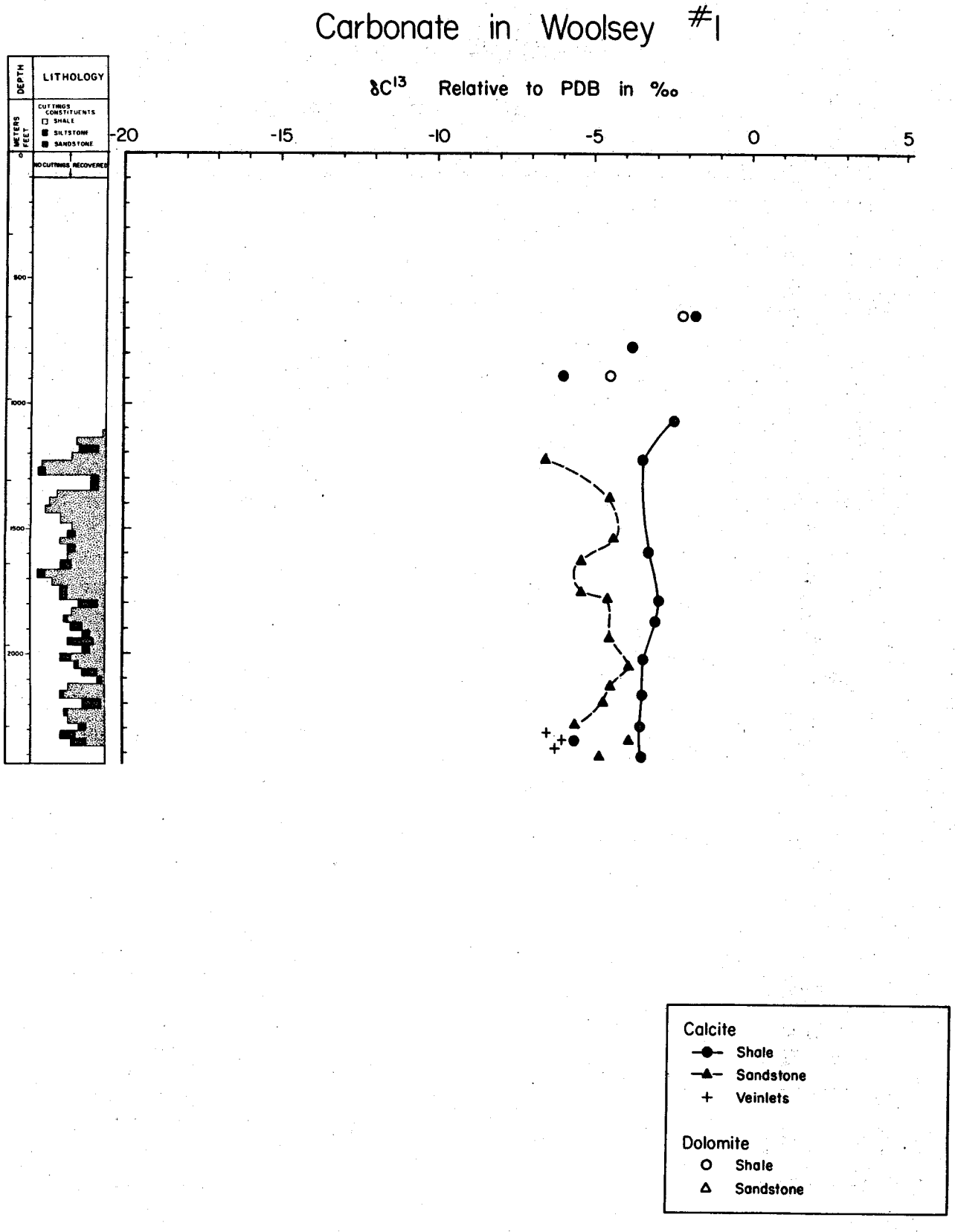
Carbonate in Woolsey #1
δC13 Relative to PDB in ‰
-20
-15
-10
-5
0
5
DEPTH
METERS
FEET
LITHOLOGY
CUTTINGS CONSTITUENTS
SHALE
SILTSTONE
SANDSTONE
NO CUTTINGS RECOVERED
500
1000
1500
2000
Calcite
Shale
Sandstone
Veinlets
Dolomite
Shale
Sandstone

Figure 48

δC^{13} values show a pattern of multiple inversions with variable amplitudes.

The pattern of alternating isotope maxima and minima is produced by variations in the degree of isotope exchange between the rocks and the water. There is an excellent correlation between δC^{13} inversions and δO^{18} inversions. The δC^{13} inversions are not as sharply defined and do not have amplitudes as great as the δO^{18} inversions, but most of the maxima and minima are at the same depths for both elements. The correlation between δO^{18} and δC^{13} inversions indicates that carbon isotope shifts are also strongly controlled by permeability; the more shale in an interval, the greater the δC^{13} values of rocks.

Figure 49 is a plot of δO^{18} versus δC^{13} in carbonates in Magmamax #2, #3, and Woolsey #1. The range of δC^{13} is about half that of δO^{18}. Data from the three wells are virtually identical. There is an approximately linear relationship between δO^{18} and δC^{13}; much of the scatter is caused by shallow unexchanged carbonates and deep vein calcite. Data from below 2000-2500' generally cluster into an area of low δC^{13} and low δO^{18}; these deep carbonates show more variation in δC^{13} and less in δO^{18} than shallow carbonates. The oxygen isotopes show little variation here largely because of the approximately constant temperature. The greater range in δC^{13} may be due to decarbonation reactions and CO_2 production.

The δC^{13} trends of calcite in sandstones, shales, and veinlets all show a general decrease in δC^{13} with increasing depth. Calcite in veinlets is 0 to 3 $^{o}/_{oo}$ lighter than in sandstones, and calcite in sandstones is generally 0 to 4 $^{o}/_{oo}$ lighter than in shales. Carbon isotopes,

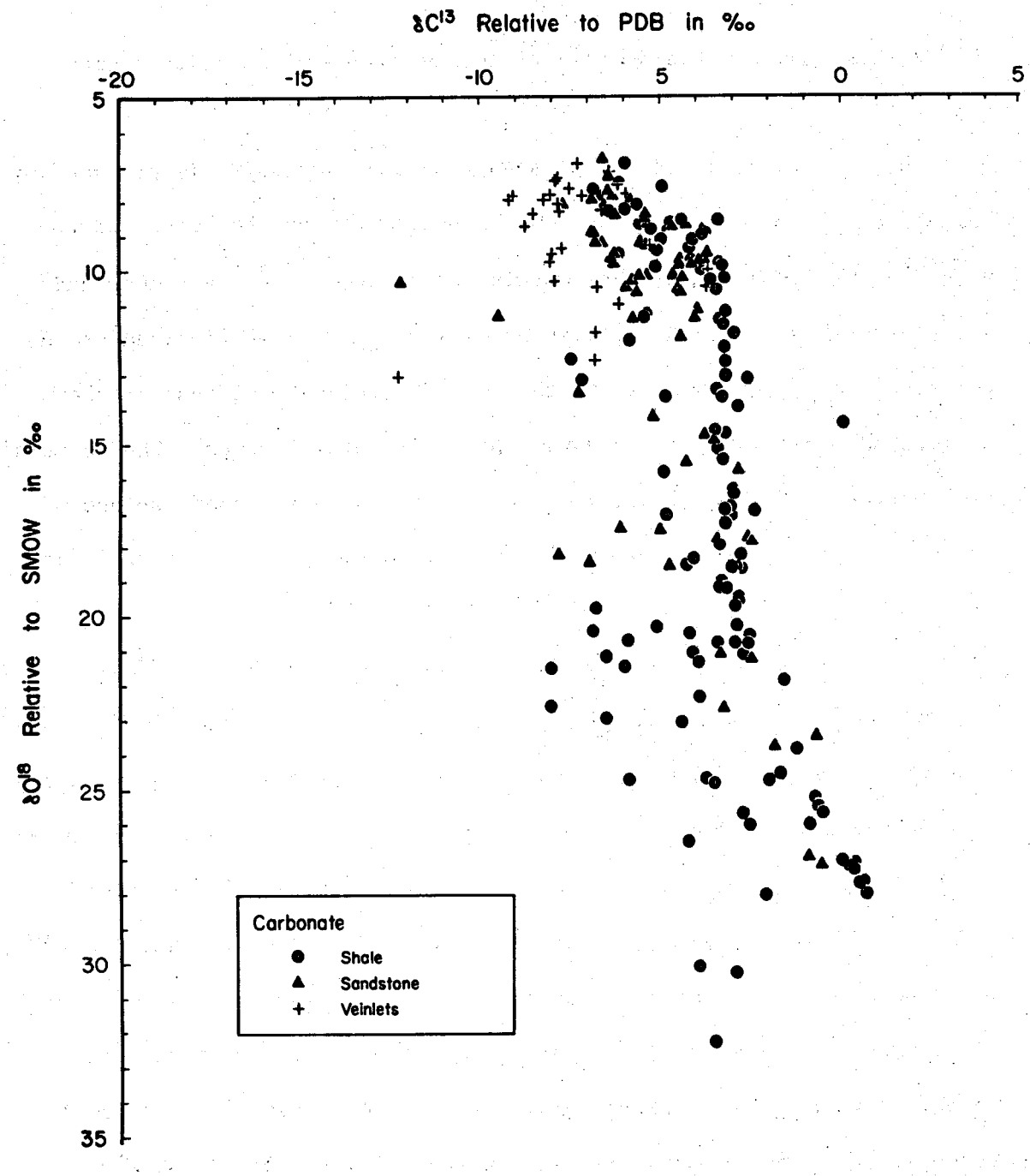
δC13 Relative to PDB in ‰
-20
-15
-10
5
0
5
5
10
15
20
25
30
35
δO18 Relative to SMOW in ‰
Carbonate
Shale
Sandstone
Veinlets

Figure 49

like oxygen isotopes, show more scatter in Magmamax #3 than in Magmamax #2.

Shale δC^{13} curves for Magmamax #2 and #3 are almost identical above 2700'; δO^{18} curves in this interval are markedly different and show much more complete exchange in the Magmamax #2 shales. Below 2700' the shale δC^{13} curves for Magmamax #2 and #3 are less similar than at shallower depths. There are vague broad δC^{13} minima below 3200' in Magmamax #3 and 3600' in Magmamax #2, which approximately correspond to the δO^{18} minima.

The δC^{13} curves for calcite in sandstone in the three wells are very different. Carbon isotopes, like oxygen isotopes, are lighter at shallower depths in Magmamax #2 than Magmamax #3, reflecting the impaired circulation in Magmamax #3. Magmamax #3 carbon values also show more variation than in Magmamax #2, but in general the calcite in Magmamax #2 sandstones above 2700' is considerably lighter than in Magmamax #3 sandstones. It is enigmatic that in the interval 1000-2700' the <u>carbon</u> isotopes of sandstones and the <u>oxygen</u> isotopes of shales in Magmamax #2 are much lighter than in Magmamax #3.

The δC^{13} curves for vein calcite in Magmamax #2 and #3 show no apparent relationship to the sandstone and shale trends. Veinlets in both wells show a rapid decrease in δC^{13} in the interval 2000-3000', and there is a vague correspondence between δO^{18} and δC^{13} inversions.

Figure 36 shows that the calcite content of the rocks decreases with depth. There is also a vague decrease in δC^{13} with decreasing carbonate abundance (Fig. 50). Temperature and salinity in the wells

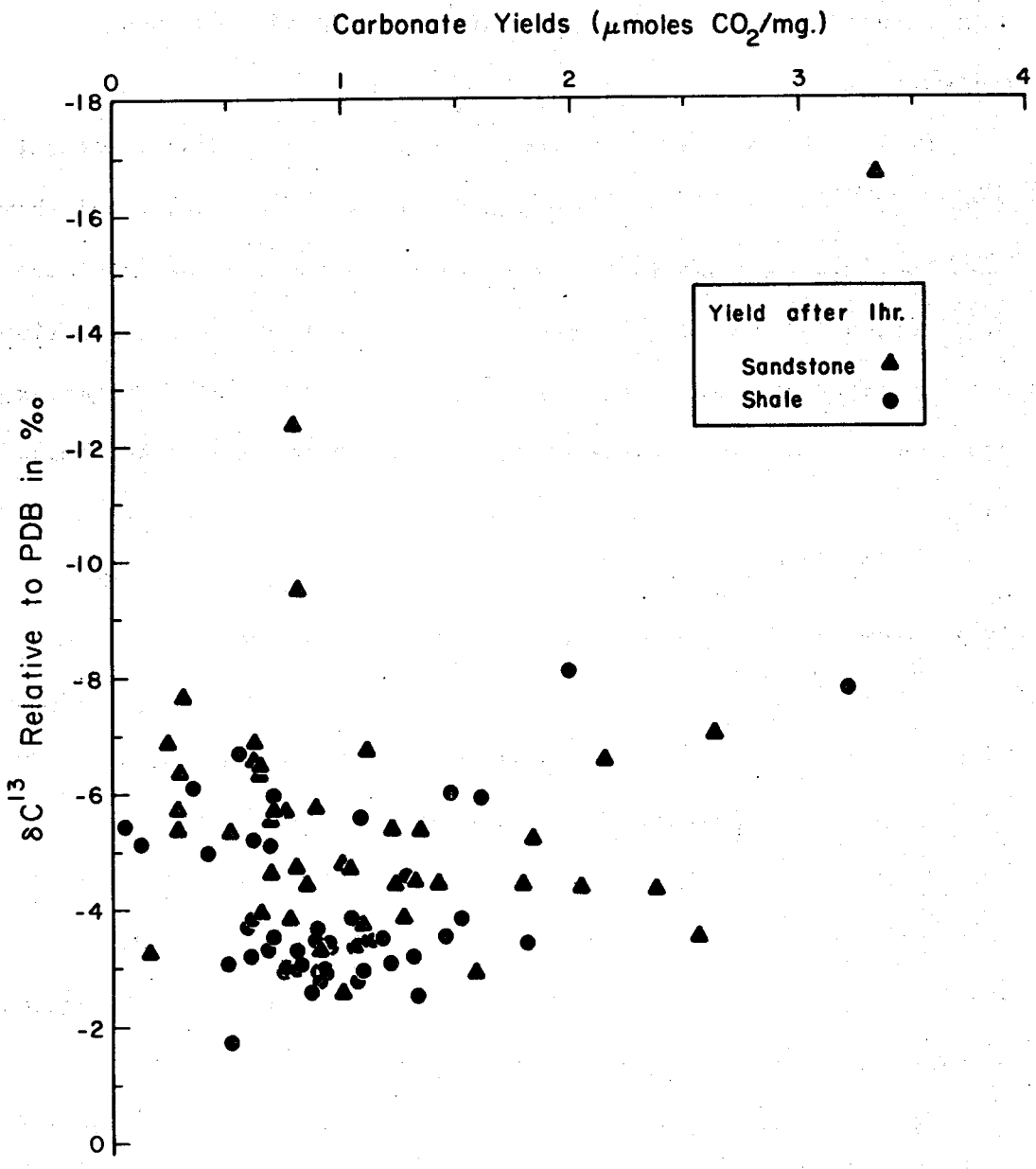
Carbonate Yields (μmoles CO_2/mg.)
0
1
2
3
4
-18
-16
-14
-12
-10
-8
-6
-4
-2
0
δC^{13} Relative to PDB in ‰
Yield after 1hr.
Sandstone
Shale

Figure 50

increases with depth; hence the solubility of calcite increases (Ellis, 1963) and calcite is replaced by higher temperature calcium-bearing minerals such as epidote, anhydrite, and tremolite. Shifts in δC^{13} reflect isotopic fractionation during decarbonation reactions (Muffler and White, 1969). The isotope minima correlate with zones where the permeabilities were greater, epidote and anhydrite replaced calcite, and perhaps where C^{13}-rich CO_2 escaped. The composition of CO_2 released in CO_2 production wells is consistent with fractionation from the calcite cement (Lang, 1959).

DOLOMITE

The isotopic fractionation of oxygen and carbon in the system dolomite-water and dolomite-bicarbonate is not very well known at low temperatures due to the difficulty of synthesizing dolomite at temperatures and pressures comparable to those of sedimentary environments. Extrapolations from high temperature experiments seem to predict, however, a 5 to 7 °/oo O^{18} enrichment in dolomite compared to syngenetic calcite (Northrop and Clayton, 1966; O'Neil and Epstein, 1966), whereas the carbon isotope fractionation is much smaller with about 2.5 °/oo enrichment of C^{13} in the dolomite (Sheppard and Schwarcz, 1970). However, many recent studies have presented evidence that the oxygen and carbon isotope fractionations observed are much smaller.

Degens and Epstein (1964), on the basis of oxygen and carbon isotopic studies of recent and ancient dolomites, concluded that recent dolomites are formed by metasomatism of pre-existing crystalline carbonate. Their conclusions were based on recent observations that the δO^{18} and δC^{13} of coexisting calcites and dolomites in several modern sediments are

essentially identical. The dolomitization process was believed to be a solid state cation exchange and reordering within calcite without alteration of the original oxygen and carbon isotopic composition of the calcite precursor. Fritz and Smith (1970) showed that secondary and chemically precipitated protodolomites have considerably smaller dolomite-calcite fractionations (3 to 4 °/oo) than expected from extrapolations from higher temperature experiments.

Many authors have noted that the oxygen isotope fractionation between calcite and dolomite is directly related to the degree of ordering of the dolomite (e.g. Northrop and Clayton, 1966; Fritz and Smith, 1970). Structurally and compositionally, the difference between dolomite and calcite is greatest when the dolomite is well crystallized and defined. Hence there is no reason to expect that the fractionation predicted for well-defined dolomites (Northrop and Clayton, 1966) would be the same as for recent, low-temperature, poorly-ordered protodolomites.

Petrologic and X-ray diffraction studies indicate that dolomite is present in shale and sandstone samples above 2000' in all three wells (Figs. 7-23). Dolomite rarely exceeds 10% in shallow sandstones, but tan shales above 1000' may contain up to 85% dolomite, ankerite, and rare siderite. With increased depth, dolomite and ankerite disappear and calcite becomes more abundant. Muffler and White (1969) indicate that the reaction may be as follows: dolomite + ankerite + kaolinite → chlorite + calcite + CO_2.

Figures 41-43 show the oxygen isotopic compositions of dolomite and coexisting calcite in sandstones and shales of Magmamax #2, #3, and

Woolsey #1. Dolomites show more scatter than the corresponding calcites, but generally parallel the calcite trend. Most samples show a 5 to 8 °/oo fractionation between dolomite and calcite; occasional samples have only a 1 °/oo fractionation. There is no apparent decrease in the observed fractionations with increased depth.

Figures 46-48 show the carbon isotopic compositions of dolomite and coexisting calcite in sandstones and shales of Magmamax #2, #3, and Woolsey #1. Dolomites are generally 1 to 3.5 °/oo heavier than the corresponding calcites; a few dolomites are slightly lighter than the corresponding calcites. The carbon isotopic compositions show no apparent relationship with depth or calcite δC^{13}, perhaps because of the sparsity of data.

Silicates and Oxides

QUARTZ

Two distinct types of sandstones were collected and analyzed to determine the δO^{18} of the constituent quartz. The first and largest group consists of pure, quartz-rich sandstones from Magmamax #3, with little matrix and little or no epidote, anhydrite, tremolite, or hematite. These sandstones are generally porous with minor (1-10%) quartz overgrowths and variable amounts of calcite cement. The second and smaller group of sandstones are from both Magmamax #2 and #3. These quartz samples are separates from extremely well-mineralized sandstones, and are the quartz which remained after the removal of epidote or hematite

for analysis. All these sandstones are alike in being very dense and nonporous.

The variations in δO^{18} of quartz in Magmamax #2 and #3 with depth are plotted on Figs. 51 and 52. In the interval 1000-3000' in Magmamax #3, the oxygen isotopic compositions of quartz in porous sandstones have a pattern of cyclic variations with .5 to 1 °/oo amplitudes around a mean composition of 13.5 °/oo. There is a very good correlation between the quartz isotopic inversions and lithology. Intervals containing abundant shale have higher values of δO^{18} than more sandy intervals; hence, like carbonates, quartz exchanges more readily in permeable zones.

Below 3000' in Magmamax #3, porous sandstones are rather sparse and their isotopic compositions show a decrease in δO^{18} to 12 °/oo at 3900'. Quartz data, like most of the calcite data, show little or no relationship to permeability below 3000'.

The general pattern of isotopic compositions of porous sandstones in Magmamax #3 is very similar to that of quartz in River Ranch #1 (Clayton and others, 1968). The River Ranch #1 quartzes have a constant composition of 13.5 °/oo above 4000', and then decrease to 11.5 °/oo at 8000'; quartz is very resistant to O^{18} exchange and has exchanged only half-way to equilibrium (Clayton and others, 1968).

At the beginning of this isotope study it was thought that porous and hence unmineralized sandstones would have had the greatest water circulation and hence the most complete isotope exchange; however, the quartz in these sandstones were found to be only partially exchanged. Later the excellent correlation found between degree of hydrothermal alternation

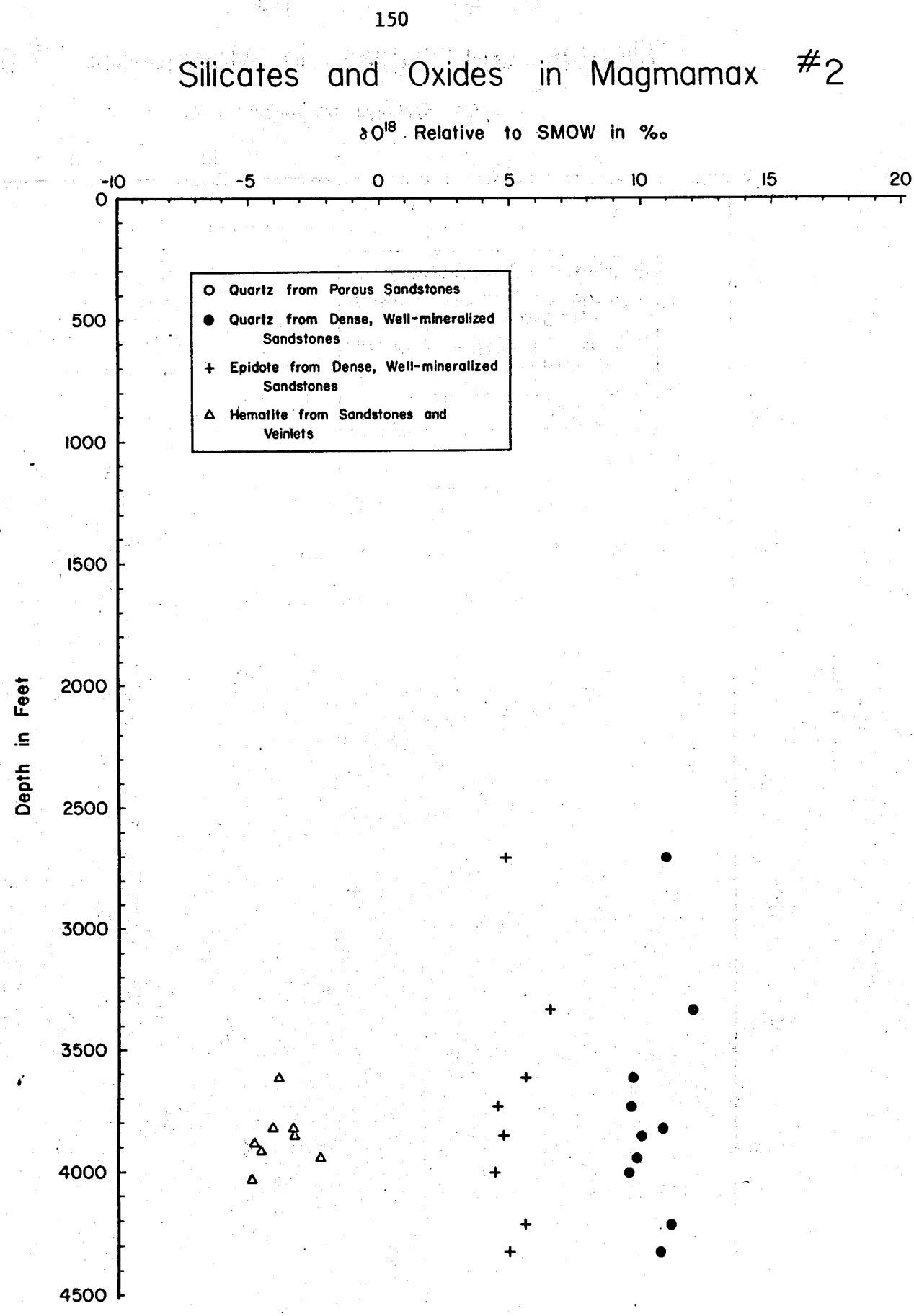
Silicates and Oxides in Magmamax #2
δO18 Relative to SMOW in ‰
-10
-5
0
5
10
15
20
0
500
1000
1500
2000
2500
3000
3500
4000
4500
Depth in Feet
Quartz from Porous Sandstones
Quartz from Dense, Well-mineralized Sandstones
Epidote from Dense, Well-mineralized Sandstones
Hematite from Sandstones and Veinlets

Figure 51

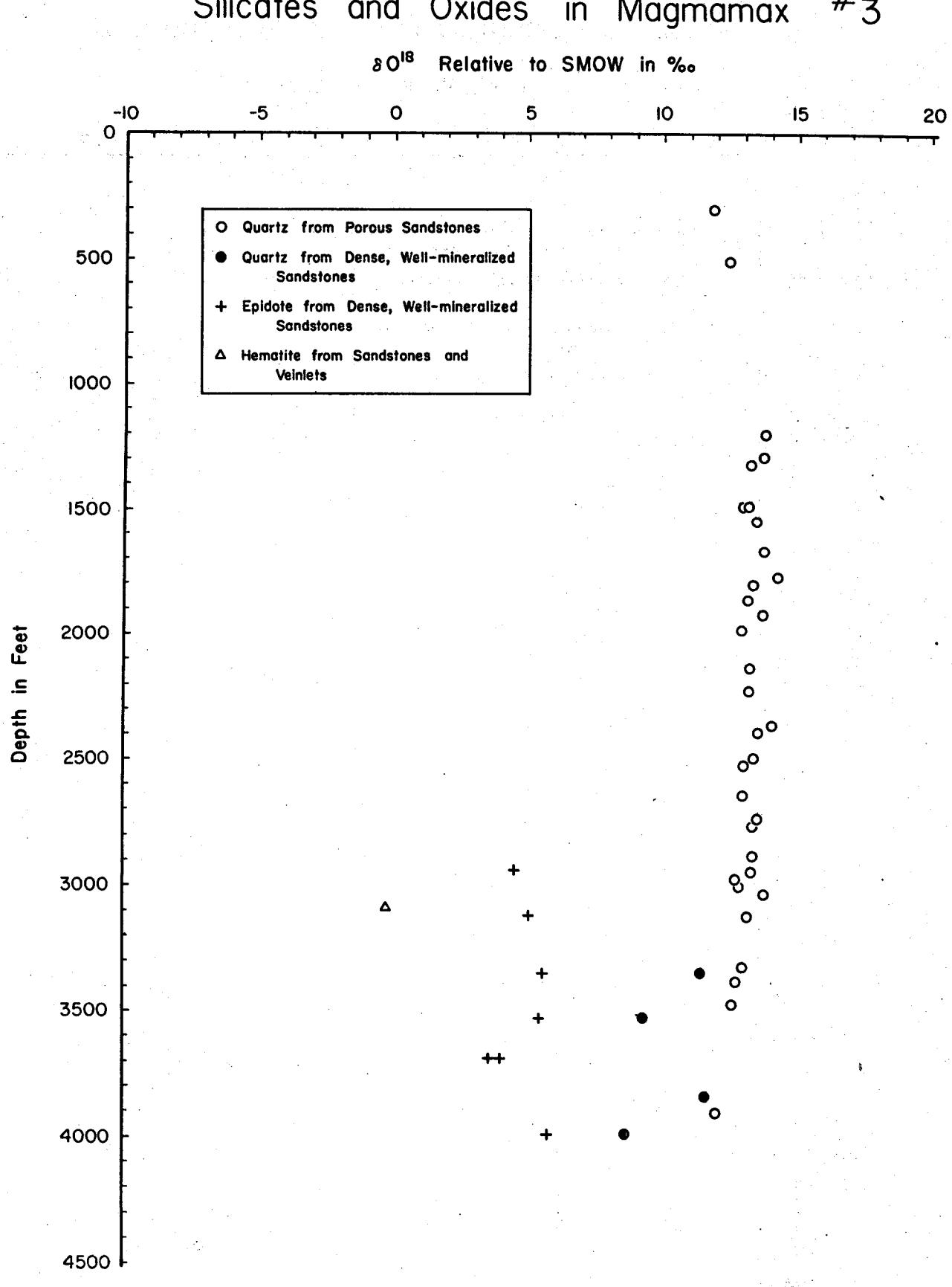
Silicates and Oxides in Magmamax #3
δO18 Relative to SMOW in ‰
-10
-5
0
5
10
15
20
0
500
1000
1500
2000
2500
3000
3500
4000
4500
Depth in Feet
Quartz from Porous Sandstones
Quartz from Dense, Well-mineralized Sandstones
Epidote from Dense, Well-mineralized Sandstones
Hematite from Sandstones and Veinlets

Figure 52

and calcite δO^{18} minima suggested that the presently unporous but highly mineralized sandstones might have had more water circulation but now are sealed. Therefore, nonporous sandstones were collected and analyzed and are generally 1 to 3 °/oo lighter than the previous group. The isotopic compositions of the quartz in well mineralized sandstones also show a definite correlation with the sandstone/shale ratio, and the more mineralized the sandstone, the lower the δO^{18}.

EPIDOTE

All the epidotes analyzed are from well mineralized sandstones; the coexisting quartz fractions of most of the sandstones were also analyzed. The oxygen isotopic compositions of both the epidotes and the coexisting quartz are plotted on Figs. 51 and 52. The δO^{18} values of epidote from both Magmamax #2 and #3 range from 3.5 to 6.5 °/oo, about 4 °/oo lighter than the associated quartz.

There is an extremely good correlation between the δO^{18} of epidote and coexisting quartz in Magmamax #2. The trends of the quartz and epidote are subparallel and have isotope maxima and minima at the same depths. The same relationship is not seen in Magmamax #3 where the quartz is less well exchanged and also where fewer coexisting quartz samples were analyzed. Quartz isotope inversions appear to be related to the permeability of the nearby rocks; the δO^{18} is generally lighter in intervals with abundant sandstone. The correlation between the δO^{18} of quartz and epidote suggests that the isotopic composition of epidote may also be related to permeability.

There apparently is no simple relationship between epidote composition, the δO^{18} of epidote, and the estimated δO^{18} of water. Studies of epidotes in regionally metamorphosed zones show that the iron content of epidotes is closely related to the fugacity of oxygen (Ernst, 1964; Brown, 1967). Keith and others (1968) in their study of epidotes in the IID wells also concluded that oxygen fugacity controls composition. There is a good correlation between hematite abundance and the high iron content of epidote in Magmamax #2; the Fe^{+3} content of Magmamax #3 epidotes shows no correlation with the hematite/pyrite ratio.

HEMATITE

Hematite was collected primarily from veinlets with a few from sandstone mineralization. The δO^{18} values range from -4.90 to -.25 °/oo as shown on Figs. 51 and 52. Eight of the hematites are from the interval 3600-4100' in Magmamax #2; one hematite is from 3085' in Magmamax #3. Three of the hematites, two at 3825' and one at 3945' in Magmamax #2, were mainly from sandstone mineralization and the coexisting quartz was analyzed separately.

Water Composition and Isotopic Equilibrium

Based on analyses from several wells, Clayton and others (1968) estimated that the oxygen isotopic composition of brines in the central part of the Salton Sea geothermal field is 2 ± .5 °/oo, and found that calcite in the interval 400(?)-7000' in River Ranch #1 was in apparent isotopic equilibrium at present temperatures with a brine of this

constant composition. No isotope analyses of water from Magmamax #2, #3, or Woolsey #1 are presently available; however, theoretical water compositions in isotopic equilibrium with calcite have been calculated using the fractionation calibration of O'Neil and others (1969), and are plotted on Figs. 53-55 for Magmamax #2, #3, and Woolsey #1, respectively. The graphs suggest that unlike at River Ranch #1, the water composition in these three wells cannot be assumed to be constant.

The range of oxygen isotopic compositions of calcite in the three wells extends from about 25 °/oo in shallow shales and sandstones to a minimum of 7 °/oo at 3000-3500'. This decrease in δO^{18} is due to exchange with the oxygen of the circulating water which has the net effect of enriching the water and depleting the calcite in O^{18}. Craig (1966) estimated that the initial composition of water in the reservoir was about -11 °/oo. As the O^{18} of calcite decreases with depth due to exchange, the O^{18} of the water should increase, and appears to reach a composition of approximately 2 °/oo.

At equilibrium, the fractionation of oxygen isotopes between calcite and water is a function of temperature, and hence <u>if</u> the calcite and water in the wells are in isotopic equilibrium at the logged temperatures, the water composition can be calculated. Unfortunately, isotopic equilibrium, like chemical equilibrium, is difficult to prove. Permeability, as well as temperature, has a strong effect on the establishment of isotopic equilibrium. If insufficient water has circulated through the rocks, the calcite will not be completely exchanged; if temperatures are too low, the reaction kinetics are too slow. It is reasonable to

Calculated Water Compositions in Magmamax #2

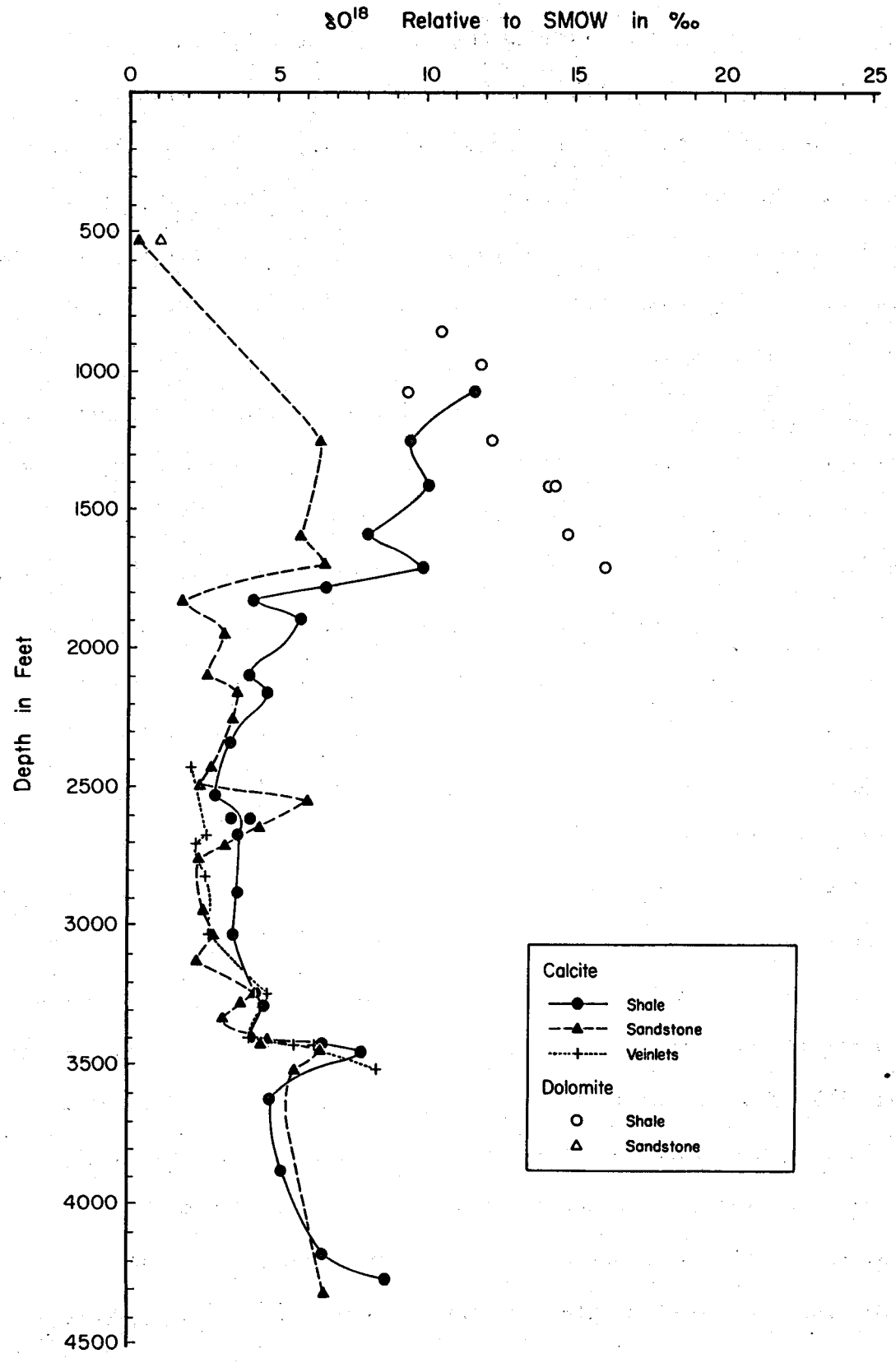

Figure 53

Calculated Water Compositions in Magmamax #3

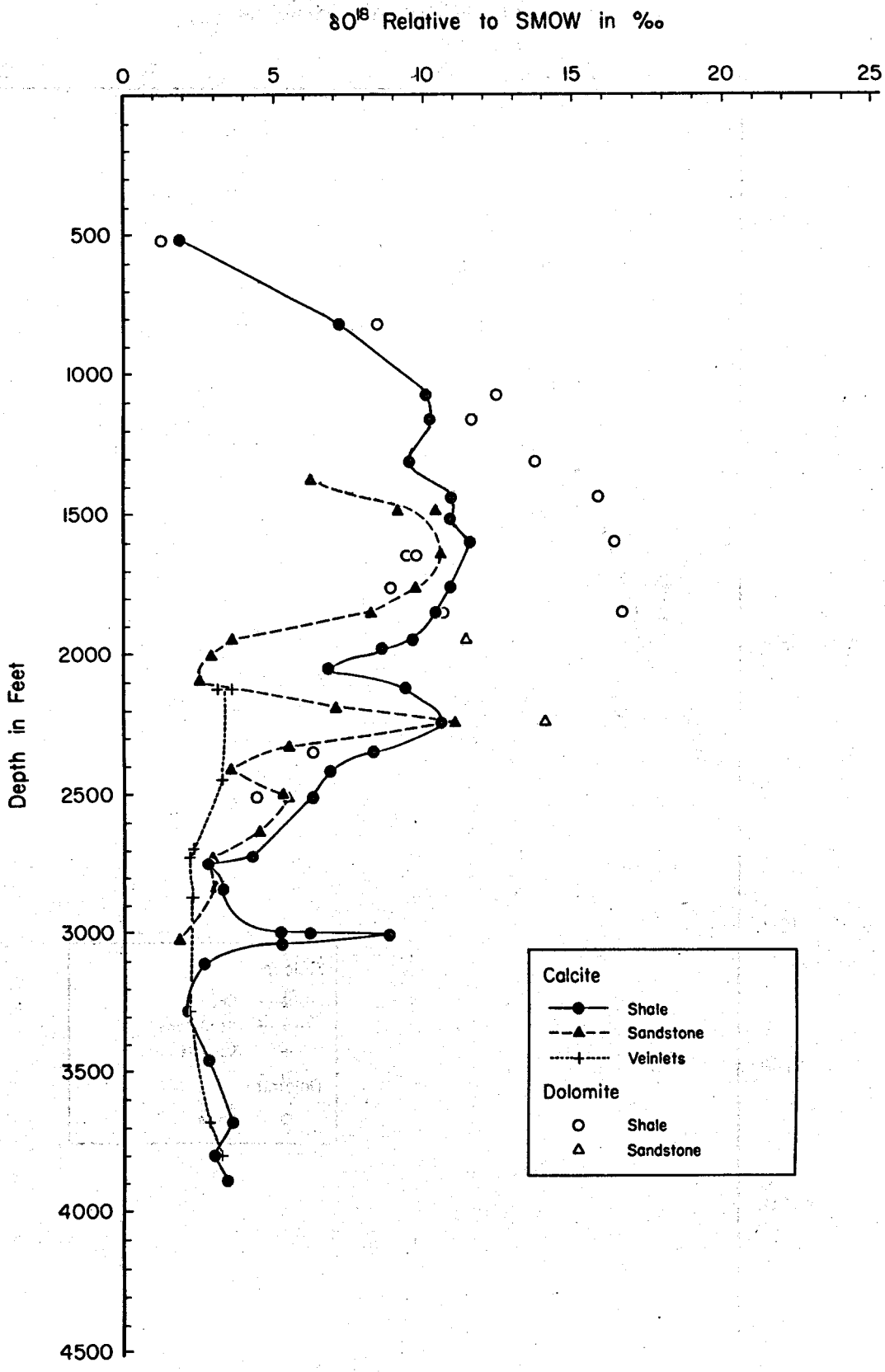

Figure 54

Calculated Water Compositions in Woolsey #1

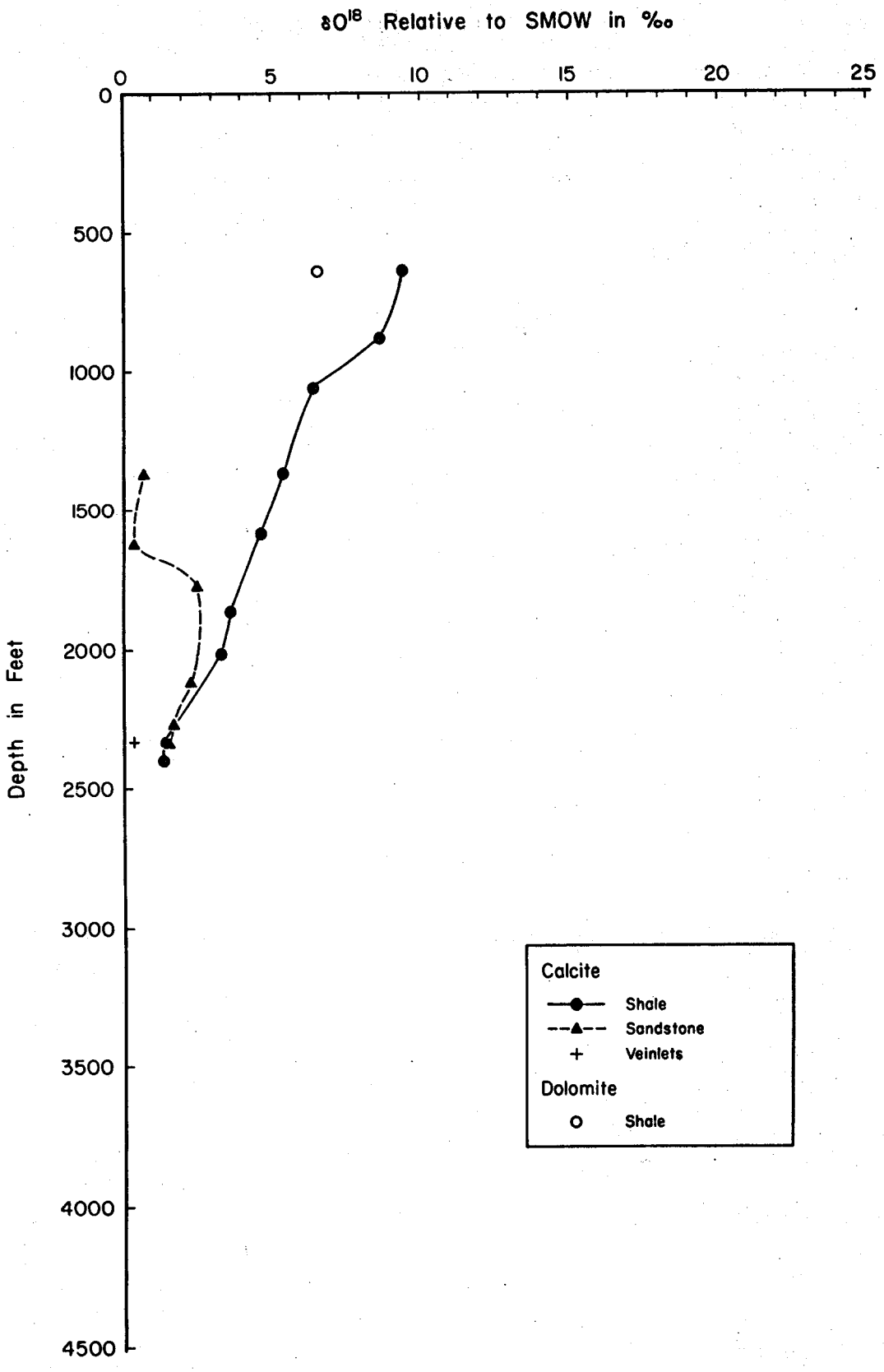

Figure 55

expect that shallow calcite will not be exchanged, and with increasing depth exchange will be more complete.

So what Figs. 53-55 show is a model of water compositions would be if all the calcite were in equilibrium at logged temperatures. Preliminary studies on fluid inclusions in Magmamax #2 indicate that mineralization occurred at approximately present temperatures (C. I. Huang, pers. com., 1976); therefore; the assumption that exchange during recrystallization and precipitation took place at logged temperatures is probably valid.

The calculated water compositions of the three wells show the same basic pattern. With increasing depth, the waters first increase abruptly in δO^{18} from -9 °/oo to about 10 °/oo at 500-1500'; the composition then decreases to a minimum of about 2 °/oo at 3000', and then increases in δO^{18} to the bottoms of the wells. The isotope patterns in Magmamax #2 and #3 are very similar, but the amplitudes of maxima and minima in Magmamax #3 are again greater. The water isotopic compositions of shales in Woolsey #1 are heavier, and those of sandstones are lighter than in the other two wells. Below 2000' in Woolsey, and 2800' in Magmamax #2 and #3 the calculated water compositions of shales, sandstones, and veinlets are within approximately 1 °/oo of each other.

The rapid increase in δO^{18} from the surface to 500-1500' is probably due to incomplete exchange in the upper shale unit. Geothermal wells throughout the Salton Trough have a 1000-2000' thick shale cap rock (Randall, 1974). This unit is very impermeable so that water/rock ratios are low, and isotope exchange between detrital carbonate and water is likely to be incomplete. Occasional samples have calculated water

compositions less than -5 °/oo, and in rare samples very close to -11 °/oo. This might suggest isotopic equilibrium with waters only slightly changed from the initial -11 °/oo. On the other hand, the measured O^{18} of the calcite in these samples is suspiciously close to the initial composition of the clastic or evaporative carbonates, so little or no exchange may have occurred. It is possible that much of the calcite in shallow samples is diagenetic rather than evaporative and hence formed in equilibrium with waters of compositions very close to -11 °/oo.

Petrologic evidence suggests that most of the calcite was formed early in the mineralization history of the rocks. The calcite was originally micritic, and has later been recrystallized to interlocking or sparry cement in sandstones. During recrystallization variable amounts of authigenic calcite were precipitated in the sandstones. Since very shallow sandstones contain abundant calcite formed at low temperatures, it is perhaps reasonable to infer that the original micrite in the sandstones and shales formed diagenetically near the surface at very low temperatures. Under these conditions, the compositions of the original calcite and the water in equilibrium with it would be close to 22 to 25 °/oo and -11 °/oo, respectively.

Below 500-1500', depending on well and relative permeabilities, there probably has been sufficient water exchanging with the calcite for isotopic equilibrium to be established. The extensive mineralization in this interval suggests water circulation has been great. Sandstones, because of their greater permeability, are in presumed equilibrium with lighter water than shales. Above 3000', the water in sandstones and

shales ranges in composition from 2 to 10 °/oo in Magmamax #2 and #3. Woolsey #1 sandstones have waters ranging between 0 and 3 °/oo.

One way to estimate the water composition is by analyzing vein calcite. Since the vein calcite is formed at equilibrium with the circulating water, if the temperature has not changed since deposition, or if the calcite has re-equilibrated to present temperatures, we can then calculate the vein water composition. If the enclosing rocks have isotope compositions similar to that of the vein calcite, the compositions of fracture waters and rock waters are probably similar; if the vein and rock calcite compositions are very different, the sources of the waters may be different, or the rock calcite is incompletely exchanged.

The vein calcite water composition curves parallel those of the enclosing rocks, and vein water is generally identical or slightly lighter than the water in nearby sandstones. Vein calcite from Magmamax #3 and from above 3000' in Magmamax #2 is in calculated equilibrium with water of about 2 °/oo at logged temperatures. Since the trends and magnitudes of the water compositions in veinlets and enclosing rocks are so similar, it is reasonable that the vein waters were derived from the nearby rocks. The reservoir rocks are largely sealed by hydrothermal mineralization so probably any water in them is located in microfractures. The slight difference between vein and rock calcite composition may be due to fractionation of the waters trapped in the open fractures during precipitation of vein calcite.

Discussion of isotopic equilibrium in the previous pages is hampered by a lack of real data on water compositions at various depths. In the

absence of water samples, the next best way to demonstrate equilibrium is to compare the isotopic compositions of two or more minerals presumed to be in isotopic equilibrium. Assuming logged temperatures, if the water compositions calculated using the two geothermometers are concordant, then isotopic equilibrium has been established between the two minerals and the brine, and the actual water composition has hence been calculated. In this study, dolomite, quartz, hematite, and epidote samples were analyzed in addition to calcite, but none of the possible mineral pairs proved to be satisfactory geothermometers over large depths.

Figures 53-55 compare the calculated water compositions in equilibrium with dolomite (Northrop and Clayton, 1966) with the corresponding water compositions calculated for coexisting calcite. About half of the dolomite waters are 1 to 2 °/oo heavier, 1/4 are 1 to 2 °/oo lighter, and 1/4 are 3 to 8 °/oo heavier than the corresponding calculated composition of the water in equilibrium with calcite. The close correspondence of water compositions calculated for the calcite-dolomite pairs indicates that shallow coexisting calcite and dolomite in shales and sandstones are approximately in isotopic equilibrium with each other. Since temperatures about 1000' are low and the rocks relatively impermeable, the apparent isotopic equilibrium between calcite and dolomite is probably original rather than due to later exchange; this suggests that both minerals are probably largely evaporative or diagenetic, and were formed in equilibrium at or near present temperatures.

The fractionation of oxygen between dolomite and calcite below 1000' is less explicable. These dolomites are apparently not in equi-

librium with coexisting calcite at present temperatures. Since dolomite is less readily exchanged than calcite (Epstein and others, 1964), these deeper dolomites may not be re-equilibrated in accordance with present temperatures and water compositions.

Figures 56 and 57 show the calculated water compositions in theoretical equilibrium with quartz at the logged temperatures using the quartz-water calibration equations of Clayton and others (1972). The calculated water compositions in equilibrium with calcite in sandstones, shales, and veinlets are also shown on the plots.

The calculated water compositions in theoretical equilibrium with quartz in the porous sandstones of Magmamax #3 show a progressive increase in δO^{18} from 0 to 6 °/oo in the interval 1200-3000', and then a decrease to 5 °/oo at 3900'. The close match between calculated water compositions for quartz in porous sandstones and calcite is probably fortuitous. Quartz in the unexchanged sediment is primarily detrital and is probably derived from igneous and metamorphic rocks in which the δO^{18} for quartz is usually in the range of +10 to 15 °/oo. Due to the compensating effects of temperature and δO^{18} of the water, this is also about the same range expected for quartz equilibrated in the geothermal system. Variations in the δO^{18} of quartz correlate very well with permeability changes, and hence are probably due to partial exchange rather than inherited differences in detrital quartz composition. The gradual decrease in quartz δO^{18} below 3000' is also probably due to greater exchange at higher temperatures.

Calculated Water Compositions in Magmamax #2

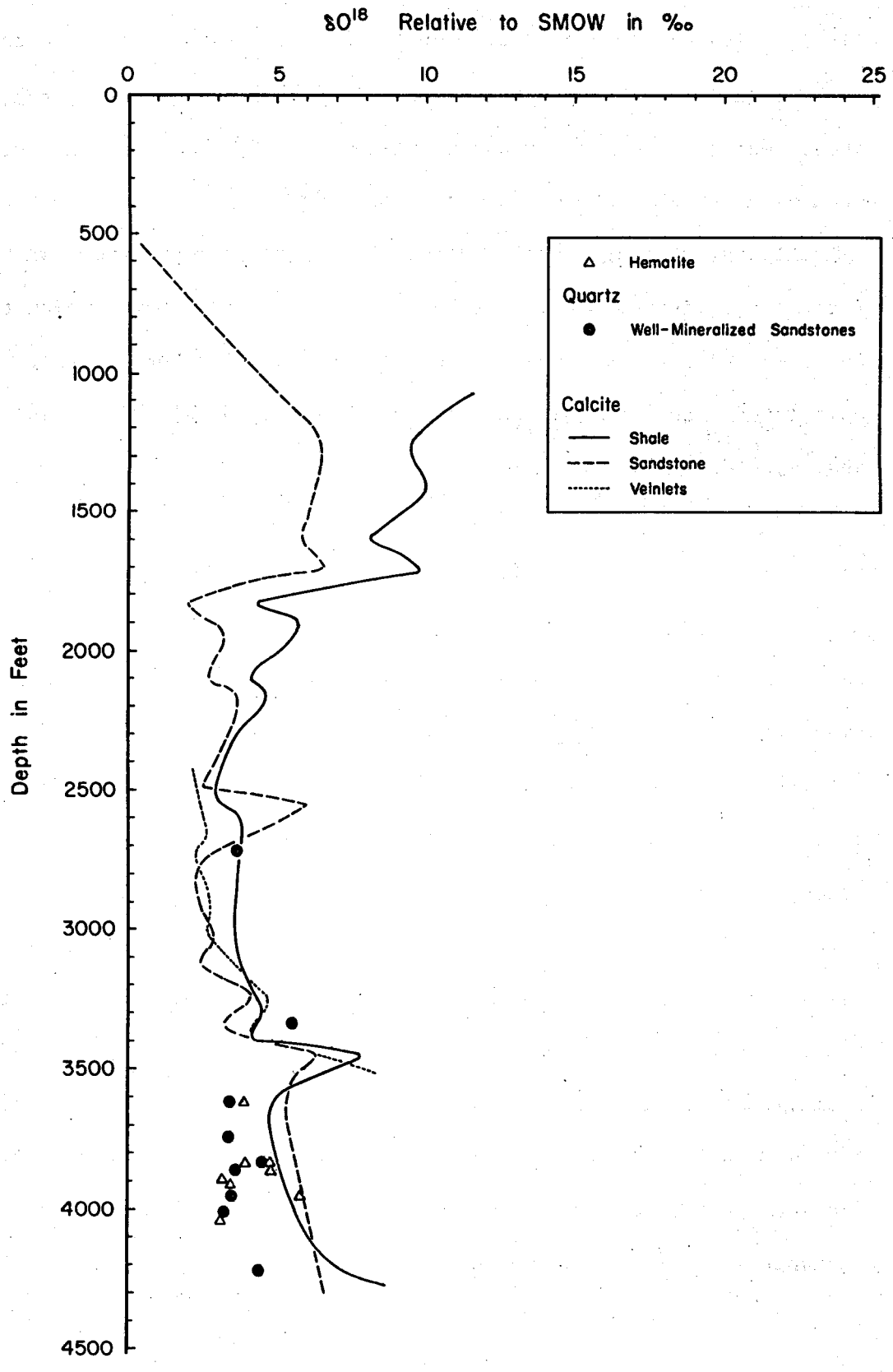

Figure 56

Calculated Water Compositions in Magmamax #3

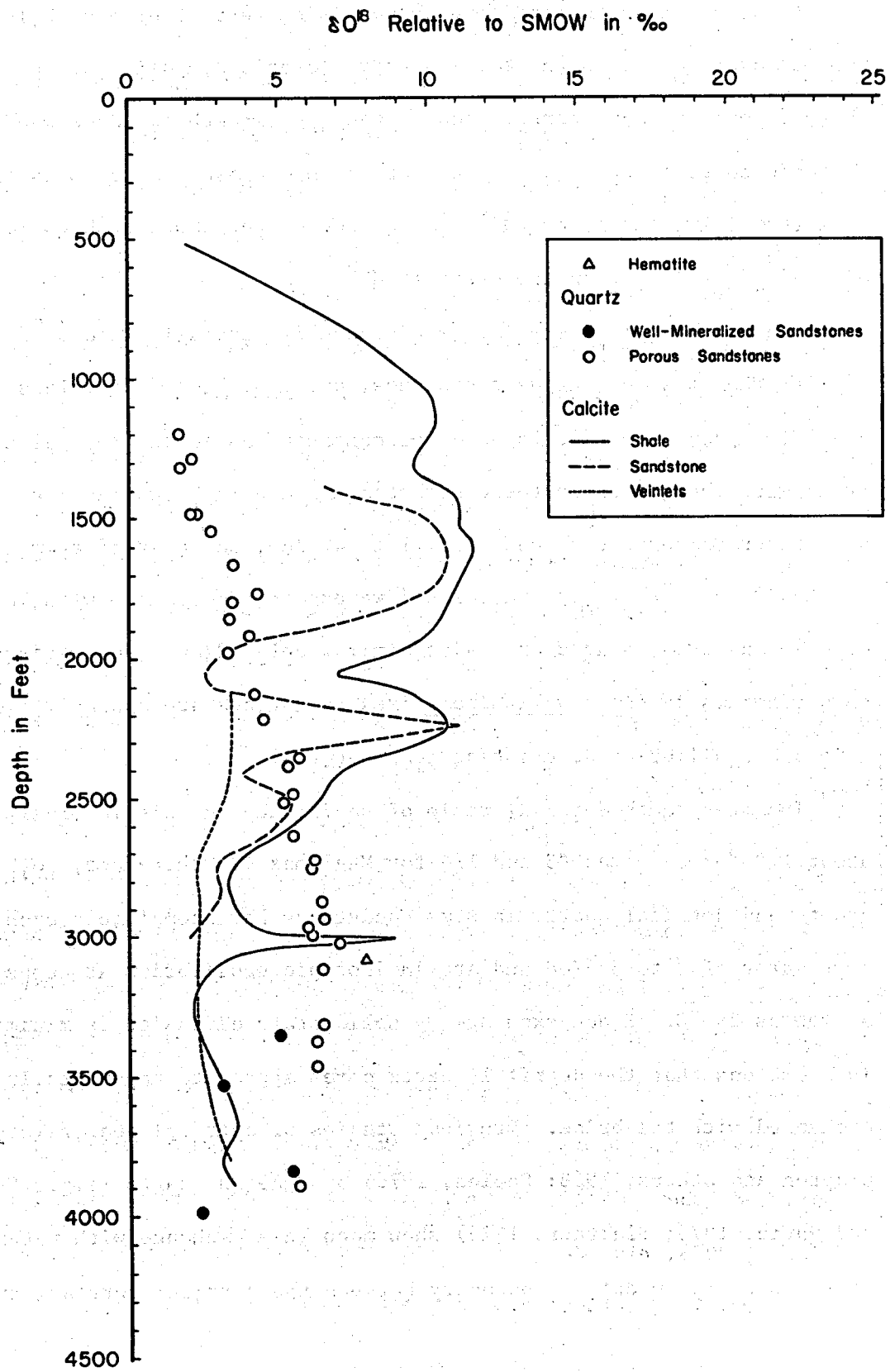

Figure 57

An alternative to partial exchange is the effect of a much lower δO^{18} of overgrowths on the total quartz isotopic composition. However, there is only a vague correlation between overgrowth abundance and isotopic composition. Since the overgrowth/detrital ratio is usually less than 1/10, the lower δO^{18} composition of the overgrowth would have only a slight effect on the overall δO^{18}.

Quartz in well mineralized sandstones is generally 1 to 3 °/oo lighter than that of porous sandstones, and most have δO^{18} values between 9 and 10 °/oo. The calculated water compositions in theoretical equilibrium with the quartz in these sandstones are also shown in Figs. 56 and 57. Water compositions range from 1 to 4 °/oo, but most of them are between 2 to 3 °/oo. The calculated waters in equilibrium with both calcite and these quartz are quite similar below 2700', suggesting that both minerals in these well mineralized sandstones are approximately in isotopic equilibrium at existing temperatures.

The overgrowth/detrital ratio of sandstones in this interval are about 1/8 for Magmamax #3 and 1/4 for Magmamax #2; therefore, both overgrowth and detrital quartz in some sandstones have completely exchanged with water of 2 to 3 °/oo and are in isotopic equilibrium at temperatures as low as 290°C. Since exchange by solid state diffusion is minimal, it is anomalous that the detrital quartz cores appear to have totally exchanged with the brine. Previous studies of detrital quartz (e.g., Clayton and others, 1968; Coplen, 1976) or igneous quartz (e.g., Eslinger and Savin, 1973; Blattner, 1975) show much less exchange with water. Although there is still an optical boundary between the detrital core and hydro-

thermal overgrowth, perhaps there has been recrystallization of the detrital core during mineralization which aided isotope exchange.

Both magnetite and hematite tend to concentrate O^{16} during equilibrium oxygen isotopic exchange. Empirical observations indicate that the fractionation of oxygen isotopes between hematite and magnetite is very slight (Clayton and Epstein, 1961), thus for a first approximation, magnetite-water geothermometers can be used for hematite-water.

In the last fifteen years several contradictory magnetite (hematite)-water fractionation curves have been calculated. The hematite-water calibration curve of Clayton and Epstein (1961) was estimated from observed fractionations between coexisting minerals, and at 320°C, the hematite-water oxygen isotopic fractionation (Δ hematite-water) is about +1.4 °/oo. The magnetite-water fractionation curve of O'Neil and Clayton (1964) is derived from experimental data in the range 400-800°C and on the observed fractionation between magnetite chiton and water at 9°C; at 320°C, the Δ magnetite-water is +3.8 °/oo. Anderson and others (1971) present a magnetite-water fractionation curve based on observations of mineral fractionations in mafic rocks; extrapolating from their curve, at 320°C Δ magnetite-water is -8.6 °/oo. Becker (1971) derived a magnetite-water fractionation curve from theoretical, experimental, and empirical data; the fractionation at 320°C is about -8.1 °/oo. The experimental magnetite-water calibration curve of Bertenrath and others (1972) shows that Δ = -9.6 °/oo at 320°C. Bottinga and Javoy (1973) estimate a magnetite-water curve for temperatures between 500-800' based on

both theoretical considerations and the data of Anderson and others (1971); at 320°C, the extrapolated Δ = -7.9 °/oo.

Extrapolations from the most recent magnetite-water fractionation curves thus show that the fractionation at 320°C is between -7.9 and -9.6 °/oo. Since the present uncertainty is about 1.7 °/oo at 320°C, the calculated water compositions cannot be estimated with any greater accuracy. The theoretical water compositions in equilibrium with hematite using Δ hematite-water = -8.1 °/oo are shown in Figs. 56 and 57. Calculated water compositions range from 3 to 8.5 °/oo, and thus the water composition is not constant.

The water compositions calculated for calcite in sandstones, shales, and veinlets in Magmamax #2 are also plotted on Fig. 56. Calcite data are very sparse below 3500' due to the general absence of calcite in permeable rocks at high temperatures. Water compositions calculated for hematite generally fall between the water compositions calculated for calcite in shale and quartz in sandstones, suggesting that the three minerals and water are all approximately in isotopic equilibrium. Due to the scarcity of hematite, veinlet and sandstone mineralization were generally combined. As has been illustrated earlier, veinlet and sandstone water compositions are not necessarily identical. Therefore, some of the scatter of the hematite data may be due to the combining of variable amounts of hematite equilibrated with waters of slightly different compositions.

Only one hematite was analyzed from Magmamax #3. The calculated water composition is shown on Fig. 57 along with the water composition trends calculated for calcite in sandstones, shales, and veinlets. There

is an excellent correlation between the high δO^{18} of the water calculated for the hematite sample, and a sharp isotope maximum calculated for water in equilibrium with nearby shale calcite. The hematite sample was collected from tiny veinlets in purple and gray shales; these types of shales tend to be impermeable. The similarity of the calcite and hematite water calculations suggests that the hematite was deposited from water very similar in oxygen isotopic composition to that circulating within the enclosing, rather impermeable, shales. Therefore not only are waters in permeable sandstones in equilibrium with the rocks, but waters in some shales as well.

Below 2700', water compositions calculated for calcite, quartz, and hematite are within about 2 $^{o}/oo$ of each other, suggesting that below here isotopic equilibrium has been established in many intervals. Above 2700', both dolomite and quartz were analyzed in addition to calcite, but neither dolomite nor quartz appear to be in equilibrium with the calcite. Vein calcites in the interval 2000-2700' often have approximately the same composition as nearby sandstones, suggesting that the calcite cement in these sandstones is in isotopic equilibrium with the water. Due to low temperatures and the impermeability of the upper shale unit above 1000', it is unlikely that hydrothermal calcite here is in equilibrium with the water. Between 1000' and 2000' there are insufficient data to conclude anything about isotope exchange; the calcite is probably only partially exchanged with the brine.

Effect of Salinity on δO^{18} Activity

In oxygen isotope geochemistry, rarely is a distinction made between the activity isotope ratio and the concentration isotope ratio because in most studies the difference between these ratios is within experimental accuracy. However, Truesdell (1974) has found that in hot highly saline fluids such as Salton Sea geothermal brines there may be a significant difference between the activity and concentration ratios due to water molecules bound into salt hydration structures.

Figure 58 shows the difference in the activity and concentration δO^{18} values of brine from a hypothetical Salton Sea well. The author collaborated on the construction of the figure; the calculations and assumptions made in the construction of the figure are presented in Olson (1976). At elevated temperatures, the salt effect may be as high as 7 $^{o}/oo$, thus without accurate water salinity data, water δO^{18} concentrations cannot be calculated with any greater accuracy. However, one can use calibration equations (e.g., O'Neil and others, 1969) to calculate water δO^{18} activities. Therefore, the water δO^{18} compositions presented in Figs. 53-57 are actually activity values, rather than concentrations.

Given accurate water salinity data, water concentration values may be calculated from activity δO^{18} values. Preliminary fluid inclusion freezing temperature data indicate that salinities in Magmamax #2 are similar to values calculated by Helgeson salinities in Magmamax #2 are similar to values calculated by Helgeson (1968) for nearby wells (C. I. Huang, pers. com., 1976), but presently there are insufficient data to estimate the actual water δO^{18} concentra-

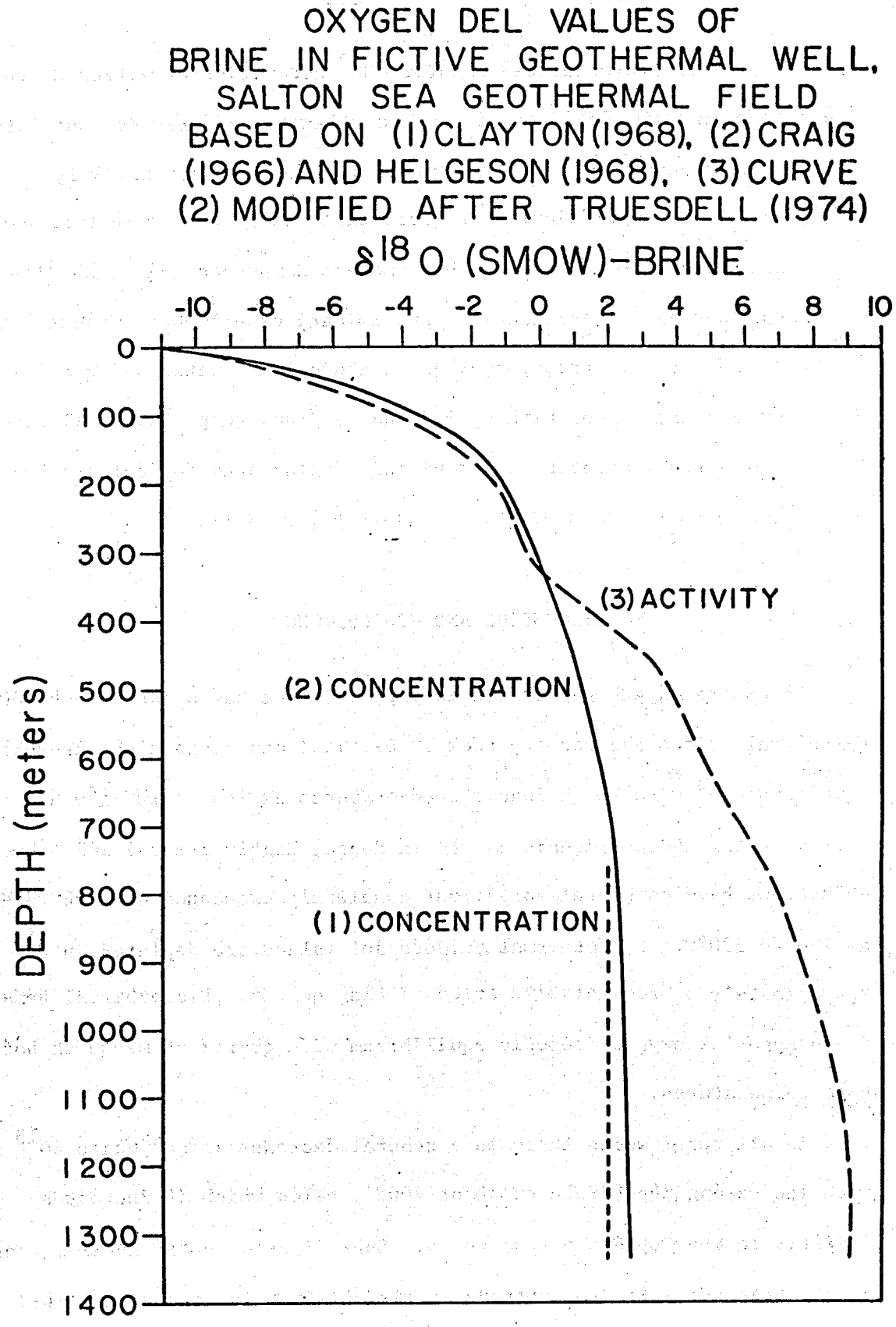
OXYGEN DEL VALUES OF
BRINE IN FICTIVE GEOTHERMAL WELL,
SALTON SEA GEOTHERMAL FIELD
BASED ON (1) CLAYTON (1968), (2) CRAIG
(1966) AND HELGESON (1968), (3) CURVE
(2) MODIFIED AFTER TRUESDELL (1974)
δ18 O (SMOW)-BRINE
-10 -8 -6 -4 -2 0 2 4 6 8 10
0
100
200
300
400
500
600
700
800
900
1000
1100
1200
1300
1400
DEPTH (meters)
(3) ACTIVITY
(2) CONCENTRATION
(1) CONCENTRATION

Figure 58

tions. Part of the variation in water δO^{18} activities of different rock types shown in Figs. 53-57 may be due to salinity differences, but large differences in salinity over short vertical intervals are unlikely.

Because of the difficulty of recrystallizing minerals in pure water, most calibrations of isotope geothermometers have been made with dilute salt solutions as "mineralizers". Preliminary experiments suggest that at 250°C the observed fractionations in the calcite-water and quartz-water systems may be too high by 1.5 and .3 °/oo, respectively (Truesdell, 1974). As a result, water δO^{18} activities calculated for calcite and quartz shown in Figs. 53-57 may be slightly too light.

DISCUSSION AND CONCLUSIONS

Extensive oxygen and carbon isotope exchange has occurred between geothermal brines and country rocks. Detrital and diagenetic carbonates have exchanged with the brines at temperatures as low as 100-150°C. Both detrital and authigenic quartz in dense, highly altered and mineralized sandstones have completely or almost completely exchanged at temperatures as low as 290°C. Hydrothermal epidote del values are depleted in O^{18} by approximately 4 °/oo relative to coexisting quartz. Hydrothermal hematite is in apparent oxygen isotopic equilibrium with quartz at measured borehole temperatures.

In all three wells there is a general decrease in carbonate δO^{18} with increasing depth down to about 3000', below which it increases slightly to the bottoms of the wells. Superimposed on the general trend is a pattern of multiple isotopic inversions; the locations and ampli-

tudes of the inversions are stratigraphically controlled. The isotopic composition of vein calcite is generally 0 to 1 °/oo lighter than calcite cement in sandstones, which in turn is 1 to °/oo lighter than calcite in shale.

There is a slight increase in δC^{13} with depth in the interval 1000-3500', below which it is approximately constant. Carbon isotope inversions are usually present at the same depths as oxygen isotope inversions. The carbon isotopic composition of vein calcite is lighter than that of sandstones, and carbon in sandstones is lighter than in shales. Shifts in δC^{13} are probably due to decarbonation reactions resulting in carbon isotope fractionation among carbonates, dissolved carbonate, and evolved CO_2.

Several isotope inversions above 2700' can be correlated between wells. What is actually being correlated are the major horizontal aquifers and aquitards. Water transport in the interval 1000-3000' is largely lateral and is stratigraphically controlled. Although the locations of the inversions are the same in the three wells, the amplitudes are different, suggesting that although the same stratigraphic unit is present in all the wells, it shows appreciable lateral variations.

Amplitudes of isotope inversions in Magmamax #3 are generally greater than those in Magmamax #2. The greater amplitude is caused by a greater variation in permeability in sandstones and shales in Magmamax #3. Water is apparently largely restricted to distinct aquifers in Magmamax #3, while in Magmamax #2 the water transport is more evenly distributed. The differences in the water distribution patterns in the three wells are probably a result of original differences in sedimenta-

tion; one possibility is that although major units are correlative and sandstone/shale ratios in Magmamax #2 and #3 are very similar above 2700', their distribution might be quite different, resulting in more evenly distributed water transport in Magmamax #2 than #3.

One of the problems of using cuttings rather than core is that in any handpicked sample of uniform chips, the individual chips are probably from several different beds within the sampled interval. If the calcite in similar-appearing chips from different beds within a 30' interval have very different isotopic compositions, the composition of the total sample represents a weighted "average" of several beds. Significant temperature fluctuations are unlikely over a 30' interval, so probably any variation in isotopic composition among similar-appearing chips from several nearby beds is due to permeability differences.

In his study of core from East Mesa geothermal wells, Coplen (1976) found as much as 8 °/oo variation in δO^{18} over several meters of homogeneous-appearing rocks. The variation within shale units (2 °/oo) was generally less than within sandstone units. Calcite in sandstone and shale beds only 10 cm apart had compositions differing by as much as 10 °/oo. Where sandstone and shale beds were thinner, their difference in δO^{18} was less. The variation in δO^{18} was largely due to differences in permeability; calcite in coarser grained sandstones had lower δO^{18} values. Calcite in thin shale beds enclosed by more permeable sandstones had isotopic compositions very close to that of the enclosing sandstone; hence the permeability of nearby rocks was important in determining the isotopic exchange of a rock. Due to the great scatter in isotopic com-

position over short distances seen in cores, when studying cuttings Coplen used bulk samples in order to average out the sharp variations.

Unfortunately, no core is available from Magmamax #2, #3, or Woolsey #1. However, it is reasonable to expect that at the higher temperatures of these wells there would be less isotopic variation or disequilibrium among homogeneous-appearing rocks over short intervals. Mesa 6-1, the hottest of the East Mesa wells is only 205°C at 8000'. Magmamax #2 and #3 reach 200° at about 1500', and 300° at 2900'. Above about 1500' in Magmamax #2 and #3, calcite in sandstones and shales is apparently not in isotopic equilibrium. Re-picked samples above 1500' frequently have quite different isotopic compositions, suggesting that there is appreciable variation in oxygen isotopic composition of these homogeneous-appearing chips; below 1500', the chips in homogeneous-appearing samples seem to have generally little variation in composition. Hence the analysis of any handpicked, uniform sample below 1500' probably is a reliable indicator of the composition of rocks within the interval, rather than an average of scattered data. Additional support for the reliability of homogeneous cuttings samples at temperatures over 200° is that the isotopic data form smooth, regular patterns which can be easily correlated with lithologic and mineralogical trends. Coplen (1976) found no correlation between the δO^{18} of calcite in bulk samples with lithologic composition, mineralogy, or geophysical logs.

Isotopic equilibrium, like chemical equilibrium, is very difficult to prove. Above 500-1500' the rocks are relatively impermeable and temperatures low; hence reaction kinetics are slow and isotope exchange

is incomplete. Above 1000', calcite and dolomite appear to be approximately in isotopic equilibrium at present temperature; since temperatures in this interval are rather low for complete exchange of detrital carbonates, the apparent equilibrium may be due to equilibrium precipitation of diagenetic carbonates.

In the interval 1500-2700' only calcite isotopic data are available. Calcite in the most permeable horizons has approximately the same isotopic composition as vein calcite, so presumably in at least some intervals calcite has totally exchanged with the brine. There are insufficient data to conclude whether the higher δO^{18} values in less permeable horizons indicates incomplete exchange or equilibration with a water of higher δO^{18} than in more permeable horizons.

Below 2500' the oxygen isotopic compositions of calcite in veinlets, sandstones, and shales converge to within approximately 1 °/oo, showing that permeability variations have less effect on isotopic composition and suggesting that all the calcite has completely exchanged with brine of the same composition. Below 2700', there is excellent agreement between water compositions calculated for quartz and hematite, and this water composition is within about 2 °/oo of that calculated to be in equilibrium with calcite at borehole temperatures. Therefore, many oxygen-bearing minerals below about 2700' are probably at or close to isotopic equilibrium with each other, and have equilibrated with a brine and δO^{18} activity of about 2 to 4 °/oo. This concordance of geothermometers may provide grounds for refuting any significant salt effect.

The consistency of calculated water compositions below 2700' suggests thorough mixing. Fractures are abundant in the interval, and minor vertical water transport within these fractures is probably partly responsible for the consistent compositions, regardless of permeability. The slight increases in calculated water compositions at the bottoms of Magmamax #2 and #3 are probably due both to lithologic changes and to a slight decrease in fracture abundance.

Above 2700', permeability variations appear to have a strong effect on isotope exchange. The large variation in calcite δO^{18} suggests that there are large differences in water isotopic composition in different lithologic units, and therefore that the waters are very poorly mixed. There has apparently been less brittle fracture above 2700', probably due to lesser mineralization and hence lesser induration of the rocks. Since fractures here are less abundant, vertical flow through shales is more difficult; the largely lateral flow of water results in large vertical variations in water composition.

The original permeabilities of the reservoir rocks, particularly the shales, have been considerably reduced by compaction and mineralization. Normally the permeability of shale is several orders of magnitude lower than sandstone; however, calcite isotopic compositions suggest that there have been only small differences in the water/rock ratios of different lithologic units. This suggests that water circulation in the reservoir is largely due to secondary rather than primary permeability. Although reservoir rocks are sealed by hydrothermal alteration, the increased mineralization makes them more susceptible to brittle fracture,

thereby increasing their effective permeability. The secondary permeability is probably caused by the development of intergranular microfractures.

Lithologic variations still have a strong effect on exchange, indicating that the creation of secondary permeability is lithologically controlled. Above 2700', microfracturing greatly aids lateral flow but apparently produces very little vertical flow. Below 2700' waters are more mixed, probably due to the development of abundant large fractures which, although largely confined to shales, apparently provide minor vertical circulation between lithologic units.

Minerals in larger fractures, such as the major fault offsetting the sedimentary section below 2700' in Magmamax #2 and the many veinlets with widths of several millimeters found below 2500' in the wells, have approximately the same chemical and isotopic compositions as minerals in the wall rocks. This suggests that the large fractures have not been major vertical water conduits since if they had, the chemical and isotopic compositions of the conduits water, and hence of the minerals precipitated, should have been very different from waters in the lithologically-controlled microfractures.

Above 2700' there is a good correlation between isotope minima and zones of high Saraband permeability; hence the isotopic compositions here reflect present rather than past permeabilities. Below 2700', the Saraband logs suggest that the present permeability is low; however, in this interval the water is well mixed and minerals in different lithologic units are in equilibrium. The abundance of veinlets in this interval also

suggests a high permeability. Either the interval is now sealed and impermeable, or the Saraband calculated permeability here is grossly inaccurate.

During the hydrothermal self-sealing of the wells, oxygen isotopic compositions of minerals may have been "frozen in". The apparent isotopic equilibrium between pairs of minerals may represent equilibrium to conditions no longer existing; the 2 to 4 °/oo water to which minerals apparently equilibrated may have been flushed away. Without analyzing formation fluids, one cannot prove conclusively whether the equilibrium between minerals is fossil or represents equilibrium under present conditions. The best evidence that the water with which the rocks have apparently equilibrated has not been later flushed away is the consistency of calculated water compositions for different minerals.

Calcite, quartz, and hematite isotopic compositions all suggest equilibration with a brine of 2 to 4 °/oo. Quartz is very resistant to isotope exchange and would be very slow to re-equilibrate to a new brine. Calcite is readily exchanged; while most of the calcite veinlets were formed early in the mineralization history, some were formed late, and many have been repeatedly refractured and healed with additional calcite. Hematite was generally the last mineral deposited. Regardless of these differences in paragenesis and exchangeability, the isotopic compositions of all three minerals suggest equilibration with the same brine; there is no evidence that this brine has been since flushed away.

Brines in the wells studied are apparently only well mixed below 2700'; above here the brines have great vertical variation in isotopic

composition. However, at River Ranch #1 Clayton and others (1968) concluded that calcite in the interval 400(?)-7000' was in isotopic equilibrium with brines of a constant composition of 2 ± .5 °/oo. Their data showed none of the strong lithologic control which is so prominent in this study.

The most plausible explanation for the discrepancy between this study and the River Ranch #1 study is that the sampling techniques used are different. Clayton and others (1968) used bulk samples rather than stones and shales caused by their relative permeabilities has therefore been averaged together. Their sampling interval is also considerably greater than in this study, hence reducing the probability of encountering rocks with anomalous δO^{18} values. Below 5700' in River Ranch #1 the calcite δO^{18} is 1 to 10 °/oo heavier than it should be if at equilibrium with the same water at the logged temperatures, and this difference is attributed to low permeability in this region (Clayton and others, 1968). The consistency of the estimated water composition between 400-5700' may be largely fortuitous.

SYNTHESIS

A major finding of this study is the effect of permeability variations on the isotopic composition and alteration of the rocks. Three nearby wells were studied in order to trace these effects laterally as well as vertically. The information in this study has been arranged into two semi-independent chapters: petrology and stable isotope geochemistry, both with a final discussion and summary of the data contained in it. The discussion below is an integration of conclusions from the previous chapters.

In evaluating a potentially-useful geothermal system, reservoir engineers are particularly interested in such topics as: the total amount of water and heat in storage, the location of the best aquifers, communication between deep and shallow aquifers, the pattern of lateral water circulation, self-sealing, and changes in reservoir rock characteristics to be expected from production and reinjection. Study of the petrology and stable isotope geochemistry provides information relating to all of these topices.

The most direct way to find the most useful aquifers in a system is to drill a well while measuring the quantity of water produced at successive horizons. Another means of determining the best aquifers is by running a Saraband log and using the computer-calculated permeability analysis; this computer program, however, was written for use in oil

wells, and expects to find oil, not extremely hot and saline brines, in the pore spaces. Saraband permeability values are hence useful only in a qualitative sense.

Saraband permeability logs for Magmamax #2, #3 (Fig. 28), and Woolsey #1 generally reflect sandstone-shale variations. Above 3000', the Saraband logs show several good aquifers. Stratigraphic correlations between wells using electrical logs is extremely difficult if not impossible due to the rapid facies changes in the Salton Trough (Randall, 1974). Correlations of aquifers using Sarabands thus are also very tenuous. However, correlations of isotopic inflections between wells clearly indicate the lateral water circulation patterns. By knowing precisely where the water is flowing, one can observe the effects of withdrawal, such as potential sealing, in the same aquifer in an adjacent well.

Mineralogical and isotopic trends do not necessarily indicate where rocks are presently permeable. The trends really only shown where water has been circulating in the past; units may not be completely sealed. However, if the unit is permeable according to a geophysical log, and petrology is consistent with a high permeability, for example: unaltered adularia rather than albite, the unit may still be a good producer. Or if several aquifers appear petrographically to be equally porous and unsealed, the horizon which the isotope data indicate has the highest water/rock ratio might be the best producer.

Below 3000', the rocks in Magmamax #2 and #3 are largely sealed by hydrothermal minerals--epidote, anhydrite, and pyrite. Although in this interval there are still minor differences in the oxygen and carbon

isotopic compositions of minerals in alternating sandstone and shale units, the calcite, hematite, and much of the quartz appear to be approximately in oxygen isotopic equilibrium with each other and with the presumed water composition. Quartz is extremely resistant to oxygen isotope exchange, and since much of the detrital quartz has been re-equilibrated, probably most of the other silicates have also re-equilibrated. A considerable volume of water was necessary to exchange with all these rocks, however, the rocks are now relatively impermeable due to self-sealing. So although the water/rock ratio in this zone is very high, the ratio only indicates a fossil permeability.

The carbon and oxygen isotopic compositions of calcite in sandstones are generally several per mil lighter than in adjacent shales due to the greater permeability of the sandstones. There is also an excellent correlation between the sandstone/shale ratio and isotopic composition. In shaley units, the oxygen isotopic composition of minerals in both the shales and sandstones is locally high; in the more sandy intervals which are presumably more permeable, the isotopic compositions of both rock types are lower. Therefore, the isotopic composition of calcite or any other mineral is strongly affected by the permeability of adjacent but different rocks. Although the detrital mineralogy and fabric of sandstones in shaley and sandy intervals may be identical, the sandstone in the sandy interval is found to be more highly altered and the minerals have more completely exchanged isotopically with the water than sandstones in shaley intervals. There is a good correlation among

the more permeable zones as indicated by the sandstone/shale ratio, isotope minima, and high abundance of late stage hydrothermal minerals.

Below 3000' in Magmamax #3 there are several very shaley intervals which, according to the low degree of isotope exchange, have had only minor water circulation. The mineral assemblages in the shales and minor sandstones are very different from assemblages in adjacent, more permeable zones. The impermeable zone assemblages appear to be relict assemblages preserved beyond their otherwise normal stability range due to the insufficient water circulation which impeded mineral reaction rates. Mineral assemblages in these impermeable zones are generally typical of rocks 1000' shallower.

In Woolsey #1, the sandstone/shale ratio is relatively high, and the higher pearmeability has resulted in mineral assemblages at shallow depths in Woolsey #1 which are typical of over 1000' deeper (and hotter) in Magmamax #2 and #3. The isotopic composition of calcite in Woolsey #1 is also much lower than at the same level in the other wells. Temperature seems to often be less important than permeability and water circulation in the kinetics of mineral stabilities.

Mineralized fractures are very abundant in Magmamax #2 and #3 below 3000'. Although the wall rocks are largely sealed, the fractures might provide sufficient permeability to make this zone a potential producer. Bodvarsson (1964) notes that "fractures of various types are the most important conductors of circulating fluids in practically all major geothermal systems." Natural hydraulic fracturing in self-sealed

areas frequently makes these zones better producers than the most porous stratigraphic units.

The mineralogy of the veinlets is very closely related to that of the adjacent wall rocks. The mineral parageneses are almost identical, and mineralization of the veinlets appears to have been largely contemporaneous with wall rock mineralization. Veinlets in the impermeable zones have the same "relict" assemblages as are found in the host rocks.

The oxygen and carbon isotopic compositions of vein minerals are also frequently closely related to those of minerals in the nearby wall rocks. The compositions of vein minerals are heavier in relatively impermeable zones; the vein waters appear to reflect the composition of nearby pore waters. The vein minerals are isotopically slightly lighter than minerals in adjacent rocks. This is probably the result of fractionation between water and minerals during the precipitation of vein minerals from an isolated fluid, or possibly due to evolution of CO_2 during hydraulic fracturing.

The close similarity between mineralogy and the isotopic composition of veinlets and enclosing rocks suggests that vein waters might reasonably be locally derived from adjacent rocks. Or if the water was derived from elsewhere, it rapidly equilibrated chemically and isotopically with the wall rocks so as to be identical to waters circulating through adjacent rocks; in this case, the water/rock ratio in the veinlets must have been very small.

Available data cannot distinguish between these two different vein-water models. Both models indicate that the veinlets were unimportant

as circulation channels; little or no water flowed in veinlets very far from the source of the water. The zone of highly fractured but otherwise nonporous rocks below 3000' does not seem to be a potential production zone.

The largest fault zone in the wells studied is located at about 2700' in Magmamax #2 (Randall, 1974). Since units below this depth cannot be correlated with any intervals in Magmamax #3, there has apparently been considerable offset. The fault zone has been extensively brecciated and mineralized, indicating abundant water circulation, but calcite and quartz in this interval are not more exchanged than in nearby rocks. Therefore, it is likely that the calcite and quartz in both the veinlets and adjacent rocks have completely exchanged and are in equilibrium with the water.

Not only are there large differences in mineralogy and isotope exchange among the various rock types, but there also are large variations between similar rock types in vertically adjacent intervals. These large vertical variations indicate that water circulation was largely lateral rather than vertical. The abundant shales serve as aquitards preventing water mixing, and the waters are consequently vertically stratified. Salinity increases with increasing depth; salinity curves approximately parallel temperature profiles (Helgeson, 1969). The variations in water composition between rock types probably parallel variations in rock permeability and isotope exchange. The lesser variation in the isotopic composition of minerals in sandstones and shales in Magmamax #2, and

the more gradual nature of its mineralogical trends probably reflects lesser vertical variation in water chemistry, and hence better mixing.

The same stratigraphic units are present above 2700' in all three wells; the individual beds, however, are different due to the rapid facies changes in the Salton Trough. Rock units in Magmamax #2 and #3 are very similar, but the units thin towards Woolsey #1 and the sandstone/shale ratio here is greater.

Several isotope inversions can be correlated between Magmamax #2 and #3, but the amplitudes of the inflections are different. Although there is very little difference in sandstone/shale ratios between the wells, the amplitudes are always significantly greater in Magmamax #3. X-ray diffraction data indicate that the amplitudes of the quartz and mica abundances in bulk samples are greater in Magmamax #3. Since quartz and mica are the most abundant minerals in sandstones and shales respectively, the x-ray data suggest that sandstones and shales are less evenly distributed and that individual sandstone and shale beds are thicker in Magmamax #3 than in Magmamax #2. This model is consistent with the isotope data. With thinner and more finely interbedded sandstone and shale beds in Magmamax #2, water in adjacent beds would have more opportunity to exchange chemically and isotopically, resulting in less variation in isotopic composition between beds, more vertical circulation, and better-mixed geothermal fluids. The difference in bedding distribution between Magmamax #2 and #3 is probably due to some slight facies change between the wells. It is peculiar that there is such a systematic dif-

ference in bedding over greater than 2700' when the wells are only one-half mile apart.

The top of the circulating geothermal system can be inferred from isotope data. There is considerable scatter in the oxygen and carbon isotopic compositions of calcite in rocks above 1500'. The inhomogeneity indicates that there has been insufficient circulation to establish isotopic equilibrium over even short vertical or horizontal distances. Below 1500' there is considerably more exchange between the water and the rocks due to greater water circulation. The top of the system approximately coincides with the base of the upper shale cap rock. Randall (1974) noted that the shale unit acts as an insulating barrier which has helped retain the heat.

The study of active geothermal systems provides a fascinating insight into the arcane mysteries of metamorphism, metasomatism, and ore genesis which have been the traditional objectives of much petrological and geochemical research. In return, such studies provide a basis for improving our understanding of geothermal systems themselves. It is my hope that this thesis has made some contribution to both these aspects.

REFERENCES

Ames, L. L. and Sand, L. B., 1958, Factors Effecting Maximum Hydrothermal Stability in Montmorillonites, Amer. Min., v. 43, p. 641-648.

Anderson, A. T., Jr.; Clayton, R. N.; and Mayeda, T. K., 1971, Oxygen Isotope Thermometry of Mafic Igneous Rocks, Jour. Geol., v. 79, No. 6, p. 715-729.

Blattner, P., 1975, Oxygen Isotopic Composition of Fissure-grown Quartz, Adularia, and Calcite from Broadlands Geothermal Field, New Zealand, with an appendix on quartz-K-feldspar-calcite-muscovite oxygen isotope geothermometers, Amer. Jour. Sci., v. 275, No. 7, p. 785-800.

Becker, R. H., ms, 1971, Carbon and Oxygen Isotope Ratios in Iron-Formation and Associated Rocks From the Hamersley Range of Western Australia and Their Implementations, Ph.D. thesis, University of Chicago.

Bertenrath, R.; Friedrichsen, H.; and Hellner, E., 1973, Fractionation of the Oxygen Isotopes O-16/O-18 in the System Iron Oxide-Water (abstr), In Deutsche Mineralogische Gesellschaft, Sektion Geochimie, Fruehjahrstagung, 1972, Referate, Fortschr. Mineral., Vol. 50, Beih. 3, p. 32-33.

Biehler, Shawn, 1964, Geophysical Study of the Salton Trough of Southern California: Ph.D. dissertation, Calif. Institute of Technology, p. 139.

Bird, D. K., 1975, Geology and Geochemistry of the Dunes Hydrothermal System, Imperial Valley of California: M.S. thesis, University of California at Riverside, Institute of Geophysics and Planetary Physics Report, No. 75-2, p. 123.

Blount, C. W., and Dixon, F. W., 1973, Gypsum-Anhydrite Equilbria in the Systems $CaSO_4$-H_2O and $CaCO_3$-NaCl-H_2O, Amer. Min., v. 58, p. 323-331.

Bodvarsson, G., 1963, An Appraisal of the Potentialities of Geothermal Resources in Iceland: Verkfraeöingafelag Islands, Timarit arg. 48, h. 5, p. 65-71.

Bottinga, Y., and Javoy, M, 1973, Comments on Oxygen Isotope Geothermometry, Earth Planet. Sci. Lett., v. 20, No. 2, p. 250-265.

Brindley, G. W., 1961, Chlorite Minerals, in Brown ed, The X-Ray Identification of Clay Minerals, Mineral. Soc., London, p. 242-296.

Brown, George, ed, 1961, The X-Ray Identification and Crystal Structures of Clay Minerals, 2nd ed., London Mineral. Soc., Clay Minerals Group, p. 544.

Brown, E. H., 1967, The Greenschist Facies in Part of Eastern Otago, New Zealand, Contrib. Min. Petrol., v. 14, No. 4, p. 259-292.

Browne, P. R. L., and Ellis, A. J., 1970, The Ohaki-Broadlands, Hydro-Thermal Area, New Zealand: mineralogy and related geochemistry, Amer. Jour. Sci., v. 269, p. 97-131.

Clayton, R. N., and Epstein, S., 1961, The Use of Oxygen Isotopes in High-Temperature Geological Thermometry, Jour. Geol., v. 69, No. 4, p. 447-452.

Clayton, R. N. and Mayeda, T. K., 1963, The Use of Bromine Pentafluoride in the Extraction of Oxygen from Oxides and Silicates for Isotopic Analysis, Geochim. Cosmochim. Acta, v. 27, p. 43-52.

Clayton, R. N.; Muffler, L. J. P.; and White, D. E., 1968, Oxygen Isotope Study of Calcite and Silicates of the River Ranch No. 1 Well, Salton Sea Geothermal Field, California, Amer. Jour. Sci., v. 266, p. 968-979.

Clayton, R. N.; O'Neil, J. R.; and Mayeda, T. K., 1972, Oxygen Isotope Exchange Between Quartz and Water, Jour. Geophy. Res., v. 77, p. 3057-3067.

Combs, J., 1971, Heat Flow and Geothermal Resource Estimates for the Imperial Valley, in, Cooperative geological-geophysical-geochemical investigations of geothermal resources in the Imperial Valley area of California: Final report (FY 1971), Contr. No. 14-06-300-2194, U. S. Bureau of Reclamation, p. 5-28.

Combs, J., and Hadley, D. M., 1973, Microearthquake Investigation of the Mesa Geothermal Anomaly, Imperial Valley, California: EOS, v. 54, p. 1213-1214.

Cook, H. E.; Johnson, P. D.; Matti, J. C.; and Zemmels, I., 1974, Methods of Sample Preparation and X-Ray Diffraction Data Analysis, X-Ray Mineralogy Laboratory, Deep Sea Drilling Project, University of California, Riverside, Institute of Geophysics and Planetary Physics, UCR Contrib. No. 74-5.

Coplen, T. B., 1973a, Cooperative Geochemical Investigation of Geothermal Resources in the Imperial Valley and Yuma Areas: University of California at Riverside, Institute of Geophysics and Planetary Physics report no. 73-48, p. 22.

Coplen, T. B., 1973b, A Double-Focusing, Double-Collecting Mass Spectrometer for Light Stable Isotope Ratio Analysis, Int. J. Mass Spectrom. Ion Phys., v. 11, p. 37-40.

Coplen, T. B., 1974, Utilization of the Sodium-Potassium-Calcium Geothermal Technique in the Imperial Valley Area, California, Institute of Geophysics and Planetary Physics report no. 74-2.

Coplen, T. B.; Kolesar, P.; Taylor, R. E.; Kendall, C.; and Mooser, C., 1975, Investigations of the Dunes Geothermal Anomaly, Imperial Valley, California, Part IV. Geochemical studies of water, calcite, and silicates. Published by the Institute of Geophysics and Planetary Physics, University of California, Riverside, p. 42.

Coplen, T. B., 1976, Cooperative Geochemical Resource Assessment of the Mesa Geothermal System, University of California, Riverside, Institute of Geophysics and Planetary Physics report no. 76-1, report to the U. S. D. I., Bureau of Reclamation.

Craig, H., 1957, Isotopic Standards for Carbon and Oxygen and Correction Factors for Mass-Spectrometric Analysis of Carbon Dioxide, Geochim. Cosmochim. Acta, v. 12, p. 133-149.

Craig, H., 1961, Standard for Reporting Concentrations of Deuterium and Oxygen-18 in Natural Waters, Science, v. 133, p. 1833-1834.

Craig, H., 1966, Isotopic Composition and Origin of the Red Sea and Salton Sea Geothermal Brines, Science, v. 154, p. 1544-1548.

Crowell, J. C., 1962, Displacement Along the San Andreas Fault, California, Geol. Soc. Amer. Bull. No. 71, p. 49.

Degens, E. T., and Epstein, S., 1964, Oxygen and Carbon Isotope Ratios in Co-existing Calcites and Dolomites from Recent and Ancient Sediments, Geochim. Cosmochim. Acta, v. 28, No. 1, p. 23-44.

de Segonzac, G. D., 1970, The Transformation of Clay Minerals During Diagenesis and Low-Grade Metamorphism: a review, Sedimentology, v. 15, p. 281-346.

Dibblee, T. W., Jr., 1954, Geology of the Imperial Valley Region, California, in, Jahns, R. H., ed., Geology of Southern California, Calif. Div. Mines Bull., 170, p. 21-28.

Doe, B. R.; Hedge, C. F.; and White, D. E., 1966, Preliminary Investigation of the Source of Lead and Strontium in Deep Geothermal Brines Underlying the Salton Sea Geothermal Area, Econ. Geo., v. 61, p. 462-483.

Downs, T., and Woodward, G. D., 1961, Middle Pleistocene Extension of the Gulf of California into the Imperial Valley, Geol. Soc. Amer. Abstr., Spec. Paper 68, p. 21.

Durham, J. W., and Allison, E. C., 1962, Stratigraphic position of Fish Creek gypsum at Split Mountain Gorge, Imperial County, California (abstr.), Geol. Soc. Amer. Spec. Paper 68, p. 22.

Elders, W. A. and Bird, D. K., 1974, Investigations of the Dunes Geothermal Anomaly, Imperial Valley, California: Part II. Petrological studies, published by IGPP, University of California, Riverside, Contri. No. IGPP-UCR-74-13, p. 14.

Elders, W. A; Rex, R. W.; Meidav, T.; Robinson, P. T.; and Biehler, S., 1972, Crustal Spreading in Southern California, Science, v. 178, p. 15-24.

Ellis, A. J., 1963, The Solubility of Calcite in Sodium Chloride Solutions at High Temperatures, Amer. Jour. Sci., v. 261, p. 259-267.

Epstein, S.; Buchsbaum, R.; Lowenstam, H.; and Urey, H. C., 1951, Carbonate-Water Isotopic Temperature Scale, Geol. Soc. Amer. Bull., v. 62, p. 417-426.

Epstein, S.; Graf, D. L.; and Degens, E. T., 1964, Oxygen Isotope Studies on the Origin of Dolomites, Chap. 13 in Isotopic and cosmic chemistry, Amsterdam, Netherlands, North-Holland Publishing Co., p. 169-180.

Ernst, W. G., 1964, Petrochemical Study of Co-existing Minerals from Low-Grade Schists, Farter Shikoku, Japan, Geochim. Cosmochim. Acta, v. 28, p. 1631-1668.

Eslinger, E. V. and Savin, S. M., 1973, Mineralogy and Oxygen Isotope Geochemistry of the Hydrothermally Altered Rocks of the Ohaki-Broadlands, New Zealand Geothermal Area, Amer. Jour. Sci., v. 273, p. 240-267.

Fritz, P., and Smith, D. G. W., 1970, The Isotopic Composition of Secondary Dolomites, Geochim. Cosmochim. Acta, v. 34, p. 1161-1173.

Griscom, A., and Muffler, L. J. P., 1971, Aeromagnetic Survey of the Salton Sea Geothermal Field, southeastern California (abstr.), Geol. Soc. Amer., Abstr., v. 3, No. 2, p. 129.

Haas, J. L., 1971, The Effect of Salinity on the Maximum Thermal Gradient of a Hydrothermal System at Hydrostatic Pressure, Econ. Geol., v. 66, p. 940-946.

Helgeson, H. C., 1968, Geologic and Thermodynamic Characteristics of the Salton Sea Geothermal System, Amer. Jour. Sci., v. 266, p. 129-166.

Helgeson, H. C., 1969, Thermodynamics of Hydrothermal Systems at Elevated Temperatures and Pressures, Amer. Jour. Sci., v. 267, p. 729-804.

Hoagland, J. R., 1976, Petrology and Geochemistry of Hydrothermal Alteration in borehole Mesa 6-2, East Mesa Geothermal Area, Imperial Valley, California, Thesis, Dept. of Geol. Sciences, University of California, Riverside.

Keith, T. E. C.; Muffler, L. J. P.; and Cremer, M., 1968, Hydrothermal Epidote Formed in the Salton Sea Geothermal System, California, Amer. Min., v. 53, nos. 9-10, p. 1635-1644.

Lang, W., 1959, The Origin of Some Natural Carbon Dioxide Gases, Jour. Geophy. Res., v. 64, No. 1.

Longwell, C. R., 1954, History of the Lower Colorado River and Imperial Depression, in, Jahns, R. H., ed., Geology of Southern California, Calif. Div. Mines Bull., v. 170, p. 56.

McCrea, J. M., 1950, On the Isotopic Chemistry of Carbonates and a Paleotemperature Scale, Jour. Chem. Phys., v. 18, p. 849-857.

Meidav, T., and Fergurson, R., 1972, Resistivity Studies of the Imperial Valley Geothermal Area, California, Geothermics, v. 1, p. 47-62.

Merriam, R., and Bandy, O. L., 1965, Source of Upper Cenozoic Sediments in the Colorado River Delta Region, Jour. Sed. Petrol., v. 35, p. 911-916.

Mook, W. G., 1968, Geochemistry of the Stable Carbon and Oxygen Isotopes of Natural Waters in the Netherlands. Ph.D. Thesis, University of Groningen, Netherlands.

Muffler, L. J. P., and Doe, B. R., 1968, Composition and mean age of Detritus of the Colorado River Delta in the Salton Trough, southeastern California, Jour. Sed. Petrol., v. 38, p. 384-399.

Muffler, L. J. P. and White, D. E., 1968, Origin of CO_2 in the Salton Sea Geothermal System, southeastern California, U.S.A., XXIII International Geol. Cong., v. 17, p. 185-194.

Muffler, L. J. P., and White, D. E., 1969, Active Metamorphism of Upper Cenozoic Sediments in the Salton Sea Geothermal Field and the Salton Trough, southeastern California, Geol. Soc. Amer. Bull., v. 80, p. 157-182.

Myer, G. H., 1965, X-Ray Determinative Curve for Epidote, Amer. Jour. Sci., v. 263, p. 78-86.

Northrop, D. A., and Clayton, R. N., 1966, Oxygen-Isotope Fractionations in Systems Containing Dolomite, Jour. Geol., v. 74, p. 174-196.

Naboko, S. I., 1970, Facies of Hydrothermally Altered Rocks of Kamchatka-Kurile Volcanic Arc, in Pacific geology, Part 2, Tsukiji Shokan Publ. Co., Tokyo, p. 23-27.

Olson, E. R., 1976, Oxygen Isotope Studies of the Salton Sea Geothermal Field: New Insights, paper submitted to the Proceedings of International Stable Isotope Conference, D.S.I.R., Wellington, New Zealand.

O'Neil, J. R., and Clayton, R. N., 1964, Oxygen Isotope Geothermometry, Chap. 12 in Isotopic and cosmic chemistry, Amsterdam, Netherlands, North-Holland Publ. Co., p. 157-168.

O'Neil, J. R., and Epstein, S., 1966, Oxygen Isotope Fractionation in the System Dolomite-Calcite-Carbon Dioxide, Science, v. 152, No. 3719, p. 198-201.

Pettijohn, F. J.; Potter, P.E.; and Siever, R., 1972, Sand and Sandstone, New York, Heidelberg, Berlin, Springer-Verlag, p. 618.

Randall, W., 1974, An Analysis of the Subsurface Structure and Stratigraphy of the Salton Sea Geothermal Anomaly, Imperial Valley, California, Ph.D. Thesis, University of California, Riverside, p. 92.

Rex, R. W., 1966, Heat Flow in the Imperial Valley of California (abstr.) Amer. Geophy. Union Trans., v. 47, No. 1, p. 181.

Robinson, P. T.; Elders, W. A.; and Muffler, L. J. P., 1976, Holocene Volcanism in the Salton Sea Geothermal Field, Imperial Valley, California, Geol. Soc. Amer. Bull., v. 87, p. 347-360.

Sand, L. B.; Roy, R.; and Osborn, E. F., 1957, Stability Relations of Some Minerals in the Na_2O-Al_2O_3-S_1O_2-H_2O System, Econ. Geol, v. 52, p. 169-179.

Sharma, T., and Clayton, R. N., 1965, Measurement of O^{18}/O^{16} Ratios of Total Oxygen of Carbonates, Geochim. Cosmochim. Acta, v. 29, p. 1347-1353.

Sheppard, S. M. F., and Schwarcz, H. P., 1970, Fractionation of Carbon and Oxygen Isotopes and Magnesium Between Co-existing Metamorphic Calcite and Dolomite, Contrib. Min. Petrol, v. 26, No. 3, p. 161-198.

Sigurdson, D. R.; Meidav, T.; and Sharp, R. V., 1971, Structure of Sediments Under the Salton Sea (abstr), Geol. Soc. Amer, Abstr., v. 3, No. 2, p. 192-193.

Skinner, B. J.; White, D. E.; Rose, H. J.; and Mays, R. E., 1967, Sulfides Associated with the Salton Sea Geothermal Brine, Econ. Geol., v. 62, p. 316-330.

Syers, J. K.; Chapman, S. L.; Jackson, J. L.; Rex, R. W.; and Clayton, R. N., 1968, Quartz Extraction From Rocks, Sediments and Soils for Determination of Oxygen Isotopic Composition, Geochim. Cosmochim. Acta, v 32, p. 1022-1025.

Taylor, H. P., Jr., 1968, Oxygen Isotope Studies of Hydrothermal Mineral Deposits, in Geochemistry of Hydrothermal Ore Deposits, Barnes, H. L., ed., Holt Rinehart and Winston, Inc., New York, p. 109-142.

Taylor, H. P., Jr., and Epstein, S., 1962, Relationship Between O^{18}/O^{16} Ratios in Co-existing Minerals of Igneous and Metamorphic Rocks, Part 2, Application to Petrological Problems, Geol. Soc. Amer. Bull., v. 23, p. 675-694.

Truesdell, A. H., 1974, Oxygen Isotope Activities and Concentrations in Aqueous Salt Solutions at Elevated Temperatures; consequences for isotope geochemistry, Earth Planet. Sci. Letters, v. 23, p. 387-396.

Truesdell, A. H., and Singers, W., 1971, Computer Calculation of Down-hole Chemistry in Geothermal Areas: New Zealand Dept. Scientific and Industrial Research, Report C.D. 2136, 145 p.

Turner, F. J., 1968, Metamorphic Petrology: Mineralogical and Field Aspects, New York, McGraw-Hill, p. 403.

Urey, H. C., 1947, Thermodynamic Properties of Isotopic Substances, Jour. Chem. Soc., Part 2, p. 562-581.

Van De Kamp, P. C., 1973, Holocene Continental Sedimentation in the Salton Basin, California: A reconnaissance, Geol. Soc. Amer. Bull., v. 84, p. 827-848.

Walters, L. J.; Claypool, G. E.; and Choquette, P. W., 1972, Reaction Rates and SO^{18} Variation for the Carbonate-Phosphoric Acid Preparation Method, Geochim. Cosmochim. Acta, v. 36, p. 129-140.

White, D. E., 1968, Environments of Generation of Some Basemetal Ore Deposits, Econ. Geol., v. 63, p. 301-335.

APPENDIX I, TABLE I

Microprobe Analyses of Authigenic Feldspar*

	1.	2.	3.	4.
SiO_2	64.66	66.00	63.86	66.30
TiO_2	--	--	--	.02
Al_2O_3	18.18	18.64	18.07	19.30
FeO	.01	.18	.01	.18
MgO	.02	.06	--	.04
BaO	.03	.19	.83	--
CaO	--	.16	--	.32
Na_2O	.49	4.83	.40	10.80
K_2O	15.14	8.70	14.55	.12
TOTAL	98.53	98.60	97.72	97.08
Mole %				
Or	95.02	53.02	94.30	.73
Ab	4.69	44.69	3.96	96.72
An	--	.81	--	1.59

* Descriptions of microprobed samples are given on page 201

TABLE II

Microprobe Analyses of Epidote

	1.	2.	3.	4.	5.	6.	7.	8.	9.
SiO_2	38.14	36.99	38.13	38.74	38.87	37.26	37.41	39.04	35.66
TiO_2	.01	.07	.1	.09	.06	.01	---	.03	.02
Al_2O_3	22.77	20.72	20.47	20.57	20.62	21.39	24.05	23.48	19.83
FeO	13.56	14.74	13.33	13.83	12.46	14.12	11.85	12.90	14.68
MnO	.15	.14	.28	.14	.19	.11	.07	.13	.38
MgO	.09	.25	.29	.19	.19	.13	.02	.16	.21
CaO	23.57	23.53	22.73	22.80	21.77	23.76	23.72	23.79	21.78
Ce_2O_3	.11	---	.17	.09	---	.02	---	---	---
F	.12	.07	.06	---	---	.08	---	.14	.08
TOTAL	98.52	96.51	95.56	96.45	94.16	96.88	97.12	99.67	92.64
Fe^{+3}	.89	.991	.91	.93	.86	.94	.78	.83	1.03
Al^{VI}	2.10	1.93	1.96	1.95	2.00	2.00	2.20	2.14	1.95

TABLE II (continued)

	10.	11.	12.	13.	14.	15.	16.	17.	18.
SiO_2	37.79	35.66	37.03	36.58	36.25	37.03	37.58	37.06	37.64
TiO_2	.03	.06	.01	.04	---	---	---	---	.04
Al_2O_3	20.16	19.95	22.57	20.52	20.71	21.90	23.99	24.08	23.17
FeO	15.17	16.21	12.59	15.80	15.63	13.87	10.89	10.76	10.38
MnO	.13	.23	.01	.11	.57	.37	.43	.74	.25
Mgo	.19	.09	.06	.06	.13	.14	---	.03	.12
CaO	23.49	23.38	23.96	23.73	23.14	23.35	23.44	23.20	24.10
Ce_2O_3	.09	---	.05	---	.16	---	---	.08	---
F	.17	---	.03	---	---	---	---	---	.1
TOTAL	97.22	95.58	96.31	96.34	96.59	96.56	96.17	95.95	95.80
Fe^{+3}	1.02	1.10	.84	1.03	1.05	.93	.73	.72	.69
Al^{VI}	1.90	1.82	2.09	1.90	1.89	2.03	2.24	2.24	2.19

TABLE II (continued)

	19.	20.	21.	22.	23.	24.	25.	26.
SiO_2	36.71	43.44	35.91	35.23	35.90	34.88	35.01	35.12
TiO_2	---	.07	.04	.08	.10	.07	.03	.06
Al_2O_3	23.78	19.51	17.58	18.80	20.99	18.44	20.42	19.27
FeO	11.46	12.07	13.70	12.72	11.29	12.53	12.24	13.70
MnO	.10	.24	.23	.05	.19	.25	.19	.22
MgO	.04	.15	.04	.29	.20	.29	.08	.32
CaO	23.97	19.59	20.21	20.48	21.39	19.80	21.57	20.15
Ce_2O_3	.08	---	---	---	---	---	.24	.02
F	.04	---	---	.03	---	.08	.10	.03
TOTAL	96.18	95.07	87.71	87.68	90.06	86.34	89.88	88.89
Fe^{+3}	.77	.82	1.02	.94	.81	.94	.88	1.00
Al^{VI}	2.17	1.88	1.84	1.96	2.12	1.95	2.07	1.98

TABLE III

Microprobe Analyses of Chlorite and Tremolite

	Chlorite		Tremolite *			
	1.	2.	3.	4.	5.	6.
SiO_2	33.22	33.35	35.49	45.39	42.68	41.75
TiO_2	.27	1.41	.02	.02	.02	---
Al_2O_3	19.62	19.54	.51	.68	.66	.75
FeO	6.95	7.54	5.15	6.65	6.35	6.50
MnO	---	.05	.32	.42	.29	.34
MgO	23.33	22.34	12.64	16.32	14.84	15.37
CaO	.14	.08	6.51	8.57	8.13	7.83
Na_2O	.29	.22	.25	.42	.32	.27
K_2O	1.59	1.94	.09	.29	.23	.12
F	.20	.20	.08	.35	.40	.21
Cl	.07	.07	.35	.33	.28	.23
TOTAL	85.68	86.74	61.41	79.44	74.20	73.37
Excess Ox	14.32	13.26	38.59	20.56	25.80	26.63
Form. Prop.	(36 Ox)	(36 Ox)	% Ferro-actinolite:			
Si	6.33	6.23				
Ti	.40	.15	18.6	17.9	19.3	19.1
Al^{IV}	1.69	1.77				
Al^{VI}	2.71	2.56				
Fe^{+2}	1.20	1.09				
Mn	.02	---				
Mg	6.32	6.52				
Ca	.017	.03				
Na	.08	.11				
K	.47	.38				
F	.12	.12				
Cl	.02	.02				
$Si+Al^{IV}$	8.02	8.00				
H_2O	16.96	18.04				
Rest	11.75	10.98				

* These totals are low probably because of the difficulty of analyzing such fine-grained material. However, the effect on major cations is likely to be uniform so that the reported ratios FeO to MgO are believed to be representative of the true values.

TABLE IV

Microprobe Analyses of Garnets *

	1.	2.
SiO_2	34.67	34.69
TiO_2	.03	.17
Al_2O_3	5.23	7.51
Cr_2O_3	---	---
Fe_2O_3	24.83	20.73
MnO	.34	.36
MgO	.10	.05
CaO	34.67	34.80
TOTAL	99.87	98.31
Mole %		
Spessartine	.7	.8
Pyrope	.4	.2
Andradite	74.6	62.0
Grossularite	24.3	37.0

* Descriptions of microprobed samples are given on page 201

Descriptions of Microprobed Samples

TABLE I

1. and 2. 3810' in Magmamax #2; pseudomorph after anhydrite(?) in shale.

3. 3500' in Magmamax #2; veinlet in green shale with epidote core.

4. 3790' in Magmamax #3; forms a band replacing shale along boundary between shale and calcite veinlet.

TABLE II

1. and 2. 3670' in Magmamax #3; veinlet in dark gray shale.

3.-5. 3670' in Magmamax #3; band in dark gray shale replaced by black epidote.

6. 3670' in Magmamax #3; veinlet of green epidote cross-cutting black epidote band (analyses #3-5).

11.-13. 3810' in Magmamax #2; veinlet in siltstone. The epidote is associated with hematite, anhydrite, and garnet (analyses #1 and 2, Table IV).

14.-15. 3810' in Magmamax #2; veinlet in green shale.

16. and 17. 3600' in Magmamax #2; veinlet in shale with adularia rim (analysis #3, Table I)

18. and 19. 2690' in Magmamax #2; pale yellowish epidote forming honeycomb breccia cement associated with adularia.

7.-10. 3670' in Magmamax #3; miscellaneous green epidote veinlets in dark gray shale associated with calcite, tremolite (analyses # 3-5, Table III) and pyrite.

20.-26. 3410' in Magmamax #2; epidote cement in miscellaneous sandstones.

TABLE III

1. and 2. 3600' in Magmamax #2; oriented chlorite in green shale.

3.-5. 3670' in Magmamax #3; fibrous tremolite in veinlets in dark gray shale. The low yields are due to epoxy volatization; however, the stoichiometries of the analyses are reasonable.

TABLE IV

1. and 2. 3810' in Magmamax #2; veinlet in siltstone. The garnet is pale honey-colored, first order gray, and is cut across by hematite, anhydrite, and epidote (analyses #11-13, Table II); it is zoned and the analyses were positioned as shown below:

APPENDIX II, TABLE I

X-ray Diffraction Analyses of Bulk Shales

	DEPTH	CALC.	QTZ.	PLAG.	KSPAR	ANHY.	EPID.	PYR.	MICA	CHL.
MAGMAMAX #2	1550'	11.2	31.0	7.2	13.2	--	--	--	34.8	2.6
	1700	17.0	38.7	6.3	7.9	--	--	--	26.8	3.4
	1940	12.1	38.3	18.2	16.8	--	--	--	11.0	3.6
	2120	14.1	42.3	14.2	14.4	--	--	--	12.3	2.8
	2330	11.6	32.9	9.9	9.7	--	--	--	28.9	6.9
	2630	14.6	38.7	15.6	3.0	--	--	--	20.0	8.1
	2780	9.9	37.0	20.2	10.0	1.7	2.5	--	12.4	6.2
	3020	11.4	22.8	22.4	3.7	--	--	--	29.7	10.1
	3230	10.8	30.1	16.8	12.2	--	--	--	21.2	8.9
	3380	11.0	30.4	20.2	--	--	--	--	28.8	9.5
	3470	--	20.3	37.8	--	6.2	--	--	21.8	13.9
	3500	5.3	15.8	37.2	--	3.5	--	1.5	20.0	16.7
	3660	2.8	19.1	24.8	24.1	6.2	--	1.5	8.2	13.4
	3780	--	23.6	27.9	19.3	7.0	3.6	1.2	4.3	13.1
	3900	3.4	20.8	23.1	19.3	2.5	7.2	--	11.1	12.5
	4020	0.7	14.5	19.1	24.7	3.3	4.3	0.5	17.8	15.1
	4170	0.9	21.9	13.2	31.4	--	7.4	0.7	10.6	14.0
	4230	0.4	21.6	18.1	20.7	--	8.2	--	20.2	10.7
	4280	0.6	20.5	19.7	21.1	--	6.4	1.5	22.0	8.1
MAGMAMAX #3	1495	11.0	26.8	9.3	6.4	--	--	--	42.5	3.9
	1780	19.5	25.3	6.1	8.4	8.2	--	--	28.9	3.5
	2060	7.5	53.7	14.1	6.7	--	--	--	12.8	5.1
	2230	12.2	36.6	12.5	6.3	--	--	--	27.7	4.7
	2400	15.6	51.6	11.1	6.3	--	--	--	10.8	5.6
	2560	19.7	35.3	11.6	2.9	--	--	--	24.4	6.1
	2710	7.9	25.9	6.5	5.1	5.0	--	--	41.2	8.3
	2830	10.7	30.4	9.5	17.8	--	--	--	24.1	7.6
	2980	2.5	44.4	18.7	18.5	--	2.3	--	5.5	8.0
	3240	5.8	21.4	15.3	21.3	--	--	--	22.9	13.2
	3420	--	36.4	24.6	20.1	--	8.4	--	--	10.5
	3640	--	20.0	14.2	14.6	24.4	--	0.8	7.0	19.0
	3730	16.1	17.6	47.3	--	--	--	1.7	4.2	13.1
	3820	2.5	15.9	40.3	--	--	13.4	2.1	18.3	7.5
	3940	--	6.1	57.0	--	24.5	--	1.2	7.6	3.6
WOOLSEY #1	1200	5.3	20.9	15.0	21.9	--	--	--	23.1	13.8
	1480	0.7	25.4	24.0	24.0	--	3.5	--	1.7	10.6
	1760	1.8	19.0	36.7	--	6.6	--	1.1	19.8	15.0
	1880	--	19.8	13.7	13.7	24.9	--	0.9	7.5	19.4
	2135	12.1	12.9	34.2	28.3	--	--	1.2	2.4	8.9
	2260	2.9	15.2	39.3	4.5	--	10.0	--	20.1	8.0
	2380	--	6.3	56.3	--	24.4	--	1.1	8.6	3.3

APPENDIX II; TABLE II

X-ray Diffraction Analyses of the Clay Fraction of Bulk Samples

	DEPTH	CALC.	QTZ.	PLAG.	KSPAR	MICA	CHL.	MONT.	TALC
MAGMAMAX #2	1550'	--	8.8	--	--	71.6	19.6	--	--
	1700	--	6.9	--	--	76.4	16.7	--	--
	1940	--	2.9	--	--	54.5	42.6	--	--
	2120	--	20.8	--	--	28.1	51.1	--	--
	2330	--	6.8	--	--	77.2	16.0	--	--
	2630	--	10.9	--	--	70.2	18.9	--	--
	2780	0.6	1.3	--	--	52.8	45.8	--	--
	3020	2.5	15.9	2.2	4.7	44.0	30.7	--	--
	3230	--	5.5	--	--	63.0	31.6	--	--
	3380	2.2	5.8	--	--	38.2	53.8	--	--
	3470	--	5.0	7.2	--	45.1	42.7	--	--
	3500	--	4.8	13.7	--	20.7	58.4	--	--
	3660	4.2	4.8	9.0	11.8	3.9	54.0	12.4	--
	3780	--	5.5	10.3	14.1	12.4	57.7	--	--
	3900	--	4.8	--	--	12.5	82.7	--	--
	4020	--	9.1	14.1	27.3	6.1	43.4	--	--
	4170	--	13.1	--	25.1	16.6	37.5	7.8	--
	4230	--	13.2	--	24.5	6.4	37.3	18.5	--
	4280	--	10.7	--	5.3	31.6	31.7	20.6	--
MAGMAMAX #3	1495	1.3	4.1	--	--	77.6	17.0	--	--
	1780	0.2	3.1	--	--	86.8	9.3	--	--
	2050	--	1.9	--	--	69.1	29.0	--	--
	2230	--	5.4	--	--	68.0	26.6	--	--
	2400	--	13.1	--	--	50.7	32.1	--	--
	2560	1.1	4.0	--	--	69.9	24.9	--	--
	2710	0.4	2.5	--	--	71.4	25.7	--	--
	2830	3.3	6.6	--	--	57.3	32.9	--	--
	2980	0.5	3.2	--	--	39.9	56.4	--	--
	3240	6.1	10.3	--	--	40.6	43.0	--	--
	3420	--	6.0	7.8	--	44.8	41.4	--	--
	3640	--	5.1	2.2	--	25.1	67.6	--	--
	3730	6.9	5.7	14.7	20.5	1.9	50.4	--	--
	3820	--	--	--	--	34.4	11.9	33.7	20.0
	3940	--	1.6	26.4	--	26.2	30.9	--	14.9
WOOLSEY #1	1200	5.2	13.1	--	--	24.5	57.2	--	--
	1480	11.4	31.0	--	--	23.6	34.0	--	--
	1760	0.5	2.4	--	--	69.6	27.5	--	--
	1880	0.9	6.0	--	--	40.9	52.2	--	--
	2135	2.1	9.3	--	--	27.0	61.5	--	--
	2260	0.3	2.0	--	--	61.6	36.0	--	--
	2380	1.6	6.9	--	--	40.9	50.6	--	--

APPENDIX III, TABLE I

Isotopic Composition of Carbonate in Cuttings from Magmamax #2

DEPTH IN FEET	CARBONATE TYPE*	O^{18} in °/oo rel. to SMOW	O^{18} in °/oo rel. to PDB	YIELD in μ moles CO_2 / mg sample **	SAMPLE DESCRIPTION
120	C	18.15	-7.79	3.20	siltstone concretions
120	D	27.11	-.57		siltstone concretions
210	G	43.29	+3.06		gastropods
520	C	22.61	-3.24	.16	sandstone
520	C	21.05	-3.33		sandstone
520	D	26.88	-.92	.25 t	sandstone
850	C	32.22	-3.51	1.45	tan shale
850	D	30.18	-2.93	6.77 t	tan shale
970	C	22.54	-8.04	1.98	tan shale
970	C	24.52	—		tan shale
970	D	30.04	-3.93	6.70 t	tan shale
1000	C	16.59	-18.89		bulk
1060	C	24.66	-5.88	1.60	gray shale
1060	D	25.93	-2.53	4.38 t	gray shale
1240	M	19.72	-6.76		red shale
1240	D	20.35	-6.86		red shale
1240	C	17.68	-3.42	2.55	very well indurated sandstone
1240	C	20.71	-2.93	.88	very pale greenish-gray shale
1240	D	27.13	+.19	1.29 t	very pale greenish-gray shale
1400	M	21.04	-2.68		shale
1400	D	25.14	-.73		shale
1400	C	20.22	-2.87	1.09	gray shale
1400	D	27.91	+.68	1.53 t	gray shale
1400	C	20.49	-2.54	.86	red shale
1400	D	27.67	--	1.23 t	red shale
1490	C	18.49	-2.77	1.06	gray shale
1580	C	14.70	-3.73	1.08	sandstone
1580	C	16.99	-3.02	1.20	gray shale
1580	D	27.04	±.34		gray shale
1700	C	15.50	-4.27	2.36	sandstone
1700	C	18.15	-2.76	.90	gray shale
1700	D	27.56	+.42	1.80 t	gray shale
1760	C	14.58	-3.17	1.30	gray shale
1820	M	11.97	-5.82		bulk
1820	C	9.60	--	.92	sandstone
1880	C	13.34	-3.41	.94	gray shale
1940	C	10.62	-5.64	.71	fine grained, well indurated sandstone
2090	C	9.60	-6.34	.64	sandstone
2090	C	11.00	--		gray shale
2150	C	11.48	-3.24		gray shale
2150	C	10.46	-5.90		sandstone
2240	C	10.22	-5.73	.75	well cemented sandstone
2270	C	20.72	-3.41	1.11	gray shale
2330	C	9.84	-3.82	1.03	gray shale
2420	C	8.20	-6.59		vein calcite from gray shale
2420	C	8.90	-6.80		sandstone
2480	C	8.38	-5.36	.51	well cemented sandstone
2510	C	8.88	-3.82	.61	gray shale
2540	C	11.82	—	.55	moderately indurated sandstone
2600	C	9.82	-3.26		gray shale
2600	C	9.09	-4.07		gray shale
2630	C	10.09	-5.34	.89	sandstone
2660	C	9.30	-4.16		gray shale
2660	C	8.23	-7.80		vein calcite
2690	C	8.85	-6.84	.24	sandstone
2690	C	7.74	-7.31		vein calcite (pure)
2720	C	8.32	-8.52		vein calcite
2750	C	7.80	-6.30		sandstone
2810	C	7.91	-8.23		vein calcite
2870	C	8.88	-3.75	.58	gray shale

Table I continued

2930	C	7.63	-6.43	.64	sandstone
3020	C	7.91	-5.74	.88	sandstone
3020	C	8.55	-4.71		gray shale
3020	C	7.92	-9.18		vein calcite
3020	C	7.75	-9.07		vein calcite
3110	C	7.21	-6.38	.29	sandstone
3200	C	9.70	-8.03		vein calcite
3200	C	9.31	-7.73		vein calcite
3230	C	9.13	-6.59	.62	ver fine grained sandstone
3230	C	9.05	-4.96	.82 d	dark gray shale
3230	C	9.48	-7.98		vein calcite
3260	C	9.31	-5.06		gray shale
3260	C	7.74	-6.71	.55	dark gray shale
3260	C	8.63	-4.62	.68	sandstone
3320	C	7.90	-6.85	.62	white sandstone
3320	C	8.04	-7.69		sandstone with epidote cement
3380	C	9.44	-6.22		sandstone with rare calcite
3380	C	8.71	-5.20	.61	very dark gray shale
3380	C	8.72	-8.72		vein calcite
3410	C	11.21	-5.38	.64 d	dark gray shale
3410	C	10.93	-6.13		calc.-anhy. veinlets in dk. gray shale
3410	C	10.26	-7.91		calc.-anhy. veinlets in dk. gray shale
3410	C	9.08	-6.74	1.11	very fine grained sandstone
3440	C	12.50	-7.45		gray shale
3440	C	13.10	-7.15		gray shale
3440	C	11.24	-9.48	.81	very fine grained sandstone
3500	C	12.98	-12.25		calc.-anhy. veinlets in green shale
3500	C	10.25	-12.18	.78	rare very fine grained sandstone
3600	C	9.41	-6.12	.35	very dark gray shale
3870	C	9.86	-5.11	.12	dark gray shale
4170	C	11.28	-5.41	.05	green shales and white sandstones
4250	C	13.54	-4.83		green shales and white sandstones
4250	C	16.93	-4.83		green shales and white sandstone
4310	C	11.37	-5.73	.28	sandstone with red hematite cement

* There are three types of carbonate : calcite (C), mixed carbonate (M), and dolomite (D). The dolomite analysis is from the same sample as the calcite analysis immediately preceding it.

** Yield values not followed by a letter are the amounts of CO_2 collected after one hour of reaction with phosphoric acid. Values followed by the letters "d" and "t" are yields after one day and the total yield after one week, respectively.

APPENDIX III, TABLE II

Isotopic Composition of Carbonate in Cuttings from Magmamax #3

DEPTH IN FEET	CARBONATE TYPE*	δO^{18} in °/oo rel. to SMOW	δO^{18} in °/oo rel. to PDB	YIELD in μmoles CO_2 / mg sample **	SAMPLE DESCRIPTION
160	G	41.48	2.38		Gastropods
490-	C	21.28	-3.99		bulk-anhy. and sand aggregates
490-	M	22.29	-3.76		bulk-anhy. and sand aggregates
490-	D	25.63	-2.76		bulk-anhy. and sand aggregates
810-	M	21.14	-6.52		anhydrite aggregate
930-	C	24.77	-3.55		gray shale
930-	D	26.45	-4.27		gray shale
1060-	M	21.47	-8.06		drilling cement aggregates
1060-	C	21.04	-4.13		pale green shale
1060-	D	26.99	-.05		pale green shale
1150-	C	20.25	-5.13	.68	red + gray shale
1150-	M	21.42	-6.03		red + gray shale
1150-	D	24.71	-2.07		red + gray shale
1270-	M	18.32	-4.09	1.50 d	red + gray shale
1270-	C	18.96	-3.32	.67	red shale
1300-	C	18.47	-4.30		gray shale
1300-	D	25.96	-.94		gray shale
1360-	C	14.84	-3.50		white sandstone
1430-	C	19.43	-2.85	.93	gray shale
1430-	M	25.60	-.57		gray shale
1430-	D	27.59	+.54		gray shale
1465-	C	17.15	-16.69	3.30	dark brown sandstone
1465-	C	18.46	-4.77	.80	white sandstone
1495-	C	19.11	-3.35	.94	gray shale
1530-	M	16.77	-3.07	1.20 d	red + gray shale
1590-	C	19.66	-2.94	.92	red shale
1590-	M	25.44	-.70		red shale
1590-	D	27.64	+.43		red shale
1620-	C	18.37	-6.98	2.62	very well cemented sandstone
1650-	C	19.17	-3.19	.60	red shale
1650-	D	20.75	-2.60		red shale
1650-	C	18.50	-2.96	.75	gray shale
1650-	D	20.45	-4.21		gray shale
1750-	C	18.53	-3.05	.50	red + gray shale
1750-	D	19.52	-2.84	1.14 t	red + gray shale
1750-	C	17.37	-6.12		whitish-tan sandstone
1840-	C	17.89	-3.37	1.06	gray shale
1840-	M	23.79	-1.30		gray shale
1840-	D	27.23	+.30		gray shale
1840-	C	15.72	-2.84	1.57	well cemented sandstone
1840-	M	17.42	-5.00		well cemented sandstone
1840-	D	23.72	-1.88		well cemented sandstone
1840-	D	21.18	-2.51		well cemented sandstone
1930-	C	10.55	-4.44	1.79	sandstone
1930-	C	16.83	-3.22		gray shale
1960-	C	15.78	-4.92	.42	gray shale
1960-	M	17.23	-3.22		gray shale
1960-	D	21.82	-1.60		gray shale
1990-	C	9.77	-4.12		sandstone-small angular chips
2050-	C	13.44	--		shale
2080-	C	9.45	-3.72		very fine grained sandstone with black unknown
2110-	C	16.30	-2.98	.76	gray shale
2110-	C	16.42	-2.98		gray shale
2110-	C	10.01	-3.70		calcite veinlets
2110-	C	10.48	-3.73		calcite veinlets
2170-	C	14.16	-5.20	1.83	sandstone
2230-	C	17.64	-2.59	1.00	sandstone
2230-	C	17.77	-2.50		sandstone
2230-	D	23.40	-.74	1.40 t	sandstone
2230-	C	16.89	--		gray shale

Table II continued

2305	C	11.83	-4.43	.84	sandstone
2340	M	14.57	-3.50		gray shale
2340	D	15.40	-3.29		gray shale
2400	C	9.65	-3.90	.85 d	sandstone
2400	C	11.55	--		gray shale
2435	C	9.28	-5.29		vein calcite
2470	C	11.09	-3.96	.65	sandstone
2500	C	11.31	-4.05	1.28 d	sandstone
2500	C	12.59	-3.22	.80	gray shale
2500	M	12.16	-3.23		gray shale
2500	D	13.05	-2.58	1.03 t	gray shale
2620	C	10.11	-5.59		sandstone
2680	C	7.81	-8.06		vein calcite
2710	C	7.63	-7.53	.55 d	vein calcite
2710	C	9.70	-4.15	1.36 d	gray shale
2710	C	8.31	-6.24		sandstone
2800	C	8.31	-5.40	.28	white sandstone with rare epid.
2830	C	8.50	-4.42	.49 d	gray shale
2860	C	7.33	-7.84		vein calcite
2980	C	11.15	-3.22	1.00 d	red shale
2980	C	13.60	-3.29	.68 d	lt. purplish gray shale
2980	C	10.19	-3.23	.67 d	dark purplish gray shale
3010	C	6.72	-6.57	.41 d	sandstone
3010	C	10.24	-3.61	.88	dark gray shale
3100	C	7.56	-4.93	.77 d	dark gray shale
3210	C	13.45	-7.26		white siltstone
3270	C	6.87	-5.96	1.39 d	light gray shale
3270	C	6.93	-7.30		vein calcite
3450	C	7.40	-6.15	.47 d	gray shale
3670	C	8.23	-6.40	.93 d	gray shale
3760	C	7.41	-7.91		vein calcite
3730	C	8.19	-5.98	.70	dark gray shale
3730	C	10.48	-6.78		vein calcite
3790	C	7.87	-7.16		vein calcite
3790	C	7.61	-6.84	.22 d	light gray shale
3880	C	8.07	-5.64	.78 d	dark gray shale

* There are three types of carbonate: calcite(C), mixed carbonate (M), and dolomite(D). The dolomite analysis is from the same sample as the calcite analysis immediately preceding it.

** Yield values not followed by a letter are the amounts of CO_2 collected after one hour of reaction with phosphoric acid. Values followed by the letters "d" and "t" are yields after one day and the total yield after one week, respectively.

APPENDIX III, TABLE III

Isotopic Composition of Carbonate in Cuttings from Woolsey #1

DEPTH IN FEET	CARBONATE TYPE*	δO^{18} in ‰ rel. to SMOW	δO^{18} in ‰ rel. to PDB	YIELD in μmoles CO_2 / mg sample**	SAMPLE DESCRIPTION
630	C	24.53	-1.78	.51	gray shale
630	D	28.02	-2.19	1.01 t	gray shale
750	C	24.67	-3.80	1.51	brown shale
870	C	20.72	-5.97	1.46	gray shale partly replaced by anhy.
870	D	23.06	-4.48	4.60 t	gray shale partly replaced by anhy.
1050	C	16.92	-2.45	1.32	red shale
1200	C	15.12	-3.45	1.16	gray shale
1200	C	8.09	-6.55	2.14	sandstone
1355	C	14.42	-3.19	1.05	gray shale
1355	C	9.73	-4.46	1.05	sandstone with iron oxide cement
1355	C	8.63	-4.37	2.04	white sandstone
1575	C	13.00	-3.24	.98	gray shale
1605	C	8.66	-5.36	1.34	sandstone
1730	C	9.20	-5.40	1.21	white sandstone
1760	C	13.89	-2.93	.78	gray shale
1760	C	10.57	-4.54	1.27	sandstone
1850	C	11.80	-2.99	.81	gray shale
1910	C	9.82	-4.48	1.31	white sandstone
2000	C	11.40	-3.39	1.80	gray shale
2020	C	9.66	-3.86	1.26	well indurated sandstone
2105	C	10.26	-4.42	1.42	very fine grained sandstone
2135	C	9.76	-3.43	.88	gray shale
2165	C	10.10	-4.68	1.03	white sandstone
2260	C	9.21	-5.54	.68	very well cemented sandstone
2260	C	10.53	-3.49	.70	light gray shale
2290	C	7.16	-6.47		vein calcite
2326	C	8.92	-3.84	.76	very fine grained sandstone
2326	C	8.67	-5.57	1.07	pale green shale
2326	C	7.76	-5.96		vein calcite
2356	C	7.52	-6.21		vein calcite
2387	C	8.56	-3.42	1.13	gray shale
2387	C	8.70	-4.79	1.00	rare white sandstone

* There are three types of carbonate: calcite (C), mixed carbonate (M), and dolomite (D). The dolomite analysis is from the same sample as the calcite analysis immediately preceding it.

** Yield values not followed by a letter are the amounts of CO_2 collected after one hour of reaction with phosphoric acid. Values followed by the letters "d" and "t" are yields after one day and the total yield after one week, respectively.

TABLE IV

Isotopic Composition of Quartz and Hematite

	Depth in Feet	δO^{18} in °/oo Relative to SMOW	YIELD in µmoles CO_2 / mg sample
QUARTZ in Magmamax #2			
Well Mineralized Sandstones	2690	10.96	15.67
	3320	11.98	16.91
	3600	9.68	16.54
	3720	9.63	16.15
	3810	10.84	16.75
	3840	10.01	16.38
	3930	9.85	16.48
	3990	9.49	15.87
	4200	11.19	16.51
	4310	10.81	16.00
QUARTZ IN Magmamax #3			
Porous Sandstones	298	11.85	16.96
	490	12.46	17.50
	1180	13.84	16.50
	1270	13.78	16.75
	1300	13.29	16.70
	1465	12.99	16.70
	1465	13.22	16.40
	1530	13.50	16.50
	1650	13.76	16.60
	1750	14.28	16.50
	1780	13.36	16.52
	1840	13.15	16.75
	1900	13.73	17.50
	1960	12.93	16.73
	2110	13.25	16.90
	2200	13.20	16.50
	2340	14.05	16.50
	2370	13.54	16.36
	2470	13.38	16.91
	2500	13.01	16.87
	2620	12.99	16.83
	2710	13.53	16.40
	2740	13.36	16.47
	2860	13.35	16.69
	2920	13.31	16.66
	2950	12.71	18.40
	2980	12.86	17.25
	3010	13.76	17.00
	3100	13.17	16.50
	3300	12.99	16.80
	3360	12.76	16.25
	3450	12.63	16.54
	3880	12.03	17.30

Table IV continued

Well Mineralized Sandstones	3330	11.50	16.24
	3510	9.41	15.40
	3820	11.69	16.39
	3970	8.76	15.43
HEMATITE in Magmamax #2			
	3600	-3.83	9.05
	3810	-3.31	10.45
	3810	-4.05	10.14
	3840	-3.26	9.80
	3870	-4.78	9.80
	3900	-4.54	8.91
	3930	-2.26	10.99
	4020	-4.90	9.75
HEMATITE in Magmamax #3			
	3070	-0.25	9.93

TABLE V

Isotopic Composition of Epidote

	Depth in Feet	δO^{18} in $^{o}/_{oo}$ Relative to SMOW	FORMULA PROPORTIONS Fe^{+3}	Al^{VI}	YIELD in μmoles CO_2 / mg sample
Magmamax #2					
	2690	4.79	.59	2.41	13.28
	3320	6.48	.69	2.31	14.05
	3600	5.55	.92	2.08	14.36
	3720	4.51	.99	2.01	13.71
	3840	4.72	1.04	1.96	13.30
	3990	4.38	.99	2.01	14.35
	4200	5.57	1.04	1.96	14.00
	4310	4.97	9.67	2.03	14.00
Magmamax #3					
	2920	4.51	.94	2.06	13.40
	3100	5.05	.94	2.06	14.35
	3330	5.61	.82	2.18	14.45
	3510	5.48	.97	2.03	13.60
	3670	4.02	.89	2.11	13.10
	3670	3.61	.92	2.08	13.85
	3970	5.81	1.04	1.96	14.74